THE INFLUENCE OF CEMENTATION ON LIQUEFACTION RESISTANCE OF SANDS

by

Jotaro Iwabuchi

Thesis submitted to the Faculty of the

Virginia Polytechnic Institute and State University

in partial fulfillment of the requirements for the degree of

Doctor of Philosophy

in

Civil Engineering

APPROVED:

G.Wayne Clough

T. Kuppusamy

J.H. Hunter

T.L. Brandon

Robert M. Jones

November, 1986

Blacksburg, Virginia

THE INFLUENCE OF CEMENTATION ON LIQUEFACTION RESISTANCE OF SANDS

by

Jotaro Iwabuchi

G. Wayne Clough

Professor and Head

Civil Engineering

ABSTRACT

Cohesionless sands are known to be susceptible to failure by liquefaction when they are saturated and subjected to earthquake shaking. Considerable study has been directed towards this subject over the past 20 years in recognition of the possibility of large-scale property damage or loss of life due to this type of failure. Recent evidence has shown that small degrees of cementation in a sand significantly reduce the likelihood of liquefication. However, the work to date has been limited to studies with conventional testing devices and simple loading paths. These devices are suspected of inducing premature failure in cemented soils, and are not capable of modeling the effects of multiaxial loading.

In this investigation, there were two major objectives. The first involved the development and fabrication of a new three-dimensional shear device with the capability of applying load to cemented sands with a minimum of stress concentration effects, and of using load paths which are more representative of the true effects of an earthquake than is possible in conventional equipment. The second concerned performance of a series of production tests to investigate the behavior of cemented sands under a range of earthquake loading paths. The production tests were largely performed using the new three-dimensional shear device.

The test results showed that cemented soils have more resistance to earthquake loading than previously thought since stress concentration effects in conventional testing do induce premature

failure through the effects of stress concentrations. On the other hand, it was found that either cemented or uncemented sands show less resistance to earthquake loadings if multiaxial stress conditions are applied to the sample as opposed to uniaxial loadings. This is important in explaining the fact that sites with seemingly similar conditions often show different behavior, since slightly different earthquake loading patterns can cause different responses. One factor explaining differences in response is found to be the mean normal stress, which is not the same for all loadings, and plays an important role in the pore pressures developed in the soil.

ACKNOWLEDGMENTS

I would like to thank prof. G. Wayne Clough whom I have respected during the years I have spent in Blacksburg. To him I owe many suggestions and improvements which have influenced the final version of this dissertation. At the completion of this dissertation, I realize that I have received quite amount of encouragement, support and friendship from him. With all these, I am very thankful to him.

I would like to express my sincere gratitude to prof. T. Kuppusamy who gave me an oppotunity to work on the cubical device. His advise and encouragement have been a key role to get this research advanced toward the completion.

I would like to mention that this research is financially supported by the National Science Foundation for two years, from 1984 to 1986. I express here my appreciation for its financial assistance.

During the period, I have met many brilliant and, sometimes hilarious, students. Some of them are:

and I have enjoyed working with 'em and do appreciate their friendship. I truly hope all of them be straight on the right truck toward their big successes.

I cannot forget helpful and kind offices and work from whom I desperately needed to complete my work. I would like to thank them for their excellent professionalism.

Finally, I have received many letters from my parents and of Chuo University. The former has taken care of my tight financial condition and the latter has urged me when I was in stumble. I thank them very much.

Table of Contents

List of Tables

List of Figures

CHAPTER I

INTRODUCTION

The term "sandy soil" often is used to connote a material that has essentially no cohesion between the soil particles. There has been a particularly intensive phase of research in this area over the past 15 years or so as a result of the finding that these materials in a saturated state can undergo liquefaction if subjected to earthquake loading. Liquefaction can lead to a loss of strength of the sand, or to the generation of large deformations even where the sand retains most of its ability to carry load. In a number of recent and historic earthquakes, significant damages and, in some cases, loss of life have occurred as a result of liquefaction. As a result, identification of the likelihood of a soil being subject to the liquefaction process has become an important issue. On the one hand, it is necessary to identify the possibility of a dangerous land mass failure. However, it is equally important not to overestimate the potential for liquefaction, since this can lead to serious economic consequences for facilities owners.

Over the past five years or so, two points have become clear which have major implications for the issue of liquefaction of sands:

1.) Cementation in sands due to either natural or artificial sources can reduce the likelihood of liquefaction.

2.) Cementation in natural sand deposits is relatively common due to a series of mechanisms that involve formation of bonds at the points of contact between the sand particles.

Because of the perceived importance of cementation on the behavior of sand during an earthquake event, a number of investigators have undertaken research into this subject. All of the previous experimental work has involved testing of cemented sands using conventional devices such as the triaxial cell or the simple shear apparatus. Although useful information has been developed in this manner on the relative importance of various parameters on the behavior of cemented sands under simple forms of cyclic loading, this type of testing is insufficient from a number of perspectives:

1.) The loading paths are simplified and are not necessarily the best models of the effects of an earthquake.

2.) The structure and strength of weakly cemented sands is particularly sensitive to the details of the testing approach.

3.) During cyclic loading with a conventional triaxial cell, the soil is subjected to extension, and the sample most often fails by necking. This is undesirable and raises questions about the validity of the failure loads determined in the test.

4.) If a simple shear device is used, it is difficult, if not impossible, to guarantee a proper bond between the platens and the cemented soil. If the bond does not exist, failure in the test will occur due to slip between the platen and the soil, a condition not representative of the soil behavior. If a tight bond is formed between the platen and the soil, sharp stress concentrations are formed in the cemented soil, causing premature, brittle failure.

These comments about testing of cemented sands in conventional devices illustrate why a new approach was considered necessary for this study.

The major objectives of the research were twofold. First, it was intended to develop a three-dimensional shear box which could apply cyclic loadings following a range of stress paths. The box was intended also to resolve most of the issues surrounding the special problems in loading of a

cemented sand. Second, using the test results of this work and that of others, it was expected to more thoroughly explain the role of cementation in the behavior of cemented sands under dynamic loadings of the type generated during a seismic event.

The three-dimensional shear box system that was developed involves not only the box itself, but also a microcomputer control and data acquisition unit, and software for the microcomputer unit. New methods were generated for preparation of samples to various levels of density and cementation, saturation of the samples, and measurement of the sample deformations. The completed system allows for a wide range of loading paths to be automatically applied to the soil through the microcomputer unit. Test information is also automatically acquired and stored for subsequent processing on a main frame computer.

During and after the three-dimensional shear box development, considerable experimental work was done. Over one hundred trial and pilot experiments were performed to check and evaluate the equipment. Twenty-four standardized tests were conducted with uncemented sands. Finally, nearly 100 more production tests were carried out using four different levels of cementation, two different densities, six types of loading paths, and four levels of loading.

The information on the research is divided into seven chapters exclusive of the introduction. Chapter II presents a background review of the previous work on cemented sands and liquefaction, and Chapter III covers concepts as to the nature of loadings during an earthquake as related to those used in the experiments of this work. Chapter IV gives the information on sample preparation techniques and experimental test program. The design and results of trial pilot tests with the three-dimensional device is provided in Chapter IV. Chapter VI presents the main results of the experimental program; discussion is provided in Chapter VII. Conclusions are presented in Chapter VIII. Appendixes are included with details on the equipment design and a user's manual for the three-dimensional shear box system.

CHAPTER II

BACKGROUND - CEMENTED SANDS AND LIQUEFACTION

2.1 Introduction

Cemented sands are recognizable when they are encountered in exposed slopes. In this environment, they are able to stand in steep bluffs, often to great heights even when only weakly cemented. An example of this behavior is given in the photographs in Figure 2.1 showing bluffs in cemented soils along the coast of California just south of San Francisco. The ability of this soil to stand in steep slopes is provided by compressive and tensile strength of the cemented sands that exists even when they are unconfined. The surprising aspect of these soils is that the unconfined tensile and compressive strengths may be very small. For example the sands in the bluffs shown along the California coast can be broken under light finger pressure (Figure 2.2) (Clough and Bachus, 1981).

The strength of cemented sands is typically neglected in geotechnical practice as a conservative expedient. Actually in many cases the geotechnical engineer simply does not know that the sand is cemented since the sampling procedures used in conventional practice disrupt the cementation bonds (Saxena and Lastrico, 1978; Frydman, et al., 1980; and Clough and Bachus, 1981). The neglect of the cementation of a sand may be acceptable for certain types of problems, but it is unnecessarily conservative for liquefaction problems.

Figure 2.1 Steep Bluff on Coastal Area near San Francisco, California.

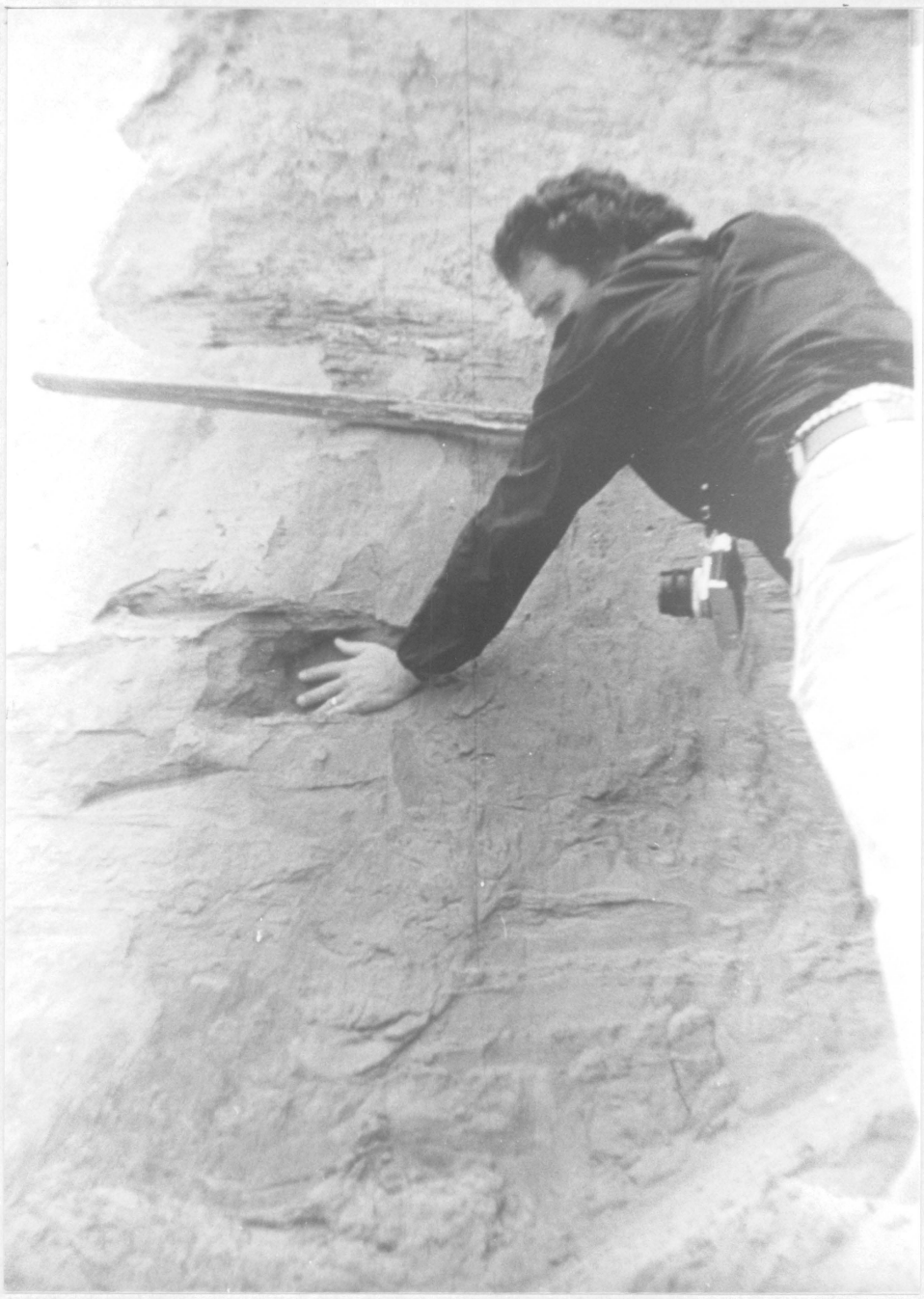

Figure 2.2 Demonstration Showing the Brittle Nature of Cemented Sand.

2.2 Cemented Sand Deposits And Cementing Agents

Cemented sand deposits come in many forms and are located in a variety of areas of the world. Table 2.1 gives a general description of a few of the more well-known cemented sands that have been cited in the geotechnical literature. These soils have generally been identified by their appearance in exposed slopes. There is no doubt that many other sands are cemented, but have not been identified as such because of the difficulty of obtaining an undisturbed sample.

While cementation adds to the strength of a sand, the spectacular natural slopes in these materials are often in a marginal stability condition. This can be especially true where erosion processes are active. In such cases, the slopes can fail suddenly since the soil near the face of the slope is unconfined and brittle. The impetus for failure can be caused by an earthquake. Examples of significant failures in cemented sands slopes during earthquakes are described in a number of references (Harp, et.al., 1978; Sitar and Clough, 1980; Shirasu Committee, 1968; Yamanouchi, et.al., 1970). The failures are typically shallow, and if the slope is steep, failure appears to be caused by tension stresses formed near the crest of the slope.

Sowers (1979) has described two forms of cemented sands. One is termed void-bound. In this case, the voids of the sand are essentially filled with the cementing agent, and the resulting soil has a low void ratio, and a high density. The second is called contact-bound, with the cementing agent found only at the points of contact between the particles. This soil has a high void ratio and can have a relatively low density. It is the latter category of sand that this work is concerned with. The contact-bound sand is subject to brittle failure if loaded in unconfined compression, and can liquefy if cyclically loaded in the undrained, saturated condition.

Cementing agents vary considerably, often being produced as a result of secondary soil development processes. Weathering, leaching and deposition, and hot and cold welding are prominent agents in cementation formation. Weathering can produce substances such as iron oxides which

Table 1. 2.1 Location of Selected Cemented Sand Deposits (After Shaffi-Rad and Clough, 1982).

No	Location	Feature	Reference
1	Along most of the Pacific coast in Cal. and Oregon.USA	Cliffs of weakly cemented sands of Quaternary marine terrace deposits and tertiary marine and dune deposits as high as 150 m (carbonates, clays, iron oxides)	Clough, et al., 1981
2	The western and southern USA	A caliche-type soft rock (precipitation of calcium carbonate)	Hamel, 1977
3	Extensive areas of the Midwestern USA and Yellow River, China	Steep bluffs. (Loess, silt, calcareous soils)	Bechwith Hamsen 1981
4	Central Guatemala	Wind blown volcanic ash deposits	Harp et al., 1978
5	Southern Japan	Pumic-flow deposits in Shirasu Plateau	Yamanouchi, et al., 1977
6	Northern Island New Zealand	Pumic-flow deposits	Yamanouchi, et al., 1974
7	Mediterranean coastline of Israel and neighboring countries	KurKar deposits. (silica sands grain, calcite crystals, small, fragment of shells, other calcarious materials	Frydman et al., 1980
8	Western and central Europe	Keuper sandstone (illitic clay minerals with calcium carbonate)	

serve to provide a weak form of cementation. Leaching and subsequent precipitation of silicates and carbonates can lead to very strong cementation if the process is prolonged. Hot welding is a process where the points of contact between the sand particles are bonded as silicates are driven into solution under the influence of heat and pressure. The heat is typically a result of volcanic activity in or near ash or soil deposits. Cold welding process is little understood and occurs only due to prolonged high pressures at the points of contact between particles (Lee, 1975). In this case, the silicates are driven into solution as in the case of hot welding. Seed (1976) has postulated that this may explain the observed time dependent gain in liquefaction resistance in some sands as they remain at rest under gravity stresses.

2.3 General Aspects Of Cemented Sand Behavior

The studies of cemented sand behavior under static loading have shown that in spite of the variety of cementing agents in the sands that there are many common facets of the behavior. Some of the more important findings are:

Static Behavior

1.) The cohesion intercept increases with level of cementation, amount of fines, and angularity of the sand.

2.) The friction angle is little affected by level of cementation, but increases with density and angularity of the sand (Shaffi-Rad and Clough, 1982).

3.) There is a small, but significant tensile strength which typically equals about 10 percent of the unconfined compressive strength. (Haruyama, 1973; Clough et al., 1981).

4.) Brittleness increases by increasing the cementation or decreasing the confining pressure. (Murata and Yamanouchi, 1978; Shaffi-Rad and Clough, 1982).

5.) The initial tangent modulus increases with confining pressure and / or the level of cementation (Clough, et al., 1981).

6.) Volumetric increases generally accompany shear failure even for cemented sands with " loose structure . " The volume changes tend to be more concentrated and somewhat larger than those for uncemented sands (Murata and Yamanouchi, 1978; Clough, et al., 1981; Shaffi-Rad and Clough, 1982)

Dynamic Behavior

1.) Dynamic shear modulus tends to be greater and damping ratios are less for cemented sands than those of uncemented sands (Sitar and Clough, 1979).

2.) Increasing the cementing agents increases liquefaction resistance (Salamone et al. 1978; Dupas and Pecker, 1979; Poulos, 1980, Frydman et al., 1980; Shaffi-Rad and Clough, 1982).

3.) Pore water pressure development of cemented sands is different from uncemented sands and models to predict the pore pressure build up may need to be modified for cemented sands (Shaffi-Rad and Clough, 1982).

4.) Weakly cemented zones within a strongly cemented matrix seem to dominate the liquefaction resistance (Frydman, et al., 1980).

Research has also shown that with proper care in the sample preparation procedures, sands cemented with small amounts of portland cement behave at least qualitatively like naturally cemented sands (Shaffi-Rad and Clough, 1982). This finding is of importance in that naturally ce-

mented sands are difficult to sample and test, and it is useful to use artificially prepared sands in laboratory studies.

2.4 Sampling And Testing Cemented Sands

The difficulties of obtaining good quality undisturbed samples of naturally cemented sands have been described by a number of authors (Frydman, et al. 1980; Saxena and Lastrico, 1978; Clough and Bachus, 1981). Even if the soil can be obtained in a sample tube, it is likely to be damaged in the process of extruding it from the tube. For these reasons, it is doubtful that any conventional investigation of cemented sands results in a realistic evaluation of the soil properties.

Because of the problems associated with sampling and testing of undisturbed samples of naturally cemented sands it is tempting to rely on in-situ testing procedures to ascertain the engineering properties. Unfortunately, most of the common and readily available methods are of the penetrometer family, and none of these techniques are able to sort out the relative influence of density and cementation. To date, the only reasonable approach seems to be in the form of pressuremeter testing, particularly of the self-boring variety (Bachus, et al., 1981).

2.5 Classification Of Cemented Sands

Cemented sands are a category of materials for which no standard classification system is appropriate. Considering the widely used Unified Classification System as an example, there is no mention of the subject of cementation. Thus, in this system, a sand can be heavily cemented or lightly cemented, and in both cases, it will be simply called a sand. To address this oversight, Rad and Clough (1982) proposed to use certain terms to classify the degree by which a sand is cemented.

Their system is shown in Table 2.2. This approach is used in the descriptions of the soils tested in this work.

2.6 Liquefaction Of Uncemented Soils

The general mechanisms causing liquefaction were described in the early days of soil mechanics (Casagrande, 1975). However, it was not until the significant damage caused by sand liquefaction in 1964 in Alaska and Niigata Earthquakes that the effects of cyclic loading in the process came under detailed study. The work of Seed and his co-workers was instrumental in developing laboratory and analytical procedures needed to form a practical infrastructure for the engineer to deal with the problem (Seed and Lee, 1966 and 1967; Seed and Idriss, 1971; Seed and Martine, 1976; Seed and Idriss, 1981; etc.)

In the intervening years since the late 1960's and early 1970's many investigators have contributed to the work on liquefaction of uncemented sands. Recently, the field has benefited from a series of excellent state-of-art reports by Seed (1979) and Ishihara (1985), and the report from the 1985 MIT workshop on liquefaction. Because of the availability of this substantive body of literature, this review of liquefaction will be brief, and primarily devoted to those aspects which bear on the topic of this research.

2.6.1 Laboratory Testing

Laboratory testing has formed the backbone of the methods for research into liquefaction. It is useful for research because control can be exerted on drainage and boundary conditions, and the loading can be defined accurately. Most laboratory testing associated with liquefaction work utilizes either triaxial or simple shear devices. The triaxial apparatus offers the advantage of simplicity, and much of the test procedure for liquefaction work is standardized (Seed and Lee, 1966; Seed and Peacock, 1971; Silver et al., 1976). The simple shear device is preferred by some in that it better

Table 2. 2.2 Classification System for Cemented Soils (after Shaffi-Rad and Clough, 1982).

Very Weakly Cemented Soils - with UCS* < 100 (kN/m^2) The cementation is almost inapparent to the touch, and undisturbed sampling is difficult if not impossible. However, freezing the soil may be a suitable technique.
Weakly Cemented Soils - with 100 < UCS < 300 (kN/m^2) The soil breaks under light finger pressure, and a block sampling technique with care can be used to obtain undisturbed samples. This soil can be easily scratched with the fingertip.
Moderately Cemented Soils - with 300 < UCS < 1000 (kN/m^2) The soil hardly breaks apart under finger pressure, and undisturbed specimens can be easily obtained from block sample. The pressure of cementation bonds between the particles is readily felt, and the soil can be scratched with the fingernail.
Strongly Cemented Soils - with 1000 < UCS < 3000 (kN/m^2) A power saw can be used to cut block samples, trimming of specimens ordinary had tools is difficult. The soils hardly break under hand pressure, and cannot be easily scratched

*: Unconfined Compressive Strength.

models the effects of an earthquake-induced shear wave transmitting through the soil (Seed and Peacock, 1968; Finn, et al., 1971; Ishihara and Yamazaki, 1980). However, both of these devices are limited in the type of stress path that can be applied to the soil.

Other types of laboratory test devices in liquefaction investigations include shaking tables, torsional shear, and three-dimensional shear boxes. The shaking table is used primarily as a large-scale simple shear apparatus, and has served to answer some of the questions about boundary effects in conventional simple shear boxes (Seed et al., 1976). Torsional shear was proposed as a device to allow for more general stress path loading than is possible with other approaches (Ishibashi and Sherif, 1974; Ishihara and Yasuda, 1975). However, this method requires the use of a hollow cylindrical specimen, and this poses difficulties in sample preparation. Also, there are still limitations in the variety of stress paths that can be applied to the soil.

Ishihara and his co-workers are apparently the only investigators that have used a three-dimensional shear box in liquefaction testing (Yamada, Y. and Ishihara, K., 1983). The three-dimensional approach offers the most latitude in load paths for liquefaction testing. This testing device and the stress paths used in it are described in Chapter III.

2.6.2 Concepts of Liquefaction

There are a number of different schools of thought concerning liquefaction. Two of these are mentioned here because they are examined in the course of this work in regard to cemented sands. One of these is the approach developed by Seed and his co-workers. It involves defining the loads which will occur in terms of an equivalent shear stress which is attributable to the design earthquake. The soil resistance which can be mobilized to resist the earthquake shear stress exceeds the soil resistance, then liquefaction is assumed to occur, regardless of the density of the sand.

Casagrande (1975) and his co-workers Castro (1975, 1977) and Poulos (1981) proposed that the resistance which can be mobilized by the soil should be determined through the critical or steady state concept. In this case, a steady-state relationship is established for a sand which serves to sep-

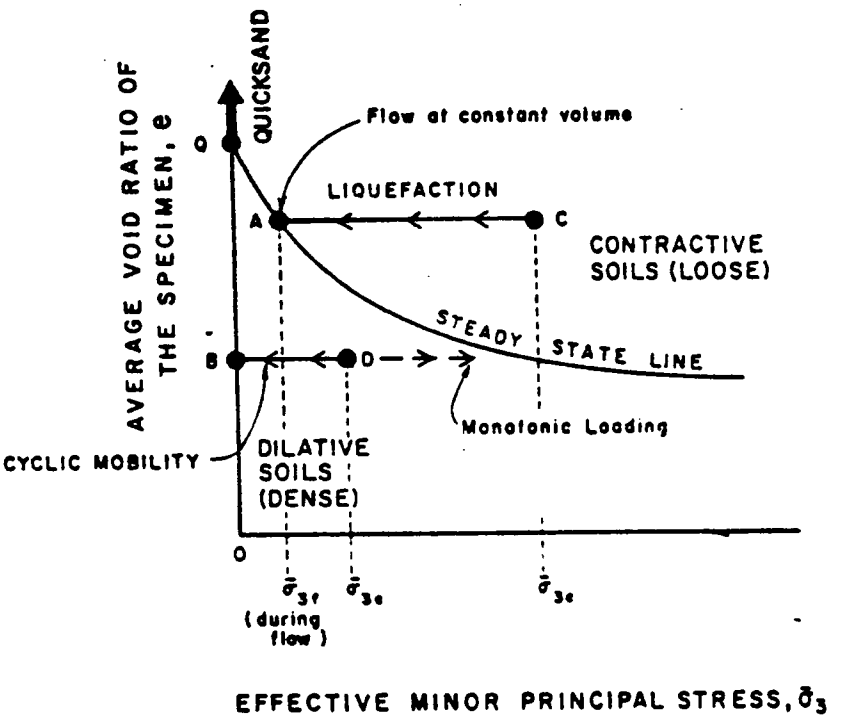

Figure 2.3 Critical State Concept for Mobility of Liquefied Sand (after Castro and Poulos, 1977).

arate soil behavior into "loose" and "dense" conditions (see Figure 2.3). Only loose sands are able to undergo true liquefaction in this concept, because only loose sands will flow and exhibit large strains after failure even if the stresses applied to the soil do not exceed those which caused the initial failure. In this approach, it is necessary to perform laboratory triaxial tests to define the steady-state line for a given sand. Details of this process are given in Poulos (1981). Notably, the sand used in this operation can be remolded, and even static tests can be employed. To determine if the sand in the field is subject to liquefaction, careful testing with undisturbed samples is needed to define the in-situ void ratio. If the sand void ratio is such that it falls on the loose side of the steady-state line, then it is potentially subject to liquefaction. If the void ratio falls on the dense side, then the soil cannot liquefy since it will not flow under the application of shear stresses.

Although the Casagrande approach has not found the popularity of the Seed approach with practicing engineers, it is useful for analysis of the potential behavior of a soil under the action of static shear stresses after a seismic event. Thus, it is used to determine if the soil can flow after the earthquake due to the action of pre-existing shear stresses induced by a slope.

2.6.3 Pore Pressure Modeling

In the event that earthquake loading does not produce liquefaction, it still may induce significant pore pressures. Thus, there is an interest in predicting the excess pore pressures that might occur during a seismic event. Many models have been proposed for this purpose. In a general sense, they may be classed as simplified and complex. A simplified model is one that requires few parameters to define it, and typically the calculations required to obtain an estimate for the pore pressures can be done by hand or with a personal computer. All of the simplified models assume fully undrained conditions. A complex model is usually based on detailed theories of mechanics, and requires a major computational effort to obtain pore pressures. Dissipation effects can also be included in the analysis. Notably, all of the models, either simplified or complex, have been proposed for uncemented sands. This investigation will examine several simplified models for their applicability for cemented sands.

Simplified pore pressure models have been proposed by Seed and Martin (1976), Sherif et al., 1978, and others. These are usually based on the idea that the pore pressures developed in a sand during undrained cyclic loading follow certain empirically derived patterns. The empirical patters are subsequently described through the use of a fitting equation, and this is used as the basis for the method of prediction. An example of this is proposed by Seed and Martin (1976). They noted that pore pressures during cyclic loading with uniform cycles can be described by:

$$r_u = \frac{1}{2} + \frac{1}{\pi} \arcsin(2 \times r_N^{1/\alpha} - 1)$$

$$\gamma_N = [\frac{1}{2}(1 - \cos \pi)\gamma_u]^{\alpha}$$

in which $r_u = u/(\overline{\sigma}_c)_i$; the excess pore pressure ratio is expressed as the ratio of the peak excess hydrostatic pore-water pressure to the initial effective confining pressure, $(\overline{\sigma}_c)_i$, and $r_N = N/N_l$; the cyclic ratio is equal to the ratio of the number of cycles required to cause liquefaction, N_l. α is the soil parameter. An average value of $\alpha = 0.7$ was reported by (Seed and Martin, 1976). Thus, if one knows the number of equivalent uniform cycles of loading expected in the design event, then the excess pore pressures can be readily calculated using the above equation. Seed et al., (1975) give simple rules that can be used to determine the number of equivalent uniform cycles of load for different events.

2.7 Liquefaction Of Cemented Sands

The subject of liquefaction of cemented sands has only recently been of interest to the engineering profession. A number of circumstances provided the impetus for the work in this area. First, in the early 1970's a number of major construction projects were undertaken in areas with cemented sands, and where there was concern about seismic loading. Project specific studies were undertaken to examine the liquefaction potential of the soil at the sites. The results of these studies were reported by Salamone, et al. (1978), Dupas and Pecker (1979), Saxena and Lastrico (1978), and Frydman et al. (1980). The basic conclusions were:

1) It is very difficult to obtain a representative samples of the weakly cemented sand deposits.

2) Even a relatively low degree of cementation in a sand serves to significantly inhibit liquefaction.

3) The liquefaction of the sand seems to be dominated by the weakest cementation element in the soil.

These studies were unable to come to specific conclusions as to how much cementation was needed to affect liquefaction potential for a given seismic loading or soil density since only one soil was typically studied, and the quality of the samples tested was subjected to question.

Other indirect evidence for cementation and its effect on liquefaction is cited by Seed (1976). He noted that the liquefaction resistance of a sand increased if the sand remained under pressure for a significant period of time. It was postulated that in these conditions cementation occurred due to cold welding at the points of contact of the sand. This effect was measurable even over a period as short as six months. In his later publications, Seed has taken this factor into account, allowing for an empirical increase of the liquefaction resistance of a sand if the period of "rest" is known for the sand. In a similar vein, Youd and Perkins (1978) have shown that the liquefaction resistance is directly correlatable to the age of a sand deposit, and that older sand deposits are more resistant to liquefaction.

More recent studies have attempted to quantify the effect of cementation on liquefaction resistance through the use of cemented sands manufactured in the laboratory to predefined cementation and density levels. Rad (1982), Saxena et al. (1985), and Milstone (1985) have used this approach. In general, the results of these studies have shown similar trends. Conclusions where the findings are the same are as follows:

1.) Cementation increases the liquefaction resistance of a sand.

2.) The effect of cementation on liquefaction resistance can be correlated to the unconfined strength of the cemented sand.

3.) Cementation in a sand can make it behave as if it were a dense uncemented sand, even though the cemented sand has a loose structure.

In addition to the points where the different studies agree, there are also points of disagreement. One of these areas concerns pore pressure development. Saxena, et al. (1985) report that the pore pressure response curve in cemented sand is very similar to that of uncemented sands. Rad (1982) concluded this was not the case, and Milstone (1985) provided evidence to explain the difference in opinions. Milstone (1985) was able to show that in a sense both were right, since if low stress ratios are applied to cemented sands, and large numbers of cycles are needed for liquefaction, then the pore pressure generation response for a cemented sand is essentially the same of an uncemented sand. However, if high stress ratios are applied to a cemented sand, the pore pressure generation response is different than that of the uncemented sand.

Some other conclusions drawn by Milstone (1985) on the effects of nonhomogeniety in a cemented sand are:

1.) The presence of a weak lens in a matrix of a stronger cemented matrix leads to a lowering of the ability of the cemented sand to carry dynamic loads.

2.) The effect of a weak lens on the stronger matrix is larger at higher stress ratios. Thus, under large earthquakes, the weak lens has a greater impact on reducing the resistance of the cemented sand than is the case in smaller earthquakes.

The research to date on the liquefaction potential of cemented sands has clarified a number of issues. However, all of the testing has been done through conventional triaxial loading, and there has been no attempt to determine the influence of stress path on the soil response. Further, it is not clear that the stress concentration effects inherent in triaxial testing do not lead to an incomplete picture of cemented sand behavior. This thesis is directed towards resolving these points.

CHAPTER III

ADVANCED TESTING DEVICES AND LOADINGS FOR LIQUEFACTION STUDIES

3.1 Introduction

Dynamic triaxial and simple shear devices are commonly used for laboratory based studies of liquefaction phenomena. Such approaches are justified on the basis of a simplified concept of the loading induced by earthquake. Typically, they produce a loading path assumed to model the passage of a one-dimensional shear wave through the soil. In this chapter, the issue of other types of loading due to earthquakes is considered. Also a review of previous three-dimensional liquefaction testing of uncemented sands is presented.

3.2 Basic Concepts Of Earthquake Loading

It is well known that, in the vicinity of the earth's surface, seismograph recordings show that both body waves (compression and shear waves) and surface waves (Love and Rayleigh waves) are detected. Often the surface waves have larger amplitudes than that of the body waves. The typical assumption that laboratory tests should model only the effects of the shear wave derives from the notion that the shear wave will produce the most damaging effects. However, there is little evidence that this assumption can be applied for all cases.

Figure 3.1 shows a seismograph recorded for the 1965 Offshore Central America earthquake (Simon, 1971) for which the typical magnitude is 6 3/4; and the focus was located 27 km (16.8 mil.)

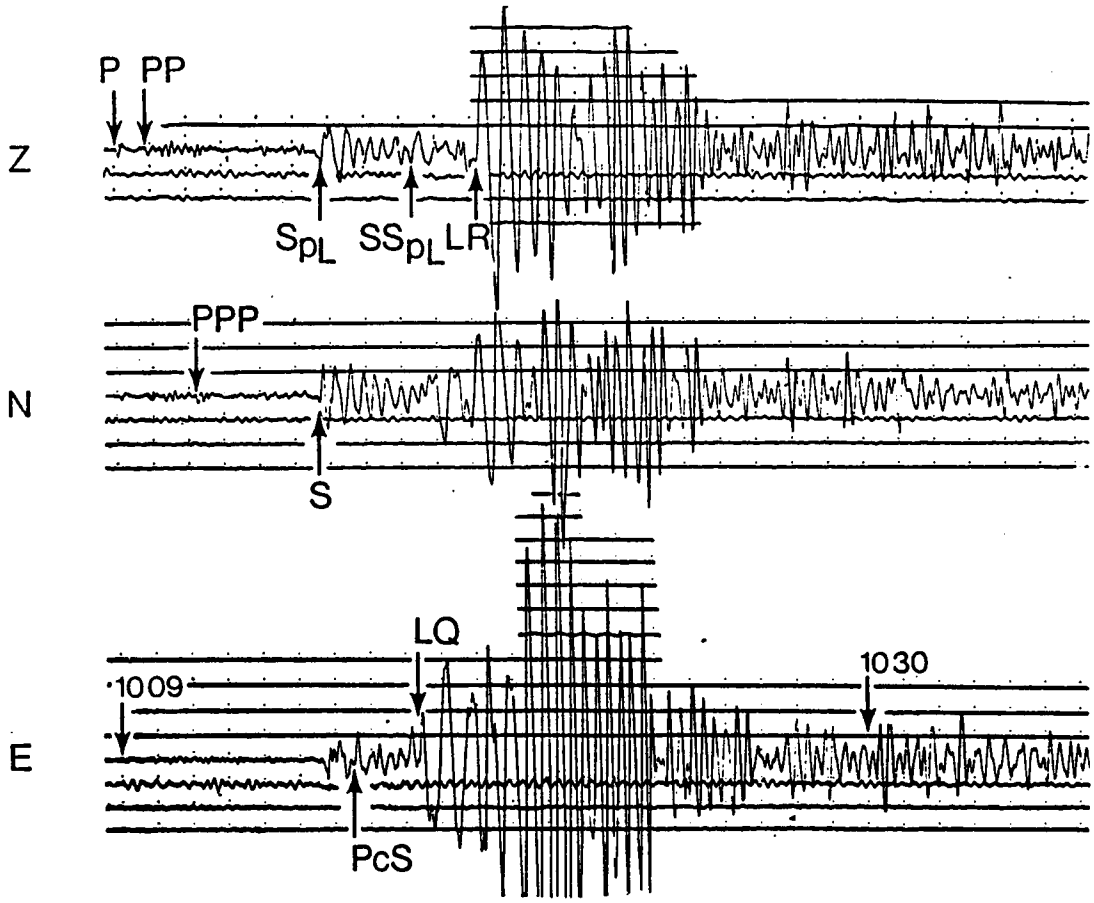

MAXIMUM MAGNITUDE 7

P: P-Wave PP, PPP & PcS: P-Waves generated by reflection of P & S-Waves

S: S-Wave Spl & SSpl: S-Waves generated by reflection of S & P-Waves

LQ: Love-Wave LR: Rayleigh-wave

Figure 3.1 Example of Seismograph - 1965 Offshore Central America Earthquake.

below the surface; shallow earthquake. The motions of the compression, shear, Love and Rayleigh waves can be seen, and it is observed that the amplitudes of the surface waves are as large, or larger than those of the body waves. Induced deformation patterns on three axes due to the passage of seismic waves are shown in Figure 3.2. It can be seen that the ground is forced to undergo a rotational type of response somewhat like that known to occur in water during ocean wave passage. Importantly, the effect is three-dimensional with simultaneous motion occurring on all axes. Three dimensional trends are commonly observed in both ground motions and accelerations (Carder and Cloud, 1959; Stauder, W.S.J., 1960; Cloud and Hudson, 1961; Gupta and Navain, 1967; Knudson, et al., 1972; Shiraki and Kajimura, 1978; Gonzlas and Yegian, 1979; Harding and Hermsen, 1981; etc).

The trends in the loadings of the surface of the earth in a seismic event suggest that the forms of loading used in the conventional triaxial and simple shear devices oversimplify the actual case. It follows that it is appropriate to consider the effects of more general loading to determine if this is important or not.

3.3 Review Of Nonconventional Testing Devices With Two- And Three-Dimensional Loading Capabilities

A number of methods have been used in geotechnical engineering to achieve loading paths beyond those that can be attained in the triaxial or simple shear types of devices. Most of this work has been directed at static applications, but recently a number of investigations have used dynamic loadings.

3.3.1 Stacked Shake Tables

This concept was used by Pyke, Seed, and Chang (1975 and 1978) to achieve multi-directional shaking of a soil sample. The procedure involved stacking a one-directional shake table onto a larger shake table which is capable of both horizontal direction and vertical shaking. The two shake

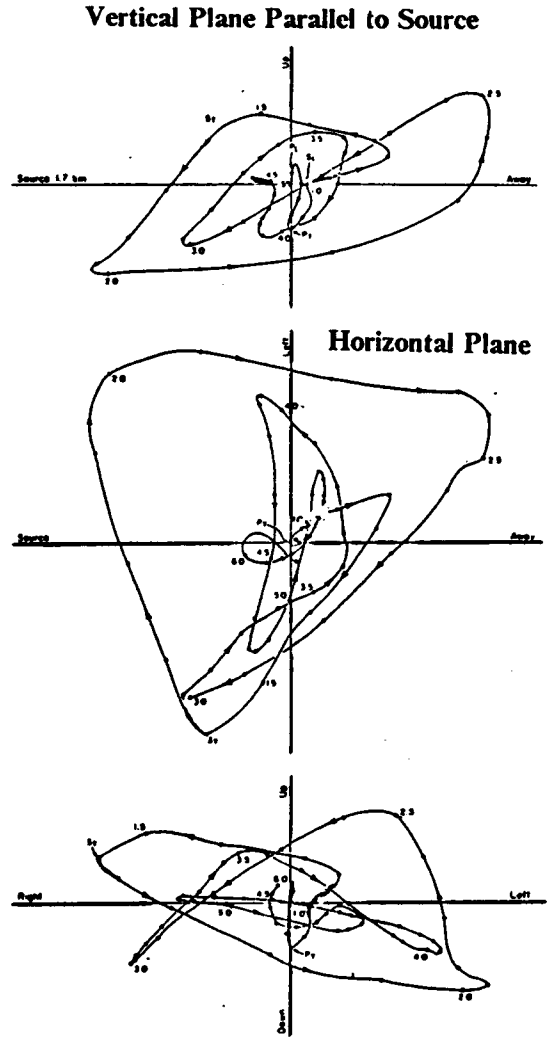

Figure 3.2 Trajectories of Particle Motion in Seismic Wave Propagation (after Carder and Cloud, 1959).

tables were aligned so that the horizontal shaking axes of the larger and smaller tables were at right angles to each other. In this manner when the tables were both operating, the soil in the smaller table subjected to horizontal shaking in two directions, and vertical shaking in one direction.

The tests were performed with the objective to see if shaking the soil in three directions simultaneously lead to differences relative to the behavior observed in shaking table tests with only one axis of shaking. The results showed that there was difference in one- and three-dimensional shaking table tests, with the three-dimensional testing giving a liquefaction resistance about 20 percent lower than that of the one-dimensional test. The tests left a great deal unanswered however, since there was no way to measure the stresses that were actually being applied to the soil, and the true principal stress rotational effect was not simulated.

3.3.2 Two Directional Simple Shear

Ishihara and Yamazaki (1980) built a cyclic simple shear test device capable of two directional loading. In this case, a 7 cm (1.18 in) diameter and 3 cm (2.75 in) thick specimen surrounded by a stack of teflon coated annular plates is set under ambient water pressure in circular chamber. The upper plane of the specimen is coupled by two rigid platens intersecting orthogonally, and the bottom is fixed to the frame. The top platens are attached by two arms by which two shear forces are applied at right angles to each other on the horizontal plane. A vertical stress is applied to the top of the specimen to simulate the gravity effect. The arrangement allows the application of two shear forces and a fixed vertical stress. Both isotropic and anisotropic conditions could be used for consolidation.

The shear forces transmitted onto the top of specimen were rotational and crisscross in pattern with a frequency of 0.25 Hz. The results of these tests indicated that the cyclic stress ratios causing 5 percent simple shear strain under multi-directional loadings were at an average of 30 percent less than those under uni-directional loadings. However, because of the inherent limitation of the de-

vice, membrane inflation and rocking motions were induced during cyclic loading. As a result the application of the test results is limited.

3.3.3 Three Dimensional Shear Devices

Many three-dimensional shear devices have been developed over the past 20 years. The primary uses for them have been in the study of the effect of the intermediate principal stress and stress path during static loading. Dynamic loading poses more difficult problems if control is to be allowed in three-dimensions. In this case, the stress applications are rapid, and each independent stress must be synchronized with the others. Further, because information is measured along three axes, a large band of data must be simultaneously recorded. For this reason, there is little history of three-dimensional dynamic loading experiments. One case which is reported is the work of Yamada and Ishihara (1983). This device was used in the investigation of the behavior of uncemented sands.

The shear box of Yamada and Ishihara (1983) has a cubical hollow frame which forms a cubical space at the center for a sample and six pressure chambers on each side of the cubical space for load application. The soil sample is located in central cubical space and is 10 cm x 10 cm x 10 cm (3.9 in x 3.9 in x 3.9 in). Six square rubber plates are attached to the frame, covering the opening to the six chambers. The soil specimen is in contact with the rubber plates during the loading process. The loading in this device is applied in each pair of the chambers, the three principal stresses can be varied independently. Movements of the rubber plates are calculated from measurements of the amount of water that flows into the chambers during the loading process. This allows an indirect determination of the strains in the soil specimen. The actual strains are not known in this device since the soil specimen deforms under the action of the rubber plates more in the center than at the edges.

The article by Yamada and Ishihara (1983) does not explain exactly how the device generates the dynamic loading. Also, no reference is given to the frequency of the load application. The paper does state that a number of different stress paths were used in the testing. The basic conclu-

sion of the study was that the strength of an uncemented sand can be on the order of 10 percent less than that determined from the conventional triaxial test under the action of the different stress paths.

3.3.4 Summary

Table 3.1 provides a listing of the multiaxial loading devices that have been used in the study of liquefaction. Only that of Yamada and Ishihara (1983) is a true three-dimensional shear device with independent control of the three principal stresses. All of the multiaxial testing has been directed at uncemented sands. The results have suggested that soils can be made to liquefy more readily in multiaxial loading than is the case in triaxial or simple shear conditions.

3.4 Stress Paths For Three-Dimensional Loading Experiments For This Investigation

Almost all soil testing investigations for earthquake problems limit the stress path to relatively simple choices. The prevailing philosophy has been to attempt to model the effects of a one-dimensional shear wave passing through the soil. This type of loading is modeled by the action of a shaking table moving along one horizontal axis. It produces cyclic shear on the horizontal plane within the soil. On a smaller scale, investigators have used the simple shear device to simulate this effect. Alternatively, engineers have relied on the triaxial test. In this case, the soil inside the sample on a 45 degree plane is subjected to alternating shear stresses. In the tests of this investigation, it was decided to use the cubical device to simulate both a simple set of loadings, and a series of others which are more complicated.

3.4.1 Simple Loading Path - Cyclic Triaxial (CTX)

The simplest loading that can be accomplished in a cubical device is one involving load application in only one direction. This process is identical to that used in the triaxial device, and since

Table 3. 3.1 Multi-Axial Dynamic Devices for Liquefaction Studies.

Reference	Type	Dynamic Loads	Boundary Condition	Sample Size
Pyke et al. (1975)	Shaking Table	Inertia forces on three orthogonal directions	No lateral deformation	91 cm (Circular) 7.62 cm (Thick)
Yamazaki Ishihara (1980)	Simple Shear	Two horizontal shear stresses	No lateral deformation by a stack of annular plates	17 cm (Diameter) 3 cm (Thick)
Yamada Ishihara (1983)	True Triaxial	Three independent principal stresses	Corners fixed	10 x 10 x 10 cm Cubical

the loading is cyclic, it is referred to as the CTX test in this work. The stress path for the CTX loading is shown in Figure 3.3, where the principal stress space is depicted in two dimensions by showing the plane representing only the hydrostatic line.

In this type of plot, the major principal stress is represented in true magnitude, but the minor and intermediate stresses are plotted in terms of the square roots of their values. In Figure 3.3, the first phase of the triaxial loading involves the application of the hydrostatic confining stress, and this moves the stress path out onto the hydrostatic line. Subsequently, in the dynamic phase of the test, the major principal stress is alternatively increased and decreased, while the other two principal stresses held constant. In Figure 3.3 this phase of the test is represented by a vertical line which passes through the stress established during initial confinement.

It is useful to consider the CTX loading in terms of octahedral stress components because some of the more complex stress paths can only be conveniently described in this manner. The octahedral stress system is represented by two stress components; namely, the mean normal stress or the octahedral normal stress, σ_{oct} and the octahedral shear stress, τ_{oct}. These are defined as follows:

$$\sigma_{oct} = \frac{1}{3}(\sigma_1 + \sigma_2 + \sigma_3) \tag{1}$$

$$\tau_{oct} = \frac{1}{3}\sqrt{(\sigma_1 - \sigma_2)^2 + (\sigma_2 - \sigma_3)^2 + (\sigma_3 - \sigma_1)^2} \tag{2}$$

in which, σ_1 = the major principal stress,

σ_2 = the intermediate principal stress,

σ_3 = the minor principal stress.

An additional parameter that is used in the octahedral stress system is the angle, θ , which defines the amount of rotation of the octahedral shear stress vector from the principal (vertical) stress axis.

$$\tan\theta = \frac{\sqrt{3}(\sigma_3 - \sigma_2)}{2\sigma_1 - \sigma_2 - \sigma_3} \tag{3}$$

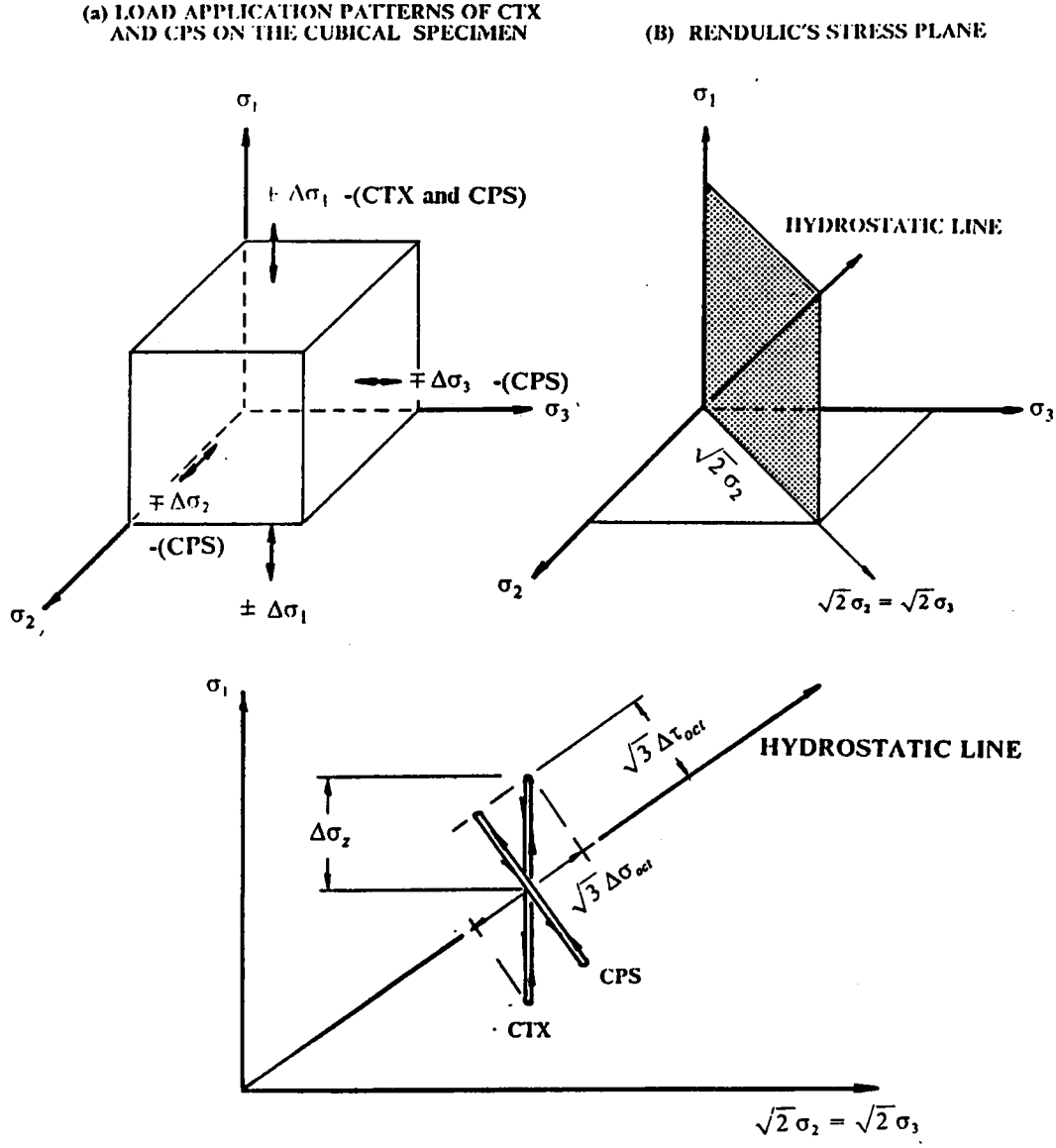

Figure 3.3 Dynamic Stress Paths of CTX and CPS on the Rendulic and Octahedral Planes.

In three-dimensional principal stress space, a stress state is represented as a point. The position of the point can be characterized in terms of the principal stress coordinates, or the octahedral normal and shear stresses. The octahedral stresses define the stress state in terms of its position relative to a plane drawn normal to the hydrostatic line. Since a stress state is a point in the three-dimensional stress space, the point will lie in one of these planes. The octahedral normal stress defines the distance the plane lies out on the hydrostatic line, while the octahedral shear stress locates the distance the stress point lies from the hydrostatic line in the normal plane (the actual distances in principal stress space for the position of the plane and the stress point are equal to $\sqrt{3}\,\sigma_{oct}$ and $\sqrt{3}\,\tau_{oct}$, respectively). In a sense, the octahedral normal stress defines the intensity of the hydrostatic stress, while the octahedral shear stress defines the intensity of the shear stress.

In this case of the CTX loading, the cyclic octahedral stress components are determined as follows:

$$\Delta\sigma_1 \neq 0; \qquad \Delta\sigma_2 = 0; \qquad \Delta\sigma_3 = 0$$

$$\Delta\sigma_{oct} = \frac{1}{3}(\Delta\sigma_1 + \Delta\sigma_2 + \Delta\sigma_3) = \frac{\Delta\sigma_1}{3} \tag{4}$$

$$\Delta\tau_{oct} = \frac{1}{3}\sqrt{(\Delta\sigma_1 - \Delta\sigma_2)^2 + (\Delta\sigma_2 - \Delta\sigma_3)^2 + (\Delta\sigma_3 - \Delta\sigma_1)^2} = \frac{\sqrt{2}\,\Delta\sigma_1}{3} \tag{5}$$

$$\tan\theta = \frac{\sqrt{3}\,(\Delta\sigma_3 - \Delta\sigma_2)}{2\Delta\sigma_1 - \Delta\sigma_2 - \Delta\sigma_3} = 0 \tag{6}$$

The equations show that as a result of the CTX loading, increases in both octahedral normal and shear stresses occur. The component of the octahedral normal stress is important in as much as it has a direct effect on the pore pressure in a saturated soil.

When considering the cyclic loading issue, the level of loading is often defined in terms of a parameter called the stress ratio. In the case of the conventional cyclic triaxial test, this is taken as:

$$\text{Stress Ratio} = \frac{\Delta\sigma_1}{2(\overline{\sigma}_c)_i} \tag{7}$$

in which, $\Delta\sigma_1$ = the applied cyclic stress.

$(\overline{\sigma}_c)_i$ = the initial effective confining stress.

Note; $\frac{\Delta\sigma_1}{2}$ = the maximum shear in the CTX test.

As defined for the conventional triaxial test, the stress ratio is the maximum cyclic shear stress, τ_{max}, divided by the initial effective confining stress. It is useful to define a comparable type of ratio in terms of the octahedral stresses, since in the case of more complex stress loadings, the original stress ratio does not work. Following the general approach of the stress ratio concept, a logical octahedral stress ratio would be the maximum cyclic octahedral shear stress divided by the initial effective octahedral normal stress, or

$$\text{Octahedral Stress Ratio} = \frac{\Delta\tau_{oct}}{(\overline{\sigma}_{oct})_i} \tag{8}$$

where, $\Delta\tau_{oct}$ = the cyclic octahedral stress,

$(\overline{\sigma}_{oct})_i$ = the initial effective octahedral normal stress.

The following equation shows how the new and old stress ratios are related for the case of the CTX type of test:

$$\frac{\Delta\tau_{oct}}{(\overline{\sigma}_{oct})_i} = \frac{\sqrt{2}}{3} \times \frac{\Delta\sigma_1}{(\overline{\sigma}_c)_i} = 0.47 \times \frac{\Delta\sigma_1}{(\overline{\sigma}_c)_i} = 0.94 \times \frac{\Delta\sigma_1}{2(\overline{\sigma}_c)_i} \tag{9}$$

Based on the foregoing result, the old stress ratio is only six percent greater than the value of the new one. The similarity of the two values provides for a degree of continuity when comparing the results of this test program with those of others. Unless stated otherwise, the new stress ratio will be used throughout this test; however, for practical purposes it is the same as the old one.

3.4.2 Simple Loading Path - Cyclic Pure Shear (CPS)

As a first step away from the CTX type of loading, one might consider cyclic pure shear. This condition would begin with the application of confining stresses in the same manner as in the

triaxial test. Subsequently, the cyclic shear is applied by alternatively increasing the vertical stress by one unit of stress, while decreasing the two horizontal stresses by one half of the vertical stress unit. In terms of octahedral stresses, this serves to increase the octahedral shear stress, while the octahedral normal stress is constant, thus, the term; pure shear loading. This type of loading better represents the effect of a one-dimensional shear wave than the CTX loading, since in the passage of a one-dimensional shear wave, the only effect is to apply alternating shear stresses to the soil, with the normal stress remaining constant. This same basic idea is accomplished in conventional simple shear testing.

The CPS stress path can be visualized in Figure 3.3, where it is represented by a line which crosses normal to the hydrostatic axis, rather than vertical to it as in the case of the CTX loading. Since the CPS avoids applying the increment of octahedral normal stress in each cycle in the CTX, it will avoid inducing an equal increment of pore pressure, a critical difference in the two loadings.

In terms of the octahedral stress equations, the cyclic portion of the CPS loading is represented as:

$$\Delta\sigma_1 \neq 0; \qquad \Delta\sigma_2 = -0.5\Delta\sigma_1; \qquad \Delta\sigma_3 = -0.5\Delta\sigma_1$$

$$\Delta\sigma_{oct} = \frac{1}{3}(\Delta\sigma_1 + \Delta\sigma_2 + \Delta\sigma_3) = \frac{1}{3}(\Delta\sigma_1 - \frac{\Delta\sigma_1}{2} - \frac{\Delta\sigma_1}{2}) = 0 \tag{10}$$

$$\Delta\tau_{oct} = \frac{1}{3}\sqrt{(\Delta\sigma_1 - \Delta\sigma_2)^2 + (\Delta\sigma_2 - \Delta\sigma_3)^2 + (\Delta\sigma_3 - \Delta\sigma_1)^2} = \frac{\sqrt{2}\,\Delta\sigma_1}{2} \tag{11}$$

$$\tan\theta = \frac{\sqrt{3}\,(\Delta\sigma_3 - \Delta\sigma_2)}{2\Delta\sigma_1 - \Delta\sigma_2 - \Delta\sigma_3} = 0 \tag{12}$$

The stress ratio is taken as the ratio of the octahedral shear stress to the initial consolidation stress, and this can be expressed in terms of the increment of major principal stress applied in this type of loading:

$$\frac{\tau_{oct}}{(\bar{\sigma}_{oct})_i} = \frac{\sqrt{2}}{2} \times \frac{\Delta\sigma_1}{(\bar{\sigma}_c)_i} = 0.707 \times \frac{\Delta\sigma_1}{(\bar{\sigma}_c)_i} = 1.414 \times \frac{\Delta\sigma_1}{2(\bar{\sigma}_c)_i} \tag{13}$$

Note that the octahedral stress ratio in this case is over 1.41 times the conventional one from triaxial loading. This points up the importance of using the octahedral stress ratio since it better expresses the level of the loading being applied to the soil. The reason for the large difference in this case lies in the fact that the cyclic major principal stress increment, $\Delta\sigma_1$, does define the maximum shear when the other principal stresses are also being changed.

3.4.3 Complex Loading Paths - Cyclic Rotational Elliptic (CRE) and Cyclic Rotational Circular (CRC)

These two loading paths represent variations on the CTX and CPS modes, with the purpose of simulating the effects of passage of other than shear waves through the soil. In the introductory discussion to this chapter, it was pointed out that during many earthquakes, the distortion of the soil along one axis will be different from that along another. For example, in the responses for many California earthquakes, the horizontal ground distortion is twice that of the vertical. To simulate this type of effect in this investigation, the cyclic rotational elliptic loading (CRE) is used. Two versions of the CRE test are used, one applied to avoid any change in octahedral normal stress, called CRE-PS (Cyclic Rotational Elliptic - Pure Shear), and another with the same type of change in octahedral normal stress as in the CTX test, called CRE-TX (Cyclic Rotational Elliptic - Triaxial).

The stress path of the CRE-PS can be seen on the " π - plane ", which is the plane normal to the hydrostatic line (Figure 3.4). The CRE-PS is an ellipse on the π - plane with the center at the intersection of the hydrostatic line and the π - plane. The octahedral shear stress rotates with the angle θ changing 0 to 360 degrees. The ellipse defines the octahedral shear stress variation. The major and minor axes depend upon the maximum and minimum $\Delta\tau_{oct}$ change; here, the minor axis is assumed to be half of the major axis. Hence, the ellipse satisfies the condition:

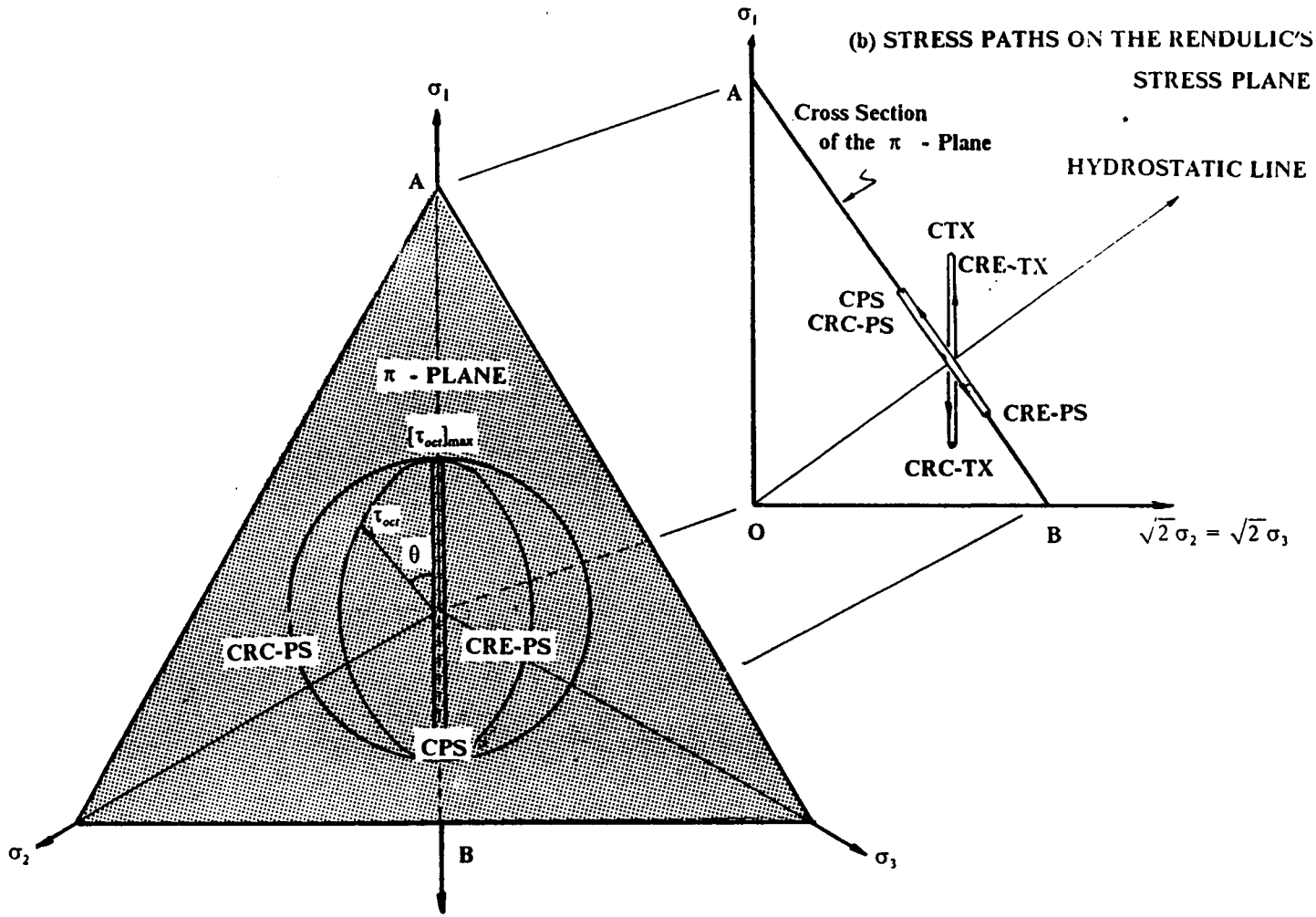

Figure 3.4 Dynamic Stress Paths of CRE-TX and CRC-TX as well as CRE-PS and CRC-PS on the Octahedral and Rendulic Planes.

$$1 = \frac{[\Delta\tau_{oct} \times \cos\theta]^2}{[(\Delta\tau_{oct})_{max}]^2} + \frac{[\frac{\Delta\tau_{oct}}{2} \times \sin\theta]^2}{[\frac{(\Delta\tau_{oct})_{max}}{2}]^2} \tag{14}$$

For an assumed value of θ, and $(\Delta\tau_{oct})_{max}$, $\Delta\tau_{oct}$ can be calculated from the above equation.

It is already defined that:

$$\Delta\sigma_{oct} = \frac{[\Delta\sigma_1 + \Delta\sigma_2 + \Delta\sigma_3]}{3} = 0 \tag{15}$$

$$\Delta\tau_{oct} = \frac{1}{3}\sqrt{(\Delta\sigma_1 - \Delta\sigma_2)^2 + (\Delta\sigma_2 - \Delta\sigma_3)^2 + (\Delta\sigma_3 - \Delta\sigma_1)^2} \tag{16}$$

$$\tan\theta = \frac{\sqrt{3}(\sigma_1 - \sigma_2)}{2\sigma_1 - \sigma_2 - \sigma_3} \tag{17}$$

In the equation (15), $\Delta\sigma_{oct}$ is zero because of the pure shear condition and in the equation (16), the left hand side, $\Delta\tau_{oct}$, is known already from the equation (14). For a known value of θ, the $\tan\theta$ value is fixed as well. Therefore, three unknown values (three principal directional loadings), $\Delta\sigma_1$, $\Delta\sigma_2$, and $\Delta\sigma_3$, can be obtained by the three equations (15, 16, and 17).

The CRE-TX stress path gives the same appearance as that for the CRE-PS path if instead of using the π - plane for the projection, the vertical plane cutting the hydrostatic axis is used. The reason for this is that the CRE-TX path lies in the same plane as does the simple CTX. The CRE-TX path is defined in an analogous manner to that described for the CRE-PS path. The stress ratio is the same that of the CTX path, since the maximum octahedral shear stress is the same.

The final loading considered in this investigation is the cyclic rotational circular (CRC). This loading is used in an effort to model the effects of those earthquakes where the distortions from the earthquake reach at equal levels in all three principal directions. The path for the CRC-PS version of the test appears as a circle in Figure 3.4. For the CRC-TX version, it describes the same shape in the triaxial plane. Values of principal stresses to simulate this path are obtained in the same

manner as described for the CRE path. Variation of the octahedral shear stress is a circular fashion and $\Delta\tau_{oct}$ is equal to the maximum octahedral shear stress, $[\Delta\tau_{oct}]_{max}$ during rotational angle changing from 0 to 360 degree. The variation of the octahedral normal stress is the similar to the CRE- TX. The stress ratio of the CRC path is identical to that of the CRE path since the maximum octahedral shear stress and the hydrostatic consolidation stress are the same.

CHAPTER IV

TEST PROGRAM AND SAMPLE PREPARATION TECHNIQUES

4.1 Introduction

The test program involved the confirmation and proof testing for the cubical device as well as production research testing. Sample preparation technique is described herein. Confirmation and proof testing work involves a range of special tests. In the production work, a total of 92 liquefaction tests were performed using two soil densities, four level of cyclic shear stresses, three soil cementation magnitudes, and six types of dynamic loadings. For purposes of the initial discussion, the tests are arranged into two basic group. Group I consists of those involving CTX and CPS loadings; details for the test units are given in Table 4.1. Those tests which followed more complex load paths (CRE-TX, CRC-TX, CRE-PS, and CRC-PS) are defined in Table 4.2. Cemented and uncemented sands were used in all the test efforts.

4.2 Basic Testing Conditions And Liquefaction Definition

Although a number of aspects of 3-dimensional testing were unique because of the nature of the test device, basic test conditions follow the conventional standards where possible (e.g. Silver et al., 1976). Aspects which were the same unless specifically identified are:

(1) Effective confining pressure, 104 kN/m^2 (15 psi) for all tests.

(2) Frequency of loading for an axis - 1 cycle per second.

Table 4. 4.1 Liquefaction Test Program - Group I.

Serial No.	Unconfined Strength (kN/m^2)	Dry Density (kN/m^3)	Type of Loading	Curing Period (Days)	Identification
LQ-1 to 4	0.0	15.06	CTX	0	Uncemented-Loose Sand
LQ-5 to 8	46	15.06	CTX	5	Very Weakly Cemented-Loose Sand
LQ-9 to 12	76	15.06	CTX	14	Weakly Cemented-Loose Sand
LQ-13 to 16	0.0	15.38	CTX	0	Uncemented-Medium Loose Sand
LQ-17 to 20	62	15.38	CTX	5	Very Weakly Cemented-Medium Loose Sand
LQ-21 to 24	94	15.38	CTX	14	Weakly Cemented-Medium Dense Sand
LQ-25 to 28	110	15.38	CTX	30	Weakly Cemented-Medium Dense Sand
LQ-29 to 32	0.0	15.06	CPS	0	Uncemented-Loose Sand
LQ-33 to 36	46	15.06	CPS	5	Very Weakly Cemented-Loose Sand
LQ-37 to 40	76	15.06	CPS	14	Weakly Cemented-Loose Sand
LQ-41 to 44	0.0	15.38	CPS	0	Uncemented-Medium Loose Sand
LQ-45 to 48	62	15.38	CPS	5	Very Weakly Cemented-Medium Loose Sand
LQ-49 to 52	94	15.38	CPS	14	Weakly Cemented-Medium Dense Sand

Table 5. 4.2 Liquefaction Test Program - Group II.

Serial No.	Unconfined Strength (kN/m^2)	Dry Density (kN/m^3)	Type of Loading	Curing Period (Days)	Identification
LQ-53 to 56	0.0	15.06	CRE-TX	0	Uncemented-Loose Sand
LQ-57 to 60	0.0	15.06	CRE-PS	0	Uncemented-Loose Sand
LQ-61 to 64	76	15.06	CRE-TX	14	Weakly Cemented-Sand
LQ-65 to 68	0.0	15.38	CRE-TX	0	Uncemented-Medium Loose Sand
LQ-69 to 72	94	15.38	CRE-TX	14	Weakly Cemented-Medium Dense Sand
LQ-73 to 76	0.0	15.06	CRC-TX	0	Uncemented-Loose Sand
LQ-77 to 80	0.0	15.06	CRC-PS	0	Uncemented-Loose Sand
LQ-81 to 84	76	15.06	CRC-TX	14	Weakly Cemented-Loose Sand
LQ-85 to 88	0.0	15.38	CRC-TX	0	Uncemented-Medium Loose Sand
LQ-89 to 92	94	15.38	CRC-TX	14	Weakly Cemented-Medium Dense Sand

(3) Pore pressure parameter, B , greater than 0.90 [back pressures 274 kN/m^2 (40 psi) or higher for all tests].

(4) Soil Samples formed by pluviation.

For consistency, liquefaction was defined in terms of the concept of the initial liquefaction. This occurs where the pore pressure accumulates and becomes equal to the level of the initial effective confining pressure (ASCE Committee Report, 1978). At this time, the initial effective confining stress, $(\overline{\sigma}_c)_i$, is approximately zero.

4.3 The Test Sand

Monterey sand #0/30 is used as the test soil for this research. This sand or ones with very similar gradations have been used by numerous investigators studying liquefaction. Table 4.3 gives the basic properties reported by Muzzy (1983) for Monterey sand #0/30. To check that the batch of sand received from the supplier was the same as that tested by others, grain size tests were performed (Figure 4.1). The tests on the Virginia Tech sand batch gave curves that show slightly more uniformity and slightly larger particle diameters than that given by Muzzy (1983). However, the differences are very small. In both cases the sand is described as uniform, with little fines, and with a median diameter of grains around 0.45 to 0.50 mm. Standard triaxial type liquefaction tests on the Virginia Tech sand batch by Milstone (1985) show the liquefaction resistance of this sand to be essentially the same as that of Muzzy (1983).

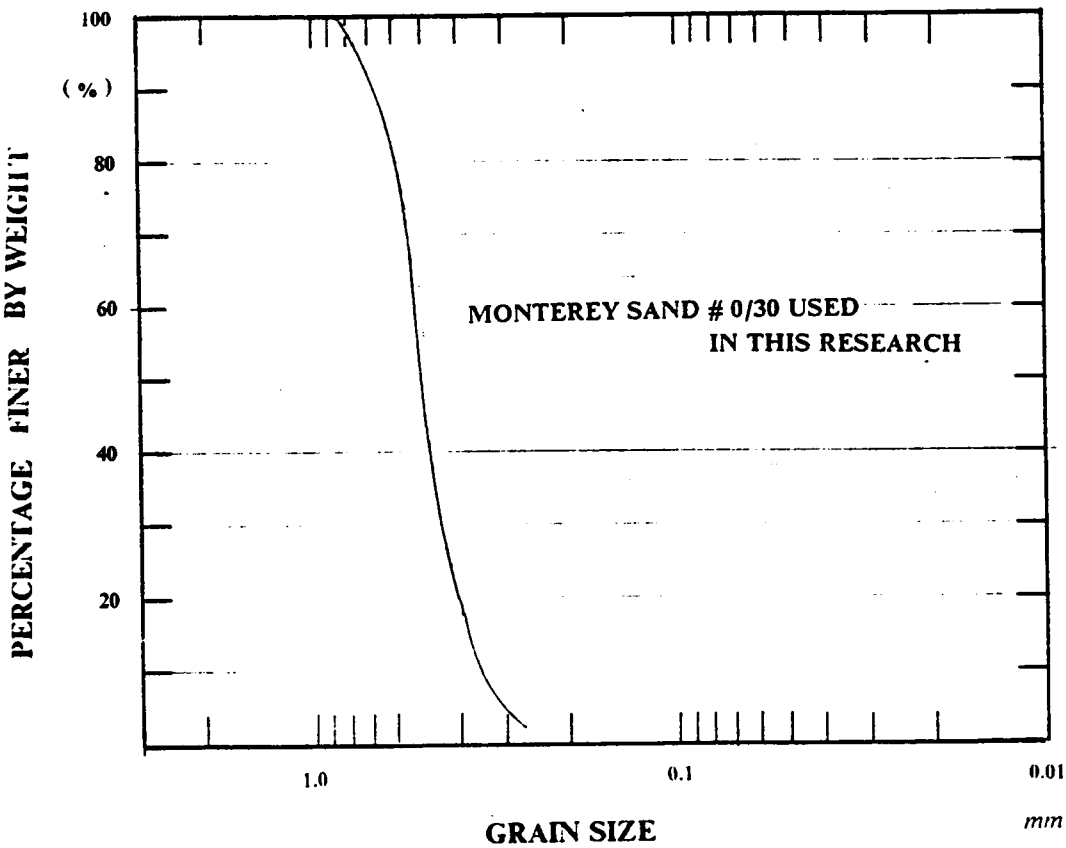

Figure 4.1 Gradation of Monterey Sand # 0/30 Used in This Research.

Table 6. 4.3 Properties of Monterey Sand # 0/30.

Properties	Monterey Sand # 0/30		
	Muzzy (1983)	Milstone (1985)	This Research
G_s	2.65	2.65	****
$\gamma_{d\,max}$ (kN/m^3)	16.58	**	**
$\gamma_{d\,min}$ (kN/m^3)	14.38	**	**
e_{max}	0.803	**	**
e_{min}	0.563	**	**
D_{50} (mm)	0.45	0.45	0.50 & 0.48
$C_u = D_{60}/D_{10}$	1.60	1.37	1.44 & 1.52
$C_c = D_{30}^2/D_{60} \times D_{10}$	1.00	0.95	1.03 & 1.08
Angularity	Subangular to subrounded		
Chemical Composition	Predominantly silica but includes fair amount of other chemicals		

4.4 Sample Preparation Method - Uncemented Sample

The pluviation technique described in several papers (e.g., Mulilis et al., 1977) is adopted to manufacture samples. This technique allows density control and development of homogeneous samples. The pluviation is done with a rainer whose basic structure consists of a hollow cube with inside dimensions of 5.08 x 5.08 cm (2 x 2 in) and a height of either 5.08 or 10.16 cm (2 or 4 in). The rainer has a diffuser plate at the top of the cube. For preparation of sand sample, the rainer is placed over a cubical vacuum mold (for details, Appendix A), and dry sand is poured over the diffuser plate and is pluviated through the cube and accumulates in the mold. A large group of experiments with this process indicated that with a drop at the height of 5.08 cm (2 in), the density of the samples is 15.07 kN/m^3 (96 pcf). If a drop height of 10.16 cm (4 in) is used, the sample density which result is 15.38 kN/m^3 (98 pcf).

At the start of the process of pluviation to obtain a density of 15.07 kN/m^3, precisely 201.5 gm (0.443 lb) of dry uncemented sand is weighed and pluviated through the rainer. At the end of the process, the top surface of the sand is expected to be as high as the top of the mold; otherwise the pluviation is repeated. In the case of the higher density, 15.38 kN/m^3 , 205.7 gm (0.453 lb) of dry uncemented sand is pluviated through the rainer using the drop height of 10.16 cm (4 in). If the sand properly fills the mold to the top, the proper density is obtained.

4.5 Sample Preparation Method - Artificially Cemented Sand

The artificially cemented sand is prepared to cover a range of strengths and densities that might be typical of a naturally occurring "cemented sand". The basic procedure is adopted from that developed by Shafii-Rad and Clough (1982). It involves adding Portland Cement (type II) with Monterey #0/30 sand. The cement-soil mix is pluviated into a cubical mold and cured in water until the desired strength is reached. A step by step description is as follows:

(1) Four plastic plates with slits on surfaces are assembled to form a mold with an inside space with dimensions of 5.08 x 5.08 x 5.72 cm (2 x 2 x 2.25 in.). The inside surfaces are coated with a silicone lubricant. A bottom plate with six small drainage holes is attached to the square mold, and, subsequently, a filter paper is placed on the plate inside the mold to prevent the passage of soil or cement.

(2) The mold with the sample top plate is weighed so that this quantity can be removed from the weight obtained with the soil in place.

(3) Enough air-dried Monterey sand #0/30 for 7 samples (2000 gram or 4.4 lb) is weighed and placed in the bowl.

(4) About 10 gm (0.022 lb) of water is added on the sand and then stirred for about 1 minute by hand using a rubber spatula. The surface of the sand should have slight moisture as a result.

(5) Dry Portland cement (Calaveras Cement, Type I-II, Low Alkali) is weighed, out in a 40 gm (0.088 lb) portion.

(6) The cement is slowly added to the sand and mixed by hand, stirring. Agitation continues 5 minutes. This procedure leads to a coating of the sand particles by cement. No free cement is allowed, and disagregation between the cement and sand is minimized.

(7) The sand-cement mixture is pluviated through a rainer. The pluviation process is identical to that of uncemented sand at the section 4.4.

(8) The excess of the sand-cement over the mold is trimmed by a steel ruler. After placing the top plate on the mold, the mold is weighed to obtain a density. As noted for uncemented sands, two densities, 15.07 kN/m^3 (96 pcf) and 15.38 kN/m^3 (98 pcf) could be obtained by changing height

of sand drop during pluviation. If the density of the sample was not within 0.5 percent of desired density, the pluviation process was repeated.

(9) The entire mold with sand is placed in a large plastic container on the top of a thin layer of coarse sand. The layer of sand allows free access of water through the holes in the bottom plate to the sample.

(10) Water is introduced to the plastic container such that the water level in the container rises approximately 1.25 cm (1/2 in) an hour. The sample is completely submerged in about three hours. The container and the sample are then placed in the humid room for curing. The time and date is recorded.

(11) After the required curing, the sample is extruded from the plastic container. The top and bottom plates of the mold were detached and the mold was loosened. The cured sample was pushed out carefully from the bottom to upward by a 5.08 x 5.08 x 5.08 cm (2 x 2 x 2 in) cubical plastic block; a 3 mm layer of the sample was forced out from the top edge of the mold. This layer was trimmed off by a wire saw. The mold was tighten, overturned, and loosened; the process was repeated, trimming off a thin layer of the bottom. This is a precautionary action since in some of the samples slightly higher concentrations of cement were observed at the very bottom. This can be a result of separation of the cement particles while the sand grains are falling down from the rainer, or while water is penetrating through the sample in presence of small vibrations. Cutting away the top and bottom of the samples reduces the likelihood of non-uniformities. The final sample dimensions are 5.08 cm height (2 in.), 5.08 cm wide (2 in.), and 5.08 cm deep (2 in.). After trimming, the sample dimension is carefully measured and its weight is recorded. The sands trimmed off could be used for water contents measurement so that density of the sample is confirmed in the submerged condition.

(12) After trimming, the sample is surrounded by a thin rubber membrane made of a dental dam. With the membrane in place, the sample is weighed and measured again as to check or or confirm measurements, and to establish the weight of the membrane (see Appendix A.3.2.[g]).

4.6 Unconfined Compressive Tests As Curing Check

Unconfined compressive strength tests were conducted frequently for the artificially cemented sands during the dynamic test program. This was done to confirm the quality of the artificially cemented sand, to establish that a given batch of cemented sand samples had the same basic response, to provide a strength value for correlation with liquefaction behavior, and to give a cemented sand quantitative identity. Conditions for the unconfined tests are:

(a) Size of Sample: 5.08 cm wide (2 in.), 5.08 cm deep (2 in.),
5.73 cm high (2.25 in.).

(b) Strain speed is 0.88 percent to the height of the samples per a minute.

(c) Period of Curing : 2.5 days, 4 days, 5 days, 14 days, 30 days.

(d) Density 15.07 kN/m^3 (96 pcf) and 15.38 kN/m^3 (98 pcf).

The unconfined tests were performed on cubical samples. In a subsequent section the strengths on cubical and cylindrical samples are compared.

4.6.1 Relation between Strength and Time of Curing

Figure 4.2 presents examples of stress-strain curves for some of samples tested. Samples with dry densities of 15.38 kN/m^3 (98 pcf) and 15.07 kN/m^3 (96 pcf) are shown in Figure 4.4 (a) and (b). As expected, the longer the period of curing, the higher the strength. However, there is no obvious difference in stiffness with curing period. The specimens with longer cures tended to fail in a more brittle mode.

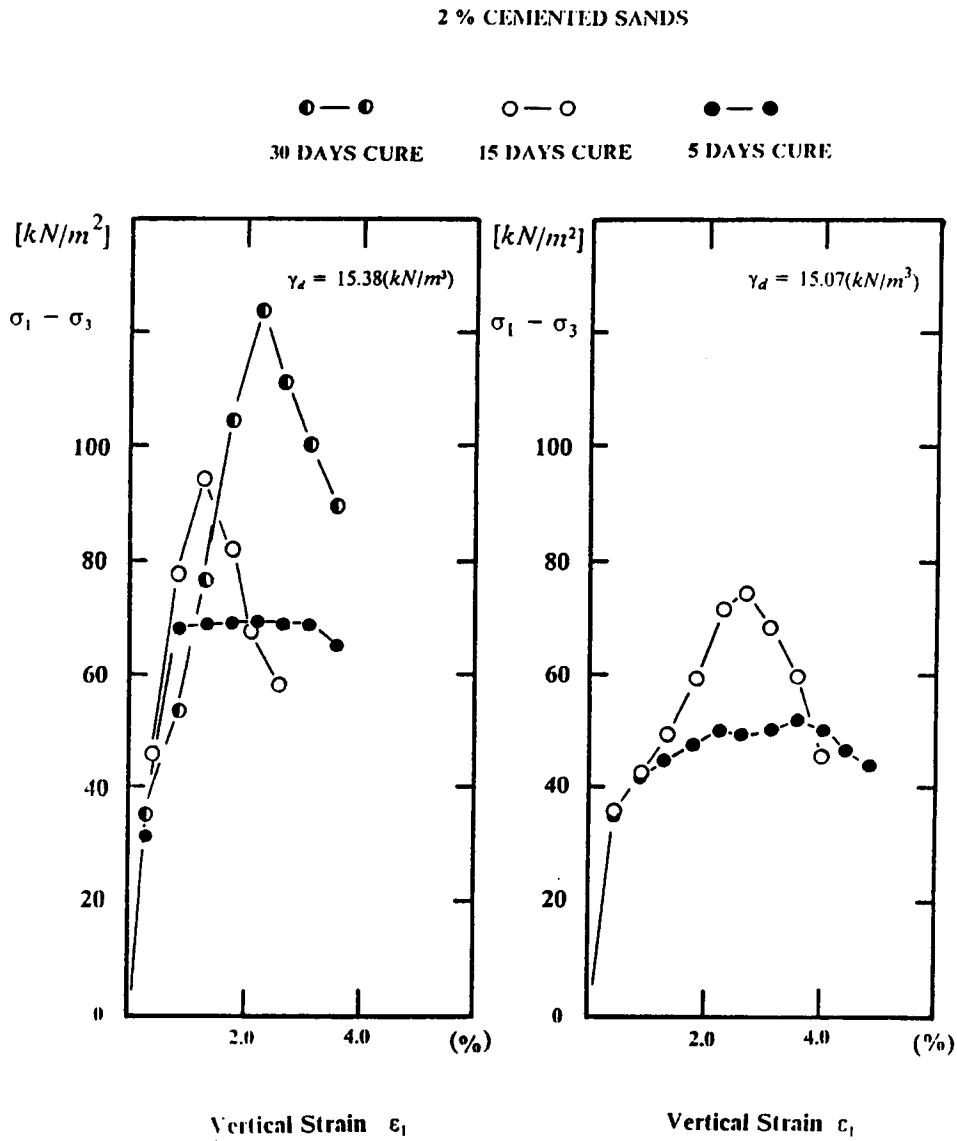

Figure 4.2 Examples of Stress-Strain Relationship of Cemented Sands by Unconfined Compressive Strength Tests.

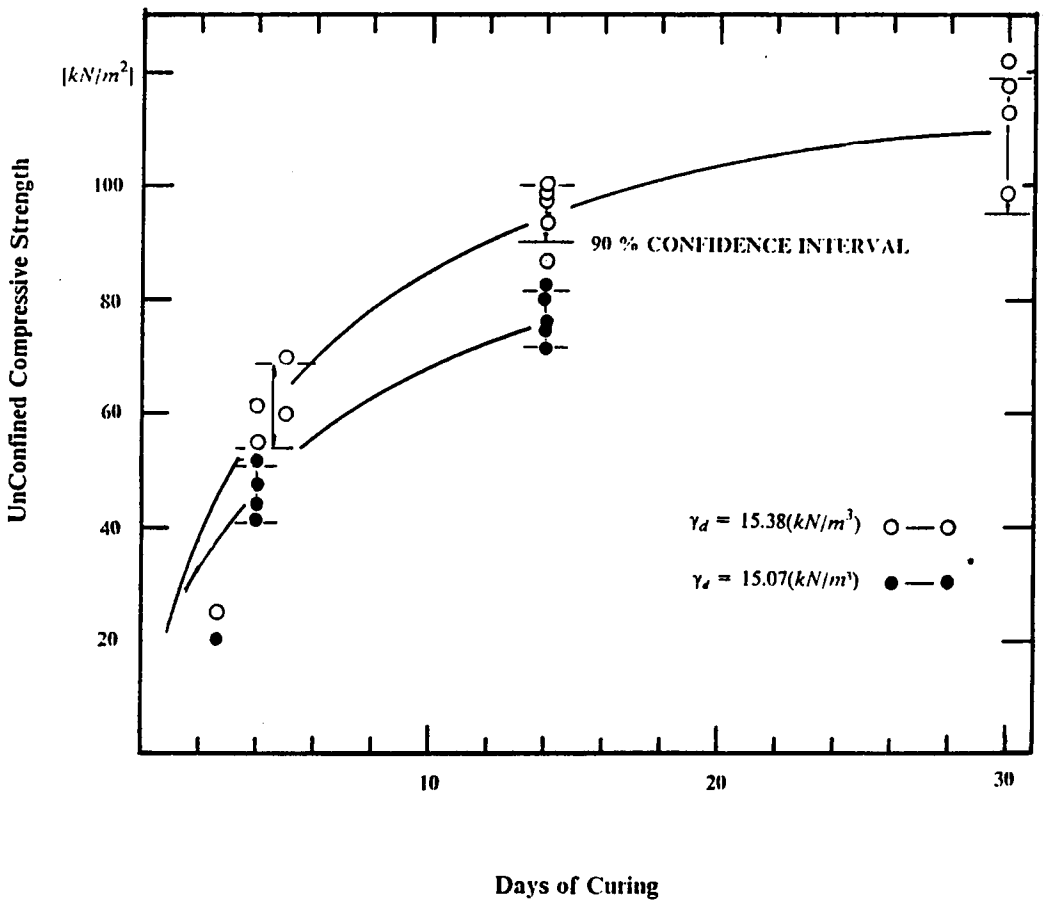

Figure 4.3 Relation between Unconfined Compressive Strength and Days of Curing.

Figure 4.3 presents the relation between strength and time of curing for sands with dry densities of 15.38 and 15.07 kN/m^3 (98 and 96 pcf). Most of the testing concentrated at curing time of 14 days, since most samples used in the experimental program fell in this range. A few tests were done at 5 and 30 days since some very weak samples were included in the program.

The following trends are observed in the results:

1.) For either density, the unconfined compressive strength increases with curing time, although most of the strength gain occurs in the first 2 weeks or so of curing, and that which occurs after 2 weeks is relatively small.

2.) There is a clear tendency for the samples with the lower dry density to have a lower unconfined compressive strength.

3.) Variations of unconfined strengths at any given curing period are typically no more than ± 5 kN/m^2 (0.7 psi) from the mean value, suggesting that the samples could be prepared to consistently yield similar properties.

Because the unconfined strength is relatively easily determined, and it serves as an index to the strength of the samples, these tests were performed frequently. Typically, one sample out of seven prepared was used for unconfined testing. A compilation of the data is given in Table 4.4.

4.6.2 Relation between Unconfined Strengths of Cubical and Cylindrical Samples

The control unconfined compression tests were performed on the same types of cubical samples as used in the production program. However, conventional testing to determine unconfined strength is done on cylindrical specimens which have a height about twice the diameter. To determine the relation between the strength of a cubical sample versus that of a cylindrical sample a few tests were performed to compare them. In Figure 4.4 the results of the tests on cylindrical

Table 7. 4.4 Average Unconfined Compressive Strengths of Cemented Sands.

Density (kN/m^3)	Curing Time (Days)	Unconfined Compressive Strength (kN/m^2)		
		Min	Mean	Max
15.07	0	0	0	0
15.07	4	40.7	45.9	51.1
15.07	14	71.2	76.0	81.0
15.07	30	N/A	N/A	N/A
15.38	0	0	0	0
15.38	4 to 5	53.6	61.0	68.5
15.38	14	89.7	94.8	100.0
15.38	30	N/A	110.0	N/A

N/A : not available

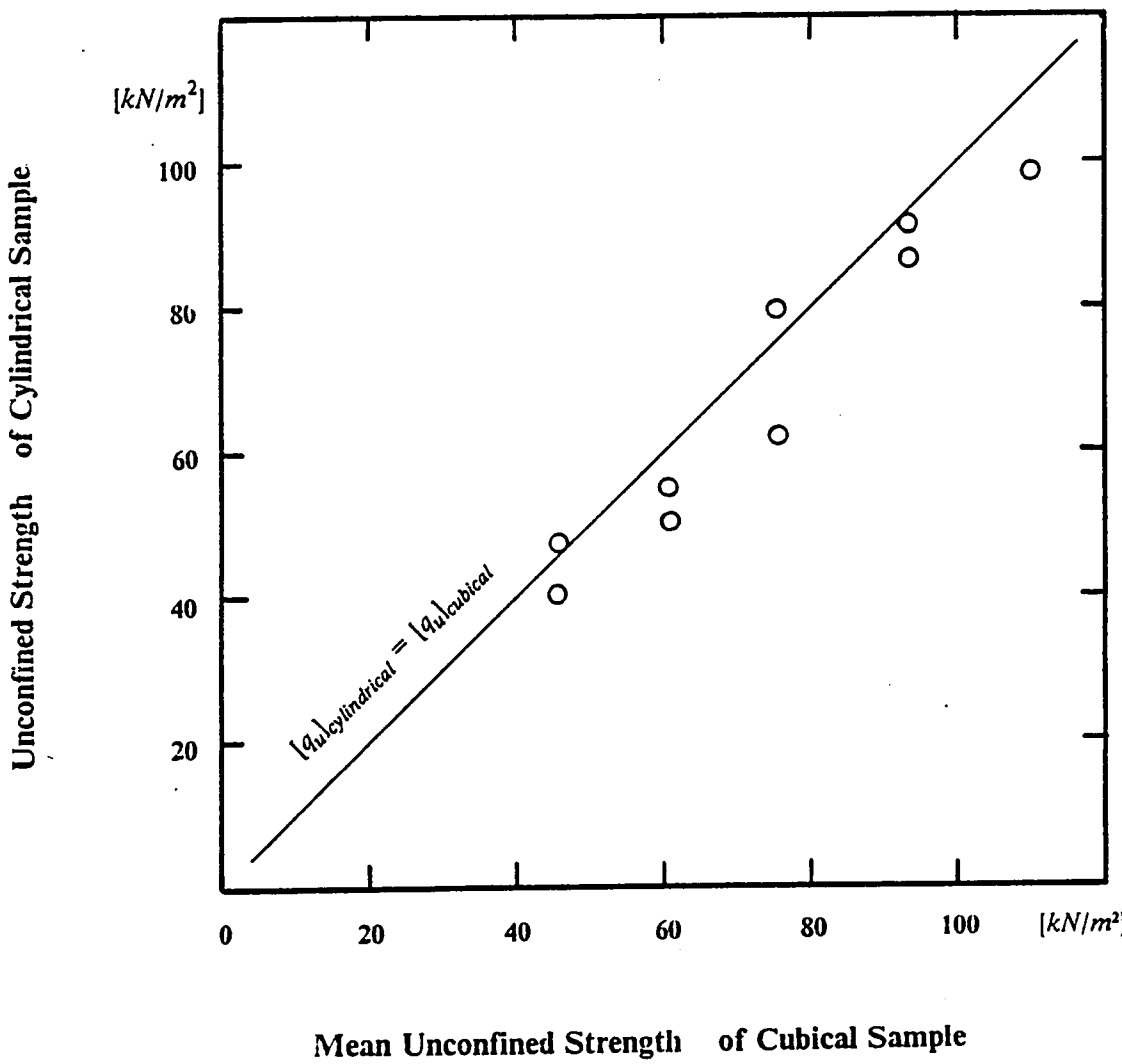

Figure 4.4 Relationship of Unconfined Strengths of between Cubical and Cylindrical Cemented Samples.

samples are compared to the mean of those on the cubical samples. The strengths are quite similar. The largest difference lies in the stress-strain response, but this behavior is not important in regard to the unconfined strengths.

CHAPTER V

DYNAMIC CUBICAL SHEAR DEVICE - DESIGN AND PROOF TESTING

5.1 Introduction

The dynamic cubical device of this investigation represents a modified version of a cubical device that was developed during an earlier study for static loading. The static cubical shear apparatus was developed by T. Kuppusamy. The primary modifications for this work involved:

1.) Development of a loading system so that three principal stresses are applied to the soil specimen in a dynamic, in-phase process.

2.) Implementation of a microcomputer data acquisition and control unit so that the tests are performed completely automatically.

3). Improvement of the pressure application membranes in the cubical shear box so that the strains occurring in the sample are as uniform as possible.

4.) Development of a procedure to allow back pressure saturation and accurate pore pressure and volume change measurements.

The resulting device is capable of applying stress-controlled dynamic loading with independent control of three principal stresses. A wide range of stress paths can be followed, and measurements

can be made of the strains in three directions, as well as pore pressures or volume change in the specimen.

5.2 System Configuration

Figure 5.1 shows a picture of the new device, hereafter referred to by the designation, DCSVT1. The cubical shear box is located at the left, the loading and drainage circuits on the panel at the right, and the microcomputer system in the front of the panel. A schematic of the system is provided in Figure 5.2. The system consists principally of two parts: (1) The 3-D shear box; and , (2) The control unit. Details related to the operation of the apparatus are given in Appendix A. A basic description of it is given in the following paragraphs.

5.2.1 Cubical Shear Box

The cubical shear box is formed by assembling six identically shaped aluminum frames in such a way that a 5.1 x 5.1 x 5.1 cm (2 x 2 x 2 in.) cubical space is created inside of the box. Preformed silicon membrane pressure modules are placed on the six sides and cover plates are used to close the cubical shear box. The pressure modules are used to apply the stress on the cubical sample. Some special features concerning these modules are given in Section 5.2.2.

A cross section of the box is shown in Figure 5.3, and the details of the various components are shown in the figure. The cover plate has the necessary ports for pressure tubes and transducers to be connected. Air pressure for loading the sample is supplied through the tubes that are fitted on the six faces. A linear variable differential transformer is attached to the center of each pressure module so that the deformations of the sample are monitored on the six sides. In the figure, the drainage tubes can be seen passing through the cubical frame and outside the top and bottom of the box. The drainage tubes are made of hard teflon and connect the specimen to the drainage circuit.

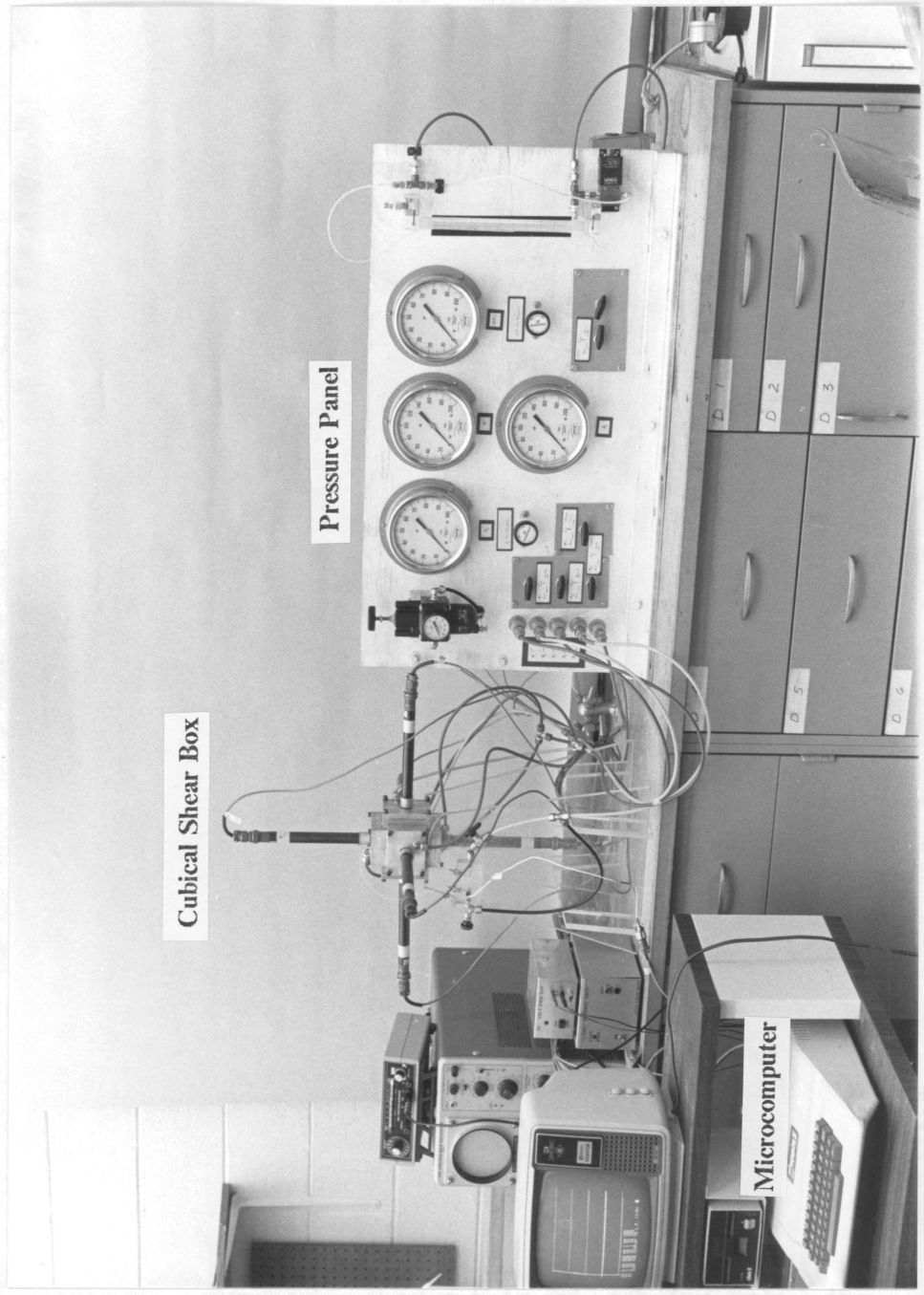

Figure 5.1 The Overall View of the Cubical Device.

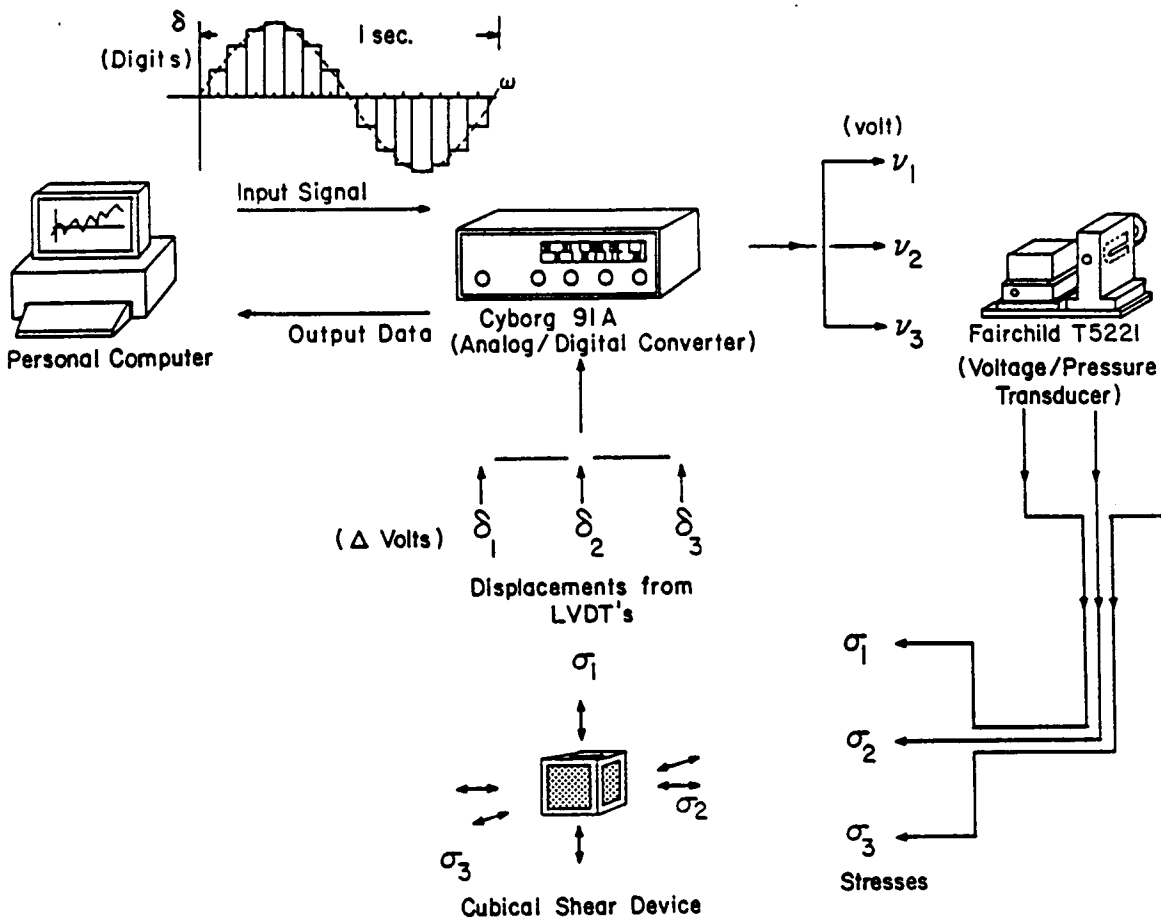

Figure 5.2 Schematic of the System Arrangement.

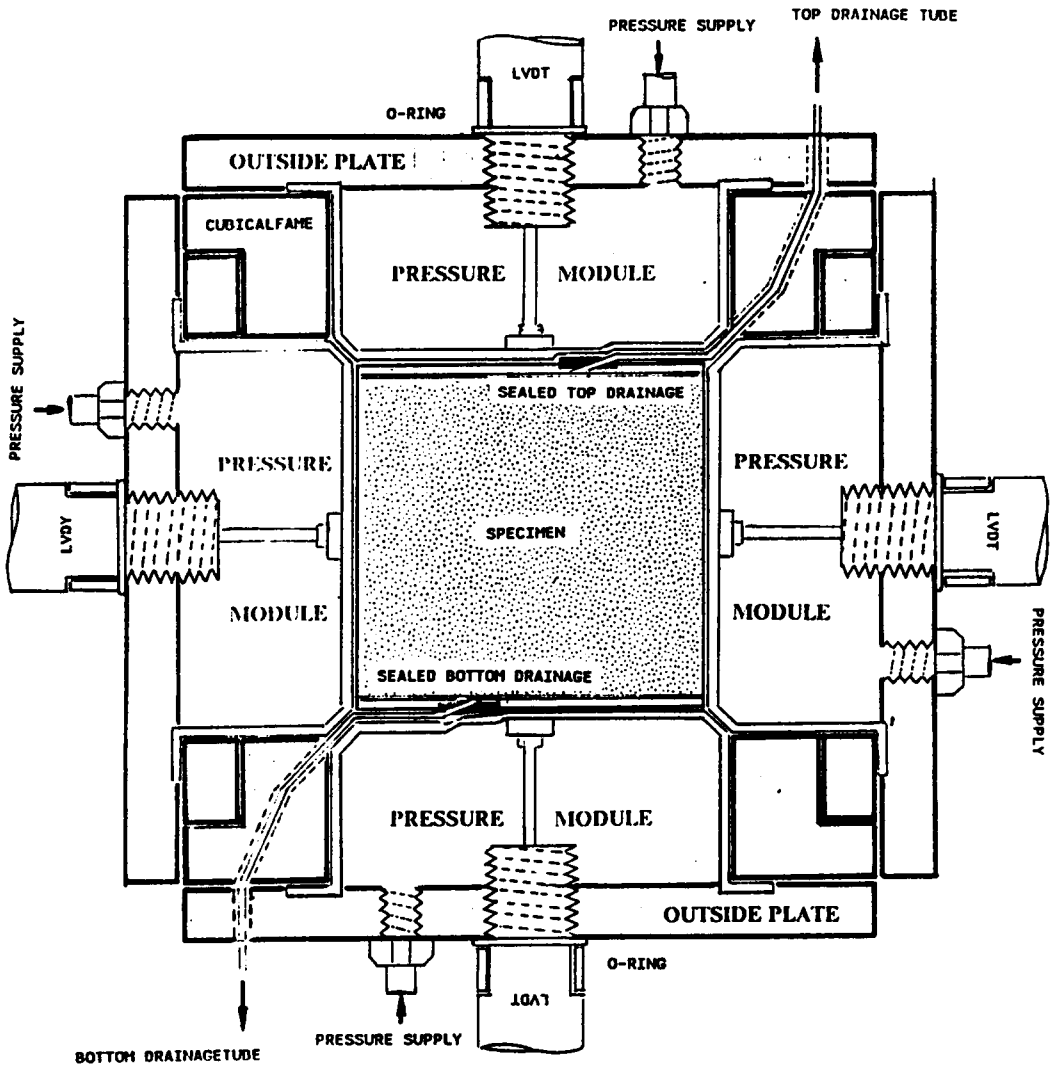

Figure 5.3 Cross Section of the Cubical Shear Box.

The sample is initially prepared in a special cubical mold which allows the specimen to be wrapped with a thin membrane. The membrane is made of dental dam rubber sheets cut to the required size (see appendix A). With the sample sealed in the membrane, a small vacuum is applied to the sand which pulls the membrane in against the sand to provide a confining pressure to it, and allow removal of the forming mold.

The inside of the box is sprayed with silicon lubricant prior to the placement of the specimen. Then, each surface of the sample is covered by a square thin teflon sheet to reduce friction between the membrane and the sample. While placing the sample into the shear box, the drainage lines are carefully carried through the box (Figure 5.4). Figure 5.5 shows the arrangement of pressure and drainage lines around the shear box. Manual air pressure regulators are used for the ambient pressure condition. Three electronic controlled air pressure regulators (see Appendix B) or voltage pressure transducers, are used for the application of three independent pressures.

The drainage lines are extended from the cubical shear box and connected to a miniature pore pressure transducer and to a water reservoir where an air-water interface is created. The back pressure is controlled by an air regulator and if volume change occurs, this is measured by a differential pressure transducer.

5.2.2 Silicon Membrane Pressure Modules

The pressure modules play the key role of transmitting to the sample the pneumatic pressure generated by the loading system. As such they must meet a number of criteria. On the one hand, they must be flexible enough to follow the sample face as it deforms under the stress application. On the other hand, they must be strong enough not to burst under the pressure, and also not to deform significantly into the space of an adjoining pressure module when the two are under different pressures. An example of the problem with excessive deformation of the pressure modules relative to each other is shown in Figure 5.6. In the extreme, this can lead to rupturing of the membrane. Although some work had been done on selecting a proper material for the pressure modules during

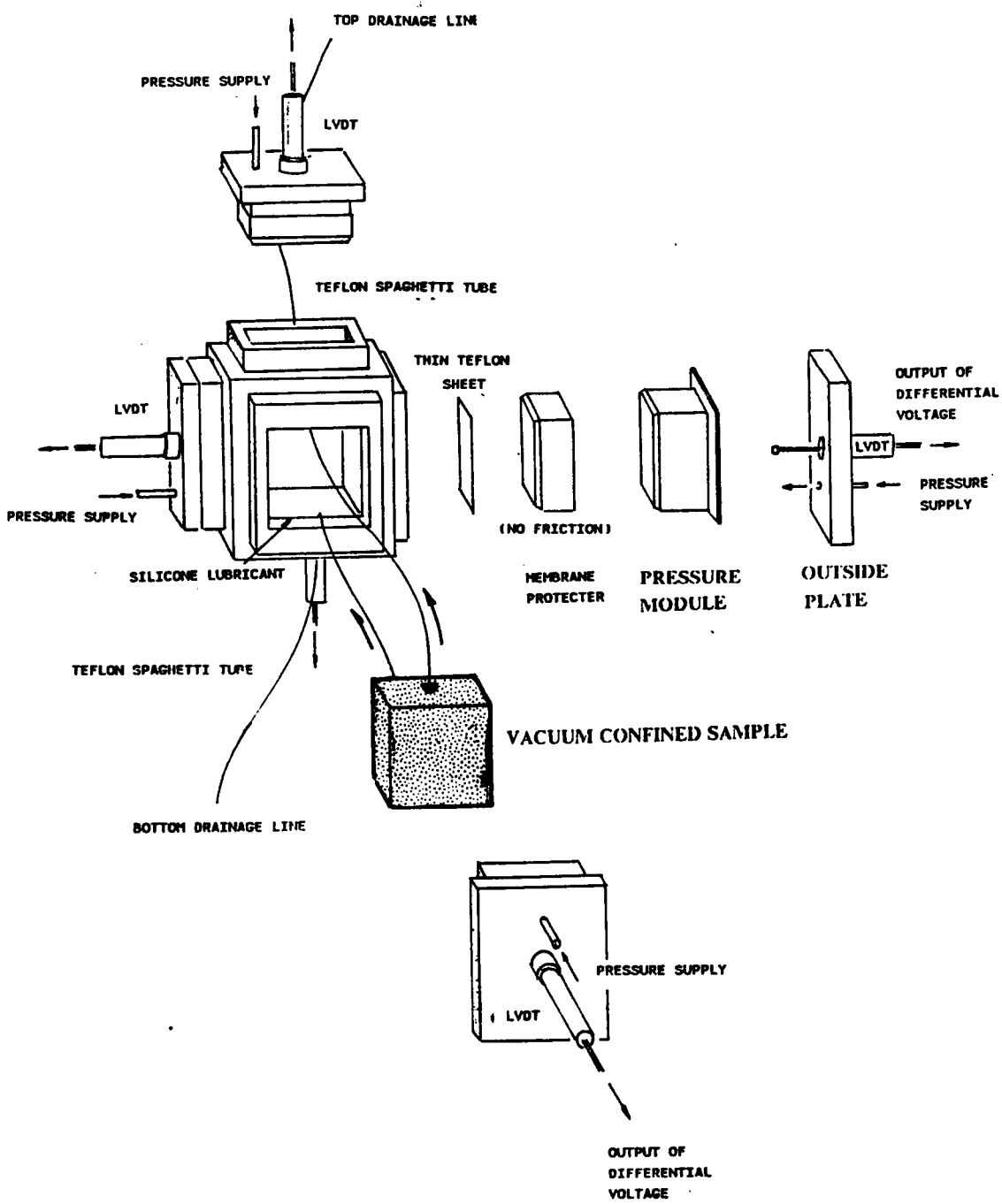

Figure 5.4 Placing a Sample and Assembling the Shear Box.

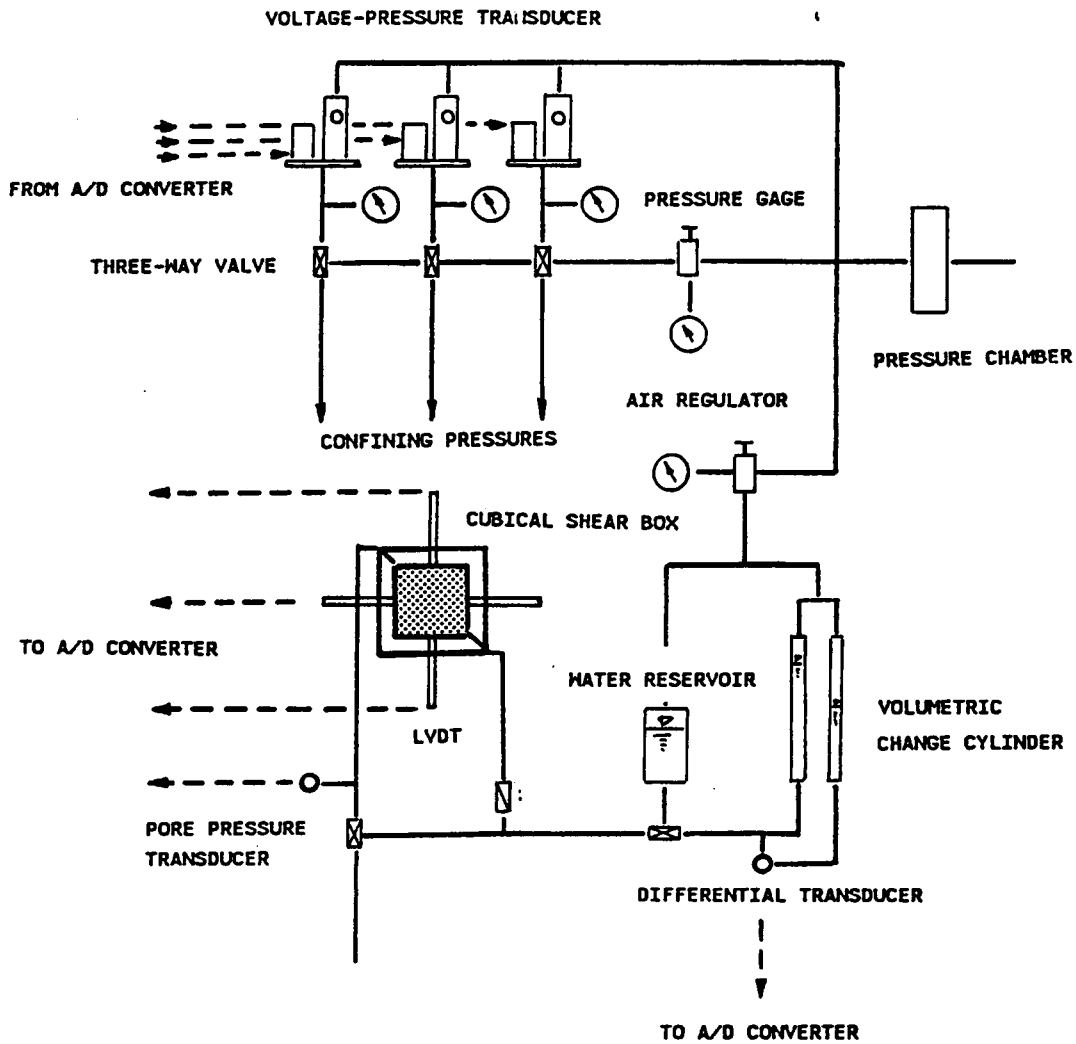

Figure 5.5 Arrangement of Pressure and Drainage Lines around the Shear Box.

the development of the shear box for static loading, the available modules proved unsuccessful in meeting the needs for this investigation, and some modification was required.

The process of developing the modified pressure module proceeded largely by trial and error. The basic idea was to find a means of softening the walls of the module while strengthening the edges where the walls meet the pressure face. The softening of the module walls was needed to allow the module pressure face to follow the soil as it deforms. Strengthening of the edges was required to help keep the module pressure face plane, and minimize any problems with interpenetration of the adjoining modules.

The solution involved two modifications of the original pressure modules. First, new silicon compound was used for higher flexibility with reduction in the thickness of the walls of the pressure module. The final thickness of the walls was 0.3 mm (0.015 in) and the elongability of the new pressure module is three times as much as the original one. Second, a simple reinforcement was found for the wall to face edges of the module. The reinforcement consists of applying a strip of frictionless masking tape over the outside surface of the module. The final modules worked well, and proved easy to make and repair.

5.2.3 Sample Membranes and The Sealing Process

The sample membranes are described in detail in Appendix A. The membranes used in the investigation worked exceptionally well. The basic process for the membranes was developed previously by T. Kuppusamy. The only modification of the system for this work was to develop a means to penetrate the top of the membrane with a drainage line in such a way that no leakage would develop around the point of penetration. If leakage occurred, it was noticeable immediately since volume changes would be observed when they were not supposed to occurs.

The procedure for sealing is described in the Operational Manual in Appendix A. It requires some skill and practice, but the process worked well and is verifiable.

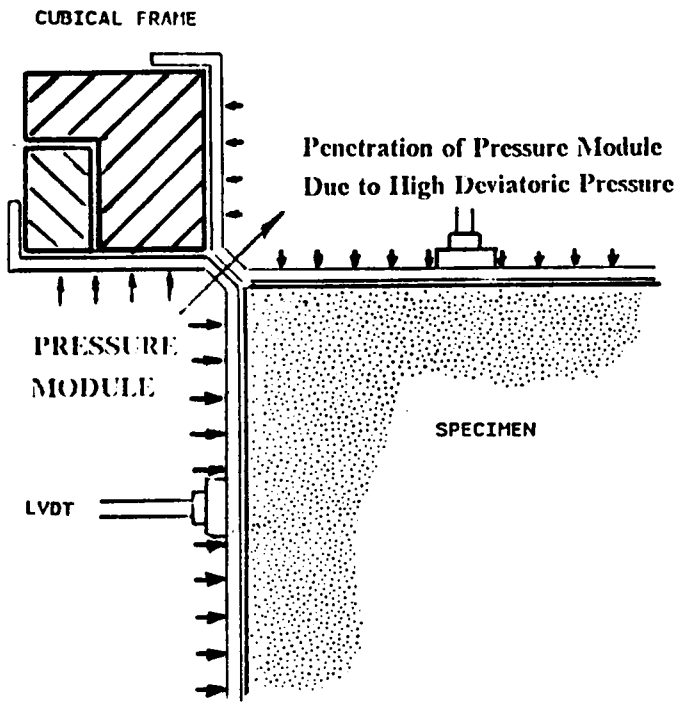

Figure 5.6 Silicon Membrane Burst in High Deviatoric Pressures.

5.2.4 Control Unit

The control unit consists of a microcomputer, an analog to digital converter, and a preamplifier. The basic system was purchased from the Cyborg company, and uses model no. ISSAC 91. The control unit has two functions. First, it serves to initiate and control the pressure regulators. Second, it acquires the data generated by the monitoring transducers. All of this is done in a dynamic environment, and requires rapid response time, and high storage capacity. The control unit allows the entire test to be done automatically, since the loads are applied and the data are acquired in one process.

The control unit coordinates a total of 11 electronic devices. Three of these are digital to pneumatic regulators for loading. The data monitoring devices consists of six LVDT's , one pore pressure transducer, and one differential pressure transducer.

5.2.5 Dynamic Three Dimensional Loading

The dynamic three-dimensional loading is activated and controlled by the control unit. The loading signal is received by the electronic pressure regulator, which converts the signal into a pressure. Next, the pressure pulse is passed to the silicon membrane pressure modules, and hence to the sample.

The control unit can process a signal in 10^{-3} seconds, thus it is able to apply pressures very rapidly. However, the electronic pressure regulators are unable to transmit the signals into pressures that fast. Thus, the electronic pressure regulators are the controlling factor in how rapidly the load can be transmitted to the sample. Fortunately, the regulators operate in optimal fashion at frequencies as high as 2 cycles per second (2 Hertz), which is sufficiently adequate for load application in earthquake testing of soils.

The form of the loading signal is controlled by software written for the microcomputer which drives the control unit. This allows the user to write a program which will follow a wide range in

load paths. In this work, this option was especially important. It made it possible to change the different principal stresses independently of each other in a phased operation.

5.2.6 Data Acquisition

Data acquisition is achieved using the monitoring devices which pass electronic signals into the A/D converter, and hence into the microcomputer for storage and processing. The storage of the particular microcomputer is limited to 48 k-bites RAM, and a floppy disk. Approximately 50 measurements per second can be handled per second in addition to the loading signals. At various intervals of the testing procedure, the data from RAM is passed onto the floppy disk. After the test, the data is displayed via the microcomputer, and simple plots can be made at that time. Finished plots are obtained by sending the data from the floppy disk to the mainframe computer.

5.3 Sample Saturation Method

5.3.1 Uncemented Samples

Initially carbon dioxide is percolated through the uncemented sample and this is used for saturating uncemented samples. The idea for this saturation method was originally introduced by Chan (1976) and based on the special relationship between CO_2 and H_2O. Since the carbon dioxide easily dissolves into water, high saturation is obtained at low back pressure. Figure 5.7 shows the drainage circuit of DCSVT1. To complete the description, assume that the sample of uncemented sand is in the 3-D shear box under a small amount of ambient pressure, say 34.5 kN/m^2 (5 psi). The following steps are taken afterwards;

(1) Set the all valves on the figure as following: T-1 (the water reservoir to the shear box), T-2 (Closed), T-3 (from the box to open air).

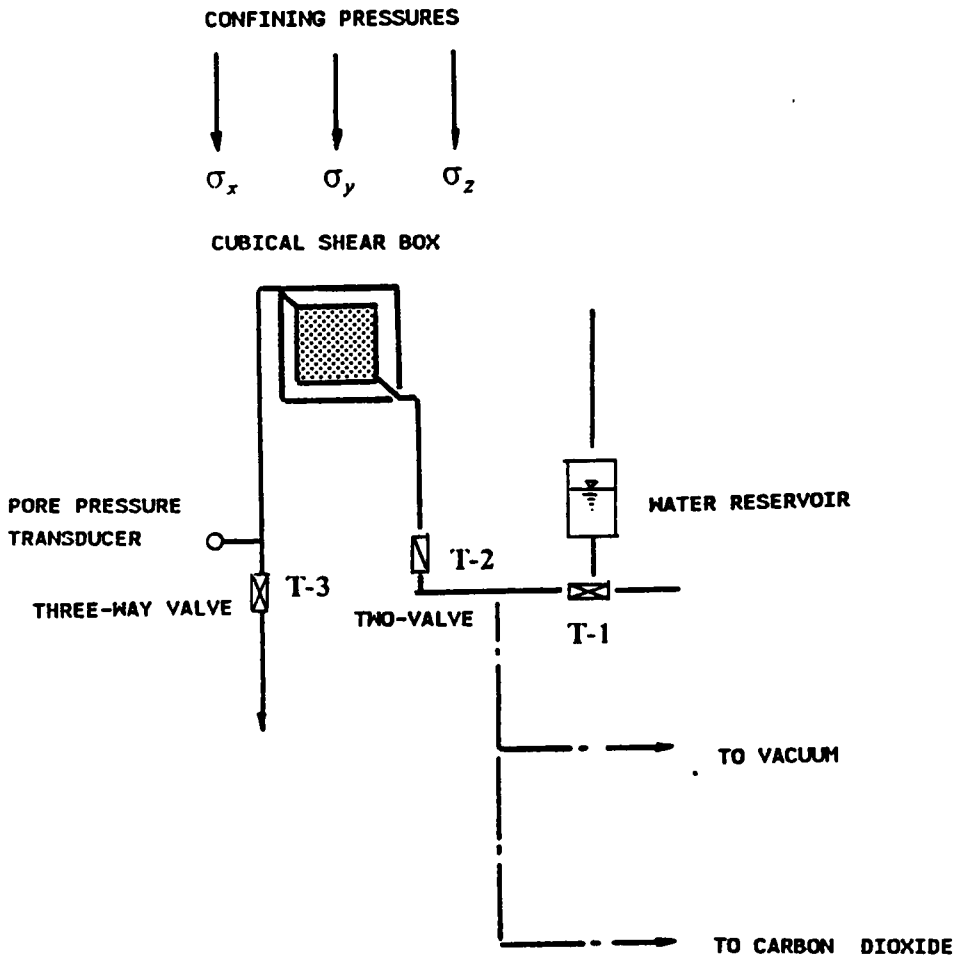

Figure 5.7 Arrangement of Drainage Lines for Saturation of Uncemented Sands.

(2) Connect the extension line between T-1 and T-2 to carbon dioxide, and then percolate carbon dioxide through the specimen by opening T-2 for 5 minutes. Note the pressure of carbon dioxide does not exceed more than 13.8 kN/m^2 (2 psi).

(3) Relocate the extension line from the carbon dioxide to the water reservoir and apply small amount of the back pressure, say 13.8 kN/m^2 (2 psi) in order that the deaired water percolates though the specimen. This step continues until the water comes out of T-3.

(4) Increase the confining and back pressures until the desired effective confining pressure is achieved. Note that the back pressure must be still low, say 69 kN/m^2 (10 psi), for the steps afterwards.

(5) Connect pore pressure and differential transducers and LVDTs to the computer, and run the test program (Appendix A), which monitors deformation and volumetric change of the specimen afterwards.

(6) Close T-1 and T-3, and watch the pore pressure (the pore pressure monitoring at this step is in the test program but it can be substituted by volt-meter). If there is any significant decrease, there is leakage. In this case, stop the procedure, and reform the sample.

(7) Read the pore pressure, close the drainage valve, increase the confining pressure. Read it again.

(8) Get the B-value by the equation below.

$$B = \frac{(y - x)}{z}$$

x: the first pore pressure

y: the second pore pressure

z: the total ambient pressure increased

B: the degree of saturation

(9) Increase the back pressure as much as the increment of the confining pressure. Open T-2.

(10) If B-value is greater than 0.95 percent, then the saturation has been done, otherwise repeat from (7) to (9).

5.3.2 Cemented Samples

Saturation of cemented soils is made difficult because the void structure is not as open as in uncemented soils. Simple back pressure saturation does not work well because undesirably high pressures have to be used. Also, the carbon dioxide technique is not suitable to help since carbon dioxide can react with the cementation agents. Recognizing the problem, Shaffi-Rad and Clough (1984) proposed the vacuum procedure, which they applied successfully to triaxial type sample. Herein, this method is modified slightly to adopt it to the cubical apparatus.

Figure 5.8 shows the arrangements to the 3-D device for the vacuum procedure. To complete the description, assume that the sample of cemented sand is in the cubical apparatus under a small amount of ambient pressure, say 34.5 kN/m^2 (5 psi). The following steps are taken afterwards;

(1) Set the all valves on the figure as following: T-1 (back pressure to the upper water reservoir), T-2 (the reservoir to the cubical box),T-3 (open),T-4 (the cubical box to the lower water reservoir).

(2) Fill the upper reservoir (UR) with deaired water, while the lower reservoir (LR) is kept empty.

(3) Apply a back pressure, 13.8 kN/m^2 (2 psi), to UR in order to flush deaired water through a sample. The water with air voids comes out of the sample for a while.

(4) Release the back pressure. Apply vacuum, 127 mm (5 in) to LR so that this time a water flow is induced by the vacuum through the sample from UR to LR.

(5) Maintain the vacuum for a period of time needed to optimize its effects. Generally it takes half an hour.

(6) Turn the T-1 from the back pressure to the vacuum and release the confining pressure.

(7) Close the T-3. And increase the vacuum up to 254 mm (10 in).

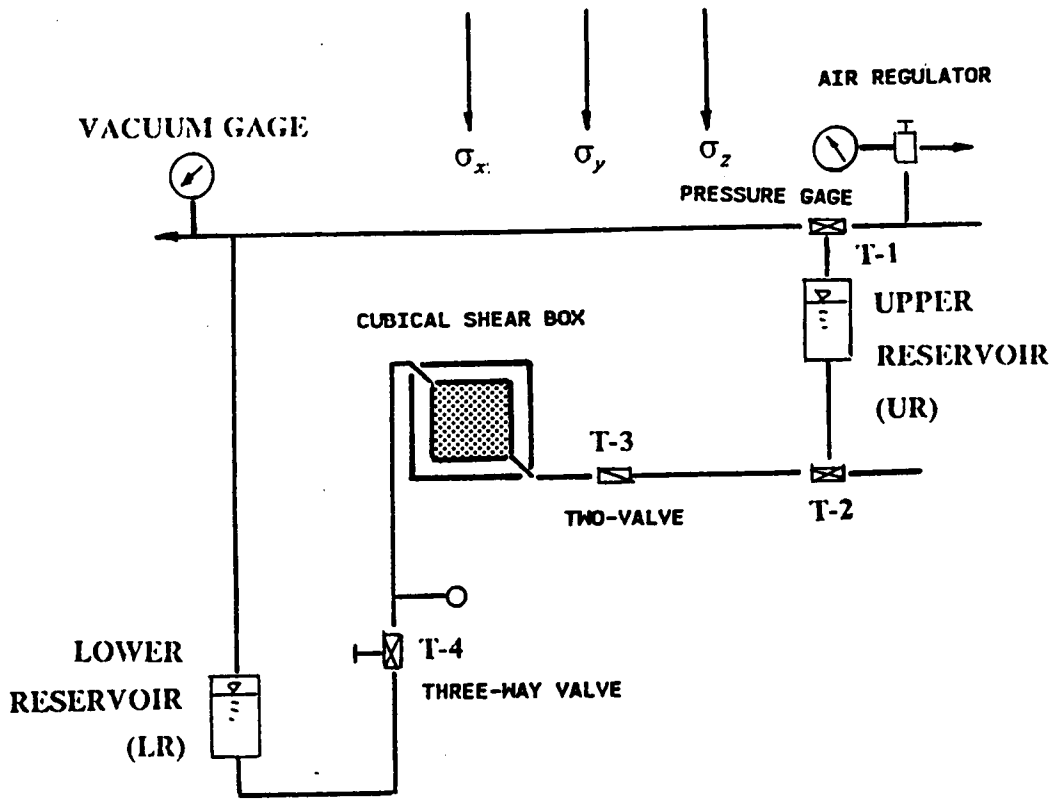

Figure 5.8 Arrangement of Drainage Lines for Saturation of Cemented Sands.

(8) The vacuum creates the effective confining pressure for 34.5 kN/m^2 (5 psi).

(9) Maintain the vacuum for a period of time needed to optimize its effects. Generally this is a short process.

(10) Set the drop between UR and LR at 1.8 m (6 feet) and percolate the water through the sample by opening the T-3.

(11) Close the T-3 and continue the application of the vacuum inside the sample for a period of 1 to 5 minutes depending on the soil type to insure a proper equilibrium inside the sample.

(12) Repeat step (10)and (11).

(13) Release the vacuum gradually meanwhile apply the ambient pressure up to 48.3 kN/m^2 (7 psi).

(14) Turn the T-1 to the back pressure and apply the back pressure at 13.8 kN/m^2 (2 psi).

(15) Close the T-3 and turn the T-4 to the fixed end.

(16) Increase the ambient pressure for 34.5 kN/m^2 (5 psi) and check the pore pressure generated. Decrease the ambient pressure, open the T-3, and turn the T-4 to LR. If the pore pressure increases about 40 percent of the ambient pressure, go on to the following procedure otherwise repeat the steps from (3) to (16). If the degree of saturation is more than 40 percent, experience shows that a back pressure of 274 kN/m^2 (40 psi) will fulfill the saturation requirement.

(17) Increase the ambient pressure and the back pressure so that the desired effective confining pressure is achieved. Note that at this time, volume change of the sample is monitored.

(18) Increase the ambient and back pressure simultaneously so that the effective confining pressure is kept unchanged and the back pressure reaches 274 kN/m^2 (40 psi). Check B values until greater than 90 percent achieved.

5.4 Static Testing To Determine Uniformity Of Strains In Samples And Measurement Consistencies

Historically, three-dimensional shear devices have had problems with nonuniform strains or stresses in the cubical samples, especially in the corners of the samples. No three-dimensional device is immune from such problems, but there are differences in the ranges over which different equipment can perform reliably, and in the accuracy with which measurements can be made. To investigate this issue for the present device, a number of checks and proof tests were performed. This section of the text presents those tests performed in the static mode. Section 5.5 covers the cyclic tests. The static tests include:

1.) Volumetric Check - This consists of performing a test, and using knowledge about the total volume change to compare against what can be calculated by the separate measurements of strains on each face of the sample. For example, the total volume change, ε_v, that occurs should be related to the individual strains by the relationship:

$$\varepsilon_v = \varepsilon_1 + \varepsilon_2 + \varepsilon_3$$

The total volume change is known through direct measurement in drained tests, and is zero if the test is undrained and no cavitation occurs. Summing the individual strains should equal the total volume change obtained by independent means if the system is working properly.

2.) Check by Comparison of Cubical Results to Those of Other Tests - In this case, a cubical test is performed to model a conventional triaxial test, and the results are checked against those of the conventional test to see if the results are reasonable.

3.) Direct Observation - This process involves a group of special tests performed with one side of the cubical box exchanged for a plexiglass plate. Using a sample prepared with a series of dark layers placed in it, the plexiglass plate allows the deformations of the sample to be visually observed.

5.4.1 Volumetric Check

The volumetric check process was conducted using a series of cubical tests performed with the conventional triaxial compression test stress path. In Figure 5.9 the volumetric and summed axial strains from two drained tests are plotted against vertical axial strain. Also shown are the stress strain curves for the two tests. As can be seen in the plot, the volumetric strain obtained by summing the individual strains determined from the LVDT measurements is very consistent in both cases with the volumetric strain determined by direct measurement to about five or six percent axial strain. In the only one of the tests which goes beyond six percent strain, the sum of the individual strains begins to diverge from the measured volume beyond the six percent strain level. The reason for this likely is related to the fact that the LVDT measurements, which only indicate the movement of the center of the sample face, become unrepresentative of the sample behavior as a whole after six percent strain since it can be seen from the companion stress-strain curve that the soil sample is beginning to fail. Looking at both of the tests from this point of view, it may be stated that the LVDT measurements are accurate up to the points where the stress-strain curves indicate failure is imminent. After failure, the sample likely distorts due to disruption by shear planes, and the local measurements by the LVDT's are not representative of the general sample deformations. Subsequently, in Section 5.3.3, direct evidence will be presented for this statement.

In Figure 5.10, a plot is given for the results of an undrained test where no volume changes occur. In examining these data, it is important to consider both the conventional stress-strain curve and the ratio of the effective principal stresses. In this case, the ratio of the effective principal stresses is a method which allows internal failure of the sample to be detected. The internal failure can occur well before it is indicated in the conventional stress-strain curve because in this test, negative pore pressures develop which allow the soil to "fail", but to continue to take load since the effective confining stresses are still increasing.

The sum of the strains determined from the LVDT's fluctuates around the zero axis line as it should until about five to six percent strain (note the similarity to the drained tests). After this point, the sum of the individual strains deviates from the zero axis. As can be seen in Figure 5.10,

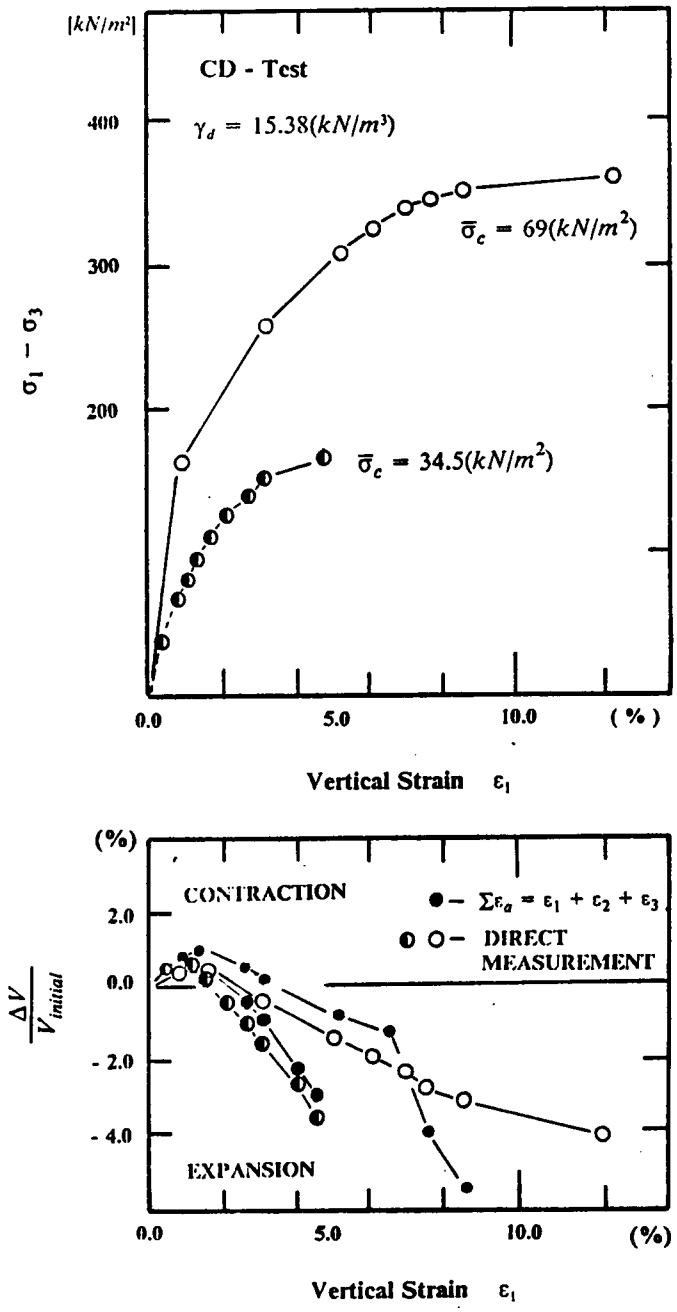

Figure 5.9 Comparison of Volumetric Strain - Consolidated, Drained, and Static Loading.

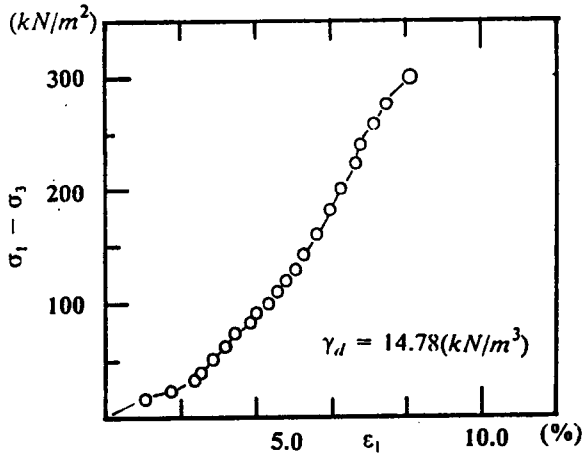

(a) Deviatric Stress vs. Vertical Strain

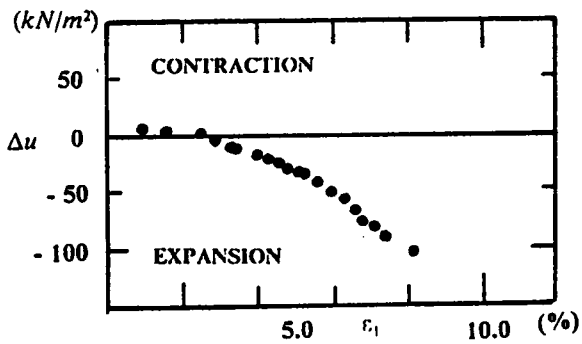

(b) Excess Pore Pressure Development

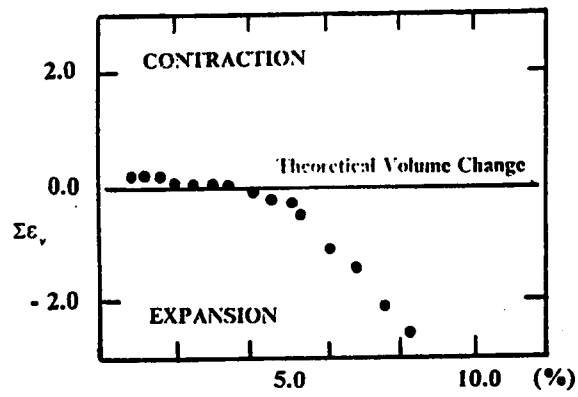

(c) Total Volumetric Strain

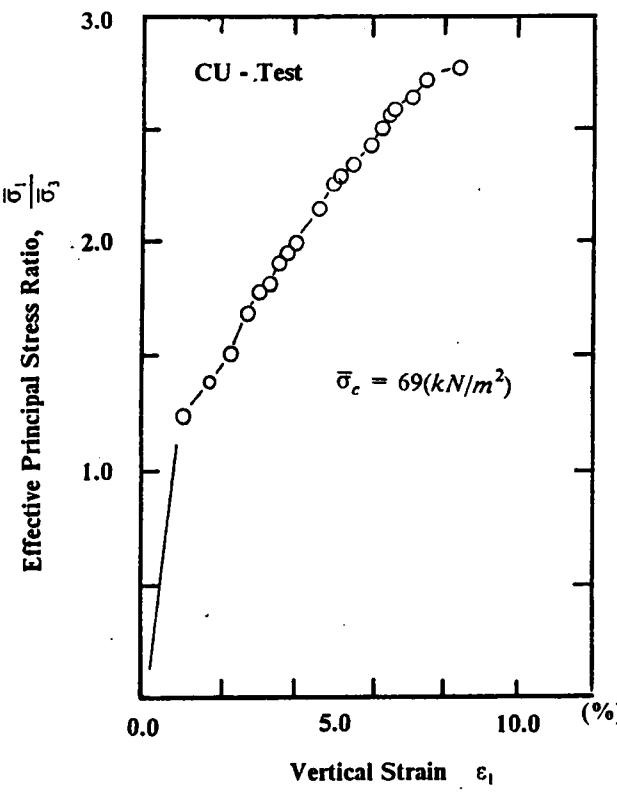

(d) Effective Principal Stress Ratio

Figure 5.10 Comparison of Volumetric Strain - Consolidated, Undrained, and Static Loading.

the axial strain at which the deviation occurs corresponds with the initiation of failure of the sample in terms of the principal stress ratio. Thus, the implication again is that the system captures the behavior well until the process of failure of the sample occurs.

The two cases shown in Figure 5.9 and 5.10 are typical of the results obtained for other checks of this type. These results tend to support the suitability of conditions up to and including the first phases of failure of the sample.

5.4.2 Comparison of Test Results Between Conventional and Cubical Devices

A number of types of tests were performed in the cubical test which were designed to mimic the conventional triaxial test. The results of two of these are shown in Figure 5.11 and 5.12. It is reasonable to expect that if the cubical device is working properly the results from the conventional versions of the tests be in close agreement with those from the conventional test device. For this purpose, conventional triaxial compression tests were performed in which conditions were kept as closely as possible to those of the cubical tests.

In Figure 5.11 and 5.12 the results of the drained triaxial and cubical "triaxial" tests are compared. The following trends are observed:

1.) The stress-strain curves from the cubical tests are essentially the same as those of the conventional triaxial tests except near failure where the cubical tests tend to show a slightly higher strength.

2.) The volume changes from the cubical tests are also very similar to those of the triaxial tests, although those from the cubical tests are consistently slightly higher than those from the triaxial tests (the volume changes shown for the cubical tests are those directly measured, not computed from summing individual strains).

The similarity of the behavior in the cubical tests to that of the triaxial tests is encouraging. The differences which do exist, particularly in the case of the volume changes is not a surprising finding. In many investigations this type of response has been observed. For example, if the results of

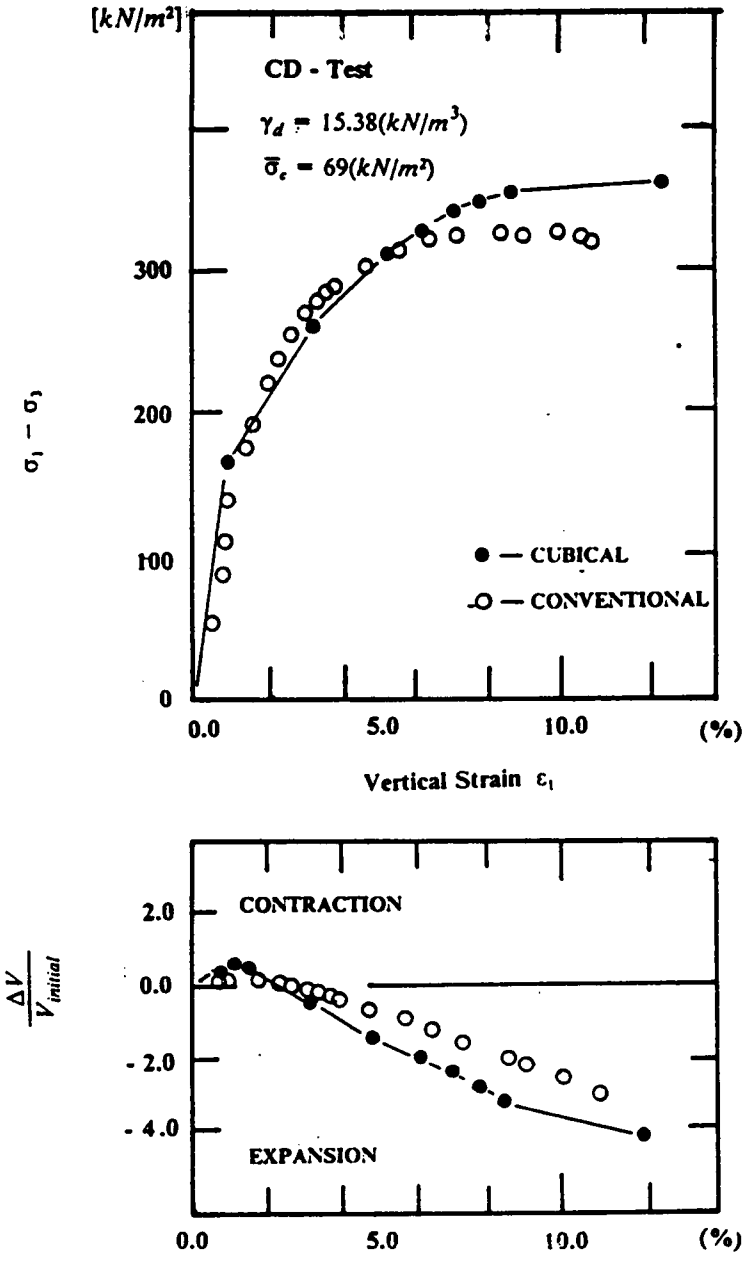

Figure 5.11 Comparison of Test Results from Cubical and Triaxial Devices - Consolidated, Drained, and Static Loading on Dense Sand.

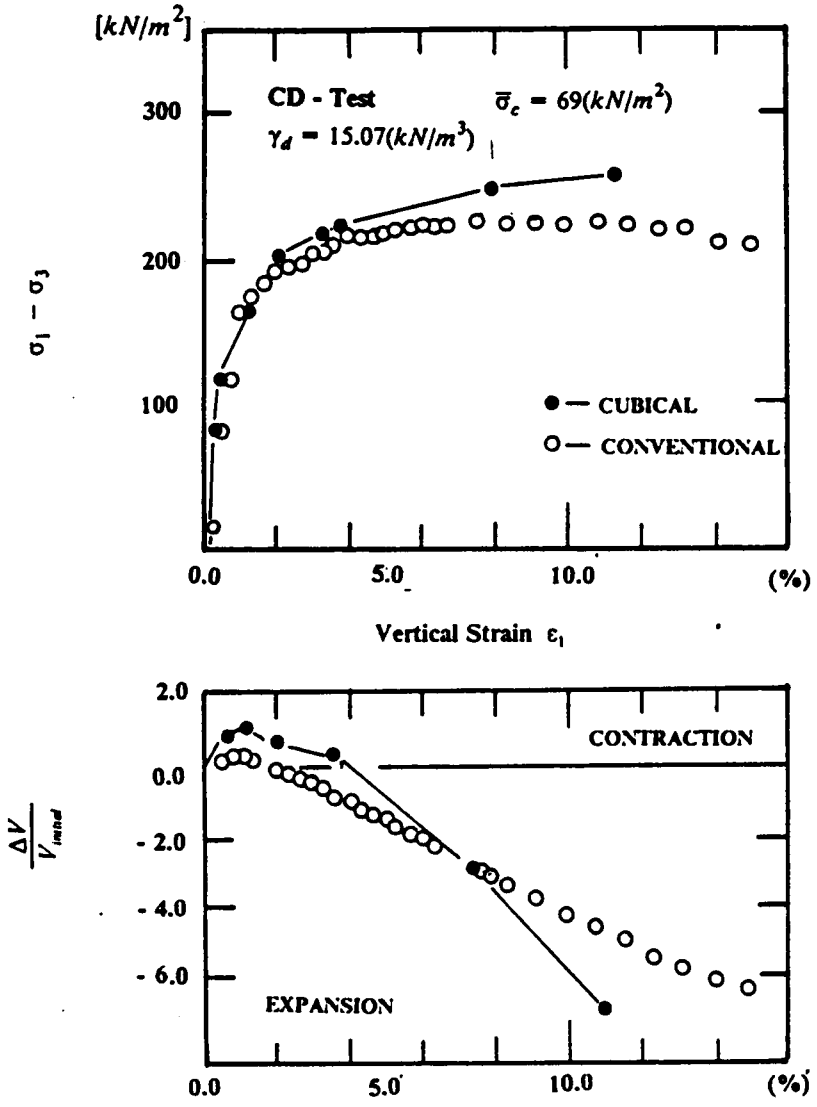

Figure 5.12 Comparison of Test Results from Cubical and Triaxial Devices - Consolidated, Drained, and Static Loading on Loose Sand.

frictionless ends triaxial tests are compared to those of conventional triaxial tests, the same effect is seen (Rowe and Borden, 1964). This effect is caused by the fact that in the conventional triaxial test there are " dead zones " within the sample body that are not involved in the shearing process. In the frictionless ends triaxial test, most, if not all, of the sample is involved, and thus, more volume change ensues. In spite of this effect, it is usually found that the strength from the different types of triaxial tests is close with that of the frictionless ends test, typically the larger. The same trend is observed in the tests of this work, except it is the cubical tests playing the role of the frictionless ends triaxial tests. Note that the cubical tests are performed with greased platens to reduce the friction.

It is useful to also examine the response of comparable consolidated undrained tests performed in the cubical and triaxial devices. In this case, instead of volume change, pore pressures are measured. The result in Figure 5.13 shows that the stress-strain responses from the two tests are similar, but are not as close as those of the cases in the drained tests. Part of the reason for this is attributable to the pore pressure behavior shown in Figure 5.13. The pore pressures in the cubical test tended to be at first larger on the positive side, and then ultimately also larger on the negative side than those from the triaxial test. These trends are a natural reflection of the volume changes in the drained tests, and thus are consistent with the trends observed earlier about the larger volume of soil being sheared in the cubical test relative to the triaxial test. Importantly, where the volume changes in the drained tests exert only a secondary effect on the stress-strain behavior of the soil, the pore pressures have a primary effect. For example, the larger initial positive pore pressures in the cubical test reduces the effective confining pressure in the sample, causing a softening of the soil stress strain response relative to the triaxial test. On the other hand, the higher negative pore pressures in the later phases of the cubical test cause the effective stresses in the cubical test to be higher than those of the triaxial test, causing a stiffening of the stress strain response of the cubical test relative to the triaxial test.

The trends in the tests shown here are repeated in other results. A good indication of the consistency of the test results is shown in Figure 5.14, where friction angles from the static cubical

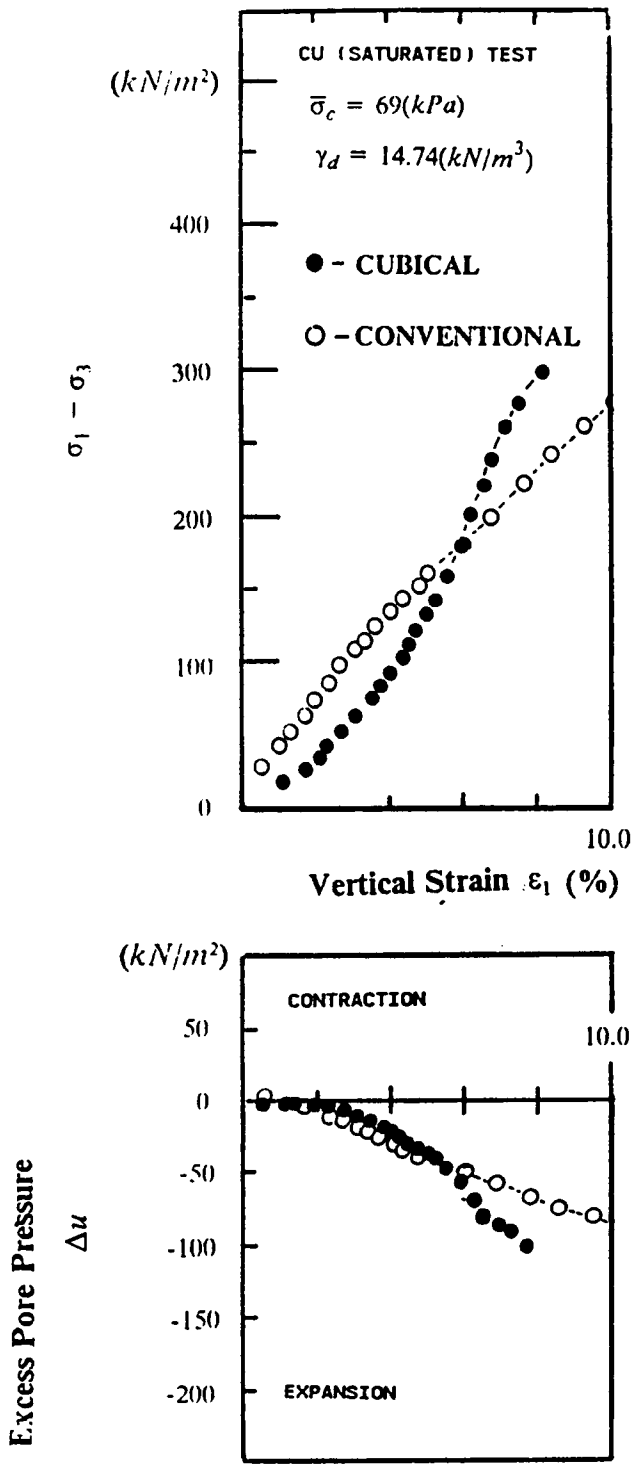

Figure 5.13 Comparison of Test Results from Cubical and Triaxial Devices - Consolidated, Undrained, and Static Loading.

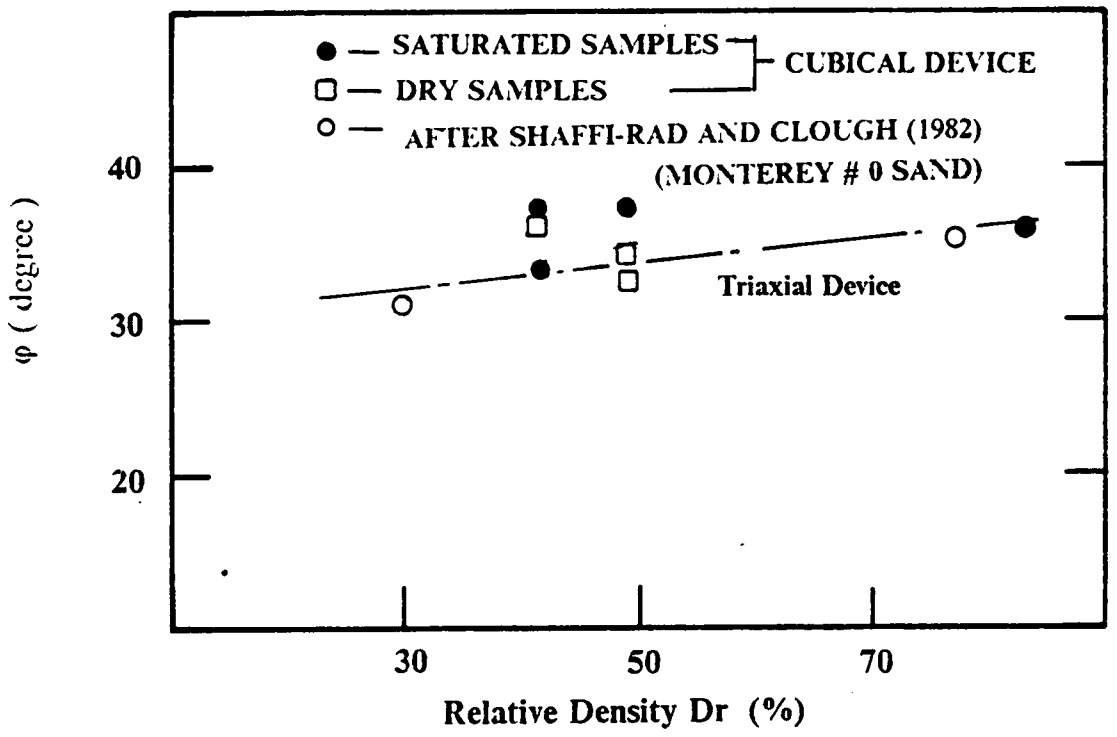

Friction Angle vs. Relative Density

Figure 5.14 Friction Angles Obtained by the Cubical Device.

tests are plotted versus those in triaxial tests. The friction angles from the cubical tests are generally slightly higher than those in the triaxial tests, but the difference is less than three degrees at best.

The results from these comparisons suggests that regardless of small nonuniformities in stresses or strains of the cubical sample, the test device yields reasonable results except in the large strain region after sample failure. It is encouraging that the small differences observed in some cases before failure are consistent with previous research, and are readily explainable in terms of basic concepts of testing and soil behavior.

5.4.3. Direct Observation of Failure and Strain Patterns

Cubical loading devices frustrate the direct observation of sample behavior since the sample is surrounded on all sides by the device. To circumvent this problem in the present case, several tests were performed where two sides of the cubical box were removed and replaced by plexiglass sheets. In these tests, the plexiglass formed a rigid boundary that prevented strains along the axis perpendicular to them. Thus, this particular version of the test utilized plane strain conditions, with the sample free to deform only along two axes. However, the pattern of deformation could be readily observed as the sample responded to the pressures applied by four of the silicon membrane pressure modules. To better observed the pattern of deformation, bands of sand stained by ink were placed at intervals in the sample. After completion of each test, a gelatin solution was circulated through the soil, and it was allowed to set up. In this condition, the sample could be removed from the box for more detailed observation.

The general trends of sample deformations and failure pattern development in the sample as visually observed in the tests are shown in Figure 5.15. In the early phases of the tests, the sample boundaries and the dark layers remained plane. Along the axis with the highest stress, the sample axis shortened, while along the axis with the smallest stress, the sample axis lengthened. As failure of the sample approached as detected by the appearance of the stress-strain curve, the development of several failure planes could be detected in the corners of the sample, although the boundaries of

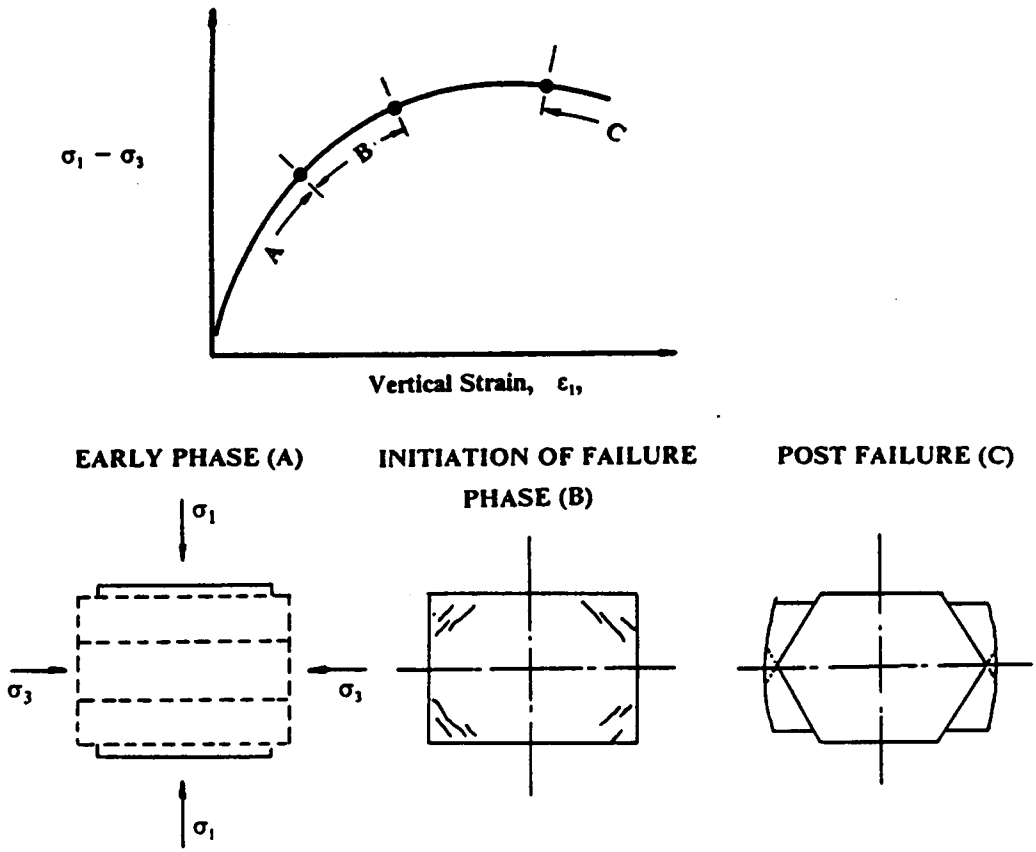

Figure 5.15 General Trends of Sample Deformations and Failure Pattern Development.

the sample remained intact. The incipient failure planes formed as angles consistent with Mohr-Coulomb theory (about 60 degrees from the horizontal plane, which was the axis of the minor principal stress). The trace of the failure planes passed from the corner of the sample and intersected the midpoint of the side of the sample. After the peak of the stress-strain curve was passed, more of the failure planes became obvious in the corners, and those that developed first became planes of large displacements and distortions of the sample. At this stage, the sample boundaries were transacted by the failure planes. In those areas of the sample where the shear planes did not develop, the soil structure continued to deform in a regular pattern.

The reason for the development of the failure planes in the corners of the sample is shown in Figure 5.16. It is in these locations that the major principal stress acts against a section of the soil which is able to move into the face of the adjacent pressure module. The fact that the failure planes form in all of the corners of the sample and are essential identical, suggests that the stress conditions up to that time are relatively uniform. Failure planes in the central portions of the sample may be incipient, but the relative movements needed to produce them cannot occur because the soil mass in these areas act in part against the face of the pressure module with the largest stress.

The conclusion of the observations in the special tests is that stresses and strains are uniform in the sample in the early portions of the tests. As the peak of the stress strain curve is approached, the failure planes begin to develop in the corners. At this stage, the stresses and, hence strains, are still reasonably uniform, since the failure planes form in a very consistent pattern, and the sample boundaries are still intact. After the peak, the strains in the sample are nonuniform, and the LVDT measurements become less representative of the soil behavior. In this condition, the system for measuring the sample deformations is obviously unable to capture the average behavior, since there is only one LVDT per side of the sample, and it is located at the center of the sample, where the deformation are the smallest.

5.4.4 Summary

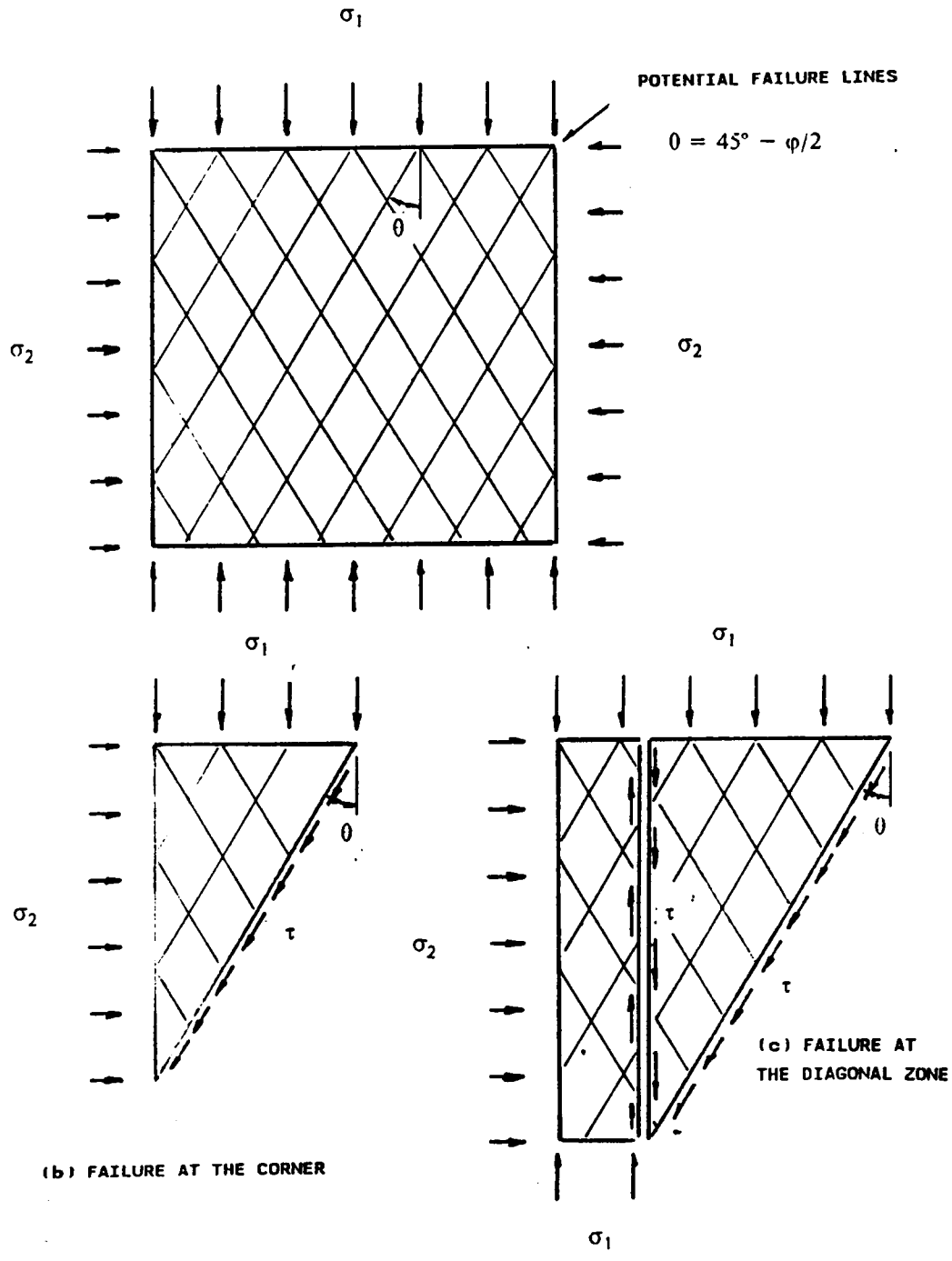

Figure 5.16 Potential Failure Lines and Possible Failure Lines.

The static tests performed to check the reliability of the strain measurement systems, and the stress and strain conditions in the cubical devices show a consistent set of trends, and all lead to the same conclusions. For behavior up to and including the initial phases of failure of the soil:

1.) The strain measurements are accurate - measured total volumetric strain approximately equals that obtained as the sum of the independently measured individual axial strains.

2.) The behavior of static cubical tests performed to mimic conventional triaxial tests is very consistent with the behavior of the conventional triaxial tests. What differences that are observed are readily explainable and reasonable.

3.) The stress and strain patterns in the cubical sample are reasonably uniform, and lead to reliable results.

For behavior after failure of the sample, it is apparent that the stresses and strains in the cubical sample become nonuniform. The larger the strains after the failure, the larger are the nonuniformities in the system, and the less representative are the measurements of the deformations from the LVDT's acting on the sides of the specimens. However, prior to this stage, the results from the cubical device are well within acceptable bounds. This is particularly important in liquefaction studies of this work, since the concern is with the initial development of liquefaction, not the large strain conditions that follow liquefaction failure.

5.5 Cyclic Uniaxial Testing To Determine Reliability Of Cubical Device Test Results

Before the cubical device was used to perform earthquake simulation tests with unusual stress paths, a testing program was performed using uniaxial cyclic loading. The load path in this case is that of the conventional triaxial test, earlier referred to as the CTX test in the Chapter III. There are two issues about reliability in the tests. First, there is the question as to the accuracy with which the cyclic loading system can produce a sinusoidal loading at one cycle per second. The second concerns, how the results obtained from the tests are consistent with those of other investigations. All of the tests done for this phase of the investigation are for uncemented sands.

5.5.1 CTX Loading

The cyclic loading in the cubical device is generated by a program written for the microcomputer control unit. The microcomputer in turn sends electronic signals to the loading devices. In Figure 5.17 the pneumatic stress pulses generated by the loading system for the case of CTX loading is plotted versus the ideal, desired curve. As can be seen, the computer generated curve is in excellent agreement with the desired curve.

Typical results from a test on a sample prepared to a density of 15.38 kN/m^3 , and loaded with a stress ratio of 0.424 are given in Figure 5.18. Shown in the figure are the excess pore pressures and the vertical and horizontal strains. The only unusual aspect of this figure is the plot of horizontal strain since this is not measured by any conventional device. The pore pressures can be seen to cycle regularly with the loading applications, and the general trend is for the pore pressures to increase. At the tenth cycle of load, the pore pressure instantaneously equals the initial effective confining stress, indicating that the condition of initial liquefaction has occurred. Both vertical and horizontal strains increase rapidly after the initial liquefaction, a behavior commonly observed in triaxial tests.

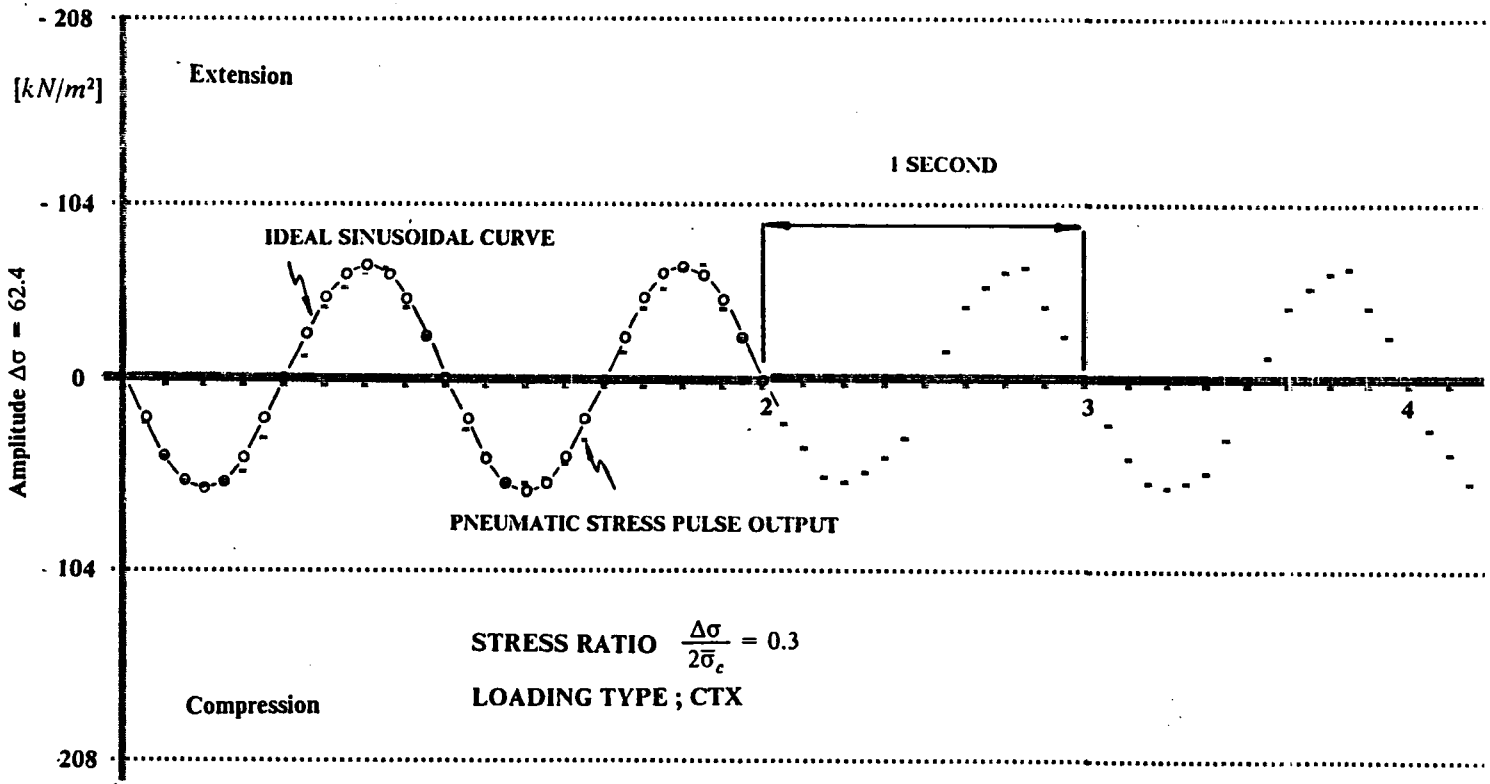

Figure 5.17 Pneumatic Stress Output and Ideal Sinusoidal Curve.

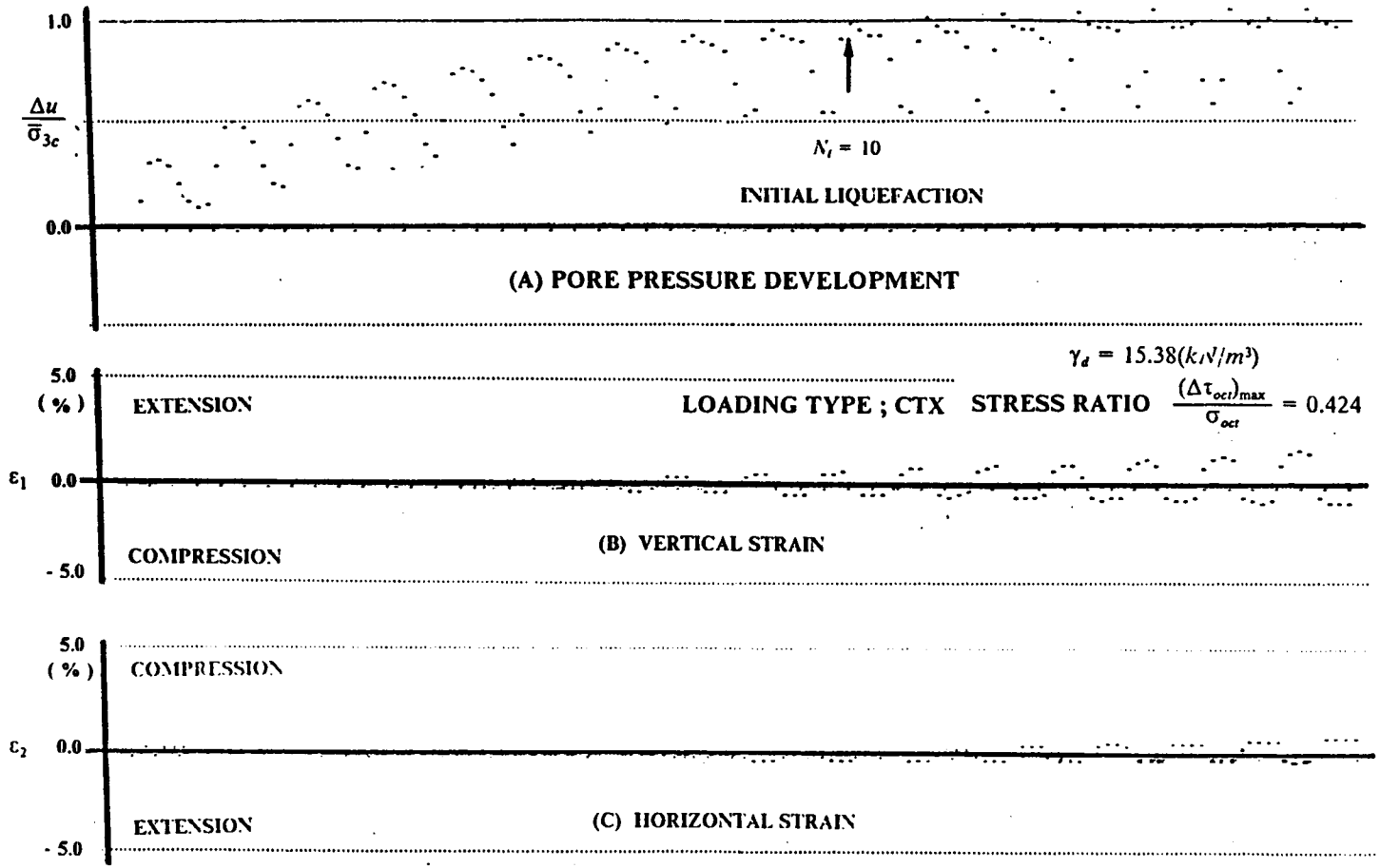

Figure 5.18 Typical Test Results by CTX in the DCSVT1.

The results in Figure 5.17 and 5.18 confirm that the loading in the system is consistent with that desired for the CTX conditions. Also, the general trends of the test results are correct.

5.5.2 Liquefaction Resistance from CTX Tests on Wet Tamped Specimens

In Table 5.1, information is provided for a series of four CTX tests that were performed on wet tamped samples of Monterey # 0/30 sand. The purpose of these tests was to obtain results that could be compared to those published in the literature for standardized test programs for this condition. Silver, et al. (1976) reported the results of cyclic liquefaction tests performed to precise standard for the triaxial test. The Silver et al. (1976) tests were conducted Monterey # 0 sand, a material which is no longer available from the supplier. The replacement for this sand is Monterey # 0/30 as used in this investigation. Monterey # 0/30 sand is similar to Monterey # 0 sand, although # 0/30 has a slightly coarser grain size. Liquefaction tests have been performed by Muzzy (1983) on the Monterey # 0/30 showing it to be slightly more resistant to liquefaction than Monterey # 0.

Figure 5.19 shows a plot of the cyclic stress ratio versus the number of cycles to initial liquefaction. In the figure, the standard results of Silver et al. (1976) and Muzzy (1983) are provided along with those of the four tests of this investigation. Observations from the results are:

1.) The trend of the data from this investigation and that of the others is very consistent.

2.) The cyclic resistances from the cubical CTX tests agree closely in magnitude with those of the Silver et al. (1976) investigation on Monterey # 0 sand, and are slightly below those of Muzzy (1983) on Monterey # 0/30.

The agreement of the results suggests that the cubical device is capable of generating high quality information in a cyclic liquefaction test. The small differences between the Muzzy results and those of this investigation may be attributed to inherent differences in preparation of the cubical and

Table 8. 5.1 Pilot Liquefaction Test Program with CTX Loading.

	Test Condition
Density	15.38 kN/m^3 for Tamped Samples 15.07 kN/m^3 for Pluviated Samples
Sample Preparation	Three layers with 25 tamping by about 0.5 kg weight and approximately 20 percent water contents for Tamped Samples Air pluviation of dry sand for Pluviated Samples
Stress Ratio	Four different levels for Tamped Samples Six different levels for Pluviated Samples
Loading Type	CTX
Test Sand	Monterey #0/30 Sand for Both Samples

AUTHOR	MATERIAL	$\bar{\sigma}_c$ (kPa)	$\gamma_d\|(D_r)$ (kN/m^3)	TEST	SAMPLE
SILVER ET AL.(1975)	MONTEREY #0	103	15.46 (60 %)	TRIAXIAL	WET TAMPED
MUZZY I (1984)	MONTEREY #0/30	103	15.46	TRIAXIAL	WET TAMPED
MUZZY II (1984)	MONTEREY #0/30	103	(60 %)	TRIAXIAL	WET TAMPED
THIS RESEARCH	MONTEREY #0/30	103	15.38	CUBICAL TRIAXIAL	WET TAMPED

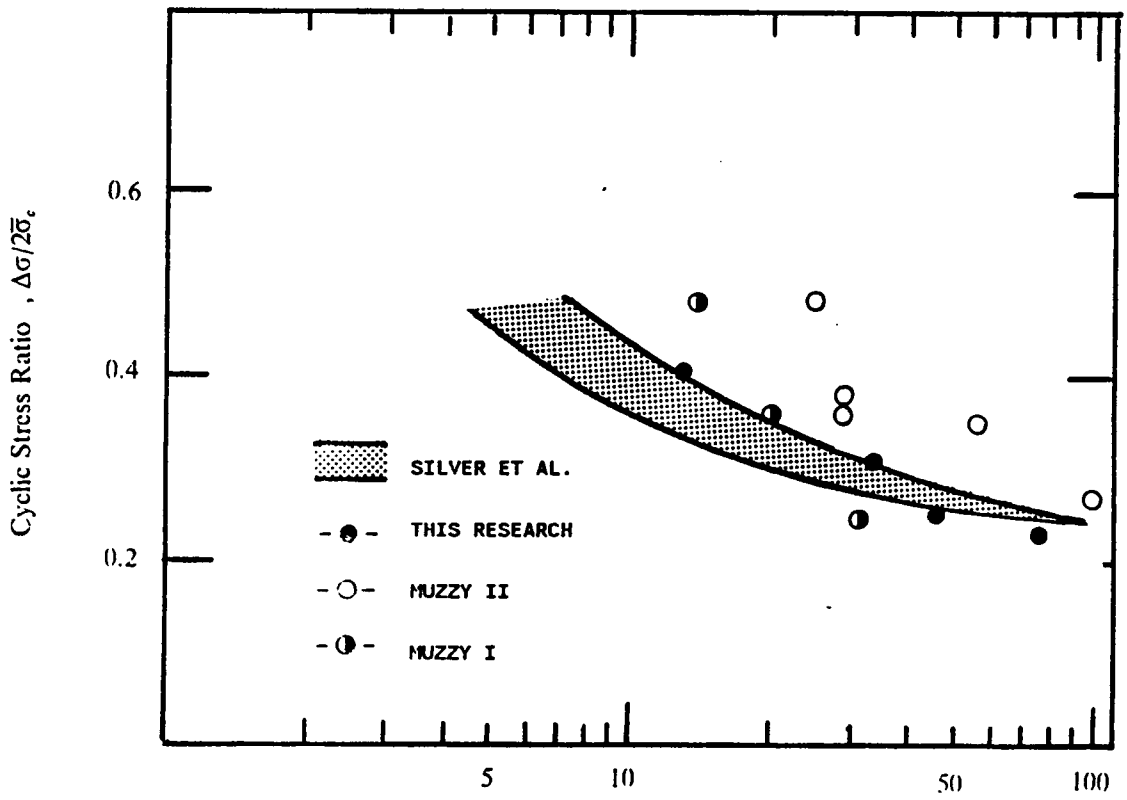

Figure 5.19 Comparison of Cyclic Shear Strengths of Wet Tamped Specimens.

triaxial samples. Not as many layers are used in the cubical samples, and thus the structure of the samples is probably not identical to that of the triaxial tests.

As a check on the monitoring system for the pore pressures, it is useful to compare the test results to recognized average ranges of pore pressures in triaxial liquefaction experiments. In Figure 5.20 the pore pressure ratio is plotted against the number of cycle in the test. The number of cycles is nondimensionalized by dividing the total number of cycles to liquefaction. A band is shown on the diagram for what was identified by Lee and Albeisa (1974) as typical response. The cubical test results largely fall within the band, although there are some differences. The most noticeable difference is for the highest stress ratio case, where the pore pressure ratios tend to be higher than those of the hand. However, this type of response has been observed in using high stress ratios even in triaxial tests (Milstone, 1985), and it is not considered unusual.

In the cubical tests, it is possible to show how the strains develop on each of the principal planes, and this is done in Figure 5.21 for the test with a stress ratio of 0.22, where each of strains is plotted against the nondimensionalized number of cycles. Each of the strains increases rapidly only near the end of the test. They all tend to become larger at about the same point. Note that the initial liquefaction occurs at strains typically of two percent or less. This is important relative to the earlier discussion of possible nonuniformities in the stresses or strains. Since initial liquefaction occurs at low strains, the conditions in the samples should remain in the well defined region.

5.5.3 Liquefaction Resistance from CTX tests on Pluviated Specimens

While the tests of Silver, et al. (1976) were performed on specimens prepared using the wet tamping method, most of the work in this investigation was done using the pluviation technique for sample preparation. As part of the general proof-testing program, a series of six CTX tests were performed on pluviated specimens (see Table 5.1). Figure 5.22 gives the plot of cyclic stress ratio versus number of cycles for the tests performed with a density of 15.07 kN/m^3, along with those

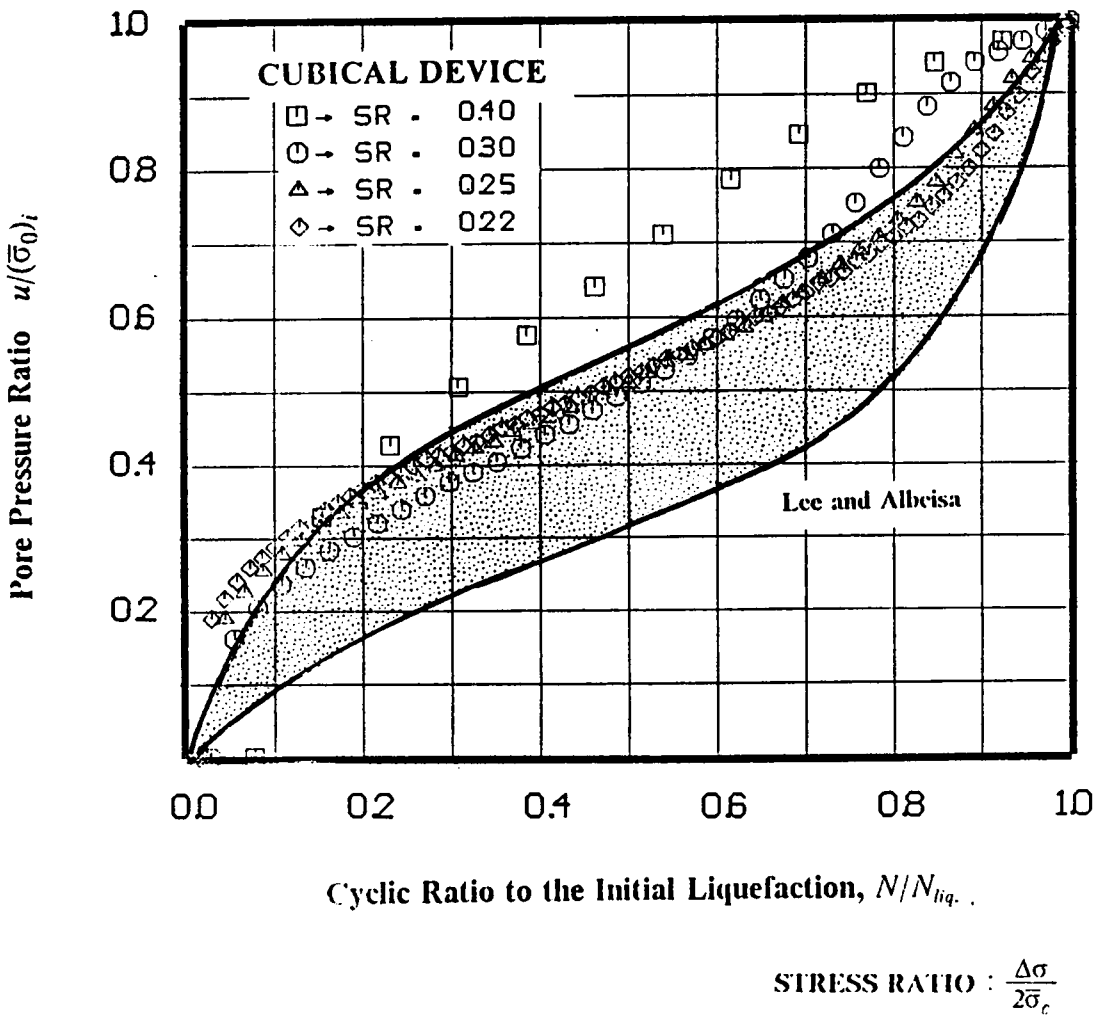

Figure 5.20 Comparison in Normalized Pore Water Pressure Development in the CTX Tests and Conventional Trends.

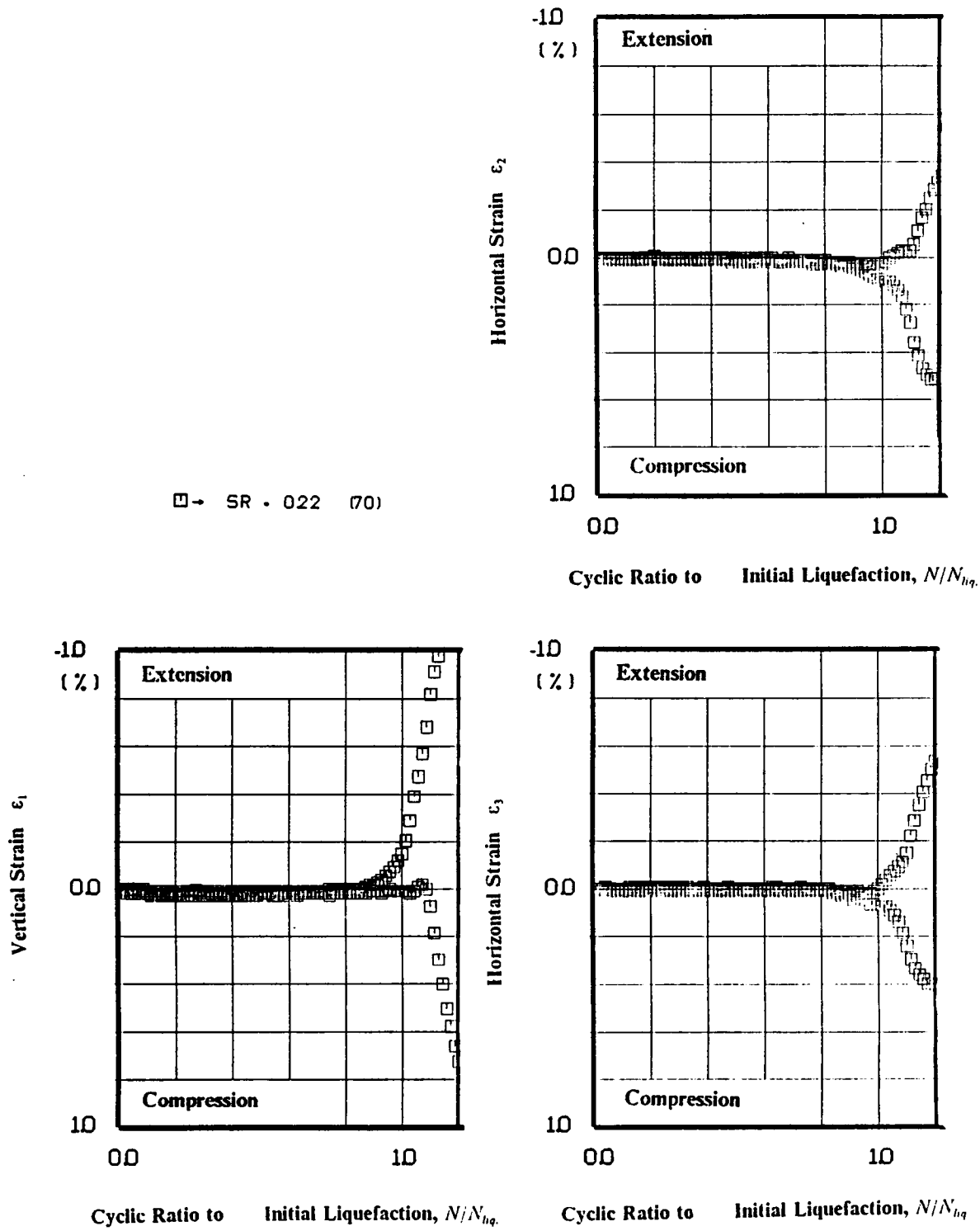

Figure 5.21 Measured Strains in a CTX Liquefaction Test.

from other similar investigations using pluviated samples. The tests of this work follow the same trend as those of the others, but the samples tend to require a slightly higher number of cycles to reach liquefaction. The reason for this is not clear, but it may be related to small differences which likely exist in sample structure, or the fact that the triaxial samples typically fail by necking on the extension cycle, a factor that does not enter into the cubical tests. Structure is important as can be seen in comparing the response of the wet specimens to that of the pluviated specimens. The wet tamped specimens are considerably stronger than those which are prepared by pluviation even though the densities are exactly the same. This finding has been observed by many investigators in triaxial tests (Mulilis, 1977).

5.5.4 Summary

The series of CTX type tests shows that the cubical device yields very reasonable information in the development of the condition of initial liquefaction. All of the test results are consistent with those of other investigations using the conventional triaxial apparatus. In addition all of the equipment and loading systems are shown to work properly.

5.6 Verification Of The Loading System Under The Complex Loading Paths

In an earlier section, the loading system is shown to produce a proper sinusoidal stress wave for the simpler loading paths. It remains to demonstrate the degree of accuracy with which the control unit can generate the stresses for the more complex cases such as the CRE-PS or the CRC-PS. These present more of a challenge since all three principal stresses are changing instead of just one. In the test, the complete rotation to finish the elliptical or circular path is done in three seconds.

Figure 5.23 presents the idealized and actual stress paths for the CRC-PS tests. The actual path is based on measured values of the principal stresses. These were measured by taking the lines for each one of the pressure modules and recording the pressure as the outlet of the line using a pressure

AUTHOR	MATERIAL	$\bar{\sigma}_c$ (kPa)	γ_d|(D_r) (kN/m^3)	TEST	SAMPLE
SILVER (1980)	MONTEREY #0	103	15.46 (60 %)	TRIAXIAL	AIR PLUVIATED
MULILIS (1977)	MONTEREY #0	55.1	15.20 (50 %)	TRIAXIAL	AIR PLUVIATED
SHAFFI-RAD('82)	MONTEREY #0	103	15.20 (50 %)	TRIAXIAL	AIR PLUVIATED
THIS RESEARCH	MONTEREY #0/30	103	15.07	CUBICAL TRIAXIAL	AIR PLUVIATED

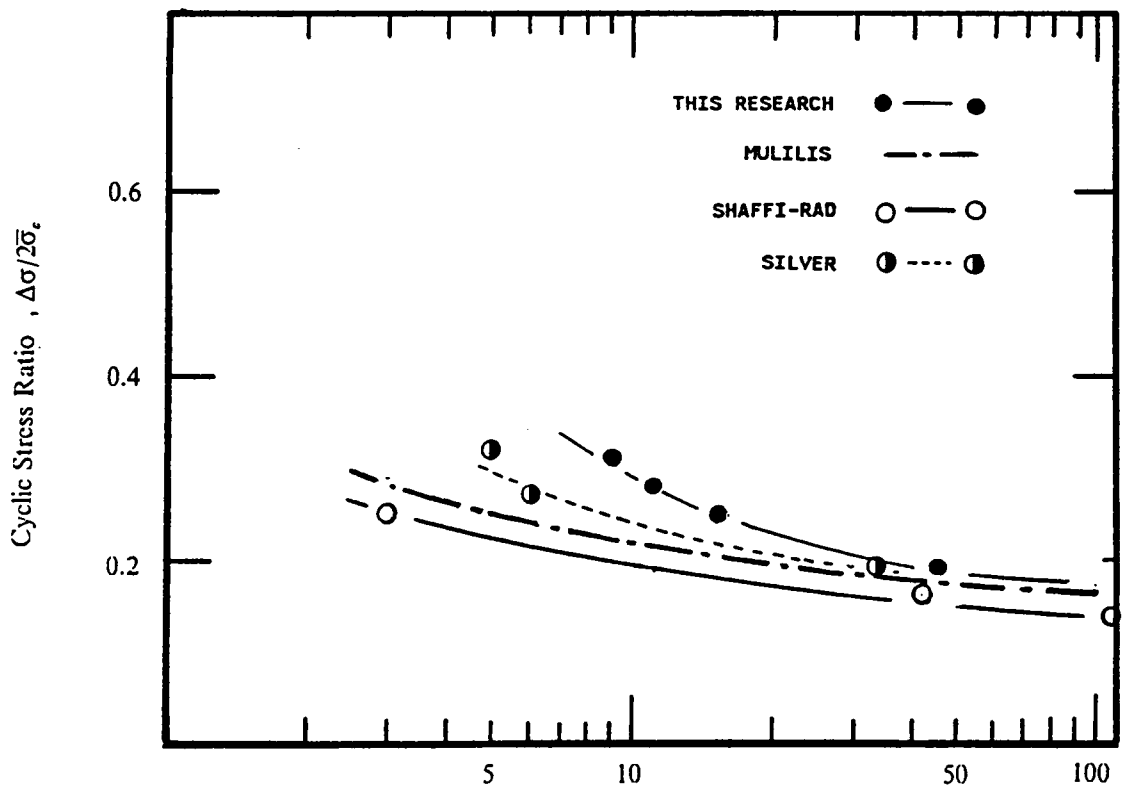

Figure 5.22 Cyclic Strengths of Air Pluviated Samples.

transducer. The actual path is close to, but not exactly the same as the ideal paths. Differences exist for the following reasons:

1.) The control unit achieves the pressure changes in finite increments, and not the smooth process described in the ideal curve.

2.) There is a certain amount of inertia in the process of moving the air through the system as the changes are called for by the control unit, because of hydraulic losses, and the fact that there is a finite amount of air involved.

The level of deviations between the ideal and the real stress paths is not considered important because it is not large, and the main impact of the process is achieved with that applied.

5.7 Summary

This chapter has presented the concept of the cubical testing system. The device is unique in its simplicity, and the fact that the microcomputer control unit allows for a wide range of load paths to be automatically applied to the soil, and for the data to be automatically recorded. Recognizing that the cubical device has some limitations in regard to uniformity of strains, a major effort was invested to define the range of strains over which the apparatus would yield reasonable and accurate results. This effort showed that the cubical shear box maintained acceptably uniform sample conditions up to and including initial sample failure. Nonuniformities developed increasingly as the strains became larger in the post-failure region. However, the post-failure situation has no impact on this work since the research focuses on pre-failure and initial failure type circumstances.

In support of the contention that the cubical device is an acceptable tool for the purposes of this work, a number of tests were performed where the conventional triaxial test was "mimicked"

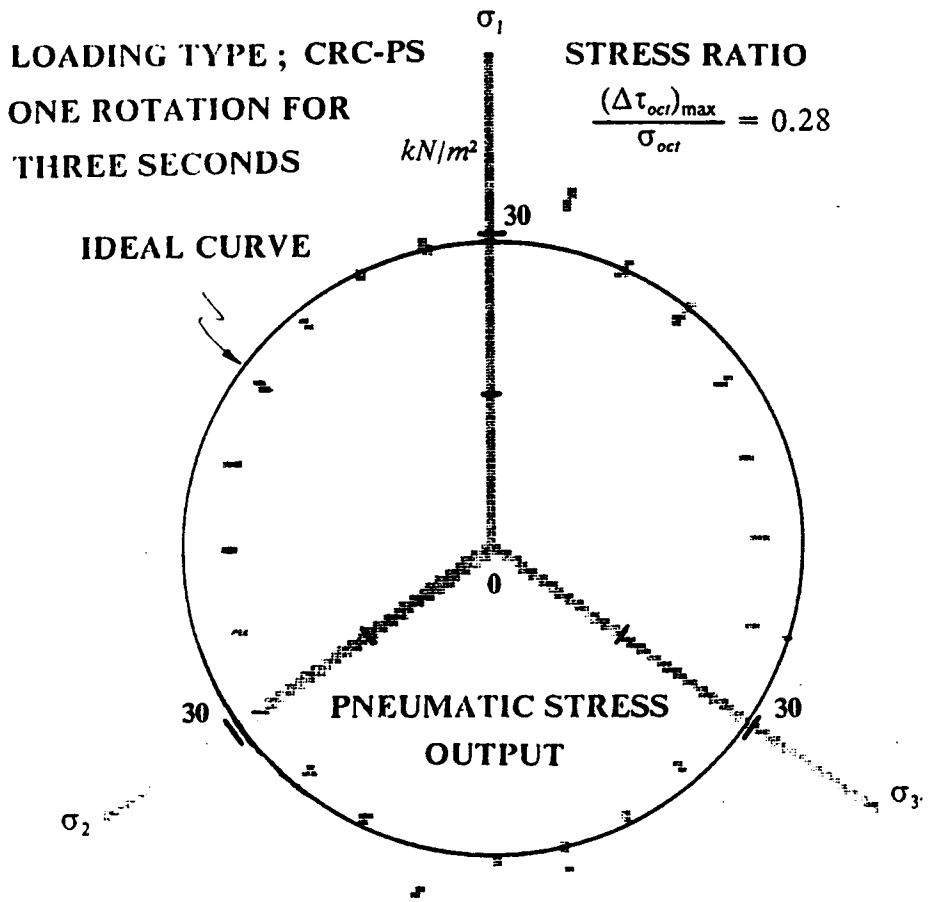

Figure 5.23 Pneumatic Stress Output of CRC-PS and an Ideal Output Curve.

by using the triaxial stress path. The results of the both static and cyclic tests are shown to be very consistent with the behavior from the conventional tests.

CHAPTER VI

TEST RESULTS

6.1 Introduction

The production tests afford an opportunity to compare the effects of a number of important variables, including :

1.) Level of cementation

2.) Type of stress path

3.) Density

As regards the level of cementation, it will be defined in terms of the unconfined compressive strength of the sand. The unconfined compressive strength value used herein is that determined in the unconfined compressive tests on the cubical samples as reported in Chapter IV.

Key information for all of the production tests is given in Table 6.1 to 6.3. The test identification numbers used in the tables are the same as used in the tables in Chapter IV, where control parameters in the tests are defined.

Table 9. 6.1 Cyclic Shear Strength by CTX.

Serial No.	Density (kN/m^3)	U.C.S.* (kN/m^2)	Stress Ratio**	Initial Liquefaction (cycles)
LQ- 1	15.07	0	0.292	9
LQ- 2	15.07	0	0.264	12
LQ- 3	15.07	0	0.235	15
LQ- 4	15.07	0	0.179	40
LQ- 4a	15.07	0	0.160	100 < N < 110
LQ- 5	15.07	46	0.329	17
LQ- 6	15.07	46	0.283	26
LQ- 7	15.07	46	0.235	48
LQ- 8	15.07	46	0.189	NL
LQ- 9	15.07	76	0.377	16
LQ-10	15.07	76	0.283	50
LQ-11	15.07	76	0.235	107 < N < 120
LQ-12	15.07	76	0.235	NL
LQ-13	15.38	0	0.424	10
LQ-14	15.38	0	0.283	15
LQ-15	15.38	0	0.235	40
LQ-16	15.38	0	0.189	89
LQ-17	15.38	62	0.424	21
LQ-18	15.38	62	0.377	23
LQ-19	15.38	62	0.283	52
LQ-20	15.38	62	0.189	NL
LQ-21	15.38	94	0.566	12
LQ-22	15.38	94	0.424	36
LQ-23	15.38	94	0.377	38
LQ-24	15.38	94	0.283	95
LQ-25	15.38	110	0.424	NL
LQ-26	15.38	110	0.424	100 < N < 120
LQ-27	15.38	110	0.377	NL
LQ-28	15.38	110	0.377	NL

* Unconfined Compressive Strength

** Cyclic Stress Ratio ; $\frac{(\Delta\tau_{oct})_{max}}{(\overline{\sigma}_{oct})_{initial}}$

NL No Liquefaction within 120 cycles.

N Number of cycles.

Table 10. 6.2 Cyclic Shear Strength by CPS.

Serial No.	Density (kN/m^3)	U.C.S.* (kN/m^2)	Stress Ratio**	Initial Liquefaction (cycles)
LQ-29	15.07	0	0.424	7
LQ-30	15.07	0	0.354	11
LQ-31-a	15.07	0	0.283	19
LQ-31-b	15.07	0	0.263	29
LQ-32	15.07	0	0.247	54
LQ-33	15.07	46	0.566	7
LQ-34	15.07	46	0.424	17
LQ-35	15.07	46	0.235	NL (Low Saturation)
LQ-37	15.07	76	0.707	8
LQ-38	15.07	76	0.566	12
LQ-39	15.07	76	0.495	26
LQ-40	15.07	76	0.389	73
LQ-41	15.38	0	0.495	10
LQ-42	15.38	0	0.424	18
LQ-43	15.38	0	0.318	22
LQ-44	15.38	0	0.247	97
LQ-45	15.38	62	0.636	7
LQ-46	15.38	62	0.424	32
LQ-47	15.38	62	0.318	NL
LQ-48	15.38	62	0.318	NL
LQ-49	15.38	94	0.848	11
LQ-50	15.38	94	0.636	19
LQ-51	15.38	94	0.566	30
LQ-52	15.38	94	0.495	100 < N < 120

* Unconfined Compressive Strength

** Cyclic Stress Ratio ; $\frac{(\Delta\tau_{oct})_{max}}{(\bar{\sigma}_{oct})_{initial}}$

NL No Liquefaction within 120 cycles.

N Number of cycles.

Table 11. 6.3 Cyclic Shear Strength by CRE-TX, CRE-PS, CRC-TX, and CRC-PS.

Serial No. (Loading)	Density (kN/m^3)	U.C.S. (kN/m^2)	Stress Ratio	Initial Liquefaction (cycles)
LQ-53 (CRE-TX)	15.07	0	0.207	9
LQ-54 (CRE-TX)	15.07	0	0.189	12
LQ-55 (CRE-TX)	15.07	0	0.141	42
LQ-56 (CRE-TX)	15.07	0	0.094	NL
LQ-57 (CRE-PS)	15.07	0	0.283	8
LQ-58 (CRE-PS)	15.07	0	0.247	17
LQ-59 (CRE-PS)	15.07	0	0.212	35
LQ-60 (CRE-PS)	15.07	0	0.141	NL
LQ-61 (CRE-TX)	15.07	76	0.330	14
LQ-62 (CRE-TX)	15.07	76	0.283	20
LQ-63 (CRE-TX)	15.07	76	0.232	38
LQ-65 (CRE-TX)	15.38	0	0.283	9
LQ-66 (CRE-TX)	15.38	0	0.232	12
LQ-67 (CRE-TX)	15.38	0	0.189	47
LQ-68 (CRE-TX)	15.38	0	0.141	NL
LQ-69 (CRE-TX)	15.38	94	0.424	16
LQ-70 (CRE-TX)	15.38	94	0.377	28
LQ-71 (CRE-TX)	15.38	94	0.283	67
LQ-72 (CRE-TX)	15.38	94	0.189	NL
LQ-73 (CRC-TX)	15.07	0	0.189	4
LQ-74 (CRC-TX)	15.07	0	0.141	12
LQ-75 (CRC-TX)	15.07	0	0.122	17
LQ-76 (CRC-TX)	15.07	0	0.094	NL
LQ-77 (CRC-PS)	15.07	0	0.283	5
LQ-78 (CRC-PS)	15.07	0	0.212	7
LQ-79 (CRC-PS)	15.07	0	0.177	24
LQ-80 (CRC-PS)	15.07	0	0.141	40
LQ-81 (CRC-TX)	15.07	76	0.471	4
LQ-82 (CRC-TX)	15.07	76	0.330	8
LQ-83 (CRC-TX)	15.07	76	0.236	21
LQ-84 (CRC-TX)	15.07	76	0.189	NL
LQ-85 (CRC-TX)	15.38	0	0.236	4
LQ-86 (CRC-TX)	15.38	0	0.189	8
LQ-87 (CRC-TX)	15.38	0	0.141	12
LQ-88 (CRC-TX)	15.38	0	0.094	NL
LQ-89 (CRC-TX)	15.38	94	0.330	12
LQ-90 (CRC-TX)	15.38	94	0.282	17
LQ-91 (CRC-TX)	15.38	94	0.236	29
LQ-92 (CRC-TX)	15.38	94	0.217	50

6.2 Liquefaction Of Cemented Sands Under CTX And CPS Loadings

6.2.1 Effect of Level of Cementation

Figure 6.1 shows the plot of cyclic stress ratio vs. number of cycles to cause liquefaction for cemented sands under CTX loading. The curves are labeled according to the unconfined compressive strength, q_u , and density, γ_d, of the soil. The curve with the label $q_u = 0.0 kN/m^2$ and $\gamma_d = 15.07 kN/m^3$ is for uncemented loose sands; with $q_u = 76 kN/m^2$ and $\gamma_d = 15.07 kN/m^3$ for weakly cemented loose sands, and with $q_u = 94 kN/m^2$ and $\gamma_d = 15.38 kN/m^3$ for weakly cemented medium dense sands. All the unconfined strengths are relatively small; however, each higher level of q_u shows a definite increase in the liquefaction resistance of the soil. In the figure, the results of the triaxial testing investigation of Shaffi-Rad and Clough (1982) are also shown. The curve obtained with DCSVT1 is somewhat higher than that of Shaffi-Rad and Clough (1982) for equivalent soil conditions. This finding will be addressed for the Chapter VII.

Figure 6.2, gives the CTX cyclic shear strengths for three soil conditions: uncemented loose sand, uncemented medium dense sand, and very weakly cemented loose sand with $q_u = 46 kN/m^2$. The figure indicates that the effect of an unconfined strength of only 46 kN/m^2 is equivalent to that due to change in density of uncemented sand from loose to medium dense. The same trend is observed in the CPS results.

The influence of cementation on cyclic shear strength is shown in Figure 6.3, in which the cyclic stress ratio to cause liquefaction in 10 and 50 cycles is plotted against unconfined compressive strength. Results are shown in the figure for two different densities. As unconfined strength increases, the cyclic stress ratio increases considerably for both densities; the curves sharply rise after the strength is about 60 to 80 kN/m^2. It is seen that the curves associated with stress ratio to cause liquefaction in 10 cycles has larger variation than in 50 cycles for both loose and medium dense sands. This indicates that the influence of cementation is more significant at a small number than

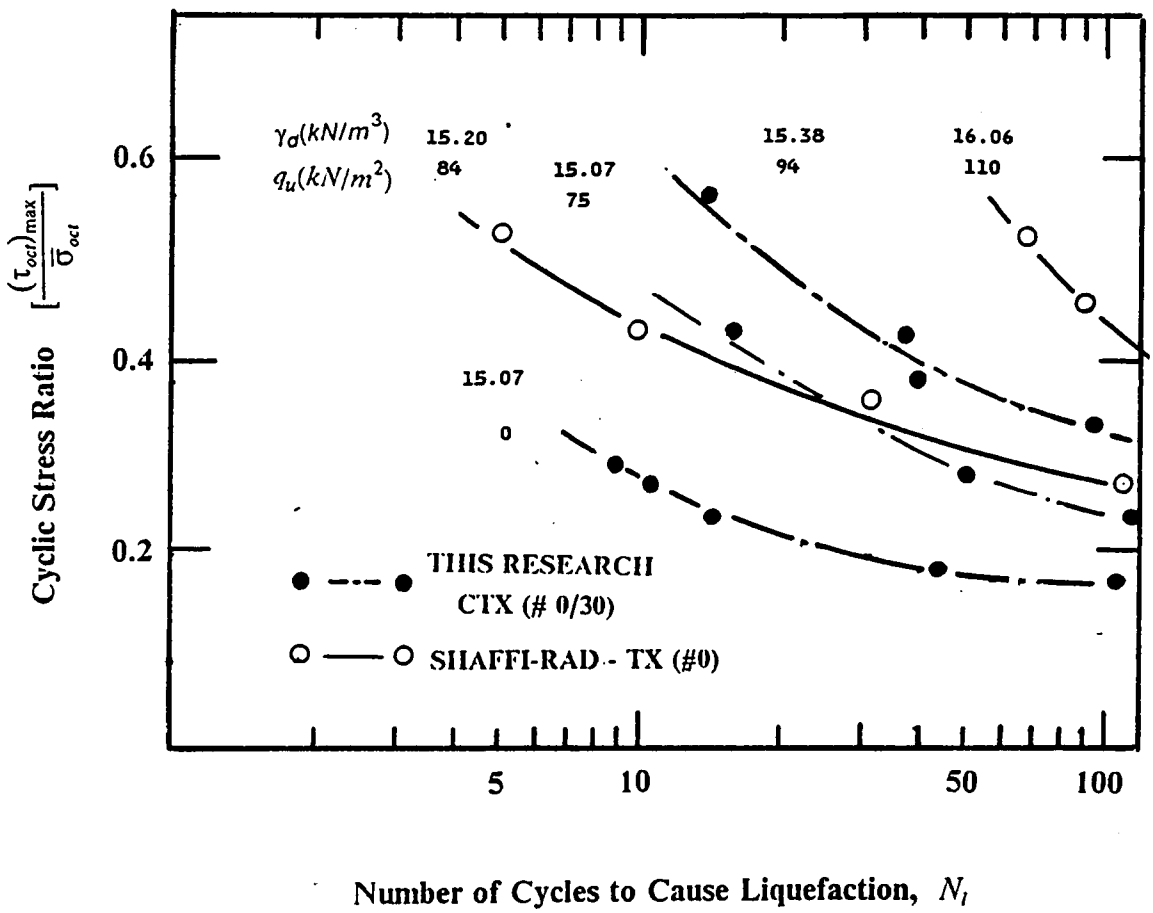

Figure 6.1 Cyclic Strengths from CTX Tests.

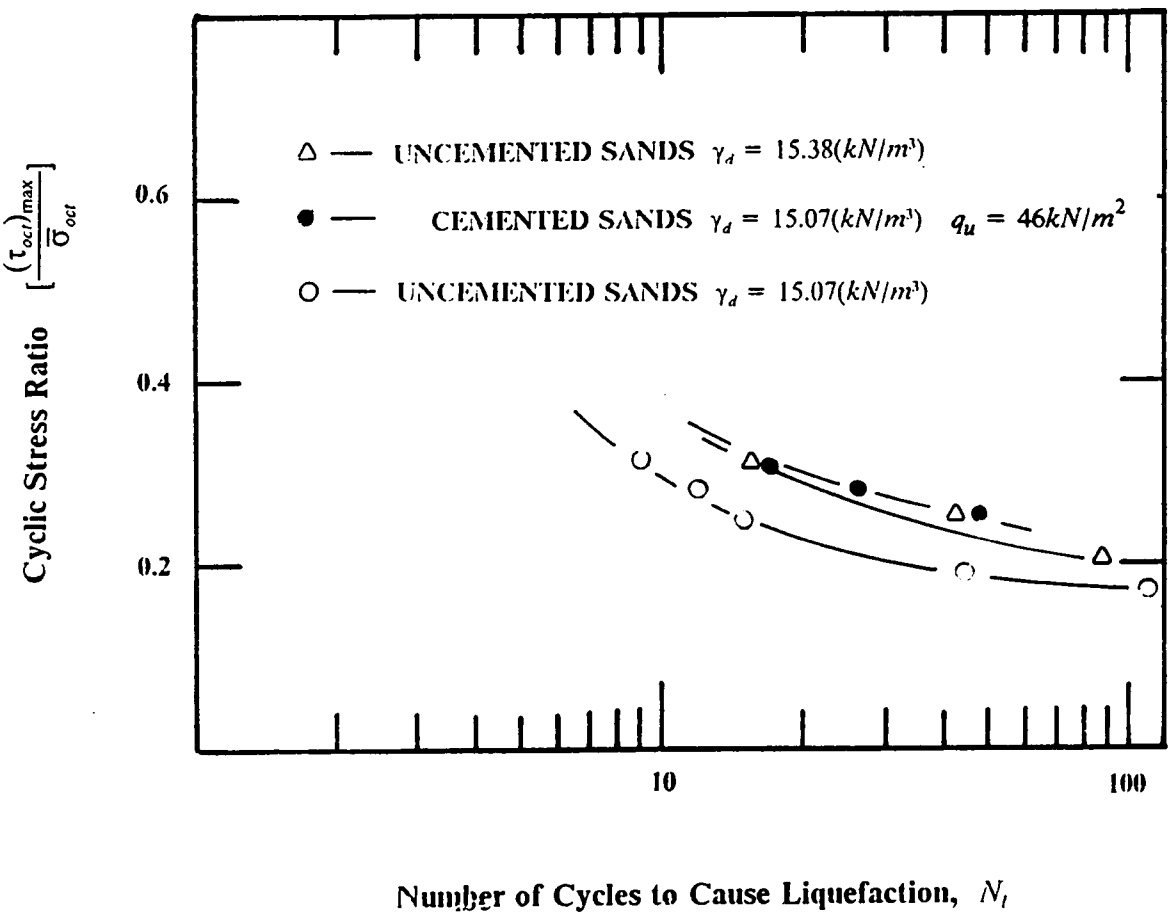

Figure 6.2 CTX Cyclic Strengths of Three Different Soil Conditions; Uncemented Loose, Uncemented Medium Dense, and Very Weakly Cemented Loose Sands.

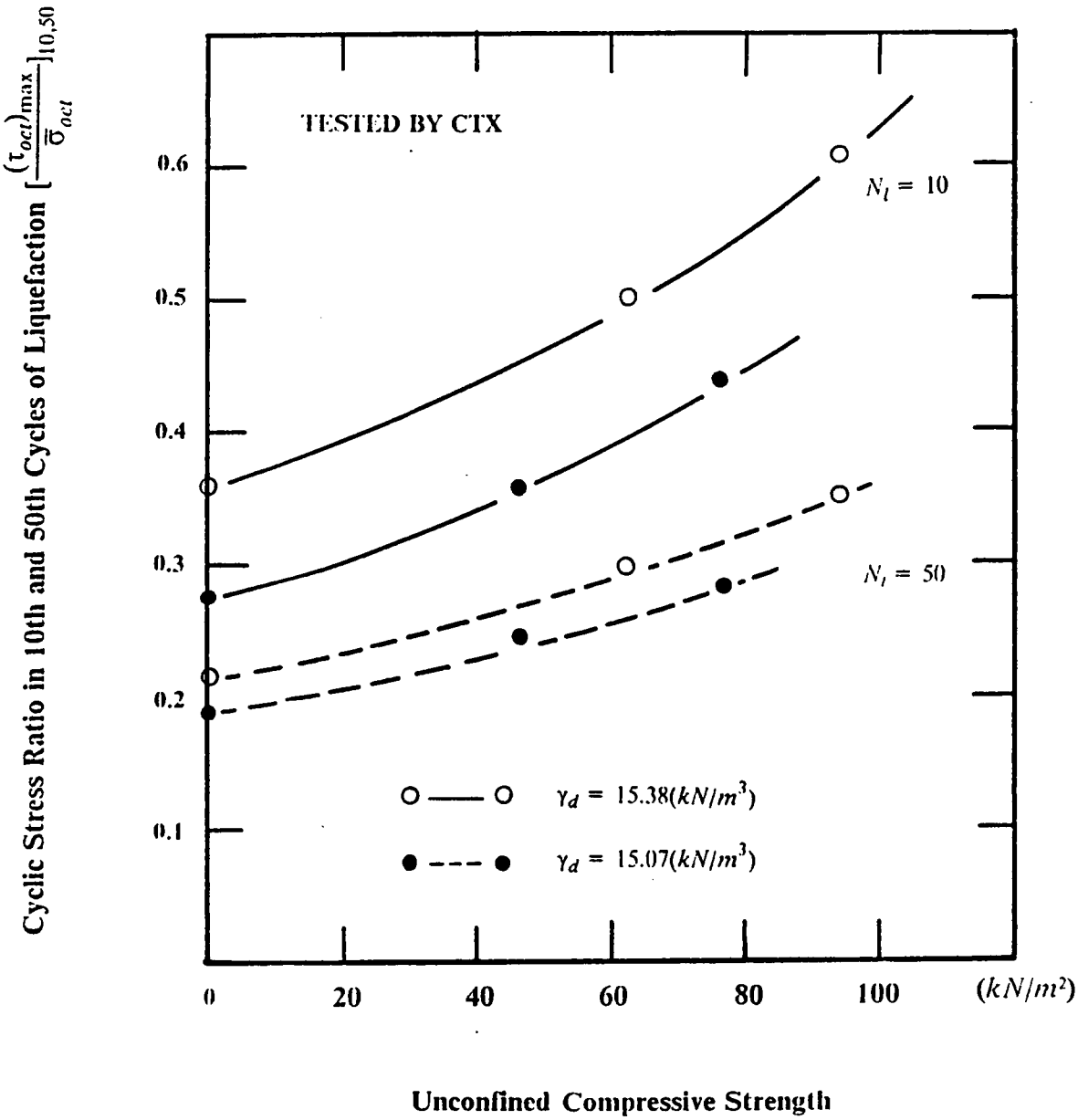

Figure 6.3 CTX Cyclic Shear Stress Ratio Causing Liquefaction in 10 and 50 Cycles as a Function of Unconfined Strength.

at a large number of cycles to cause liquefaction. Also, the difference in the stress ratio is larger for 10 cycles than for 50 cycles. An alternative way to view the relative stress ratio differences is given in Figure 6.4, where the cyclic stress ratio of cemented sands is subtracted from those of uncemented sands. The figure shows cementation is more effective at a high level of cyclic shear stress ratio. The same trend is noticed for the other types of loadings.

6.2.2 Effect of Density in Cemented Sand

Figure 6.5 (a) and (b) show the relationship between number of cycles and unconfined compressive strengths for two different densities at stress ratios of 0.4 and 0.5 for CTX and 0.5 and 0.6 for CPS tests, respectively. For uncemented sands ($q_u = 0.0kN/m^2$) the number of cycles to cause liquefaction, when it is loose, are substantially different from those when it is dense. As unconfined strength is increased due to cementation the difference in the number of cycles required to liquefy dense and loose samples is reduced. For example, if the unconfined strength is $q_u = 80kN/m^2$, there is virtually no difference. Hence the density has little role to play at this stage. It is interesting to note that the level of cementation at $q_u = 80kN/m^2$ is not very high, i.e., it is not a "strongly" cemented sand, yet the density effect is minimal.

6.3 Liquefaction In CRE-TX, CRC-TX, CRE-PS, And CRC-PS Loadings

6.3.1 Uncemented Sands

The relationship between the cyclic stress ratio and the number of cycles to cause liquefaction for the CTX, CRE-TX, and CRC-TX tests for uncemented loose and medium dense sands are shown in Figure 6.6. In both cases, the more complex stress paths with principal stress rotation effects yield the smaller cyclic strengths. Ranking of the tests from the highest strength to the lowest is CTX, CRE-TX, and CRC-TX, with those from the CTX about 25 percent and 40 percent to those from the CRE-TX and the CRC-TX tests, respectively.

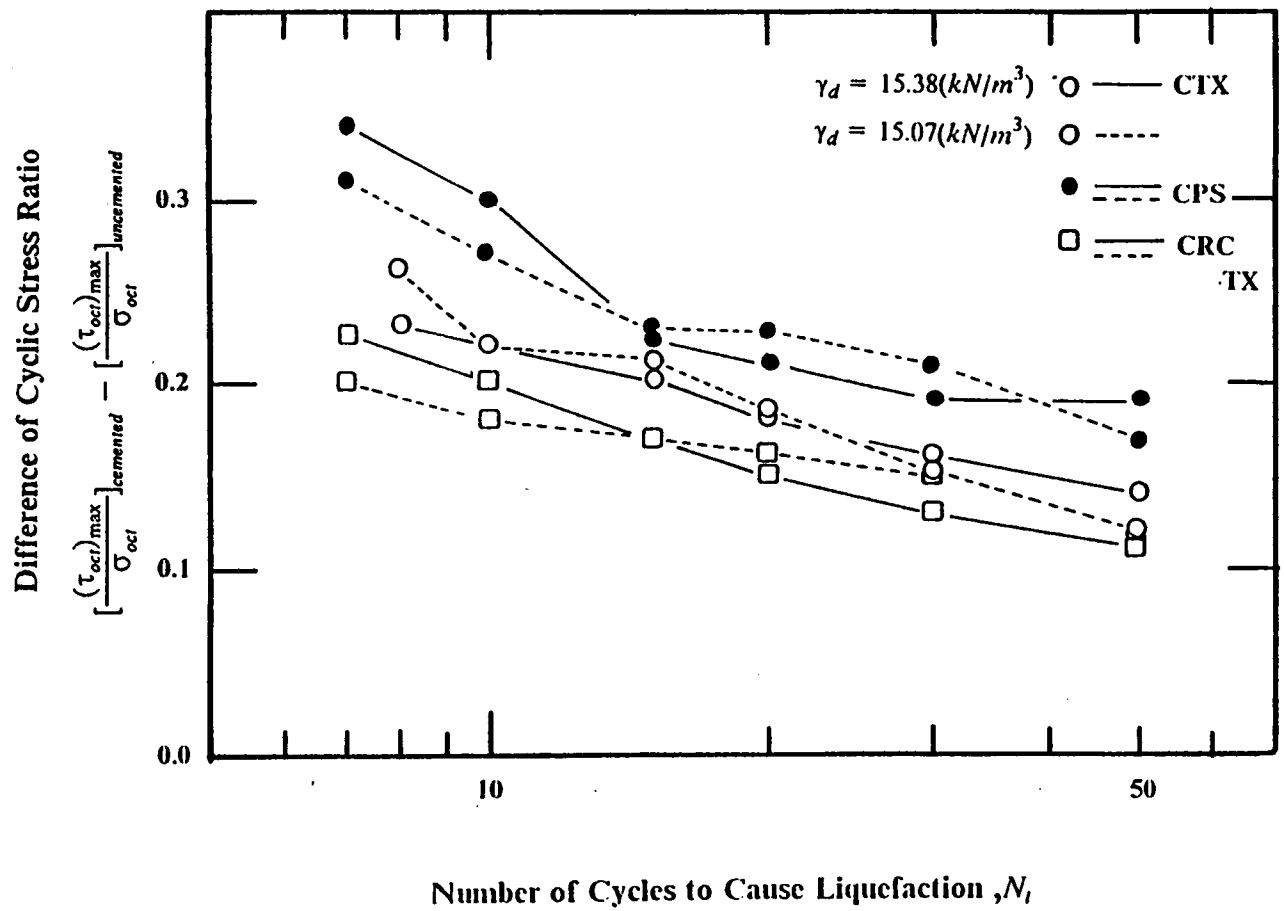

Figure 6.4 Difference in Cyclic Shear Strength between Cemented and Uncemented Samples versus Number of Cycles to Cause Liquefaction.

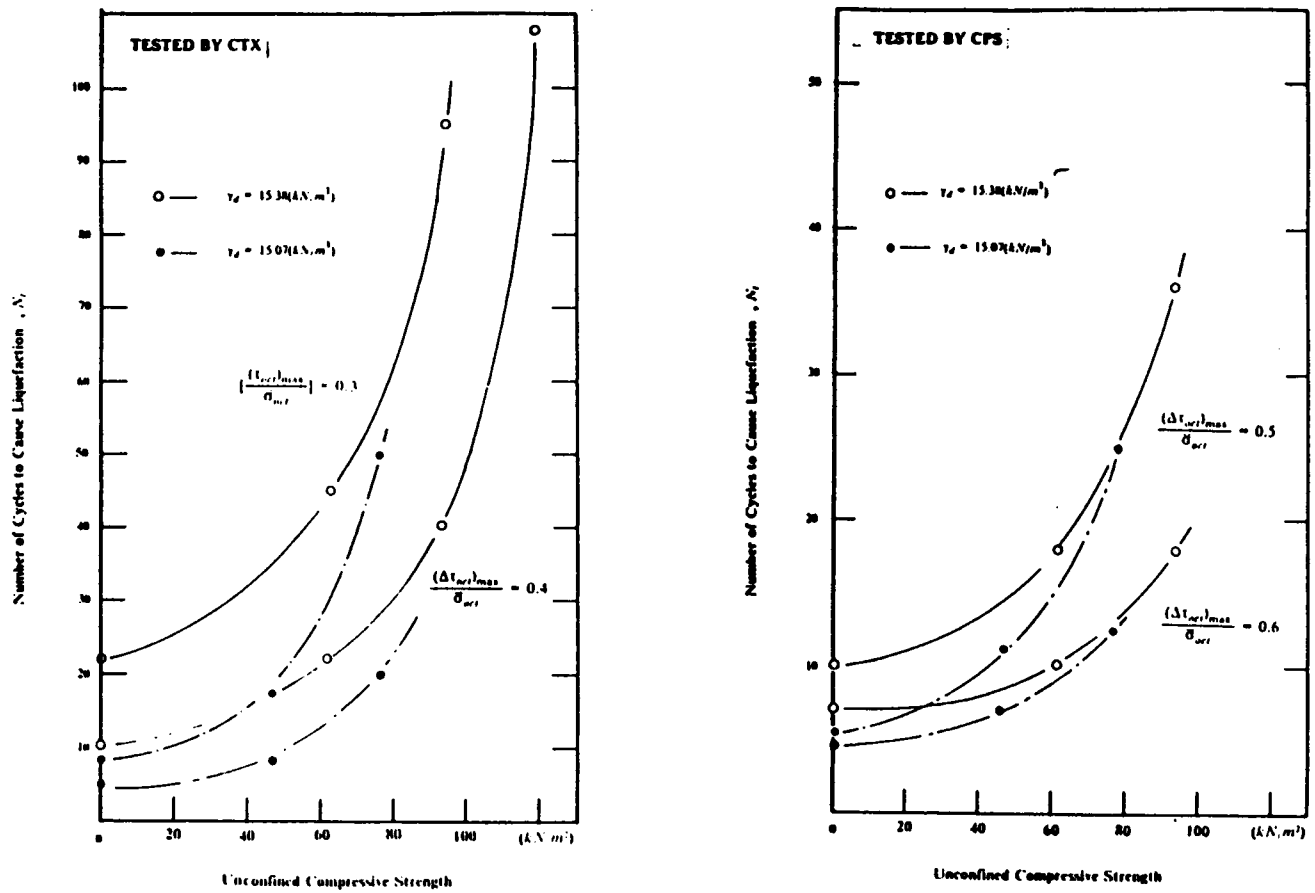

Figure 6.5 Relative Contribution to Cyclic Strength by Density and Cementation.

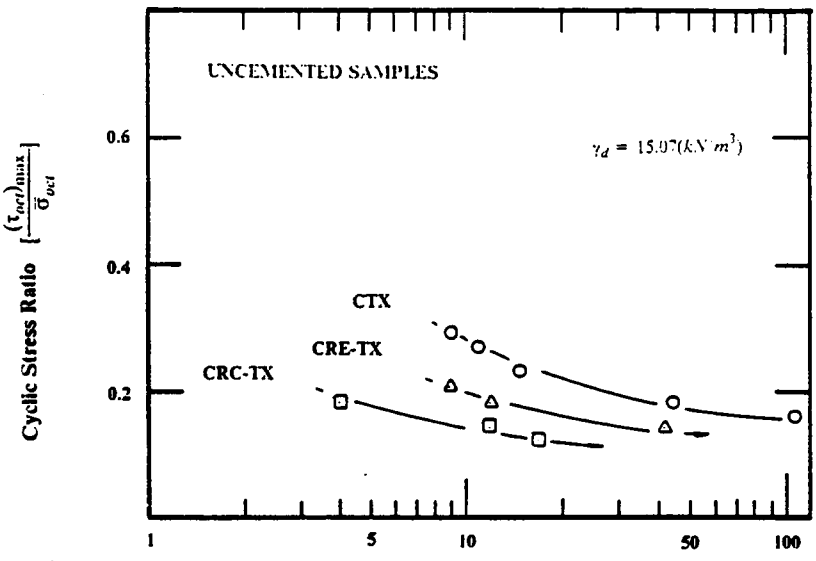

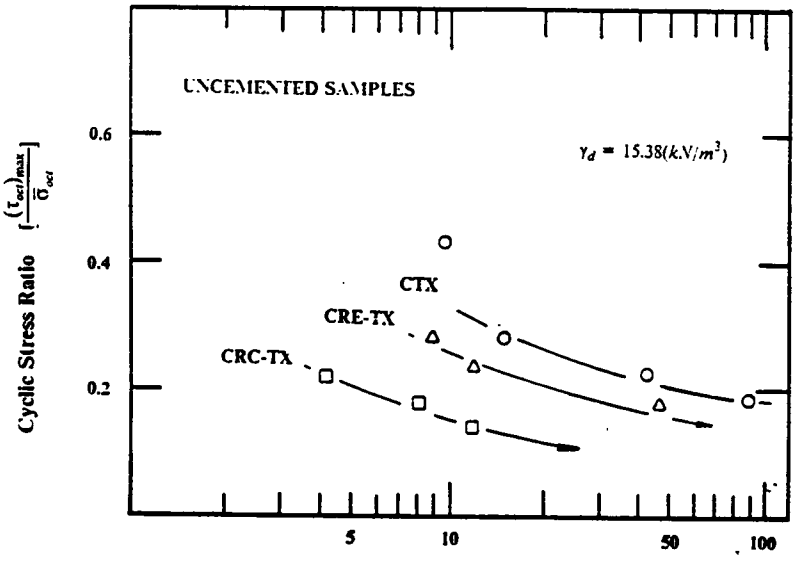

Figure 6.6 Cyclic Strength by the TX Series of Loading for Uncemented Sands.

Figure 6.7 presents similar data to that in Figure 6.6, except that it is for the PS series of loadings. The relationships between the cyclic strengths from the different tests is the same as for the TX series, with the rotational tests yielding the lowest strengths.

A comparison of the cyclic strengths of the TX series of tests against those of the PS tests (Figure 6.6 vs. 6.7) shows that the TX tests consistently give lower strengths. This finding will be discussed further in Chapter VII.

6.3.2 Cemented Sands

The results of the TX series of tests on samples with cementation and no cementation, and for loose and medium densities are shown in Figure 6.8. In this figure, the cyclic strength to cause liquefaction in 10 and 50 cycles is plotted against unconfined compressive strength of the soil. As with uncemented sands, the rotational type tests (CRE-TX and CRC-TX) provide lower strengths, but the effect is reduced as cementation increases. The rotational tests, CRE-TX and CRC-TX, give strengths for the cemented sands on the order of 15 percent to 30 percent less than that of the CTX case, respectively.

Another trend which is observed in Figure 6.8 is that the difference between the results of the uncemented and cemented sands is larger at 10 cycles than it is at 50 cycles to liquefaction. Thus, the suggestion is that the effect of cementation will be larger in greater levels of seismic shaking.

6.4 Pore Pressure Development

6.4.1 Uncemented Sands

Nondimensionalized pore pressure generation curves are useful for comparing the results of different types of tests. In this case, the excess pore pressure measured in a test is divided by the initial effective hydrostatic stress, and plotted against the number of cycles in the test divided by the

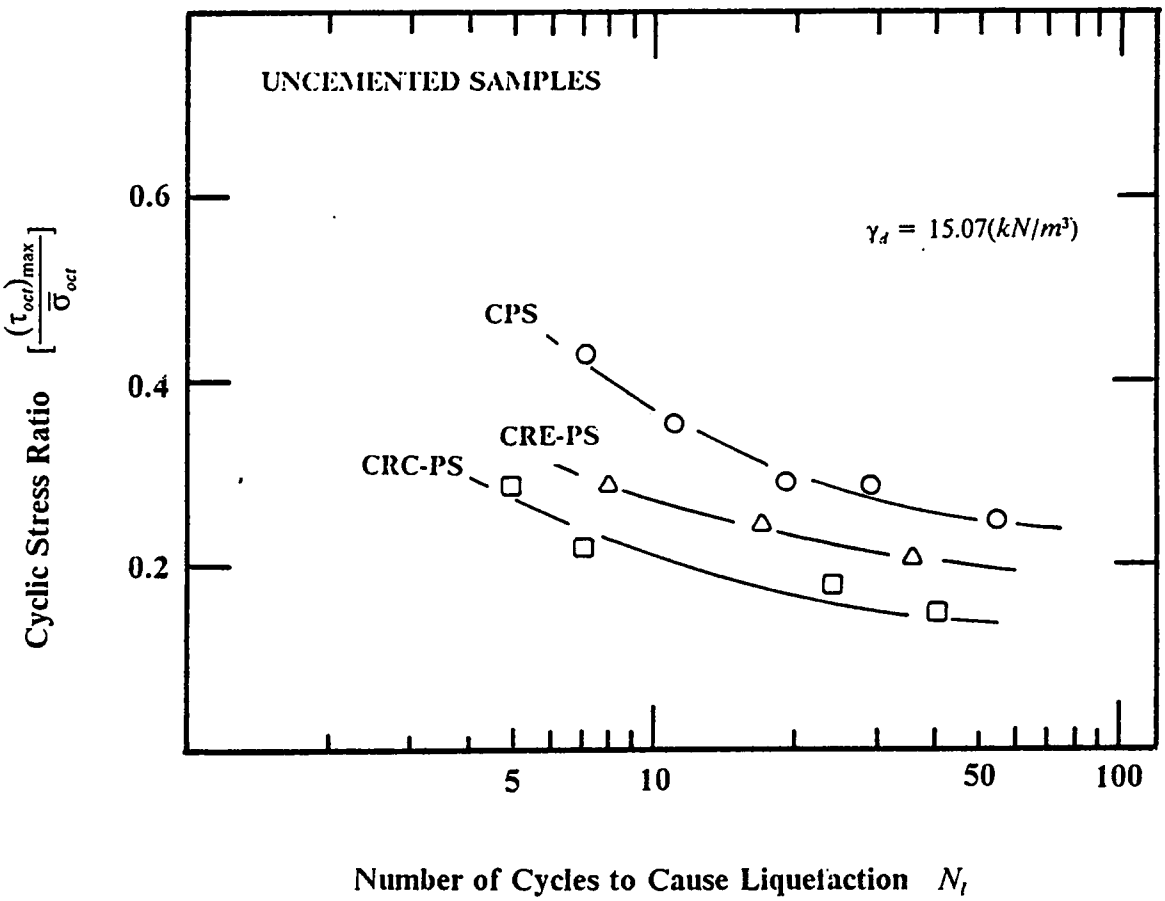

Figure 6.7 Cyclic Strength by the PS Series of Loading for Uncemented Sands.

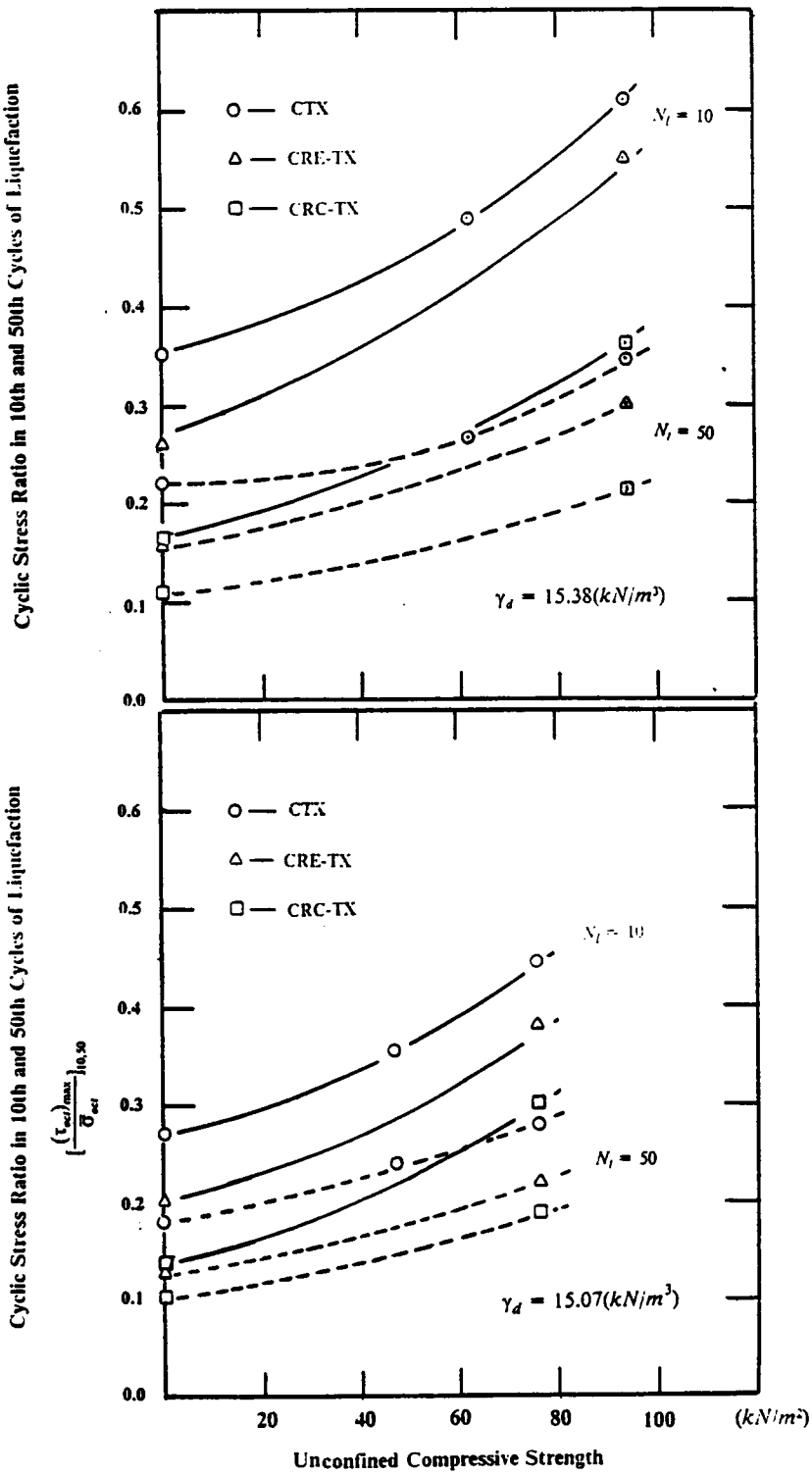

Figure 6.8 Difference in Cyclic Shear Stress Ratios in 10 and 50 Cycles among the TX Series of Loading.

number of cycles in the test to liquefaction. Figure 6.9 shows typical pore pressure generation curves for the CTX, CPS, CRE-TX, and CRC-TX tests on uncemented loose sands at low stress ratios. All of the curves are very similar, showing a convex shape in the early stages followed by an ascending straights line until initial liquefaction.

The effect of stress level on CPS tests is shown in Figure 6.10. As the stress ratio increases the pore pressure curve tends to become more convex in shape. This same trend is observed for the other stress paths and densities.

6.4.2 Cemented Sands

The pore pressure generation curves for cemented sand tested by CTX, CRE-TX, CRC-TX, and CPS are shown in Figure 6.11 for a stress ratio of about 0.3. All of the curves tend to be similar, showing a moderately convex shape.

The effect of high stress level on the CPS tests is shown in Figure 6.12. The pore pressure generation curves obtained with stress ratios of 0.636, 0.707 for cemented loose samples, and 0.848 for a cemented medium dense sample show jumps or discontinuities. These jumps are thought to be due to sudden breakage of the cementation in the soil structure due to higher stress ratio; test results for lower stress ratios do not show these types of features.

6.5 Relationship Between Pore Pressure Development And Octahedral Shear Strains

In the previous discussion, pore pressure development in the test results is presented in a conventional format. In this section we will consider the results in terms of a more general plot. The form of the plot involves pore pressure ratio versus the octahedral shear strain that develops in a test. The octahedral shear strain is defined as :

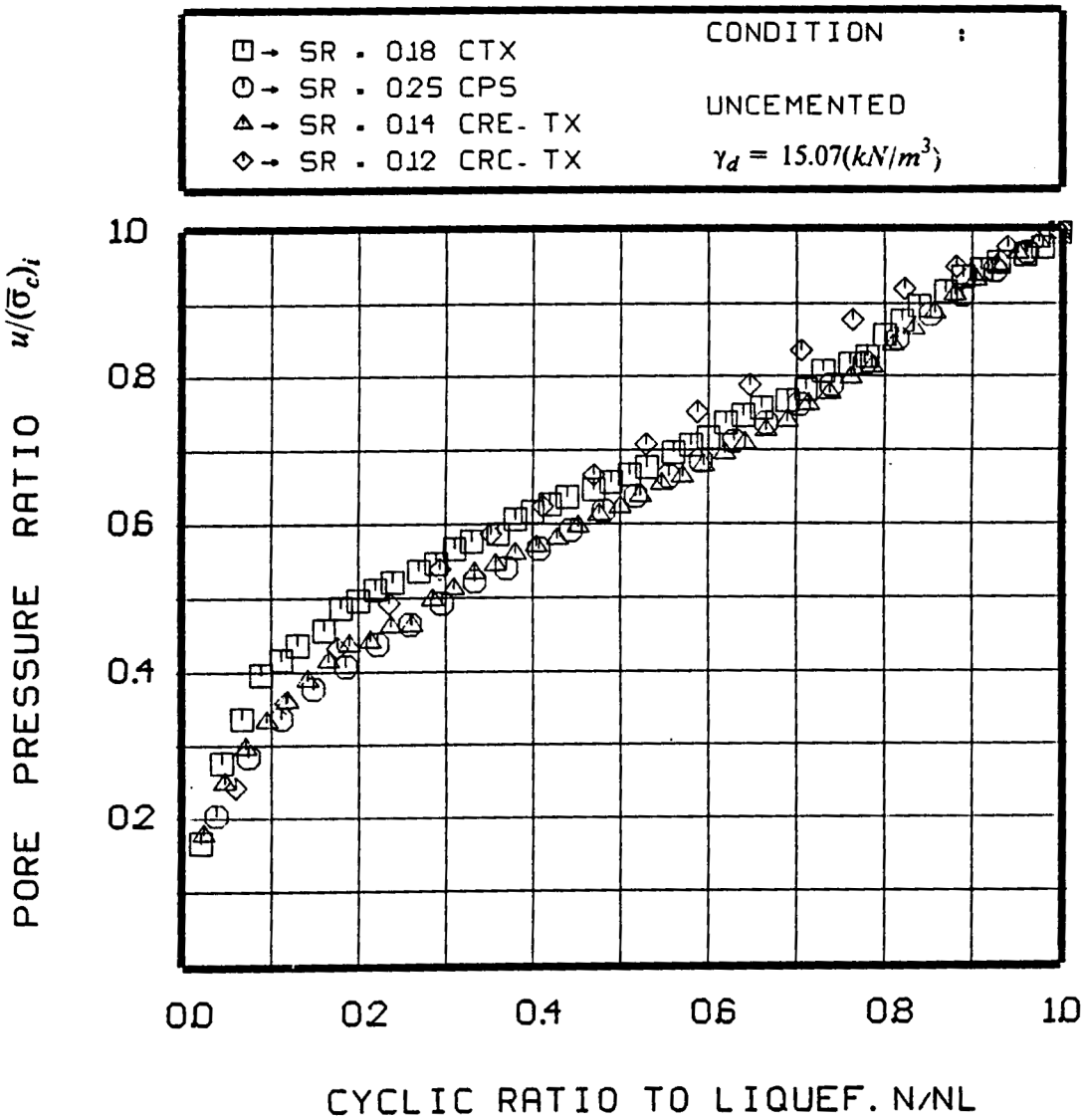

Figure 6.9 Typical Pore Pressure Generation Curves of Uncemented Sands at Low Stress Ratios.

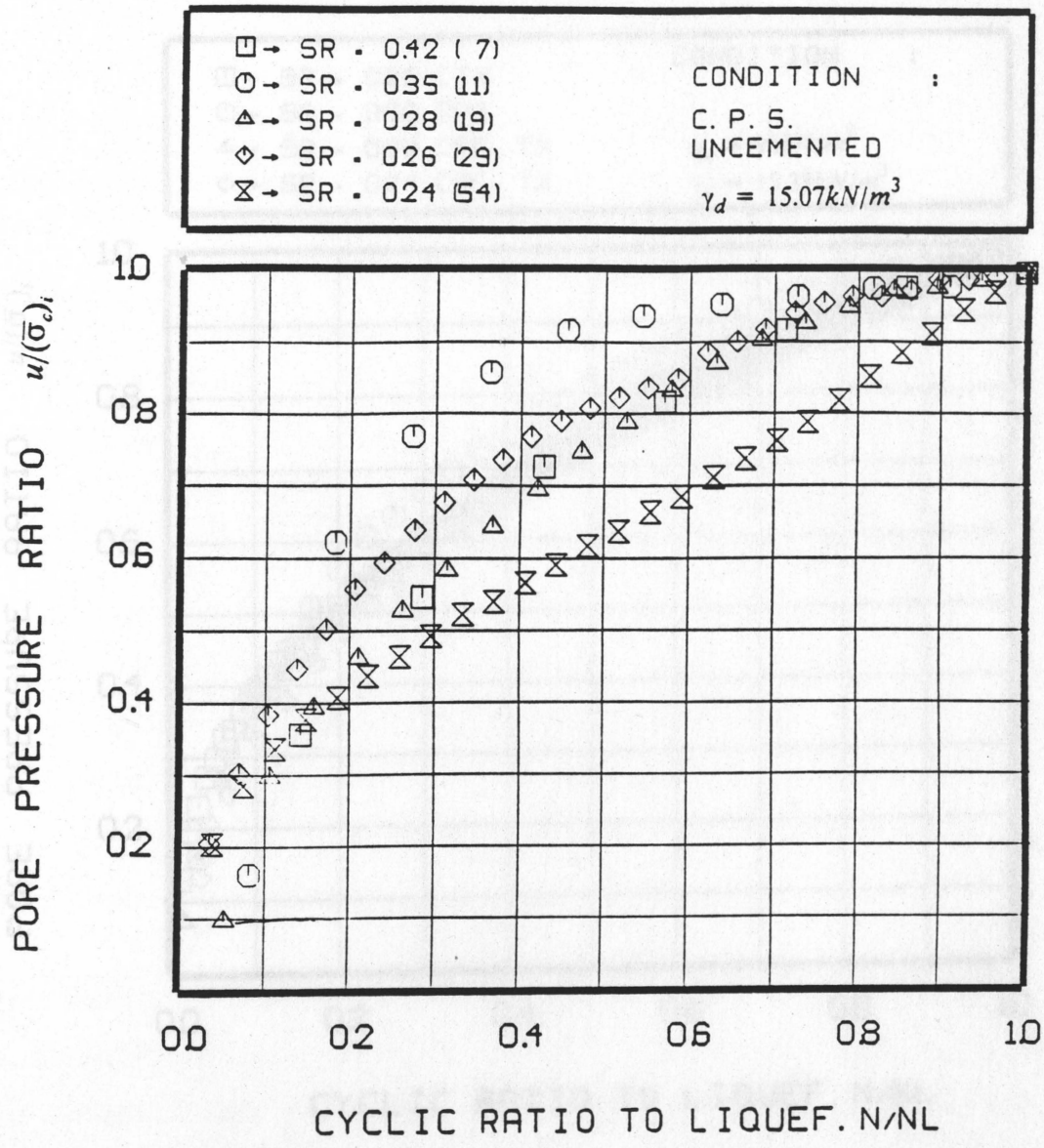

Figure 6.10 Pore Water Pressure Generation Curves in CPS Tests on Uncemented Sands.

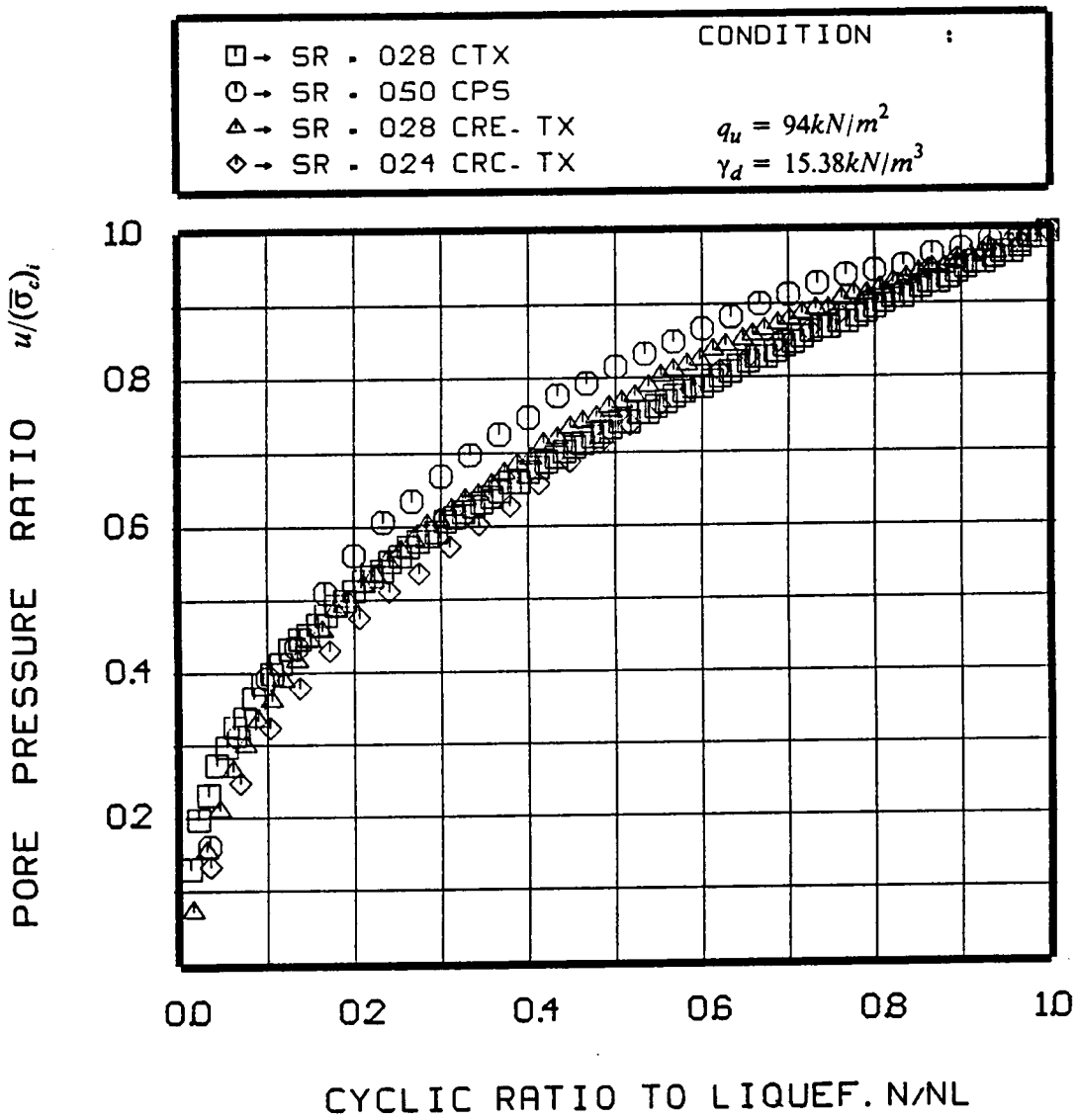

Figure 6.11 Typical Pore Pressure Generation Curves of Cemented Samples.

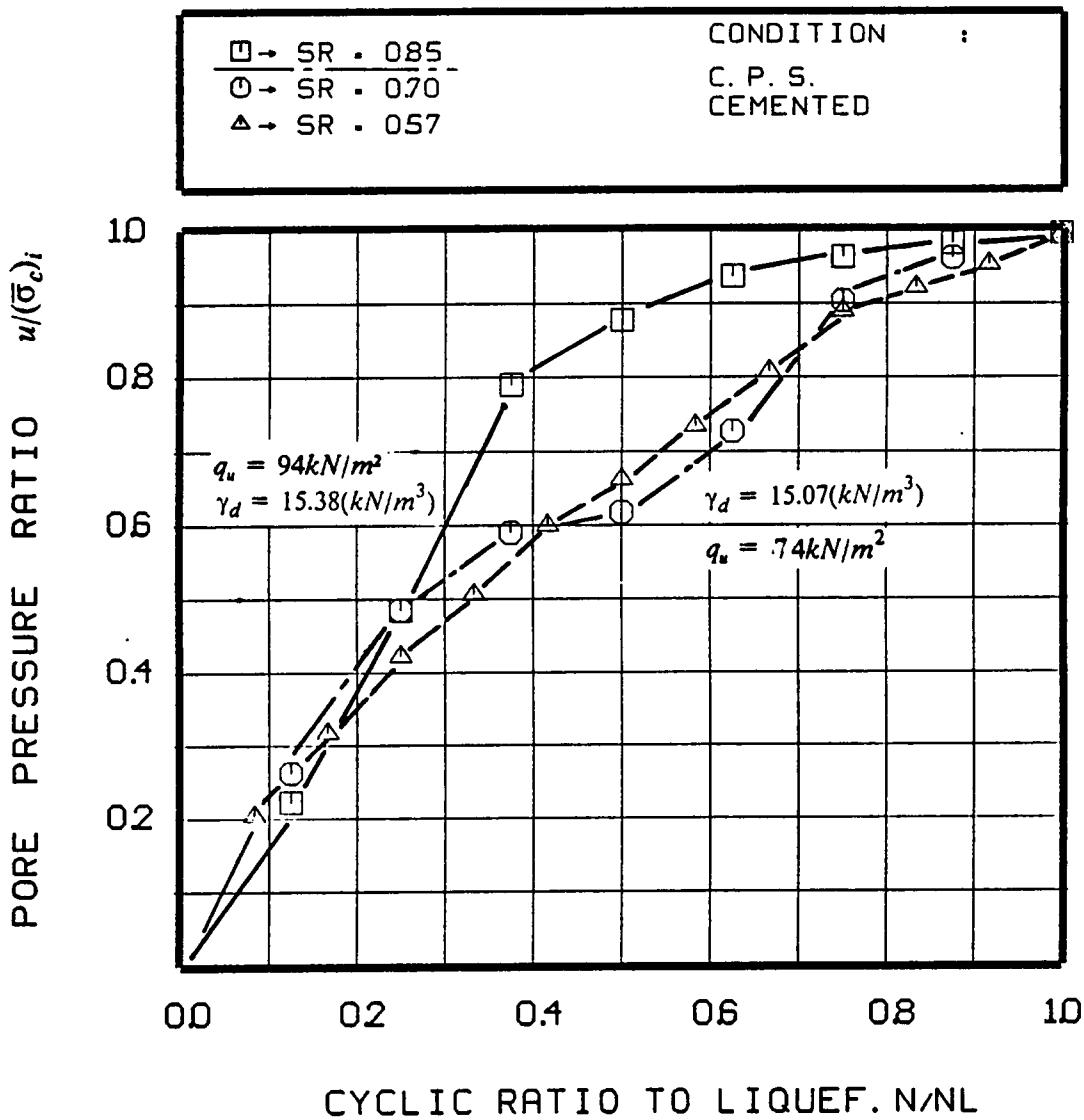

Figure 6.12 Discontinuities in Pore Pressure Generation Curves on CPS.

$$\gamma_{oct} = \frac{2}{3} \times \sqrt{(\varepsilon_1 - \varepsilon_2)^2 + (\varepsilon_2 - \varepsilon_3)^2 + (\varepsilon_3 - \varepsilon_1)^2}$$

The octahedral shear strain is considered appropriate as a parameter defining the response of the soil in these tests since it brings a measure of the strain in all three principal directions, not just one as is the case in most definitions.

6.5.1 Uncemented Sands

In Figure 6.13, the pore pressure ratio is plotted versus the octahedral shear strain for a series of tests with different stress paths. The tests were selected so that they represent cases where the number of cycles to liquefaction is in the range of 15. This means that the numbers of the cycles to liquefaction in the tests are : (1) similar in magnitude; and, (2) small enough to model the number of cycles normally encountered in a earthquake. The pore pressure curves are all very similar, and show a gradual trend in development of shear strains as the pore pressure increases towards initial liquefaction. In the case with a density of 15.07 kN/m^3, the octahedral shear strain reached at a value of about one percent when initial liquefaction occurs, and this is seen to be independent of the stress path. When the density is 15.38 kN/m^3, liquefaction is reached at an octahedral strain of about 0.4 percent.

When the number of cycles to initial liquefaction increases, the strains tend to develop more slowly, and initial liquefaction can occur with much less than one percent strain and the shape of the curve changes. In Figure 6.14 results for CTX tests with the number of cycles to liquefaction of 45 for a loose sand and 40 and 88 for medium dense sand are compared to that for a CTX test with small cycles to liquefaction.

6.5.2 Cemented Sands

The relationship between pore pressure ratio and octahedral shear strain for cemented sands is different than that for uncemented sands as can be seen by comparing the data in Figure 6.15 and

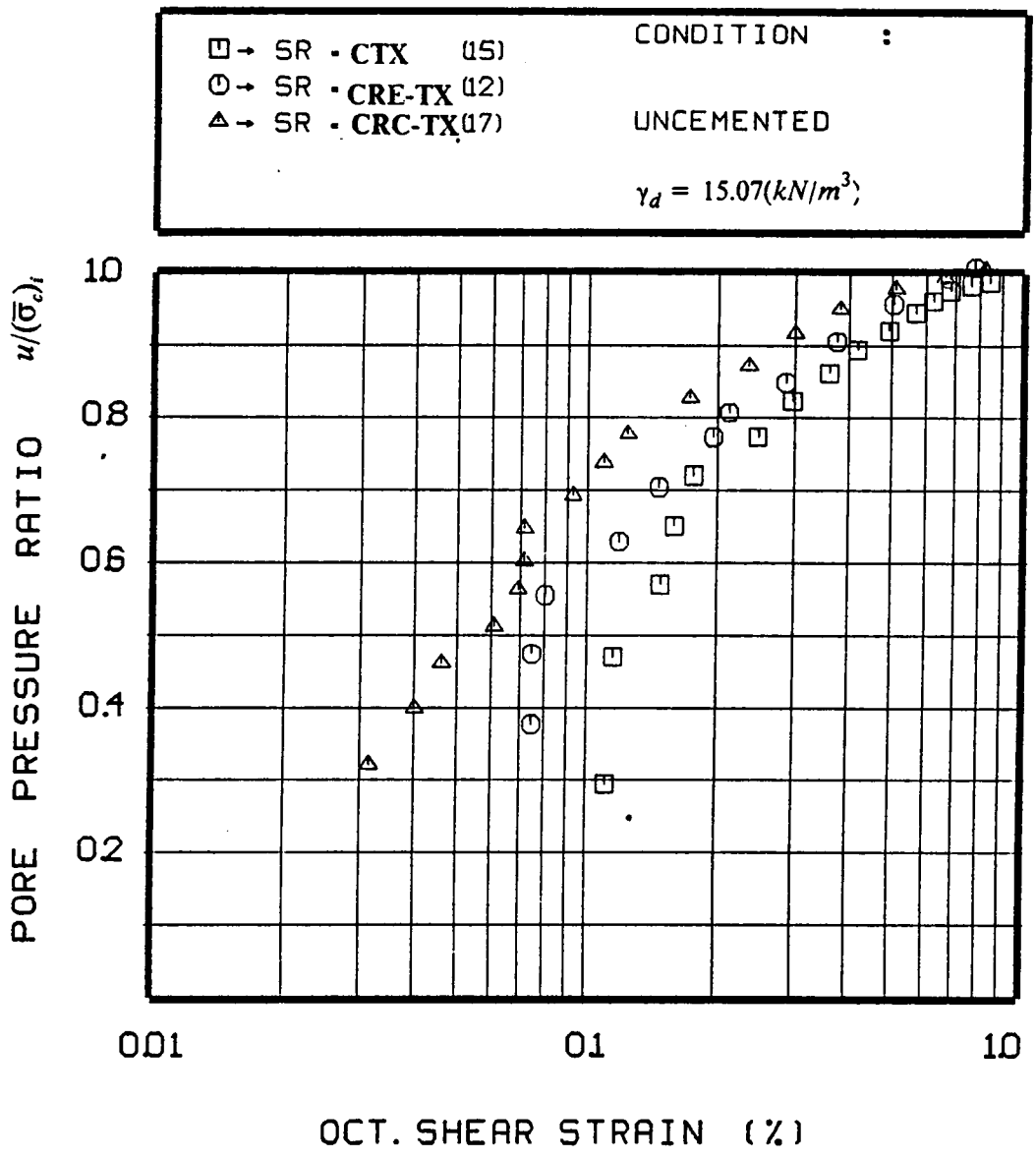

Figure 6.13 Relationship between Pore Pressure Development and Octahedral Shear Strain of Uncemented Samples at Small Numbers of Cycles to Liquefaction.

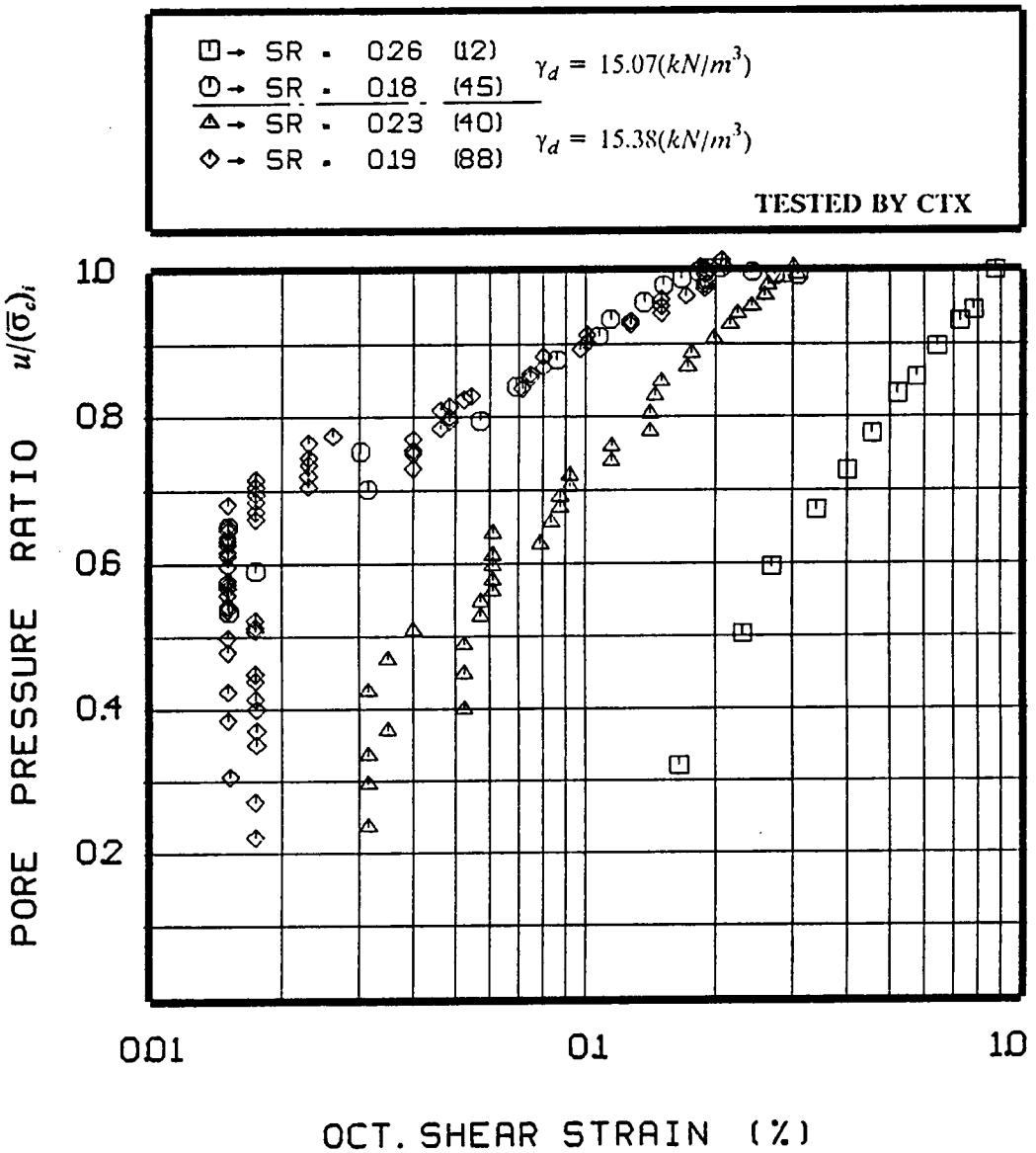

Figure 6.14 Relationship between Pore Pressure Ratios and Octahedral Shear Strain for Uncemented Samples at Large Numbers of Cycles to Liquefaction.

6.16 to that for uncemented sands in Figure 6.14. The cemented sands show that the octahedral shear strains in these materials develop very slowly as the pore pressure ratio rises to values as high as 0.8. After this, the octahedral shear strains increase rapidly with small change in pore pressure ratio. The fact that the form of the pore pressure curve in this diagram is so different from that of uncemented sands makes this type of response a type of signature for cementation in sand.

Interestingly, regardless of the type of stress path, level of stress ratio or number of cycles to liquefaction, initial liquefaction tends to occur at 0.2 to 0.4 percent octahedral shear strain. This type of consistent behavior might be used in further studies to develop a new means for predicting pore pressure development in cemented sands.

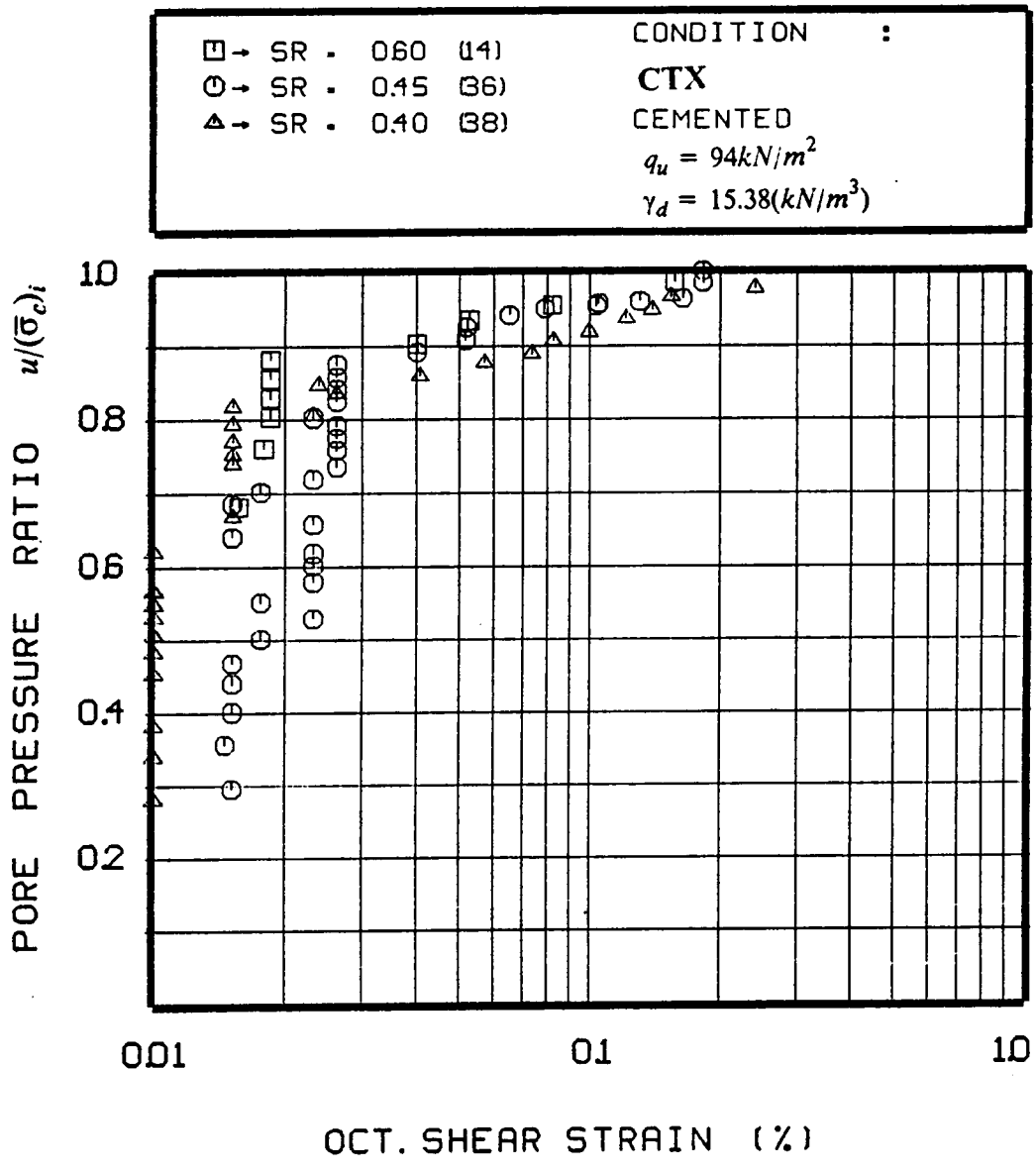

Figure 6.15 Typical Relation between Pore Pressure Ratios and Octahedral Shear Strain for Cemented Samples on CTX.

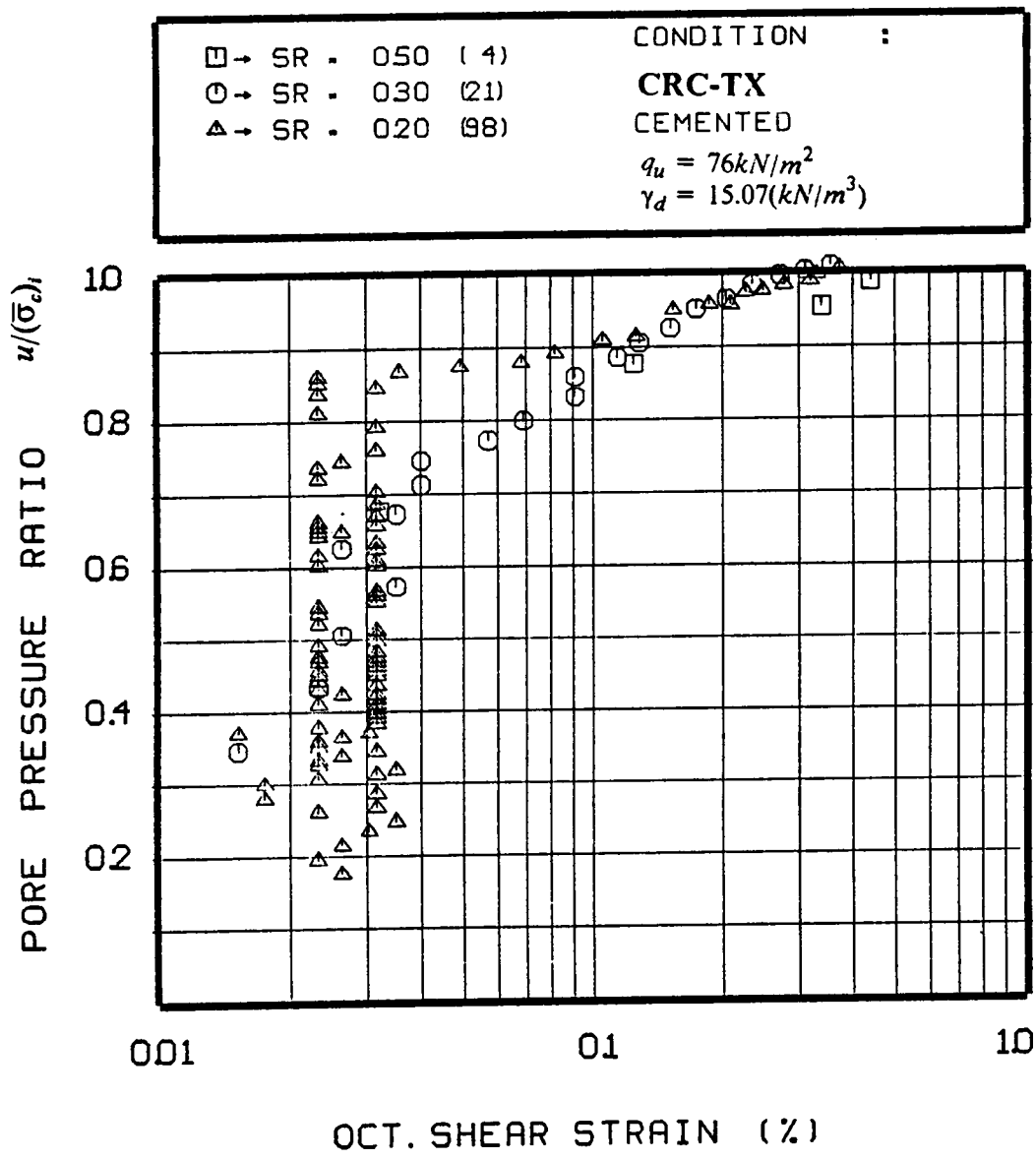

Figure 6.16 Typical Relation between Pore Pressure Ratios and Octahedral Shear Strain for Cemented Samples on CRC-TX.

CHAPTER VII

DISCUSSION OF TEST RESULTS

7.1 Liquefaction Resistance Determined in DCSVT1 Using the CTX Loading on Cemented Sands Versus That From the Conventional Triaxial Device

One of the motivations for undertaking the design and fabrication of the DCSVT1 was to ascertain if stress concentrations in the conventional triaxial test caused premature failure of cemented sand samples, and hence, led to an underestimation of the liquefaction resistance of these soils. In Figure 7.1 the stress ratios from liquefaction tests in both cubical and triaxial devices are plotted versus the number of cycles required to produce liquefaction for cemented samples. The samples have comparable densities and strengths.

The tests performed in the cubical device yielded consistently higher numbers of cycles to liquefaction, although the degree of this effect is greater at high stress ratios than at low ones. The greater liquefaction resistance developed in the tests with the DCSVT1 supports the notion that stress concentration effects are minimized in this apparatus. The fact that the differences in the results are greatest at high loads is also consistent with this idea since stress concentrations would have more impact when the loads are greater, and, thus, lead to lower strengths for the triaxial tests relative to those from the DCSVT1.

It may be remembered that comparisons of test results for uncemented sands as obtained from the DCSVT1 and triaxial tests showed that for pluviated samples, the DCSVT1 also gave higher liquefaction resistances than the triaxial test. However, the differences in this case were not as large

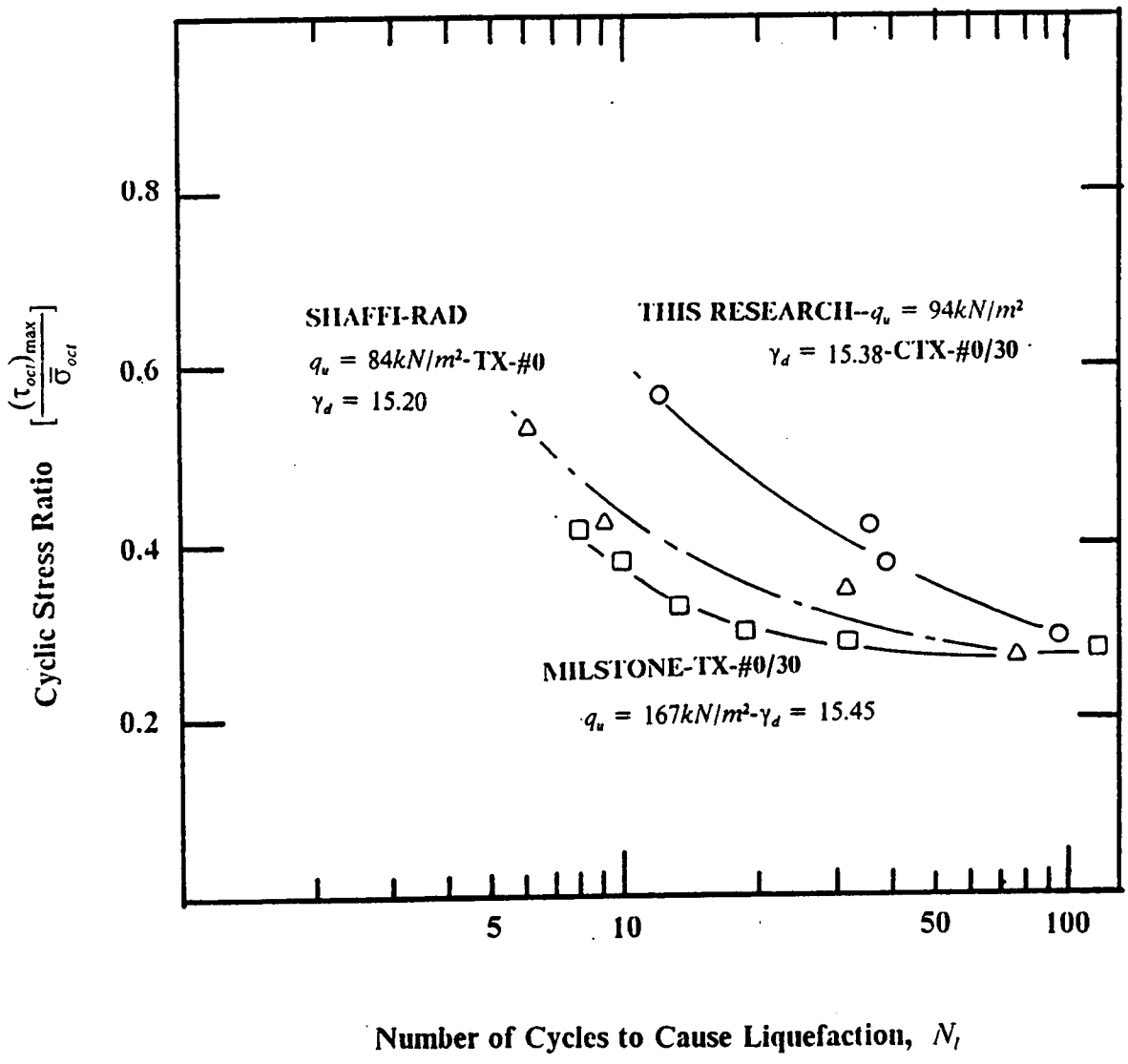

Figure 7.1 Cyclic Strengths of Cemented Sands with DCSVT1 and Conventional Triaxial Device.

as observed for the cemented sands. This seems reasonable since stress concentration effects are likely to be more prominent in cemented sands than uncemented sands.

7.2 Liquefaction Resistance in Cyclic Pure Shear Versus Cyclic Triaxial Shear Loadings

As was explained in Chapter III, the cyclic pure shear stress path differs from that of the cyclic triaxial shear in that no changes occur in mean normal stress when the shear loading is applied, while this is not the case in the triaxial loadings. The change in the mean normal stress occurs in the triaxial test on each loading cycle, and because the soil sample in the test is saturated, the change in the mean normal stress is directly reflected in a change in pore pressure.

In Figure 7.2, the stress ratios from CTX and CPS tests for uncemented and cemented samples with comparable conditions are plotted versus the number of cycles to liquefaction. The CPS tests consistently yield higher liquefaction resistances than the CTX tests for both cemented and uncemented sands. This can be explained in terms of the lower excess pore pressures that develop in the CPS tests. This observation is not surprising. Similar behavior is found when comparing conventional simple shear and triaxial liquefaction results, and, although the stress conditions in the simple shear test are not completely understood, it is accepted that the loading in this device applies very little, if any, mean normal stress increase during cyclic loading. Because the lateral stress conditions in the simple shear test are not fully understood, the stress ratio is defined in terms only of the cyclic shear and the effective vertical stress applied to consolidate the soil:

$$\text{Stress Ratio} = \frac{\tau}{(\bar{\sigma}_v)_i} \qquad \text{(Simple Shear Test)}$$

Making assumptions about the degree of lateral stress generated in the simple shear test allows one to theoretically relate the simple shear stress ratio to that of the triaxial test (Seed and Peacock, 1971). However, the theoretical equivalency has been shown to be inconsistent with actual test results, and this is in large part attributed to the fact that less pore pressure develops in the simple

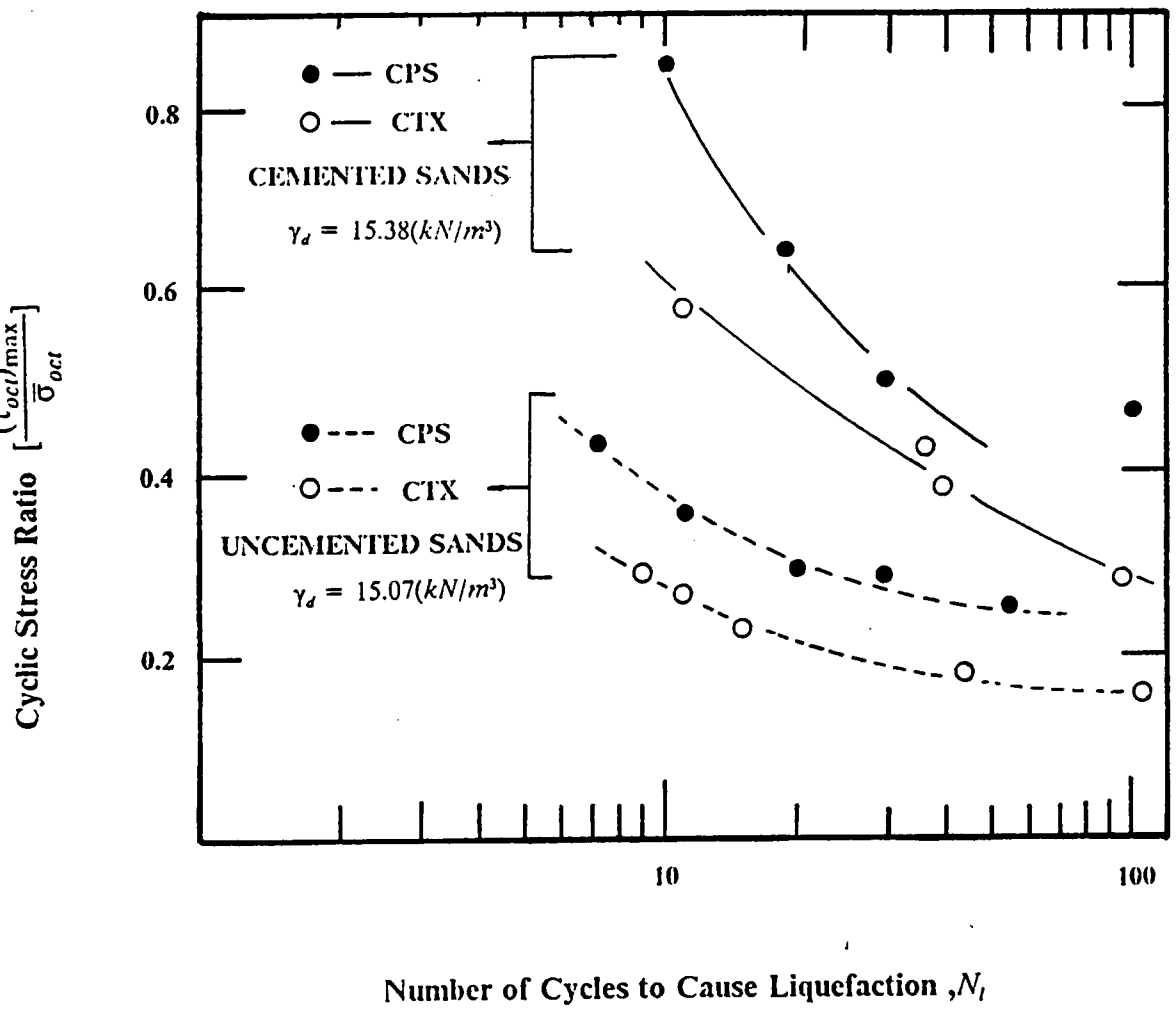

Figure 7.2 Cyclic Strengths of Cemented Sands Using CTX and CPS.

shear test than in the triaxial test as a result of the difference in mean normal stress changes in the two tests. In the end, an empirical correction is typically used to generate a correlation between the tests. The result allows for about a 15 percent modification on the theoretical correction for the triaxial test results to make them the same as simple shear, with the 15 percent factor caused by the reduced pore pressure in the simple shear test.

In Figure 7.2 the CPS liquefaction resistance at any number of cycles and for either uncemented or cemented sand is 22 to 33 percent higher than those for CTX tests. Note that no theoretical correction is needed to relate the CPS to the CTX tests since the use of the octahedral stress ratio concept allows for a direct comparison, and in terms of directly known stresses. The differences in the CPS and CTX test results are fully accounted for by the differences in stress paths in the two tests. This shows that if an earthquake induces a CPS type of loading and not a CTX type, the CTX result will underestimate the soil strength. Of course, even the CPS loading simplifies the problem since it is only representative of a one-dimensional wave passage through the soil.

7.3 Liquefaction Resistance in Complex Loading Versus Simplified Loading

As was shown in Figure 6.6 to 6.8, the cyclic tests with rotational effects in the loading (CRE-TX, CRC-TX, CRE-PS, CRC-PS) lead to a lower liquefaction resistance for either uncemented or cemented sands relative to the CTX or CPS tests. This finding for uncemented sands is consistent with that of other investigations where multiaxial loading is used (see discussion in Chapter III). Also, it is observed that the "TX" series of tests in all cases leads to lower strengths than that of the comparable "PS" series of tests. In table 7.1 the liquefaction strengths of the various tests for the condition where the soil liquefied in 10 cycles is given relative to that of the CTX test.

The following conclusions can be drawn:

Table 12. 7.1 Relative Strengths in Different Types of Stress Paths.

UNCEMENTED SAND

γ_d (kN/m^3)	CRE-TX/CTX	CRC-TX/CTX	CPS/CTX	CRE-PS/CTX	CRC-PS/CTX
15.07	-25	-42	+32	0	-25
15.38	-27	-50	+22	-	-

CEMENTED SAND

15.07	-23	-33	+33	-	-
15.38	-15	-41	+25	-	-

1.) Reduction of strengths due to the rotational loading are greater for uncemented sands than cemented sands.

2.) The CRC series of loadings causes a greater reduction in strength than does the CRE loading.

3.) The reduction in strengths in the case of CRC loadings are as high as 50 percent.

The reasons for the effects of the rotational types of loading can only be speculated upon. One clear difference in the situation with the more complex paths is that the principal stresses are rotating and the planes upon which the maximum shear is applied also rotate within the sample during cyclic loading. In either the CTX or CPS type of loading, the maximum shear planes only have one orientation.

The fact that the CRC series of tests has a greater effect than the CRE series is apparently caused by the application of the same maximum shear on all planes in the test. The CRE loading has a less severe shear in some directions than others, while that in the CRC case is uniform.

Given the lower resistance in the rotational loadings, it then follows that where soils are subjected to the simultaneous passage of different wave types, liquefaction is more likely to occur than where only a one-dimensional wave passes. If this were the only effect to influence the behavior of sands under seismic loading, and we assumed that in practice we always used one-dimensional type tests to define the strength of the soil, our predictions of liquefaction should be on the unsafe side where the multiwave loading occurs. However, there are many other factors which are as important as multiwave effects that make simple conclusions about predicting liquefaction resistance inadvisable. Actually, the trend in practice is towards the use of empirical correlations based on the results of in-situ tests for predicting liquefaction potential in sands. However, the effects of the multiaxial loadings are important to understand in explaining differences in soil responses at different sites. It is clear based on the results of the tests of this investigation that a sand can undergo liquefaction at some sites where the multiaxial loading occurs, while the same sand under the same

conditions may not liquefy if one-dimensional loading is the primary factor. This information helps explain some of the scatter often seen in empirical type correlation with observed field behavior.

7.4 Pore Pressure Development Patterns

Pore pressure development responses in the tests are depicted in Chapter VI in terms of two types of nondimensional plots. In the first, the pore pressure ratio is plotted against the nondimensionalized number of cycles in the test. In the second, the pore pressure ratio is plotted versus octahedral shear strain that develops in the test. The following trends are observed:

1.) As observed by Milstone (1985), the trend of pore pressure development for a cemented sand is affected by the stress level applied in a test.

2.) The pore pressure ratio plots against number of cycles to liquefaction tend to be somewhat different for the "PS" series of tests than those for the "TX" series of tests.

3.) The pore pressure ratio plots against octahedral shear strain of uncemented sand at small number of cycles to liquefaction are different than those at large number of cycles to liquefaction.

4.) The relationship between pore pressure ratio and octahedral strain for cemented sands is different than that for uncemented sands.

At high stress ratios for cemented sands, sudden changes in pore pressure generation curves are observed. These are thought to be caused by the fracture of the cemented soil structure due to high stress level.

7.5 Simplified Pore Pressure Modeling in Cemented Sands

The simplified model proposed by Seed and Martin (1976) for uncemented sands is discussed in Chapter II. Basically, this model proposes an empirical curve fitting for the relationship between pore pressure ratio, and nondimensionalized number of cycles to liquefaction. The relationship proposed by Seed and Martin (1976) has a general form, although they note that the constants which define its actual location can be selected on the basis of average behavior for uncemented sands. The equation and the constant for uncemented sands is as follows:

$$\gamma_u = \frac{1}{2} + \frac{1}{\pi} \arcsin(2 \times \gamma_N^{1/\alpha} - 1)$$

where $\alpha = 0.7$ is the average value.

Because of nature of the equation, the curve using the recommended constant is " S " shaped. In the case of cemented sands this form of curve does not fit most of the behavior types observed. The " S " shaped curve tends to be applicable only for very weakly cemented sands, low stress ratios, and CTX types of loadings. Other conditions in cemented sands tend towards a simple convex curve with no reversals in curvature; therefore, the nature of the curves is not like that of the Seed and Martin model (1976).

All pore pressure generation curves for cemented samples are plotted in Figure 7.3. These curves converge in a band, and a simplified model for this response can be developed. The relationship is:

$$r_u = a \times r_N^{1/\alpha}$$

where, r_u is the pore pressure ratio, denoted as $u/(\overline{\sigma}_c)_i$

r_N is the cyclic ratio, denoted as N/N_l

a and α is coefficient.

Values of $\alpha = 4$ or 1.5 provide bounds to the upper and lower curves for all of the data in Figure 7.3. An $\alpha = 2.1$ provides a fitting of the center of the response data (Figure 7.4). There is a very good match between the predicted and observed response. Apparently, the simplified equation for pore pressure ratio can be used to make accurate prediction of the pore pressures for cemented sands.

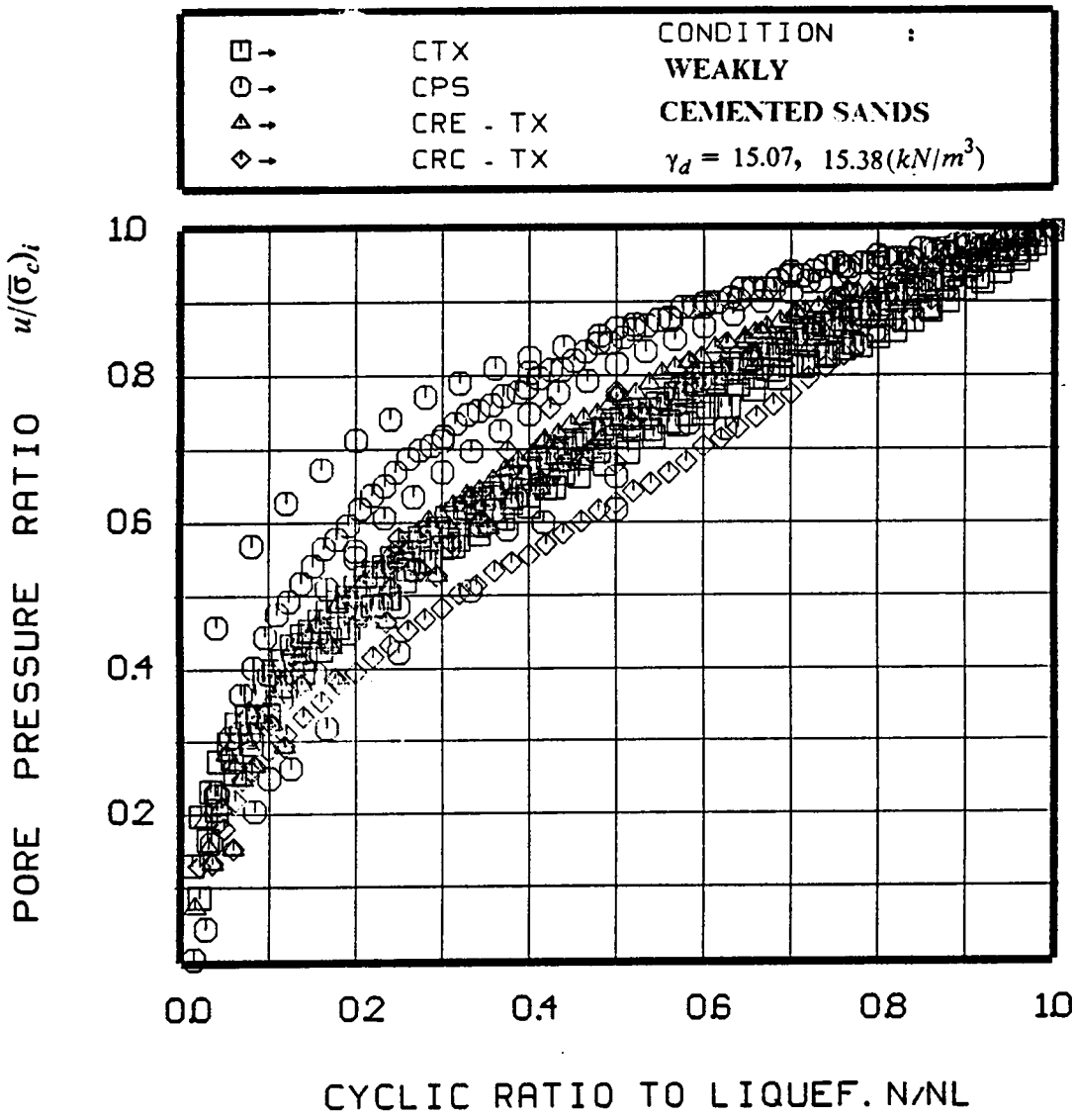

Figure 7.3 Summary of Pore Pressure Ratios vs. Cyclic Ratios for Cemented Sand Tests.

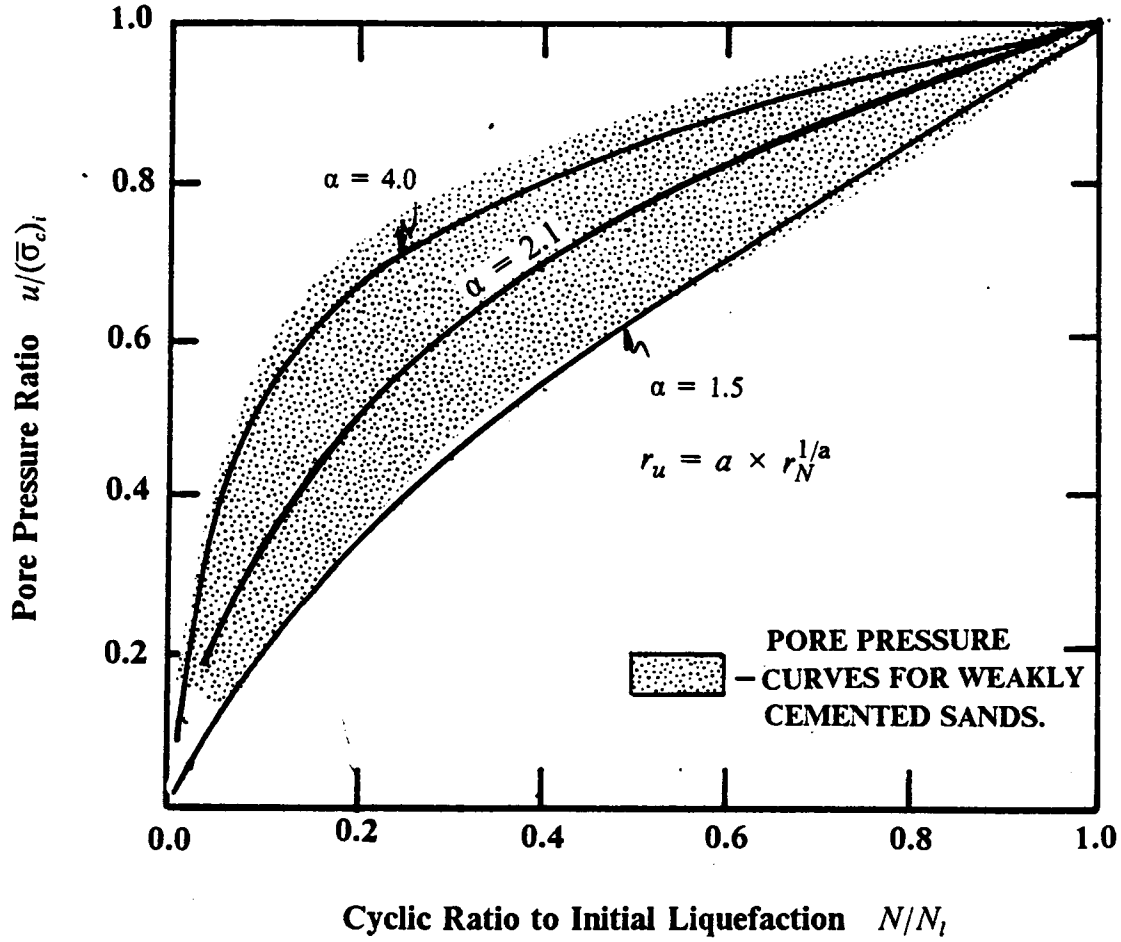

Figure 7.4 Predicted Pore Pressure Ratios with the Simplified Equation.

CHAPTER VIII

SUMMARY AND CONCLUSIONS

This investigation was undertaken with two main objectives. The first involves the development of a three-dimensional testing device to allow for better modeling of the effects of liquefaction due to earthquake loading on soils, particularly cemented soils. The second concerns sorting out the effects of a range of parameters on liquefaction of cemented sands when such materials are subjected to earthquake loadings.

Testing to model the effects of earthquakes on soils has largely concentrated on attempting to simulate the passage of a one-dimensional wave through the soil. This is usually done via a conventional triaxial device in which stresses are changed along only one axis, or in a simple shear device which allows alternating application of shear stresses on the horizontal plane of a soil sample. Both of these devices have advantages, but they are limited to modeling only a one-dimensional wave effect, and can cause stress concentrations in a cemented specimen.

In some cases it is enough to simulate an earthquake by modeling only the case of a one-dimensional wave passing through the soil. However, this is generally not true, since there is evidence that soils in many cases are subjected to multiaxial loading during a seismic event. Some studies of this type of loading have been performed, but the devices used have not allowed a full study of the problem. The evidence from the reported multiaxial loading of soils suggests that soils liquefy at lower stress levels if multiaxial loading is involved. Thus, if we were to assume that we based on practice of predicting liquefaction resistance only on simple tests which ignore multiaxial loading, our conventional prediction would be unconservative. Of course, there are many other factors that tend to complicate this picture, and these serve to counter the effects of not modeling the multiaxial loading. Nevertheless, it is important to understand the effects of multiaxial loading

to help explain why certain sites may liquefy, when sites with very similar soil and water conditions do not.

The three-dimensional device developed in this study uses a stress controlled system to load the soil. Each of the three principal stresses can be controlled independently, and , as a result, a wide range of loading paths can be applied. In addition to the cubical shear box itself, one of the keys to the apparatus is the implementation of a microcomputer control system for the device that controls the application of the stresses, and automatically monitors the information from the test. The system can be operated with suitable accuracy to load rates of 2 to 3 cycles per second, fast enough for the modeling of an earthquake.

A series of standardized loading paths were designed for the test program with increasing levels of complexity. At the simplest level, the test is designed to model the stress path of the conventional triaxial test. Experiments performed in this mode are useful since the results can be compared to those obtained in the conventional tests. Other forms of cyclic stress paths involved pure shear, and a series of what are referred to as rotational elliptical and rotational circular of either the pure shear or the triaxial mode. The pure shear test loading is distinct in that only shear stresses are cycled and no normal stress changes occur. This is not the case in the triaxial test. The rotational elliptical path attempts to model the situation where the cyclic soil stresses along the horizontal axis are twice those of the vertical axis. The rotational circular path represents the circumstances where the cyclic stresses in the soil mass are equal along all axes. Depending upon the type of earthquake, it may be said that one of these stress systems will simulate the effects. For example, the conventional triaxial or pure shear tests addresses the case where the one-dimensional wave predominates. On the other hand, the rotational elliptical or circular path models earthquake conditions where multiaxial loading occurs.

The complex stress paths are further subdivided as being tied to either the triaxial or pure shear modes. In the triaxial mode, an increment of mean normal stress is included in the loading which

is the same as that used in the conventional triaxial test. In the pure shear mode, no increment of mean normal stress is added to the loading, as is the case in a pure shear test.

A comprehensive series of tests were performed to define the range of strains over which the three-dimensional shear box could be expected to achieve accurate results. It was found that the device worked well until the sample reached initial failure, after which the measured strains became unrepresentative of the sample behavior as a whole. Fortunately, this was found to involve a condition where the strain levels were in the range of five or more percent. Such conditions are beyond the interest of this work, since the main interest is in initial liquefaction, and this occurs at strain levels of one to two percent.

The production test program with the cubical shear device involved about 100 tests on uncemented and cemented sands. All of the samples for the tests were prepared by pluviation. The cemented sands were created by adding a small amount of Portland cement to the sand before the sand was pluviated into the sample mold. Special procedures were developed to avoid particle segregation during the pluviation process, and it was found that the samples could be prepared with consistent properties. After pluviation, the cemented samples were submerged in water for about 15 days in most cases to allow for wet curing. Both dense and loose densities were prepared as well as weak to strong levels of cementation.

The principal conclusions of the test program are as follows:

1.) The cubical shear box allows for accurate testing of uncemented and cemented sands under a wide range of cyclic loading paths.

2.) The conventional cyclic triaxial test can be modeled using the cubical system, and the results of the two types of tests are in general agreement for uncemented sands.

3.) The cubical shear box shows that cemented sands have a greater resistance to liquefaction than is found in triaxial tests, probably because of stress concentrations that are set up in the cemented sands in the conventional test.

4.) Resistance to liquefaction for either uncemented or cemented sands is higher in pure shear loading than in triaxial loading because the triaxial test induces an increment of mean normal stress in every cycle which causes higher pore pressures than in pure shear.

5.) The stress paths that simulate the passage of more than one wave type through the soil during an earthquake (multiaxial loading) lead to a lowered liquefaction resistance relative to the triaxial or pure shear condition. This applies to both cemented or uncemented sands.

6.) The most severe form of loading is that applied in the rotational circular stress path, apparently because this involves applying equal cyclic shearing to all planes in the sample rather than only one or several as in the case of the other tests.

7.) The complex stress paths using the mean normal stress increment as in the triaxial test consistently yielded lower strengths than those without it. As in the case of the simple tests, this increment causes a rise of pore pressure that does not exist in the pure shear case, and leads to premature failure of the soil.

8.) Special considerations have to be given to the use of simplified pore pressure models for cemented sands since the form of the pore pressure development curves vary depending upon the stress level.

9.) The relationship between the pore pressure ratio and the octahedral strain developed in the sample during a test is different for a cemented sand as opposed to that for an uncemented sand. It is believed that this unique relationship could be used to formulate special models for cemented sands.

Bibliography

(1) Bachus, R.C., Clough, G.W., Sitar, N., Shaffi-Rad, N., Crosby, J., and Kaboli, P., " Behavior of Weakly Cemented Soil Slopes under Static and Seismic Loading Conditions," Volume II , U.S.G.S., Contract No. USGS 14-08. 0001-18380, Report No. 51, July, 1981.

(2) Saxena, S.K. and Lastrico, R.M., " Static Properties of Lightly Cemented sands, " Journal of the Geotechnical Engineering Division, ASCE, No. GT12 Proc. Paper 14259, Dec. 1978, pp 1449-1464.

(3) Frydman, S., Hendron, D., Horn, H., Steinback, J., Baker, R., and Shaal, B., " Liquefaction Study of Cemented Sands, " Journal of the Geotechnical Engineering Division, ASCE, Vol. 106, No. GT3, March, 1980.

(4) Clough, G.W. and Bachus, R.C., " An Investigation of Sampling disturbance in Weakly Cemented Soils, " Proceedings, Eng. Foundation Conference in Updating Subsurface Sampling and In-situ Testing, Santa Barbara, California, January, 1981.

(5) Hamel, J., " Large Scale Laboratory Direct Shear Tests on Desert Alluvium, " Presented in 15th Symposium on Rock Mechanics, Custer State Park, South Dakota, Sept., 17-19, 1977.

(6) Bechwith, G.H. and Hansen, L.A., "The Calcareous Soils of the South Western United States," Presented at ASTM symosium on Calcareous Soils, Ft. Landerdale, Florida, Jan. 20, 1981.

(7) Harp, E.L., Wilson, R.C., Weiczorek, G.F., and Keefew, D.K., " Landslides from the February 4, 1976 Guatemala Earthquakes Implications for Seismic Hazard Reduction in the Guatemala City Area, " Proceedings Second International Conference on Microzonation, San Francisco, California, 1978.

(8) Yamanouchi, T., Mochinaga, R., Gotoh, K., and Murata, H., " Status of Cut-off Slopes in a Pumice Flow Soil Deposit and their Applications to the Design Standards for an Expressway, " Proceedings of the 9th International Conference on Soil Mechanics and Foundation Engineering, Tokyo, 1977.

(9) Yamanouchi, T., " On the Shirasu Distributed in New Zealand, " Shin-Sabo, No. 92, 1974, pp 6-9 (in Japanese).

(10) Sitar, N., Clough, G.W., and Bachus, R.C., " Behavior of Weakly Cemented Soil Slopes under Static and Seismic Loading Conditions, " Report No. 44, The John A. Blume Earthquake Engineering Center, Stanford University, June, 1980.

(11) Shirasu Committee, " Ebina Earthquake and Resulted Foundation Disasters, " Soils and Foundations, Vol. 16, No. 9, 1968, pp 47-59.

(12) Yamanouchi,T., Taneda,S, and Kimura, T.," Damage Features in 1968 Ebino Earthquakes from the Viewpoint of Soil Engineering," Soils and Foundations, Vol. 10, No. 2, June 1970, pp 129-144.

(13) Sowers, G.B. and Sowers, G.F., " Introductory Soil Mechanics and Foundations, " 3rd Edition, MacMillan Company, New York, 1979.

(14) Lee, K.L., " Foundation of Adhesion Bonds in Sands at High Pressure, " Report No. UCLA. Eng. 7586, UCLA, School of Engineering and Applied Science, Los Angeles, California, Oct., 1975.

(15) Seed, H.B., " Evaluation of Soil Liquefaction Effects on Level Ground During Earthquakes," the ASCE National Convention, Philadelphia, ASCE, New York, New York, 1976, pp1-104 or " Recent Development in Evaluating the Potential for Soil Liquefaction and Foundation Failure during Earthquakes, " Proceedings, Inaugural Symposium, John A. Blume Earthquake Engineering Center, 1976, pp 11- 116.

(16) Shaffi-Rad, N. and Clough, G.W., " The Influence of Cementation on the Static and Dynamic Behavior of Sands, " Report No. 59, The John A. Blume Earthquake Engineering Center, Final Report. Contract No. USGS 14-08-0001-19763, Dec., 1982.

(17) Haruyama, M.," Geological, Physical and Mechanical Properties of ' shirasu ' and its engineering classification, " Soils and Foundations, Vol. 13 No. 3, 1973, pp 45-60.

(18) Clough, G.W., Sitar, N., and Bachus, R.C., " Cemented Sands under Static Loading, " Journal of the Geotechnical Engineering Division, ASCE, No GT6 Proc. Paper 16319, June, 1981, pp 799-817.

(19) Murata, H. and Yamanouchi, T., " Dilatancy and Failure Mechanism in the Undisturbed Shirasu, " Vol. 18, No. 2, Soils and Foundations, Jun., 1978, pp 59-67 (in Japanese).

(20) Sitar, N., and Clough, G.W., " Behavior of Slopes in Weakly Cemented Soils under Seismic Loading, " Proceedings, 2nd U.S. National Conference on Earthquake Engineering, Stanford University, 1979, pp 1006-1015.

(21) Salamone, L.A., Singh, H., and Fischer, J.A., " Cyclic Shear Strength of Variably Cemented Sands, " Proceedings of the ASCE Geotechnical Engineering Division Specialty Conference on Earthquake Engineering and Soil Dynamics, Vol. II, Pasadena, California, June, 1978, pp 819-835.

(22) Dupas, J.M. and Pecker, A., " 'Static and Dynamic Properties of Sand-Cement, " 'Jr. of the G.E. Division, ASCE, No. GT3, Mar., 1979.

(23) Poulos, H.G., " A Review of the Behavior and Engineering Properties of Carbonate Soils, " Research Report No. R381, The University of Sydney, School of Civil Engineering, Dec., 1980.

(24) Casagrande, A., " Liquefaction and Cyclic Deformation of Sands- A Critical Review, " Proceeding of the Fifth Pan American Conference on Soil Mechanics and Foundation Engineering, Buenos Aires, Argentina, 1975.

(25) Seed, H.B. and Lee, K.L., " Liquefaction of Saturated Sands during Cyclic Loading, " Jr. of the Soil Mechanics and Foundation Engineering Division, ASCE, No. SM6, Proc. Paper 4972, Nov. 1966.

(26) Lee, K.L. and Seed, H.B., " Dynamic Strength of Anisotropically Consolidated Sand, " Jr. of the S.M. and F. Division, ASCE, Vol. 93, No. SM5, Proc. Paper 5451, Sept., 1967, pp 169-190.

(27) Seed, H.B. and Idriss, I.M., " Simplified Procedures for Evaluating Soil Liquefaction Potential, " Jr. of the S.M. and F. Division, ASCE, No. SM9, 1971, pp 1249-1273.

(28) Martine, P.P. and Seed, H.B., " Simplified Procedure For Effective Stress Analysis of Ground Response, " Jr. of the G.E. Division, ASCE, GT6, 1976, pp 739-758.

(29) Seed, H.B. and Idriss, I.M., " Evaluation of Liquefaction Potential of Sand Deposits Based on Observations of Performance in Previous Earthquake, " In-Situ Testing to Evaluate Liquefaction Susceptibility, ASCE National Convention, St.Louis, 1981.

(30) Seed, H.B., " Soil Liquefaction and Cyclic Mobility Evaluation for Level Ground during Earthquakes," Jr. of the G.E. Division, ASCE, No. GT2, Proc. Paper 14380, Feb., 1979, pp 201-251.

(31) Ishihara, K., " Stability of natural deposits during earthquakes, " Eleventh International Conference of Soil Mechanics and Foundation Engineering, San Francisco, Cal.,1985.

(32) Committee on Earthquake Engineering, Commission on Engineering and Technical Systems, and National Research Council, " Liquefaction of Soils During Earthquakes, " National Academy Press, Washington, D.C., 1985.

(33) Seed, H.B. and Peacock, W.H., " Test Procedures for Measuring Soil Liquefaction Characteristics, " Jr. of the S.M. and F. Division, ASCE, No. SM8, Proc. Paper 8330, Aug., 1971, pp 1099-1119.

(34) Silver, M.L., Chan, C.K., Ladd, R.S., Lee, L.K., Tiedemann, D.A., Townsend, F.C., Valera, J.E., and Wilson, J.H., " Cyclic Triaxial Strength of Standard Test Sand, " Jr. of the G.E. Division, ASCE, No. GT5, Proc. Paper 12145, May, 1976, pp 511-523.

(35) Peacock, W.H. and Seed, H.B., " Sand Liquefaction Under Cyclic Loading Simple Shear Conditions, " Journal of the Soil Mechanics and Foundations Division, ASCE, Vol. 94, SM 3, 1968, pp 689-708.

(36) Lian Finn, W.D., Pickering, D.J., and Bransby, P.L., " Sand Liquefaction in Triaxial and Simple Shear Tests," Jounal of the Soil Mechanics and Foundation Division, ASCE, SM4, 1971, pp 639-659

(37) Ishihara, K. and Yamazaki, F., " Cyclic Simple Shear Tests on Saturated Sand in Multidirectional Loading, " Soils and Foundations, Vol. 20, No.1, 1980, pp 45-59.

(38) De Alba, P., Seed, H.B., and Chan, C.K., " Sand Liquefaction in Large-Scale Simple Shear Tests, " Jr. of the G.E. Division, ASCE, No. GT9, 1976, pp 909-927.

(39) Ishibashi, I. and Sherif, M.A., " Soil Liquefaction by Torsional Simple Shear Device, " Jr. of the G.E. Division, ASCE, No.GT8, Proc. Paper 10752, Aug., 1974, pp 871-887.

(40) Ishihara, K. and Yasuda, S., " Sand Liquefaction in Hollow Cylinder Torsion under Irregular Excitation, " Soils and Foundations, Vol. 15, No. 1, 1975, pp 45-59.

(41) Yamada, Y. and Ishihara, K., " Undrained Deformation Characteristics of Loose Sand Under Three-Dimensional Stress Conditions, " Soils and Foundations, Vol. 21, No. 1, 1981, pp 97-107.

(42) Castro, G., " Liquefaction and Cyclic Mobility of Saturated Sands," Jr of the GE Division, ASCE, GT6, 1975, pp 551-569.

(43) Castro, G. and Poulos, S., " Factors Affecting Liquefaction and Cyclic Mobility," Jr of the GE Division, ASCE, GT6, 1977, pp 501-516.

(44) Poulos, S., " The Steady State of Deformation, " Jr of the GE Division, ASCE, GT5, 1981, pp 553-562.

(45) Seed, H.B. and Martin, P.P., and Lysmer, J., " Pore-Water Pressure Changes During Soil Liquefaction, " Jr. of the G.E. Division, ASCE, No. GT4, 1976, pp 323-346.

(46) Sherif, M, Ishibahshi, I., and Tsuchiya, C., " Pore-Pressure Prediction during Earthquake Loadings," Soils and Foundation, Vol. 18, No. 4, 1978.

(47) Seed, H.B., et al., " Representation of Irregular Stress Time Histories by Equivalent Uniform Stress Series in Liquefaction Analysis," Report No.EERC 75-29, Earthquake Engineering Research Center, University of California, Berkeley, Calif., Oct., 1975; Partially Available in Jr. of the G.E. Division, ASCE, No.GT2, Feb., 1979, pp 217-219.

(48) Yond and Perkins, " Mapping Liquefaction - Induced Ground Failure Potential, " Jr. of the G.E. Division, ASCE, No. 104, GT6, 1978, pp 433-446.

(49) Saxena, S.K., " Behavior of Cemented Stabilized Sands Under Static and Dynamic Loads," Report to the National Science Foundation, Grant No.CEE 83-13935, Part I, 1985.

(50) Milstone, S.B., " Influence of Cementation to Liquefaction Resistance, " Unpublished M.E. thesis, Virginia Tech., 1985.

(51) Simon, B.R., " Earthquake Interpretations, " William Kaufmann, Inc., Los Altos, Cal., 1981.

(52) Carder, D.S. and Claud, W.K., " Ground Motions Generated By Underground Nuclear Explosions, " Journal of Geophysical Research, Vol., 64, No.10, 1959, pp 1471-1487

(53) Stauder, W.S.J., " Three Kamchatka Earthquakes, " Bulletin of Seismological Society of America, Vol. 50, No. 3, 1960, pp 347-388.

(54) Cloud, W.K.and Hudson, D.E., " A Simplified Instrument for Recording Strong Motion Earthquakes, " Bulletin of Seismological Society of America, Vol. 51, No. 2, 1961, pp 159-174.

(55) Gupta, H. and Naviar, H., " Crustal Structure in the Himalayan and Tibet Plateau Region from Surface Wave Dispersion," Bulletin of Seismological Society of America, Vol. 57, No. 2, 1967, pp 235-248.

(56) Kndudson, C.F., Perez, V., and Matthusin, R.B., " Strong Motion Instrumental Records of the Managua Earthquake of Dec. 23, 1972, Bulletin of Seismic Society of America, No.64, 1974, pp 1049-1067.

(57) Shiraki, K. and Kajimura, Y., " Statistic Method Estimating The Seismic Reponse of Light Secondary Systems, " I Mech E Conference Publication 1978-12, Mechanical Engineering Publications Limited for The Institution of Mechanical Engineers, London, November, 1978.

(58) Gazetas, G. and Yegian, M., " Shear and Rayleigh Waves in Soil Dynamics, " Jr. of the G.E. Division, ASCE, Proc. Paper 15053, No. GE12, Dec., 1979, pp 1455-1470.

(59) Harding, S. and Harmsen, S.," Surface Motion Over A Sedimentary Valley for Incident Plane P and SV Wave," Bulletin of Seismological Society of America, Vol. 71, No. 3, 1981, pp 655-670.

(60) Pyke, R., Seed, H.B., and Chan, C.K., " Settlement of Sands under Multidirectional Shaking, " Jr. of the G.E. Division, ASCE, No. GT4, April, 1975, pp 379-398.

(61) Seed, H.B., Pyke, R.M., and Martine, G.R., " Effect of Multiaxial Shaking on Pore Pressure Development in Sands," Jr of the GE Division, ASCE, GT1, 1978, pp 27-43.

(62) ASCE Committee Report, Committee on Soil Dynamics of the Geotechnical Engineering Division, " Definition of Terms Related to Liquefaction, " Jr. of the G.E. Division, ASCE, No. GT9, 1978, pp 1197-1200.

(63) Muzzy, M.W., " Cyclic Triaxial Behavior of Monterey No. 0 and No. 0/30 Sands, " Unpublished M.A. Thesis, Colorado State University, 1983.

(64) Chan, K.C., et al., " Sand Liquefaction in Large-Scale Simple Shear Tests," Jr. of the GE Division, ASCE, GT9. Sept., 1976, pp 909-926.

(65) Rad, S. N. and Clough, G.W., " New Procedure for Saturating Specimen, " Jr. of the GE Division, ASCE, Vol. 110, No. 9, 1984, pp 1205-1218.

(66) Rowe, P.W. and Borden, L., " Importance of Free Ends in Triaxial Testing," Journal of the Soil Mechanics and Foundations Div., ASCE, Proc. 3753, 1964, pp1-27.

(67) Lee, L.K. and Albeisa, A., " Earthquake Induced Settlement in Saturated Sands, " Jr. of the S.M. and F. Division, ASCE, No. GT4, April, 1974.

(68) Mulilis, J.P., Seed, H.B., Chan, K.C., Mitchell, J.K., and Arulanandan, K., " Effects of Sample Preparation on Sand Liquefaction, " Jr. of the G.E. Division, ASCE, No. GT2, Proc. Paper 12760, Feb., 1977.

(69) Silver, L.M., Tatsuoka, F., Phukunhaphan, A., and Avramidis, A.S., " Cyclic Undrained Strength of Sand by Triaxial Test and Simple Shear Test, " Proceedings, 7th International Symposium of Earthquake Engineering, India, 1981.

APPENDIX A

OPERATION MANUAL FOR DCSVT1

A.1 INTRODUCTION

This manual is addressed to the usage of DCSVT1 toward static and dynamic soil tests. The manual describes test procedures in sequence with instructions related to the operation of the DCSVT1. To follow the directions, the system should be set up as described in the following sections. Step by step directions for the soil test are shown afterwards. The computer software for the soil tests is listed at the end. The necessary materials and equipment are introduced in Appendix B.

A.2 INITIAL SET UP

Each unit of the device is described in Chapter V; therefore, the description of the system arrangement refers only to the initial set up of the cubical shear box, the pressure panel, an analog-digital converter, and a microcomputer.

A.2.1 Cubical Shear Box

The aluminium cubical shear box assembly as decribed in chapter V is equipped with pressure modules on all the six faces for pressure applications. These modules are made of RTV silicone rubber (General Electric RTV 660, see Appendix B). Molding of the silicone rubber needs the

special mold which is shown in Figure A.1. The silicone compound is poured into the mold taking care not to allow any air bubbles entraped; this is done by vacuum boiling. Then it is baked in the oven for three hours. The detailed procedure of making the silicone module out of the RTV compound can be found in the manual MOLDMAKERS supplied by the General Electric.

A.2.2 Pressure Panel

Figure A.2 shows the connection circuit of the panel and Figure A.3 shows the locations of the various units on the panel. The inhouse air pressure of 180 psi in the laboratory is connected to the pressure chamber (1) which absorbs small fluctuations of the supplied air pressure when the compressor is running. Then, the pressure is transmitted to six lines; one for the confining pressure, one for the back pressure(2), one for the air filter (3), and three for voltage-pressure transducers (4), hereafter abribiated as VPT.

The air filter (2) cleans the compressed air from the chamber and sends 20 psi compressed air with which the VPTs can regulate the output pressure according to the voltage received. The source pressure is obtained from the pressure chamber (1). The output pressure is monitored by pressure gages (5). The air regulator (6) controls the confining pressure. It has a gage (7) to monitor the output pressure, and is connected to three three-way valves (8). Therefore, either a constant confining pressure or different pressure on each of the faces can be easily applied. The line from the chamber to the air regulator (9) controls the back pressure and the pressure is monitored by the gage (10). The line extends to the water reservoir (11) and to the volume change gage (12). Through the water, the air pressure is transformed to the water pressure, then extended to the three-way valve (13) which selects lines between the reservoir and the volume change measuring cylinder.

Before applying the pressure to a sample, check the following:

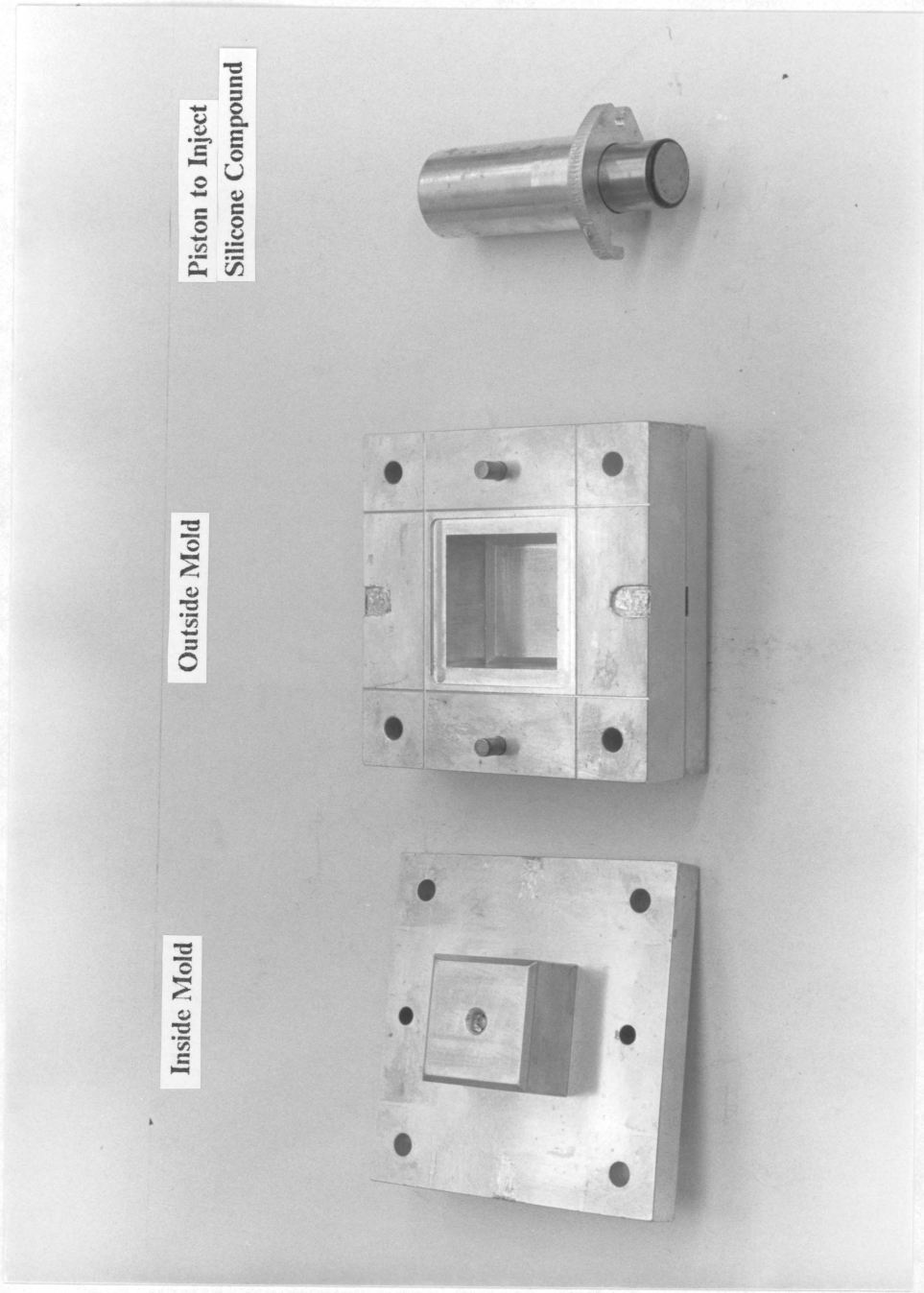

Figure A.1 Special Mold for Silicone Pressure Module.

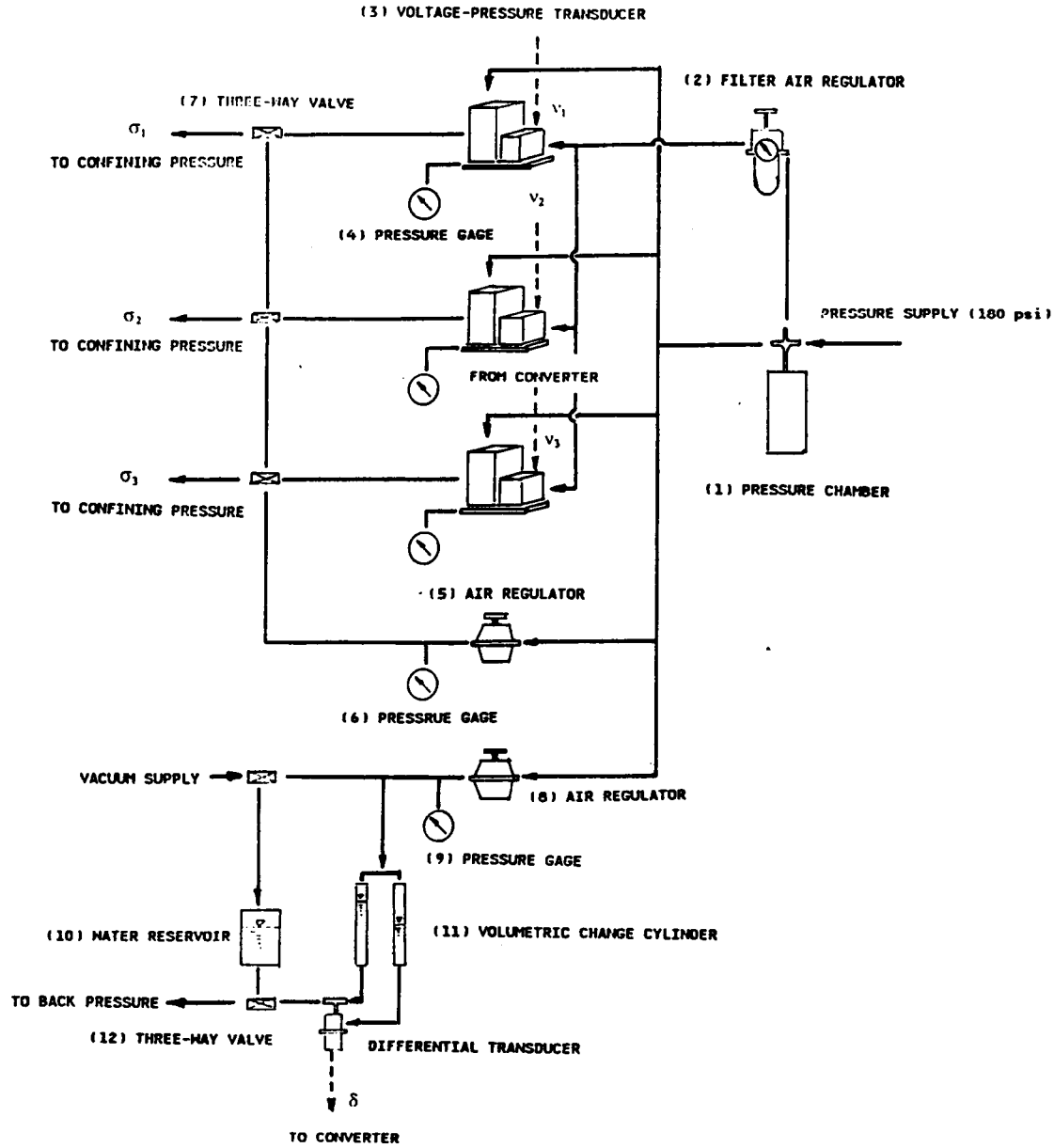

Figure A.2 Connection Circuit of The Pressure Panel.

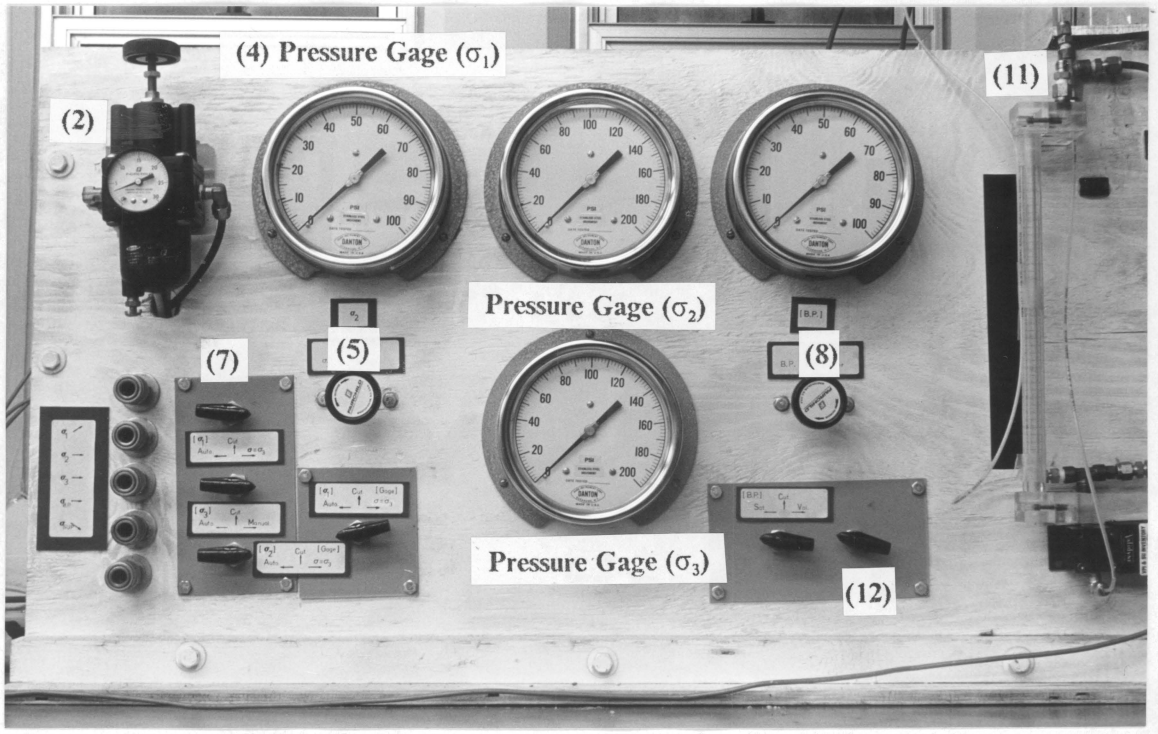

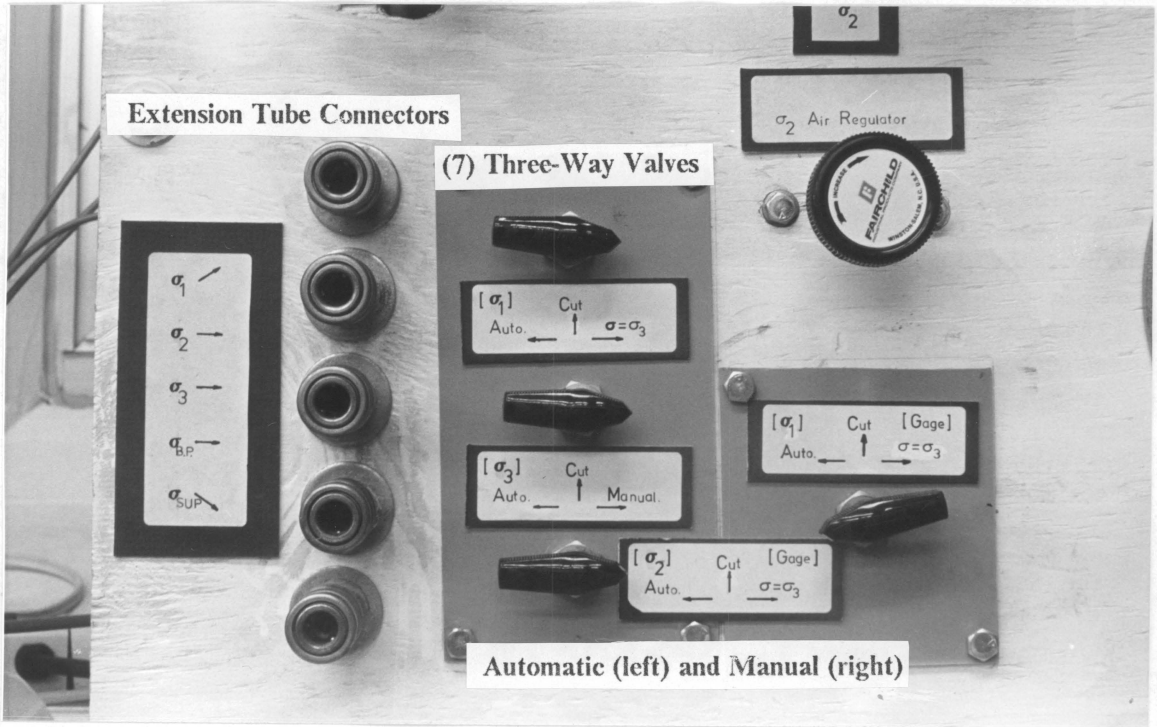

Figure A.3 The Front View of The Pressure Panel.

(i) Disconnect the extension tubes from the cubical box (see the locations of these tubes connected on the panel in Figure A.3).

(ii) All three three-way valves (8) are set to have the pressure from the air regulator (5); the directions of the valves are written on the panel. Then, open the pressure regulator gradually until the pressure gage (7) reads 5 psi. If it does, release the pressure.

(iii) The three-way valve (13) is set to have the back pressure from the water reservoir (11). Then, open the air regulator (9) gradually until the gage (10) reads 5 psi. Release the pressure.

(iv) The air filter (2) is fully open so that the gage on the filter reads 20 psi.

(v) The drainage tubes from the inside of the cubical box are connected to the panel.

A.2.3 The Analog-Digital Converter

The setup of the A/D converter is important for proper selection of the working voltage range. Five switches, S-7 ,10 ,and 12 on the main board, S-2 on the interface card I-130, and S-3 on the preamp I-140 are needed to be set properly ; the location of the switches can be seen when the top lid of the converter is opened. The setup of the switches is shown in Table A.1.

The converter is connected to the transducers with the extension board which is attached at the back of the converter. The board has 16 input and 4 output channels. The proper connection for the transducers is summarized in Table A.2.

The A/D converter and the microcomputer are connected by a interface cable. The one end of the cable is embedded on the slot number 2 in the microcomputer and the other is inserted on the socket on the A/D converter. The A/D converter and the I-140 preamp system are connected by a interface cable. One end of the cable is attached on the interface card I-130 which is embedded on the slot number 2 in the converter and the other is attached on the extension socket in the

Table 13. A.1 Set Up of the DIP Switches in the Converter.

	-1-	-2-	-3-	-4-	Note
S-7	on	on	off	off	Input Voltage Range ± 5 Volt.
S-10	on	off	off	off	Output Voltage Range ± 10 Volt.
S-12	EXT	**	**	**	Power Supply 15 Volt.
S-2	on	off	on	off	Input Voltage ± 100 mV.
S-3	on	off	off	off	Input Voltage ± 100 mV.

Table 14. A.2 Chanel Connections for Reading of Surrounding Electrical Circuits

(Analog to Digital Conversion).

A/D Channel No.	-0-	-1-	-2-	-3-
LVDT*	op**(+) z-a op(+) z-b	op(+) x-a*** op(+) x-b	op(+) y-a op(+) y-b	
Diff. Trans.	-	-	-	op(+)

Channel	earth	earth	earth	earth
LVDT	op(-) z-a op(-) z-b	op(-) x-a op(-) x-b	op(-) y-a op(-) y-b	- -
Diff. Trans.	-	-	-	op(-)

A/D S-1 on I-140	-0-	-1-	-2-	-3-
P.P.trans.	op(+)	-	-	op(-)

(*) : input (+) and (-) to the LVDTs are provided by 24 volts power supply.

(**) : (op) stands for output.

(***) : A pair of LVDTs for a direction of z is denoted as (-a) and (-b).

Table 15. A.3 Chanel Connections for Controlling the VPTs.

(Digital to Analog Conversion).

D/A Channel No.	-0-	-1-	-2-	-3-
VPT & PP.Trans	ip*(+) to z	ip(+) to x**	ip(+) to y	ip(+) to pp.trans.

Channel	earth	earth	earth	earth
VPT & pp.trans	ip(-) from z	ip(-) from x	ip(-) from y	ip(-) from pp.trans.

(*) : (ip) stands for input.

(**) : z, x, and y are the loading directions.

preamp system. These connections have been set already. For the details, refer Apple Based Laboratory Computer System Reference Manual (The Hardware Portion of ISAAC System).

A.2.4 Microcomputer

A soil test program is written using BASIC and LABSOFT. Two languages are employed by running the APPLE DOS 3.1 and APPLESOFT sequentially at the beginning. Insert the DOS in the floppy disk, and type " IN#6 ". This stores necessary commands for disk operational system and BASIC. Do the same procedure for APPLESOFT. The details for the DOS and APPLESOFT are described in APPLE II Tutorial and Labosoft Reference Manual (Labosoft Language), respectively.

A.3 TEST PROCEDURE

The test procedure is as follows:

(1) Membrane Making

(2) Sample Set Up

(3) Test

(4) Data Compilation

A.3.1 Membrane Making

The materials required are : (1) thin rubber sheet, (2) draft tape, (3) plastic liquid rubber cement, (4) rubber cement, and (5) teflon spaghetti tube (see Appendix B). Make two types of membranes, a cylindrical membrane and square membranes, which are used in the sample preparation. The direction for making the membranes are given hereafter:

CYLINDRICAL MEMBRANE

(a) Cut a rectangular sheet of size 6 x 8.25 in. (Figure A.4.a) from the thin rubber sheet.

(b) Put a draft tape on the left margin as shown in the figure. The draft tape prevents the margin from rolling and shrinking when glue is applied on.

(c) Paint rubber cement over the margin, and overlap the area with the other side of the sheet so that it turns out to be cylindrical.

(d) Peel the tape off (Figure A.4.b). Make sure there are no wrinkles and air voids remaining over the margin. Stretch the margin to eliminate any air voids if present.

SQUARE MEMBRANE

(a) Cut a square sheet of thin rubber of size 2.25 x 2.25 in. (Figure A.5.a).

(b) Make a pin hole at the point shown in Figure A.5.a.

(c) Insert teflon Spaghetti tube into the hole, and adjust the length of the tube so that the tip is roughly at the center of the square sheet. It is recommended that the mouth of the tube be trimmed into an acute angle and the wide mouth be placed facing against the plate so that the total area of the mouth becomes wider for drainage.

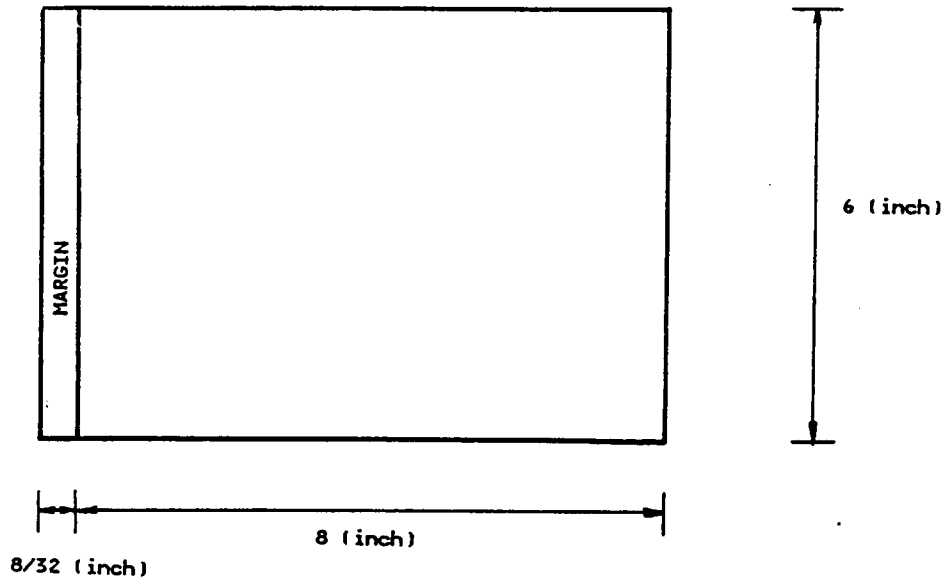

(a) THIN MEMBRANE PLATE

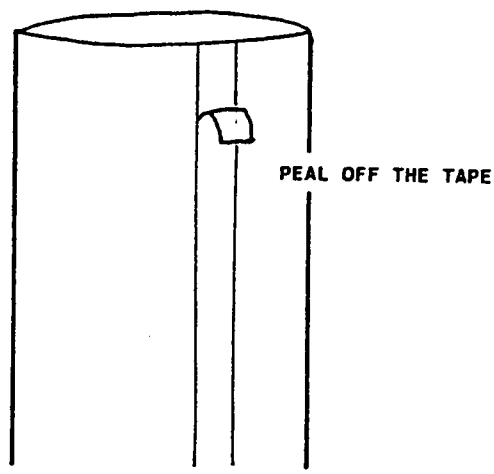

(b) CYLINDRICAL MEMBRANE

Figure A.4 Size of Cylindrical Membrane.

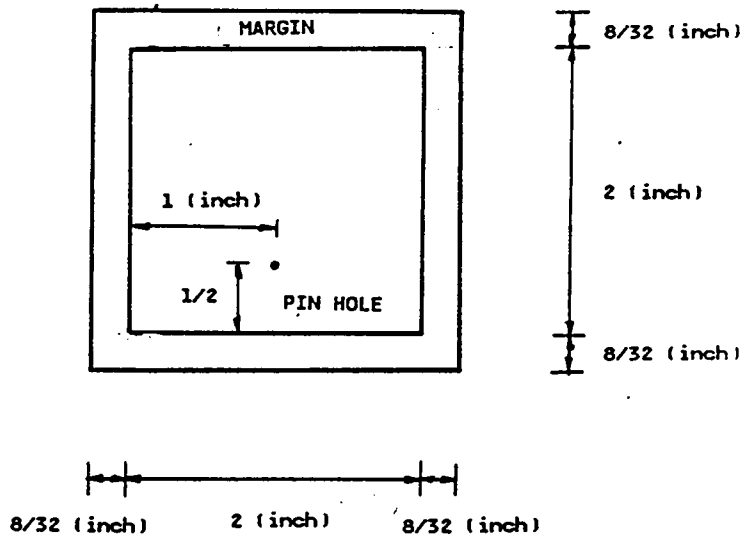

(a) SQUARE MEMBRANE

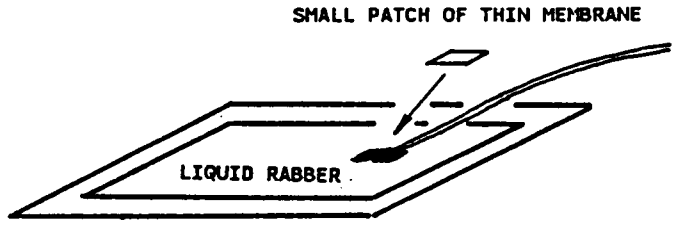

(b) SEALING

Figure A.5 Size of Square Membrane.

(d) Put liquid rubber at the intersection of the sheet and the tube from the top and bottom side of the sheet, and then, place the small patch of the thin rubber as shown in Figure A.5.b.

(e) Make another square flat sheet for the bottom cover.

A.3.2 Sample Set up

A sample is wrapped by the membranes in a special mold (Figure A.6); and then it is confined with vacuum. Finally, the cubical sample is placed in the cubical shear box. This sequential procedure is described as following:

(a) Place the cylindrical membrane (see A.3.1) inside the mold, and then, wrap the mold with inside out.

(b) Apply vacuum to the mold. Tighten the membrane around the bottom of the mold by a rubber band, and stretch the membrane from the top of the mold to eliminate any wrinkles on it. Pick up the teflon tube which is not attached to the square membrane, and hold the tip of the tube. Insert it into the top drainage canal in the cubical frame from inside to outside (ref. Figure 4.3). Do the same for the bottom drainage.

(c) Fit the nuts (cf.tube fitting in Appendix B) to the ends of the tubes coming out of the top and bottom drainage canals, and then connect them to the drainage board (Figure A.7).

(d) Now, look at the bottom of the vacuum mold. Paint Rubber Cement on the flat rectangular margin of the membrane on the bottom of the mold. Take the square membrane coming out of the bottom drainage line, and then, place it over the glued area.

(e) Press well and make sure no wrinkles and air voids are present. Note that most of the leakages occur around here.

(f) Turn over the mold. Place a filter paper and a porous teflon paper in the order, at the bottom of the mold.

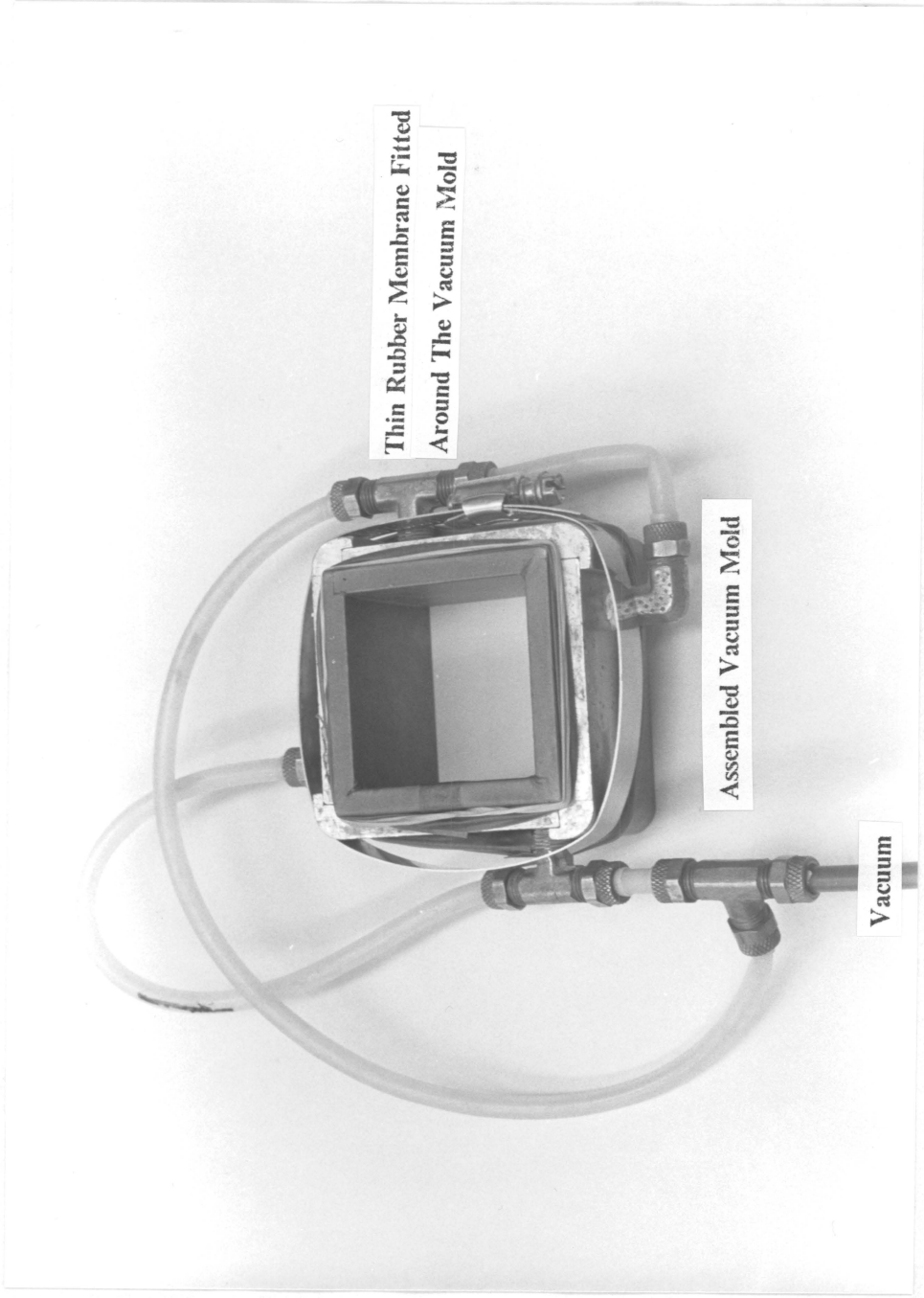

Figure A.6 Vacuum Mold for Sample Set Up.

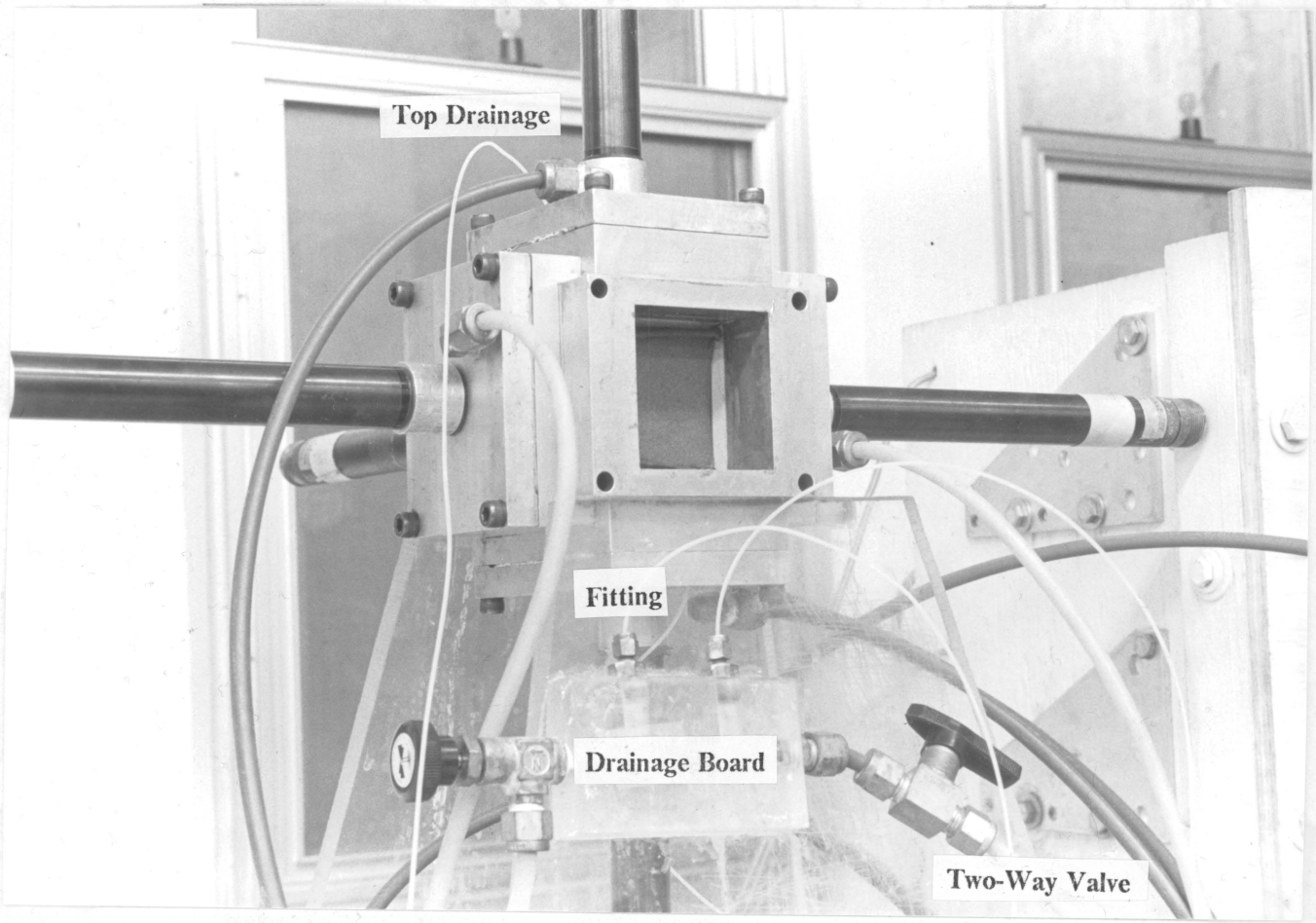

Figure A.7 Front View of The Drainage Board.

(g) Place the soil specimen inside of the mold.

(h) Spread a porous teflon paper and a filter paper at the top surface of the specimen.

(i) Seal the top of the membrane with the other square membrane by the same manner as (c) and (d). Note that the direction of the tubes leading out of the top and the bottom must go opposite so that they accord the locations of the drainage canals in the cubical frame (ref. Figure 4.3).

(j) Release the vacuum to the mold gradually and apply it to the soil specimen through the drainage board.

(k) At this stage, the soil specimen is vacuum frozen. Push it with a finger and confirm the sample confined with the vacuum. If soft, there is some leakage (Figure A.8).

(l) Take off the membrane from the mold, and disassemble the mold. Trim excess part of the thin membrane.

(m) Measure the size and the weight of the specimen. Note that the weight of the rubber membrane, filter papers, and teflon porous paper must be subtracted from the total weight, however, if the rubber sheets are cut as the sizes shown in Figure A.4 and 5, the total weight is 6.2 gram. The weigth of the filter paper is 0.8 gram and that of the teflon paper is neglegible. The thickness of the rubber is approximately 0.20 mm and that of the filter paper is approximately 0.25 mm. Thickness of the teflon papter is neglegible.

(m) Bring the specimen near the cubical box, and push the excess tubes inside to outside through the drainage canals. Place the sample inside the box (Figure A.9).

(n) Close the box with the silicone membrane pressure modules. Apply small amount of confining pressure, say 5 psi, by opening the air regulator, then, release the vacuum (Figure A.10)

The sample is ready to be tested.

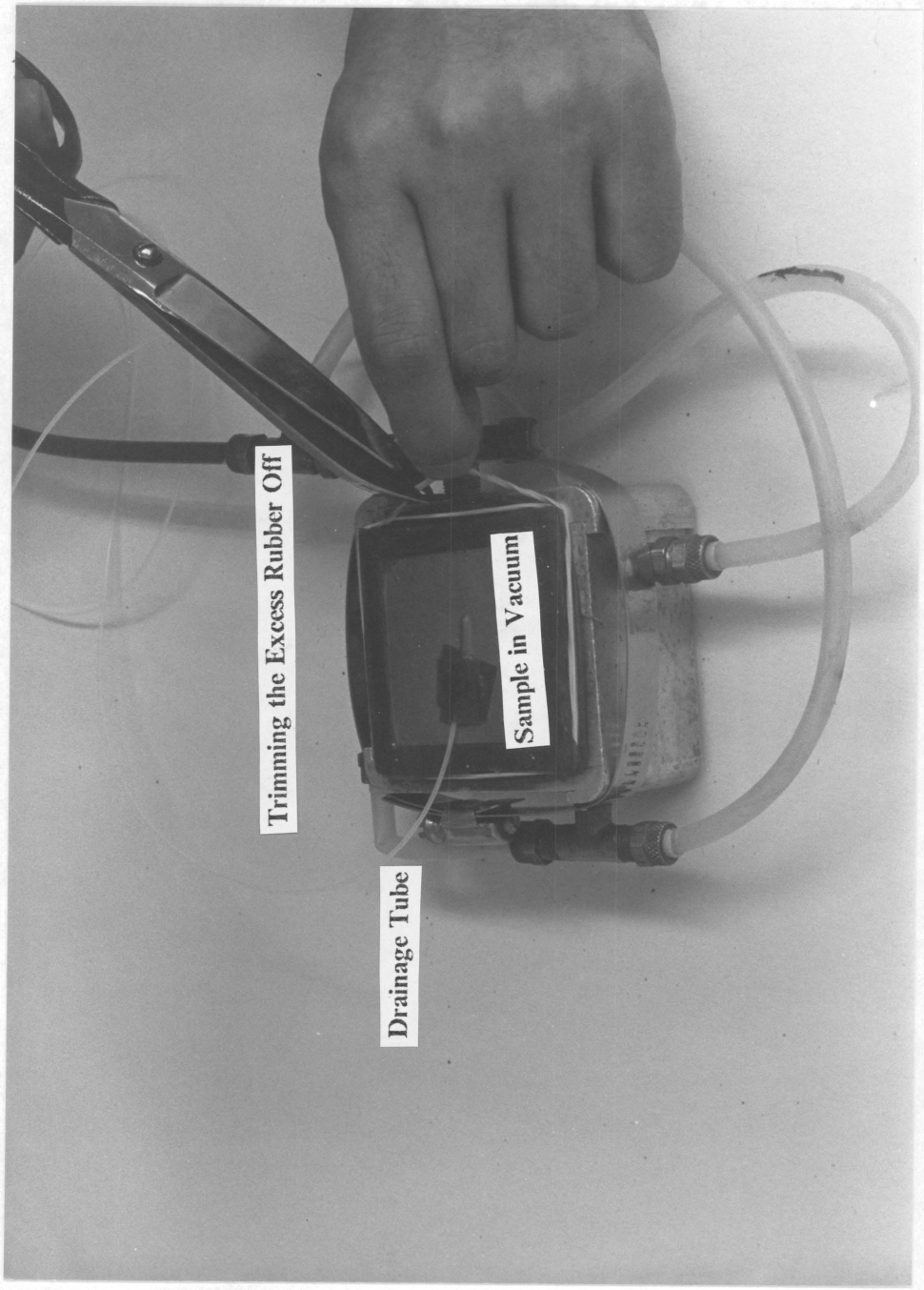

Figure A.8 The Top of the Sample in the Vacuum Mold Is Sealed By The Square Membrane.

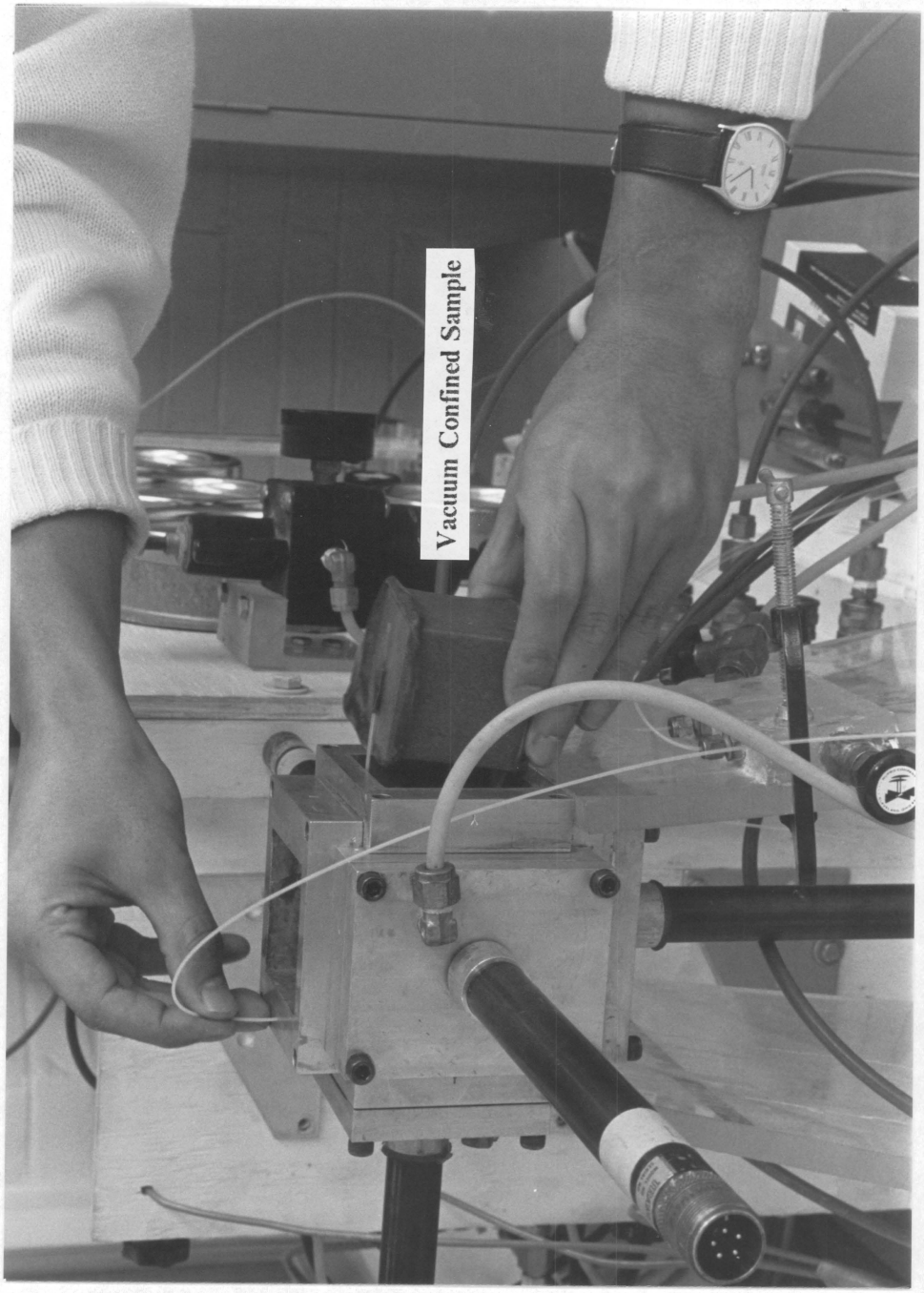

Figure A.9 Vacuum Confined Samples in The Shear Box.

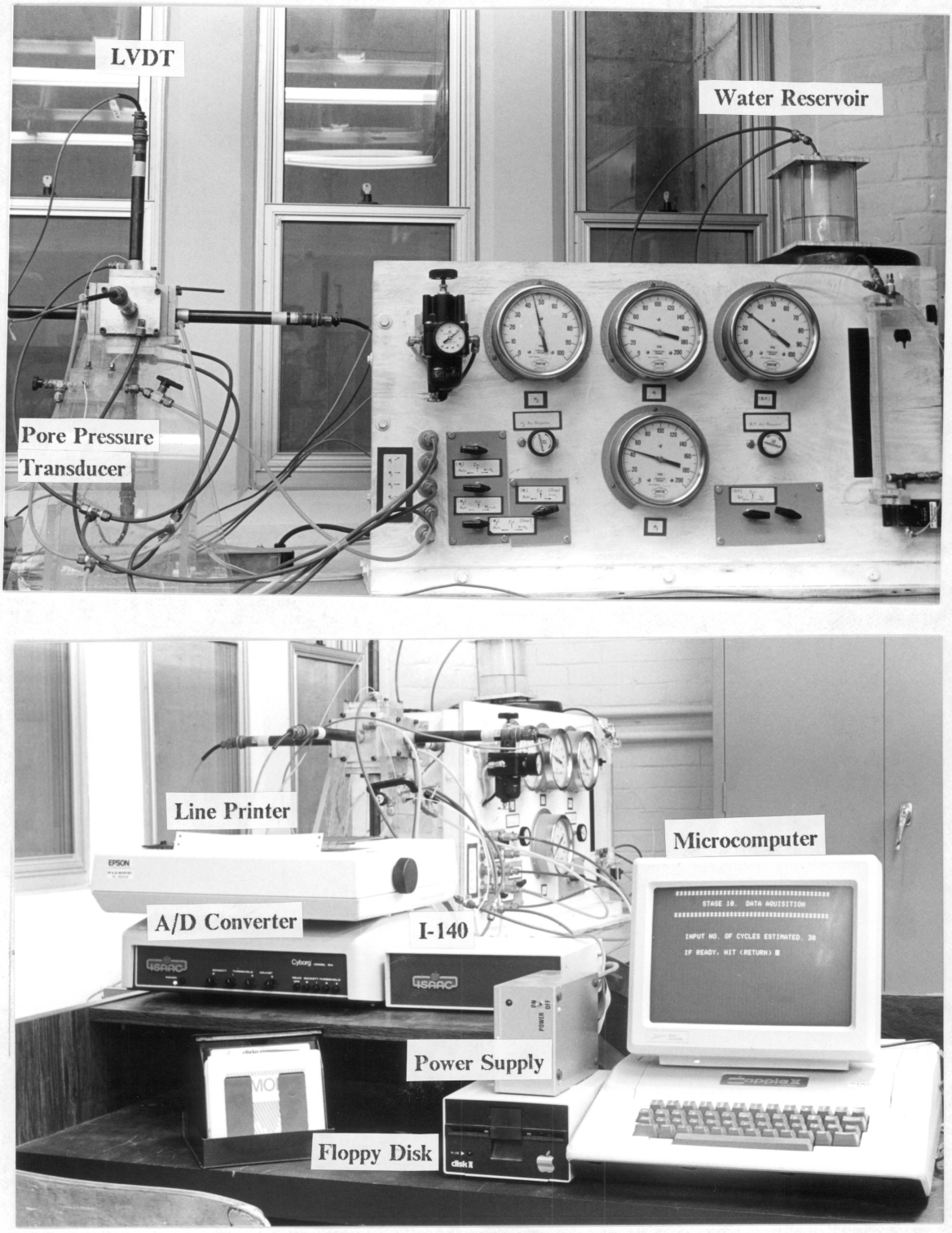

Figure A.10 Ambient Pressure Is Applied to The Box and The Test Is About to Start.

A.3.3 Test

Run the program called " SOIL TEST " and choose the option; static test or dynamic test. Up to the consolidation procedure, the process is the same for both tests. The test procedure is divided into three sections; (1) consolidation, (2) static loading, and (3) dynamic loading .

CONSOLIDATION

(1) Set the three-way value of drainage selection to the water reservoir.

(2) Input the information sequentially on the screen display: (a) NAME OF THE FILE, (b) TITLE OF THE TEST, (c) CONDITION OF THE TEST, and (d) SERIAL NUMBER OF THE TEST.

(3) Input the initial condition of the soil such as the size (inch), weight (lb), and water contents (percent).

(4) Input the consolidation and drainage condition so that the screen display confirms the condition of the test such as " consolidated and drained test with volumetric measurement " or the others.

The computer stores the input information on the disk; sequentially it executes the initial reading of the sample in terms of the initial location and volume of the sample in the cubical shear box. These steps can be repeated from the beginning by inputting the order, if anything wrong in the process.

(5) Saturate sample. The details of the procedure are explained in the Chapter V. The screen display instructs briefly about this procedure with reference to the operation of the pressure regulators and three-way values on the panel.

(6) The desired back pressure and effective confining pressure are set by two pressure regulators. The three independent pressure for three directions are activated by the program with input of the initial loading condition. Since the three-way valves are on the pressures from the manual air

pressure regulators, the three independent pressures do not affect the sample. The necessary instruction for this procedure is seen on the screen display. At this stage, the four pressure gages show amount of the pressure according to the input values.

(7) Change the drainage line from the water reservoir to the volumetric change measurement cylinder by turning the three-way valve.

(8) Input the amount of time for consolidation in minutes.

The steps instructed lead to the completion of the process up to the consolidation.

STATIC LOADING TEST

(1) Very quickly turn the three-way valves of the pressure sauces from the manual pressure regulator to the others. Also, according to the drainage condition, undrained or drained, the three-way valve of the drainage selection must be set.

(2) Input the target pressures for three directions of the sample and the time interval. Loading and measurement are automatically done. During this step some of the tentative options such as " no increment of of load but measurement ", " end of the test ", and so on, are asked.

(3) At the end of the test, three-way valves of the pressure sources are to return to the manual pressure regulator and the the valves of the drainage selection to the water reservoir.

(4) Slowly release all pressures by turning the regulators on the panel.

DYNAMIC LOADING

(1) Do the same as directed in (1) of the static loading .

(2) Input one of the loading types; (a) CTX, (b) CPS, (c) CRE-TX, (d) CRC-TX, (e) CRE-PS, and (f) CRC-PS and the stress amplitude which is the ratio of the increment of the vertical stress divided by the effective confining pressure.

(3) Input the number of cycles to be loaded. The loading and measurement are automatically performed.

(4) At the end of the test do the same on the three-way valves described on the steps (3) and (4) in the static loading test.

A.3.4 Data Compilation

Measured values are automatically stored on the diskette under the name input at the beginning of the test. The screen display asks if monitoring the data is wanted. If so, the data is plotted on the screen or written on the line printer depending on the optional number chosen by the user. In the case that the data is sent to the main frame, insert VICITERM and run; this connects the microcomputer to the main frame computer and the data is ready to be sent to there. For details, consult " User's Manual of VICITERM " (Appendix B).

A.4 "SOIL TEST" LISTING

The listing of the program " SOIL TEST " is given below. The program is written by BASIC; however, the commands related to the A/D converter and the screen display are written by using LABSOFT commands. For further details, consult LABSOFT manual.

```
10  REM  ******************
20  REM
30  REM       SOIL TEST
40  REM
50  REM  ******************
60  REM
65  HOME
70  PRINT : PRINT : PRINT : PRINT
90  PRINT "      (1) STATIC  TEST"
95  PRINT
100  PRINT "      (2) DYNAMIC TEST"
110  PRINT
120  INPUT "      SELECT (1) OR (2) ";S
130  PRINT
140  HOME
150 J$ =  CHR$ (4)
160  IF S = 1 THEN  PRINT J$;"RUN STATIC TEST"
170  IF S = 2 THEN  PRINT J$;"RUN DYNAMIC TEST"
180  END

10  REM  *************************
12  REM
14  REM        STATIC  3-D TEST
16  REM       PROGRAM (JUN.'86)
18  REM         BY J. IWABUCHI
19  REM
20  REM  *************************
22  REM
23  DIM A(200): DIM B(200): DIM C(200)
26  DIM RD(200,7)
27 FF(0) = 0.0762:FF(1) = 0.0753:FF(2) = 0.0758:FF(3) = 0.625:FF(4) = 0.
    01254
28 FF(6) = 0.625:FF(7) = 0.0125
29  DEF  FN V1(X) = (X * 0.14661 - 0.76103) * 409.6
30  DEF  FN V2(X) = (X * 0.15591 - 0.94164) * 409.6
31  DEF  FN V3(X) = (X * 0.14166 - 0.51020) * 409.6
32  DEF  FN PV(X) = X / 409.6 - 4.945
33  DEF  FN PP(X) = X * 2 / 40.96 - 200
90  HOME
91  PRINT : PRINT : PRINT : PRINT : PRINT
93  PRINT "****************************************": PRINT : PRINT

95  PRINT "            STATIC 3-D TEST": PRINT
96  PRINT : PRINT : PRINT
97  PRINT "****************************************": PRINT : PRINT
98  INPUT "               IF READY, HIT (RETURN) ";Y$
99  HOME
100  PRINT "****************************************": PRINT
110  PRINT "****************************************": PRINT
```

```
115  PRINT : PRINT
120  INPUT "   NAME OF FILE  ";A$
121  PRINT : PRINT
125  INPUT "   TESTED BY     ";B$
126  PRINT : PRINT
130  INPUT "   DATE          ";C$
131  PRINT : PRINT
135  INPUT "   SOIL          ";D$
140  PRINT : PRINT
141  SPEED= 10
142  PRINT "                  THANKS /     "
143  SPEED= 254: HOME
150  PRINT "****************************************": PRINT
152  PRINT "      STAGE 2. INITIAL CONDITION  ": PRINT
155  PRINT "****************************************": PRINT
160  PRINT "    ENTER THE SIZES OF SAMPLE  ": PRINT : PRINT
165  INPUT "      Z (INCH) = ";X(1): INPUT "      Y (INCH) = ";X(2):
     "      X (INCH) = ";X(3): PRINT
170  INPUT "    WEIGHT OF SAMPLE (DRY) (LB) = ";W: PRINT
171  INPUT "    WATER CONTENT (%)           = ";WC: HOME
172 X(4) = X(1) * X(2) * X(3)
175  HOME : PRINT
180  PRINT "****************************************": PRINT
185  PRINT "      STAGE 3. ENVIRNMENT OF TEST ": PRINT
190  PRINT "****************************************": PRINT
193 CN$ = "UNCONSOLIDATION - "
194 DR$ = "UNDRAIN TEST "
195  INPUT "   CONSOLIDATION  (1) OR NOT (0)  ";CN: IF CN = 1 THEN CN$
     "CONSOLIDATION - "
196  PRINT
200  INPUT "   DRAIN TEST     (1) OR NOT (0)  ";DR: IF DR = 1 THEN DR$
     "DRAIN TEST "
201  PRINT
205  PRINT "   ";CN$;DR$
210  PRINT : INPUT "   IS THAT RIGHT ? (Y/N) ";Y$: IF Y$ = "N" THEN
     175
215  PRINT : PRINT
220  IF DR = 1 THEN  PRINT "   VOLUMETRIC CHANGE WILL BE MEASURED "
222  IF DR = 1 THEN  GOTO 227
225  PRINT "   PORE PRESSURE WILL BE MEASURED  "
227  SPEED= 10
228  PRINT "                          "
229  SPEED= 254
230  HOME : PRINT
235  PRINT "****************************************": PRINT
240  PRINT "      STAGE 4. SAMPLE PREPARATION  ": PRINT
245  PRINT "****************************************": PRINT : PRINT
250  PRINT "   (1) WRAP SAMPLE IN MOLD": PRINT
252  PRINT "   (2) APPLY VACUUM TO SAMPLE, 5 HG IN ": PRINT
254  PRINT "   (3) SET SAMPLE IN BOX ": PRINT
```

```
256  PRINT "    (4) APPLY CONF.PRESS., SAY 5 PSI ": PRINT
258  PRINT "    (5) OUT VACUUM AND OPEN VALVES": PRINT
260  PRINT "    (6) INCREASE PRESSURE TO 10 PSI": PRINT
262  PRINT "    (7) SET LVDT AND TRANSDUCER ": PRINT
264  INPUT "    IF READY TO GO AHEAD, HIT (RETURN)  ";Y$
266  HOME : PRINT
270  PRINT "*****************************************": PRINT
275  PRINT "         STAGE 5. INITIAL READING ": PRINT
280  PRINT "*****************************************": PRINT
285 J$ =  CHR$ (4): REM  CTRL-J
290  PRINT J$;"OPEN";A$: PRINT J$;"DELETE";A$
295  PRINT J$;"OPEN";A$: PRINT J$;"WRITE";A$
300  PRINT B$: PRINT C$: PRINT D$
305  PRINT X(1): PRINT X(2): PRINT X(3): PRINT W
310  PRINT CH: PRINT DR
315  PRINT J$;"CLOSE";A$
316 J = 0
320  GOSUB 1000
322  PRINT : PRINT
325  INPUT "       ANYTHING WRONG ? (Y/N) ";Y$: IF Y$ = "Y" GOTO 266
330  HOME : PRINT
335  PRINT "*****************************************": PRINT
340  PRINT "      SATGE 6. SAMPLE SATURATION ": PRINT
345  PRINT "*****************************************": PRINT
350  PRINT "    FOR CO-2 METHOD ": PRINT
355  PRINT "    (1) FLUSH CO-2 "
357  PRINT "    (2) FLUSH H-2-O"
359  PRINT "    (3) INCREASE CON. AND BACK PRESS. "
360  PRINT "    (4) MEASURE B-VALUE ": PRINT
362  PRINT "    FOR VACUUM METHOD": PRINT
364  PRINT "    (1) FLUSH H-2-O, SAY 1 HOUR "
366  PRINT "    (2) RE-SET 5 PSI AND 10 HG"
368  PRINT "    (3) CHECK AIR VOIDS FLOWING OUT": PRINT
370  PRINT "    (4) WAIT ANOTHER 1 HOUR "
372  PRINT "    (5) INCREASE C.P. AND B.P.,GET B(%) "
373  PRINT
375  INPUT "    READY TO GO AHEAD  ";Y$
380  HOME : PRINT
390  PRINT "*****************************************": PRINT
395  PRINT "      STAGE 7. STRESS APPLICATION  ": PRINT
400  PRINT "*****************************************": PRINT
405  PRINT " EFFECTIVE PRINCIPLE STRESSES ": PRINT
406  INPUT "    STRESS (Z)    (PSI) ";S1: PRINT
407  INPUT "    STRESS (Y)    (PSI) ";S2: PRINT
408  INPUT "    STRESS (X)    (PSI) ";S3: PRINT
409  PRINT : INPUT "    BACK PRESS. (PSI) ";BP: PRINT
411 SZ = S1 + BP:SY = S2 + BP:SX = S3 + BP
419  PRINT
420  INPUT "       ANYTHING WRONG ? (Y/N) ";Y$: IF Y$ = "Y" THEN  GOTO 3
     30
```

```
454  HOME : PRINT
455  PRINT "*****************************************": PRINT
460  PRINT "     STAGE 8. AUTO-CONTROLL CHECK ": PRINT
465  PRINT "*****************************************": PRINT
470  PRINT "   (1) MAKE SURE NO AIR VOIDS IN TUBE  "
472  PRINT
475  INPUT "   (2) INPUT CON.P.AT THE PRESENT ";P
480 P1 =  FN V1(P):P2 =  FN V2(P):P3 =  FN V3(P)
481  & AOUT,(DV) = P1,(C#) = 0
482  & AOUT,(DV) = P2,(C#) = 1
483  & AOUT,(DV) = P3,(C#) = 2
485  PRINT
486  PRINT "   (3) CHECK PRESS AT AUTO-CONT.  "
487  PRINT
490  PRINT "   (4) IF OK , TURN T.W.VALVES"
491  PRINT
492  INPUT "   (5) DONE ?   ";Y$
493  PRINT
495  PRINT "   (6) INCREASE B.P. WHILE C.P. CHANGES"
497  PRINT
500  INPUT "   (7) READY ? ";Y$
501 J = 1
502  GOSUB 1000
505 DZ = (SZ - P) / 5:DY = (SY - P) / 5:DX = (SX - P) / 5
508 VZ = P:VY = P:VX = P
510  FOR I = 1 TO 5
515 VZ = VZ + DZ:VY = VY + DY:VX = VX + DX
516 ZZ =  FN V1(VZ):YY =  FN V2(VY):XX =  FN V3(VX)
520  & BEEP
522  & AOUT,(DV) = ZZ,(C#) = 0
523  & AOUT,(DV) = YY,(C#) = 1
524  & AOUT,(DV) = XX,(C#) = 2
525  & PAUSE = 10
526  NEXT I
529 J = 2: GOSUB 1000
530  IF CH$ (  ) "CONSOLIDATION - " THEN  GOTO 560
532  PRINT : PRINT
535  PRINT "   SAMPLE IN CONSOLIDATION PROCEDURE   ": PRINT
537  PRINT
540  INPUT "  SET TIMER FOR CONSOLIDATION (MIN) ";TM
542  PRINT
545 TM = TM * 60: & PAUSE = TM
546  FLASH
547  & BEEP ON
548  INPUT "       TIME IS UP, HIT (RETURN) ";Y$: NORMAL : & BEEP STOP :
      HOME : PRINT
549 J = 3
550  GOSUB 1000
555 ST = 0
560  HOME : PRINT
```

```
565  PRINT "****************************************": PRINT
570  PRINT "       STAGE 10.  STATIC LOADING  ": PRINT
575  PRINT "****************************************": PRINT
580  PRINT : PRINT
585  PRINT "LOADING PROCESS  (1) LINEAR INCREMENT OR ": PRINT
586  PRINT "                 (2) NON-LINEAR   ''   ": PRINT
587  INPUT "                 INPUT (1) OR (2) ";LS
590  PRINT : PRINT
595  INPUT "IF READY, HIT (RETURN) ";Y$
597  PRINT : PRINT : PRINT
598  PRINT "****************************************"
600  IF LS = 1 THEN  GOSUB 1500
610  IF LS = 2 THEN  GOTO 640
612 DZ = TZ / IX:DX = TX / IX:DY = TY / IX
614  FOR LP = 1 TO IX
616 A = SZ + DZ * LP:B = SX + DX * LP:C = SY + DY * LP
617 J = J + 1: GOSUB 1000
618 A(J) = A:B(J) = B:C(J) = C: GOSUB 1600
622  & PAUSE = TT
623  PRINT
624  PRINT "PRESENT STRESS LEVEL (Z) ";A
625  PRINT "PRESENT STRESS LEVEL (X) ";B
626  PRINT "PRESENT STRESS LEVEL (Y) ";C
627  PRINT "PRESENT STEP             ";LP
628  & PAUSE = 10
629  NEXT LP
630  INPUT "          CONTINUE  (Y/N) ? ";Y$
635  IF Y$ <  > "N" THEN  GOTO 580
640  HOME : PRINT : PRINT : PRINT : PRINT : PRINT
651  INPUT "NEXT TARGET EFFECTIVE STRESS (Z) ";A
652  INPUT "NEXT TARGET EFFECTIVE STRESS (X) ";B
654  INPUT "NEXT TARGET EFFECTIVE STRESS (Y) ";C
656 A = A + SZ:B = B + SX:C = C + SY
657  PRINT : PRINT : PRINT
658  INPUT "ANYTHING WRONG ? (Y/N)  ";N$
660  IF N$ = "Y" THEN 640
662 J = J + 1: GOSUB 1000
664 A(J) = A:B(J) = B:C(J) = C: GOSUB 1600
665  PRINT : PRINT
666  INPUT "          CONTINUE  (Y/N) ? ";Y$
668  IF Y$ <  > "N" THEN  GOTO 640
669  INPUT "      ARE YOU SURE  (Y/N) ? ";Y$
670  IF Y$ <  > "Y" THEN  GOTO 580
675  GOTO 800
710  END
800  HOME
810  PRINT J$;"MON C,I,O"
815  PRINT J$;"APPEND";A$
820  PRINT J$;"WRITE";A$
825  PRINT S1: PRINT S2: PRINT S3: PRINT BP: PRINT SR
```

```
827  PRINT J
830  FOR L = 0 TO J
831  PRINT A(L): PRINT B(L): PRINT C(L)
835  FOR I = 0 TO 7
840  PRINT RD(L,I)
845  NEXT I
850  NEXT L
880  PRINT J$;"CLOSE";A$
885  PRINT J$;"NOMON C,I,O"
890  PRINT : PRINT
900  INPUT "   OUTPUT DATA (Y/N)  ?  ";OP$
905  IF OP$ = "Y" THEN  PRINT J$;"RUN DATASHEET"
910  END
1000  REM  ***********************
1002  REM
1004  REM   SUBROUTINE READING
1005  REM
1006  REM  ***********************
1008  REM
1010  FOR L = 0 TO 2
1015  & AIN,(TV) = Q,(C#) = L,(FU) =  FN PV(RAW%)
1020 Q = Q * FF(L)
1025 RD(J,L) = Q
1030  NEXT L
1034  IF J < 4 THEN  GOTO 1036
1035  IF DR <  > 1 THEN  GOTO 1038
1036  & AIN,(TV) = Q,(C#) = 3,(FU) =  FN PV(RAW%)
1037 Q = Q * FF(4): GOTO 1040
1038  & AIN,(TV) = Q,(D#) = 1,(C#) = 0,(FU) =  FN PP(RAW%)
1040 RD(J,3) = Q * FF(3)
1045  HOME : PRINT
1050  PRINT "****************************************": PRINT
1055  PRINT "      DISPLACEMENTS(IN)   STRAIN (%) ": PRINT
1060  IF J <  > 0 THEN  GOTO 1065
1061 RD(J,4) = 0.0:RD(J,5) = 0.0:RD(J,6) = 0.0:RD(J,7) = 0.0
1062  GOTO 1100
1065 JM = J - 1
1066  IF J > 3 THEN JM = 3
1070  FOR I = 0 TO 3
1075 IN = I + 4:II = I + 1
1080 RD(J,IN) = (RD(J,I) - RD(JM,I)) / X(II) * 100
1082  NEXT I
1100  PRINT " Z-DIR.  ";RD(J,0)"      ";RD(J,4): PRINT
1105  PRINT " Y-DIR.  ";RD(J,1)"      ";RD(J,5): PRINT
1110  PRINT " X-DIR.  ";RD(J,2)"      ";RD(J,6): PRINT
1112  PRINT " V OR P  ";RD(J,3)"      ";RD(J,7): PRINT
1113  PRINT : PRINT "      AT THE PREVIOUS LOADING STEP  ": PRINT
1115  PRINT "****************************************": PRINT
1120  & BUZZ
1125  & PAUSE = 5
```

```
1130  RETURN
1500  HOME
1502  PRINT "****************************************": PRINT : PRINT
1504  PRINT "    SET TARGET STRESS LEVEL AND TIME ": PRINT
1506  PRINT "****************************************": PRINT : PRINT
1508  INPUT "   TARGET EFFECTIVE STRESS LEVEL (Z) ";TZ: PRINT
1510  INPUT "   TARGET EFFECTIVE STRESS LEVEL (X) ";TX: PRINT
1512  INPUT "   TARGET EFFECTIVE STRESS LEVEL (Y) ";TY: PRINT
1514  INPUT "   TIME SPENT ON STRESS APPLICATION  ";TS: PRINT
1516  INPUT "   NO. OF STEPS TO COMPLETE LOADING  ";IX: PRINT
1518  PRINT : INPUT "   IS THAT RIGHT ? (Y/N) ";Y$: IF Y$ = "N" THEN
      1500
1520 TT = TS * 60 / IX
1560  RETURN
1600 A1 =  FN V1(A):B1 =  FN V2(B):C1 =  FN V3(C)
1610  & AOUT,(DV) = A1,(C#) = 0
1620  & AOUT,(DV) = B1,(C#) = 1
1630  & AOUT,(DV) = C1,(C#) = 2
1640  RETURN


1  LOMEM: 16384
10  REM  ************************
12  REM
14  REM         MONITOR D. TEST
16  REM
18  REM  ************************
20  REM
25  DIM LV(408,3): DIM RD(3,7)
30 FF(0) = 0.0763:FF(1) = 0.0753:FF(2) = 0.0758
32 FF(3) = 1.500:FF(4) = 0.01254
35  DEF  FN PV(X) = X / 409.6 - 4.945
36  DEF  FN PP(X) = X * 4 / 40.96 - 200
40 EMAX = 105.4:EMIN = 89.3
45  HOME : PRINT : PRINT : PRINT
50  INPUT "   INPUT NAME OF FILE  ";A$: PRINT
55  PRINT "   READING HAS BEEN STARTED   "
60 J$ =  CHR$ (4)
65  PRINT J$;"MON C,I,O"
70  PRINT J$;"OPEN";A$
75  PRINT J$;"READ";A$
80  INPUT B$: INPUT C$: INPUT D$
85  INPUT X(1): INPUT X(2): INPUT X(3): INPUT W
90  INPUT CN: INPUT DR
95  INPUT S1: INPUT S2: INPUT S3: INPUT BP: INPUT SR
100  FOR J = 0 TO 3
105  FOR I = 0 TO 7
110  INPUT RD(J,I)
115  NEXT I
120  NEXT J
```

```
125  INPUT N
130  FOR L = 0 TO N
136  FOR M = 0 TO 15
138 I = L * 16 + M
140  FOR J = 0 TO 3
145  INPUT LV(I,J)
150  NEXT J: NEXT M: NEXT L
155  PRINT J$;"CLOSE";A$
160  PRINT J$;"NOMON C,I,O"
180  REM  ***********************
182  REM
184  REM      MONITOR SECTION
186  REM
188  REM  ***********************
189 X(4) = X(1) * X(2) * X(3)
200 UW = W / X(4) * 12 ^ 3
202 RLD = (UW - 89.3) / (105.4 - 89.3) * 105.4 / UW
204  IF DR = 1 THEN  GOTO 206
205 L4 = LV(0,3):L4 =  FN PP(L4): GOTO 207
206 L4 = LV(0,3):L4 =  FN PV(L4):L4 = L4 * FF(4)
207 L1 = LV(0,0):L1 =  FN PV(L1):L1 = L1 * FF(0)
208 L2 = LV(0,1):L2 =  FN PV(L2):L2 = L2 * FF(1)
209 L3 = LV(0,2):L3 =  FN PV(L3):L3 = L3 * FF(2)
210 NN = (N - 1) * 16
211  FOR I = 1 TO NN
213 LZ = LV(I,0):LZ =  FN PV(LZ):LZ = LZ * FF(0)
214 LV(I,0) = (LZ - L1) / X(1) * 100
215 LY = LV(I,1):LY =  FN PV(LY):LY = LY * FF(1)
216 LV(I,1) = (LY - L2) / X(2) * 100
217 LX = LV(I,2):LX =  FN PV(LX):LX = LX * FF(2)
218 LV(I,2) = (LX - L3) / X(3) * 100
219  IF DR = 1 THEN  GOTO 222
220 LP = LV(I,3):LP =  FN PP(LP):LV(I,3) = (LP - L4) * FF(3): GOTO 228
222 LP = LV(I,3):LP =  FN PV(LP):LP = LP * FF(4)
225 LV(I,3) = (LP - L4) / X(4) * 100
228  NEXT I
230  REM  ************************
231  REM
232  REM     SHEAR STRAIN (OCT)
233  REM
234  REM  ************************
300  REM  *************************
301  REM
302  REM      GRAPHIC SYSTEM
303  REM
304  REM  *************************
305  REM
310  TEXT : HOME : PRINT : PRINT
```

```
315  PRINT "****************************************": PRINT
320  PRINT "            MONITOR SYSTEM": PRINT
325  PRINT "****************************************": PRINT : PRINT
326  PRINT "     (0) PORE PRESS.  VS. CYCLE ": PRINT
330  PRINT "     (1) VOL. CHANGE  VS. CYCLE ": PRINT
332  PRINT "     (2) OCT S.STRAIN VS. CYCLE  ": PRINT
335  PRINT "     (3) DATA SHEAT (PRINT OUT) ": PRINT
340  PRINT "     (4) FINITO !    ": PRINT
345  INPUT "     ENTER OPTION NUMBER        ";OP
350  IF OP = 4 THEN  END
355  IF OP = 3 THEN  GOTO 500
356  IF OP <  > OR THEN  GOTO 310
357 N% = N / 50:K = N% + 2
360  IF OP = 2 THEN  GOTO 400
362 IT = 1
363  GOSUB 450
364 SS = S3 - BP
365  FOR J = 1 TO 49
370 M = (IT - 1) * 50 + J
371  IF DR = 0 THEN Y% = 75 - 114 / SS * LV(M,3)
372  IF DR = 1 THEN Y% = 116 + LV(M,3) * 570
373  IF Y% < 2 THEN Y% = 1
374  IF Y% > 155 THEN Y% = 155
375 X% = 5 * J + 10:XX% = X% + 1
380  HPLOT X%,Y% TO XX%,Y%
381  PRINT "** X ** ";X%" ** Y ** ";Y%
382  NEXT J
385  INPUT "   DUMP THE DISPLAY TO L.P. (Y/N)  ";Y$
386  IF Y$ <  > "Y" THEN  GOTO 394
387  PRINT  CHR$ (4);"PR#2"
388  PRINT  CHR$ (9);"GDR"
389  PRINT  CHR$ (4);"PR#0"
394 IT = IT + 1
395  IF IT > K THEN  GOTO 310
398  GOTO 363
400  REM  **********************
448  GOTO 310
450  HGR : HCOLOR= 3
455 CL = 75:CB = CL + 1
460  HPLOT 1,CL TO 278,CL
461  HPLOT 1,CB TO 278,CB
462  HPLOT 9,2 TO 9,158
463  HPLOT 10,2 TO 10,158
465  FOR I = 0 TO 25
467 II = 10 * I + 20:JJ = II + 1
470  HPLOT II,CB TO JJ,CB
473 CB = CB + 1: HPLOT II,CB TO JJ,CB
475 CB = CL + 1
480  NEXT I
483 C1 = 2:C2 = 40:C3 = 115:C4 = 154
```

```
485  FOR I = 7 TO 277
487 II% = I / 2:J = 2 * II% - I
490  IF J = 0 THEN  GOTO 495
493  HPLOT I,C1: HPLOT I,C2: HPLOT I,C3: HPLOT I,C4
495  NEXT I
496 I = 0
498  RETURN
500  PR# 2
505  PRINT  CHR$ (27)"4"
506  PRINT  CHR$ (27)"H"
507  PRINT  CHR$ (9); CHR$ (1)
509  PRINT : PRINT
510  PRINT "                              ************************************
     *****": PRINT
515  PRINT "                   LIQUEFACTION DATA SHEET I ": PRINT
520  PRINT "                              ************************************
     *****": PRINT
525  PRINT "            TYPE OF SOIL : ";D$: PRINT
530  PRINT "                    DATE : ";C$: PRINT
535  PRINT "               TESTED BY : ";B$: PRINT
540  PRINT "                              =========  INITIAL CONDITION  =====
     ====": PRINT
545  PRINT "    1) SIZES OF SAMPLE ": PRINT
550  PRINT "                  Z-DIR. (INCH) : ";X(1): PRINT
555  PRINT "                  Y-DIR. (INCH) : ";X(2): PRINT
560  PRINT "                  X-DIR. (INCH) : ";X(3): PRINT
564  PRINT : PRINT
565  PRINT "    2) WEIGHT OF SAMPLE ": PRINT
570  PRINT "                  DRY WT.  (LB) : ";W: PRINT
575  PRINT "                  UNIT WT.(PCF) : ";UW: PRINT
580  PRINT "                  R.DENSITY (%) : ";RLD: PRINT : PRINT
585  PRINT "                              =========  VOLUMETRIC CHANGE  =====
     =====": PRINT : PRINT
590  PRINT "    1) AFTER SATURATION (C.P.) = 10 PSI
591  PRINT
595  PRINT "       Z-STRAIN (%)  = ";RD(1,0)
596  PRINT "       Y-STRAIN (%)  = ";RD(1,1)
597  PRINT "       X-STRAIN (%)  = ";RD(1,2)
598  PRINT "       V-STRAIN (%)  = ";RD(1,3): PRINT
600  PRINT "    2) AFTER K-O LOAD (P.V.) = ";S1" PSI ": PRINT
605  PRINT "       Z-STRAIN (%)  = ";RD(2,0)
606  PRINT "       Y-STRAIN (%)  = ";RD(2,1)
607  PRINT "       X-STRAIN (%)  = ";RD(2,2)
608  PRINT "       V-STRAIN (%)  = ";RD(2,3): PRINT
610  PRINT "    3) AFTER CONSOLIDATION (B.P.) = ";BP" PSI "
615  PRINT "       Z-STRAIN (%)  = ";RD(3,0)
616  PRINT "       Y-STRAIN (%)  = ";RD(3,1)
617  PRINT "       X-STRAIN (%)  = ";RD(3,2)
618  PRINT "       V-STRAIN (%)  = ";RD(3,3): PRINT
620  PRINT  CHR$ (12)
```

```
625 NN = N * 2 + 2
630  PRINT "                                  ************************************
     *****": PRINT
635  PRINT "                       LIQUEFACTION DATA SHEET II ": PRINT
640  PRINT "                                  ************************************
     *****": PRINT
642  PRINT "  STRESS RATIO  ";SR: PRINT : PRINT
645  PRINT "  CYCLE      Z-STRAIN              Y-STRAIN              X-STRAI
     N             V-STRAIN ": PRINT
650 NN = N * 2 + 2
655  FOR I = 1 TO NN
660 II% = I / 2
670  PRINT "   ";II%"          ";LV(I,0)"         ";LV(I,1)"      ";LV(I,2)
     "      ";LV(I,3)
680  NEXT I
681  PR# 0
685  GOTO 310


10   REM  ************************
12   REM
14   REM      DYNAMIC TEST
16   REM                 NO.2
18   REM         BY J. IWABUCHI
19   REM
20   REM  ************************
22   REM
25   DIM LV(900,3)
26   DIM RD(3,7)
27 FF(0) = 0.0762:FF(1) = 0.0753:FF(2) = 0.0758
28 FF(3) = 0.625:FF(4) = 0.01254
29   DEF  FN V1(X) = (X * 0.14661 - 0.76103) * 409.6
30   DEF  FN V2(X) = (X * 0.15591 - 0.94164) * 409.6
31   DEF  FN V3(X) = (X * 0.14166 - 0.51020) * 409.6
32   DEF  FN PV(X) = X / 409.6 - 4.945
35   GOTO 90
40   FOR L = 0 TO N
41 M = 8 * L
42   FOR K = 0 TO 7
45 I = M + K
50   & AIN,(TV) = Q,(C#) = 0:LV(I,0) = Q
51   & AIN,(TV) = Q,(C#) = 1:LV(I,1) = Q
52   & AIN,(TV) = Q,(C#) = 2:LV(I,2) = Q
53   IF DR = 1 THEN  & AIN,(TV) = Q,(C#) = 3
54   IF DR = 0 THEN  & AIN,(TV) = Q,(D#) = 1,(C#) = 0
55 LV(I,3) = Q
60   & AOUT,(DV) = A(K),(C#) = 0
63   & PAUSE = 0.1
70   NEXT K
72   & BEEP
```

```
75  NEXT L
80  GOTO 610
90  HOME
91  PRINT : PRINT : PRINT : PRINT : PRINT
93  PRINT "****************************************": PRINT : PRINT : PR

94  PRINT "            LIQUIFACTION TEST": PRINT
95  PRINT "       PURE SHEAR DYNAMIC LOAD  ": PRINT
96  PRINT : PRINT : PRINT
97. PRINT "****************************************": PRINT : PRINT
98  INPUT "                IF READY, HIT (RETURN) ";Y$
99  HOME
100  PRINT "****************************************": PRINT
105  PRINT "     STAGE 1. IDENTITY OF FILE ": PRINT
110  PRINT "****************************************": PRINT
115  PRINT : PRINT
120  INPUT "   NAME OF FILE  ";A$
121  PRINT : PRINT
125  INPUT "   TESTED BY     ";B$
126  PRINT : PRINT
130  INPUT "   DATE          ";C$
131  PRINT : PRINT
135  INPUT "   SOIL          ";D$
140  PRINT : PRINT
141  SPEED= 10
142  PRINT "                  THANKS !     "
143  SPEED= 254: HOME
150  PRINT "****************************************": PRINT
152  PRINT "      STAGE 2. INITIAL CONDITION  ": PRINT
155  PRINT "****************************************": PRINT
160  PRINT "    ENTER THE SIZES OF SAMPME  ": PRINT : PRINT
165  INPUT "      Z (INCH) = ";X(1): INPUT "      Y (INCH) = ";X(2): IN
     "      X (INCH) = ";X(3): PRINT
170  INPUT "    WEIGHT OF SAMPLE (DRY) (LB) = ";W: HOME
171 X(4) = X(1) * X(2) * X(3)
175  HOME : PRINT
180  PRINT "****************************************": PRINT
185  PRINT "      STAGE 3. ENVIRNMENT OF TEST ": PRINT
190  PRINT "****************************************": PRINT
193 CN$ = "UNCONSOLIDATION - "
194 DR$ = "UNDRAIN TEST "
195  INPUT "   CONSOLIDATION  (1) OR NOT (0)  ";CN: IF CN = 1 THEN CN$ =
     "CONSOLIDATION - "
196  PRINT
200  INPUT "   DRAIN TEST     (1) OR NOT (0)  ";DR: IF DR = 1 THEN DR$ =
     "DRAIN TEST "
201  PRINT
205  PRINT "   ";CN$;DR$
210  PRINT : INPUT "   IS THAT RIGHT ? (Y/N) ";Y$: IF Y$ = "N" THEN  GO
     175
```

```
215  PRINT : PRINT
220  IF DR = 1 THEN  PRINT "   VOLUMETRIC CHANGE WILL BE MEASURED "
222  IF DR = 1 THEN  GOTO 227
225  PRINT "   PORE PRESSURE WILL BE MEASURED  "
227  SPEED= 10
228  PRINT "                          "
229  SPEED= 254
230  HOME : PRINT
235  PRINT "****************************************": PRINT
240  PRINT "      STAGE 4. SAMPLE PREPARATION  ": PRINT
245  PRINT "****************************************": PRINT : PRINT
250  PRINT "   (1) WRAP SAMPLE IN MOLD": PRINT
252  PRINT "   (2) APPLY VACUUM , 5 HG IN ": PRINT
254  PRINT "   (3) SET SAMPLE IN BOX": PRINT
256  PRINT "   (4) APPLY CONF.PRESS., SAY 5 PSI ": PRINT
258  PRINT "   (5) CUT VACUUM AND OPEN VALVES": PRINT
260  PRINT "   (6) INCREASE PRESSURE TO 10 PSI": PRINT
262  PRINT "   (7) SET LVDT AND TRANSDUCER ": PRINT
264  INPUT "   IF READY TO GO AHEAD, HIT (RETURN)  ";Y$
266  HOME : PRINT
270  PRINT "****************************************": PRINT
275  PRINT "        STAGE 5. INITIAL READING ": PRINT
280  PRINT "****************************************": PRINT
285 J$ =  CHR$ (4): REM  CTRL-J
290  PRINT J$;"OPEN";A$: PRINT J$;"DELETE";A$
295  PRINT J$;"OPEN";A$: PRINT J$;"WRITE";A$
300  PRINT B$: PRINT C$: PRINT D$
305  PRINT X(1): PRINT X(2): PRINT X(3): PRINT W
310  PRINT CN: PRINT DR
315  PRINT J$;"CLOSE";A$
316 J = 0
320  GOSUB 1000
322  PRINT : PRINT
325  INPUT "       ANYTHING WRONG ? (Y/N) ";Y$: IF Y$ = "Y" GOTO 266
330  HOME : PRINT
335  PRINT "****************************************": PRINT
340  PRINT "      STAGE 6. SAMPLE SATULATION  ": PRINT
345  PRINT "****************************************": PRINT
350  PRINT "   FOR CO-2 METHOD ": PRINT
355  PRINT "   (1) FLUSH CO-2 "
357  PRINT "   (2) FLUSH H-2-O"
359  PRINT "   (3) INCREASE CON. AND BACK PRESS. "
360  PRINT "   (4) MEASURE B-VALUE ": PRINT
362  PRINT "   FOR VACUUM METHOD": PRINT
364  PRINT "   (1) FLUSH H-2-O, SAY 1 HOUR "
366  PRINT "   (2) RE-SET 5 PSI AND 10 HG"
368  PRINT "   (3) CHECK AIR VOIDS FLOWING OUT "
370  PRINT "   (4) WAITE ANOTHER 1 HOUR "
372  PRINT "   (5) INCREASE C.P. AND B.P.,GET 3 (%) "
373  PRINT
```

```
375  INPUT "   READY TO GO AHEAD  ";Y$
380  HOME : PRINT
390  PRINT "****************************************": PRINT
395  PRINT "      STAGE 7. STRESS APPLICATION  ": PRINT
400  PRINT "****************************************": PRINT
405  INPUT "   EFFECTIVE OVERBURDEN PRESS. ";S1: PRINT
410 S2 = 0.45 * S1:S3 = S2
415  PRINT "   EFFECTIVE HORIZONTAL PRESS. ";S2: PRINT
420  INPUT ".  IS THAT RIGHT ?   (Y/N) ";Y$
425  IF Y$ = "Y" THEN  GOTO 440
430  PRINT
432  INPUT "   STRESS (Z)   (PSI) ";S1: PRINT
434  INPUT "   STRESS (Y)   (PSI) ";S2: PRINT
436  INPUT "   STRESS (X)   (PSI) ";S3: PRINT
440  PRINT : INPUT "   BACK PRESS.   (PSI) ";BP: PRINT
442  INPUT "   STRESS RATIO       ";SR
443 DS = SR * S1 / 4:DK = DS / 2
444 S1 = S1 + BP
445 S2 = S2 + BP
446 S3 = S3 + BP
447  FOR I = 0 TO 2
448 A = S1 + DS * I:A(I) =  FN V1(A)
449  NEXT I
450 A(3) = A(1):A(4) = A(0):A(5) =  - A(1):A(6) =  - A(2):A(7) =  - A(1)

452  HOME : PRINT
455  PRINT "****************************************": PRINT
460  PRINT "     STAGE 8. AUTO-CONTROLL CHECK ": PRINT
465  PRINT "****************************************": PRINT
470  PRINT "   (1) MAKE SURE NO AIR VOIDS IN TUBE  "
471  PRINT
475  INPUT "   (2) INPUT CON.P.AT THE PRESENT ";P
480 P1 =  FN V1(P):P2 =  FN V2(P):P3 =  FN V3(P)
481  & AOUT,(DV) = P1,(C#) = 0
482  & AOUT,(DV) = P2,(C#) = 1
483  & AOUT,(DV) = P3,(C#) = 2
485  PRINT
486  PRINT "   (3) CHECK PRESS AT AUTO-CONT.  "
487  PRINT
490  PRINT "   (4) IF OK , TURN T.W.VALVES": PRINT
492  INPUT "   (5) DONE ?   ";Y$
493  PRINT
495  PRINT "   (6) INCREASE B.P. WHILE C.P. CHANGES ": PRINT
500  INPUT "   (7) READY ? ";Y$
501 J = 1
502  GOSUB 1000
505 DZ = (S1 - P) / 5
508 VZ = P:VY = P:VX = P
510  FOR I = 1 TO 5
515 VZ = VZ + DZ
```

```
516 ZZ =  FN V1(VZ)
520  & BEEP
522  & AOUT,(DV) = ZZ,(C#) = 0
523  & AOUT,(DV) = YY,(C#) = 1
524  & AOUT,(DV) = XX,(C#) = 2
525  & PAUSE = 10
526  NEXT I
528  & PAUSE = 30
529 J = 2: GOSUB 1000
530  IF CH$ <  > "CONSOLIDATION - " THEN  GOTO 560
532  PRINT : PRINT
535  PRINT "   SAMPLE IN CONSOLIDATION PROCEDURE   ": PRINT
537  PRINT
540  INPUT "  SET TIMER FOR CONSOLIDATION (MIN) ";TM
542  PRINT
545 TM = TM * 60: & PAUSE = TM
546  FLASH
547  & BEEP ON
548  INPUT "       TIME IS UP, HIT (RETURN) ";Y$: NORMAL : & BEEP STOP :
      HOME : PRINT
549 J = 3
550  GOSUB 1000
560  HOME : PRINT
565  PRINT "****************************************": PRINT
570  PRINT "       STASE 10.  DATA AQUISITION   ": PRINT
575  PRINT "****************************************": PRINT
580  PRINT : PRINT
585  INPUT "   INPUT NO. OF CYCLES ESTIMATED. ";N
590  PRINT : PRINT
595  INPUT "   IF READY, HIT (RETURN) ";Y$
597  PRINT : PRINT : PRINT
598  PRINT "****************************************"
600  GOTO 40
610  PRINT J$;"MON C,I,O"
615  PRINT J$;"APPEND";A$
620  PRINT J$;"WRITE";A$
625  PRINT S1: PRINT S2: PRINT S3: PRINT BP: PRINT SR
630  FOR J = 0 TO 3
635  FOR I = 0 TO 7
640  PRINT RD(J,I)
645  NEXT I
650  NEXT J
655  PRINT N
656  FOR J = 0 TO 3
657  PRINT LV(0,J)
658  NEXT J
659  FOR L = 1 TO N
660  GOSUB 1200
665  NEXT L
```

```
680  PRINT J$;"CLOSE":A$
685  PRINT J$;"NOMON C,I,O"
690  PRINT : PRINT
695  PRINT "   OK / IT'S DONE     ": PRINT
700  INPUT "   MONITOR THE DATA ? (Y/N) ";OP$
705  IF OP$ = "Y" THEN  PRINT J$;"RUN MONITOR"
710  END
1000  REM  ***********************
1002  REM
1004  REM   SUBROUTINE READING
1005  REM
1006  REM  ***********************
1008  REM
1010  FOR L = 0 TO 2
1015  & AIN,(TV) = Q,(C#) = L,(FU) =  FN PV(RAW%)
1020 Q = Q * FF(L)
1025 RD(J,L) = Q
1030  NEXT L
1035  & AIN,(TV) = Q,(C#) = 3,(FU) =  FN PV(RAW%)
1038 Q = Q * FF(4)
1040 RD(J,3) = Q
1045  HOME : PRINT
1050  PRINT "****************************************": PRINT
1055  PRINT "      DISPLACEMENTS(IN)   STRAIN (%) ": PRINT
1060  IF J = 0 THEN  GOTO 1100
1065 JM = J - 1
1070  FOR I = 0 TO 3
1075 IN = I + 4:II = I + 1
1080 RD(J,IN) = (RD(J,I) - RD(JM,I)) / X(II) * 100
1082  NEXT I
1100  PRINT " Z-DIR.  ";RD(J,0)"      ";RD(J,4): PRINT
1105  PRINT " Y-DIR.  ";RD(J,1)"      ";RD(J,5): PRINT
1110  PRINT " X-DIR.  ";RD(J,2)"      ";RD(J,6): PRINT
1112  PRINT " V OR P  ";RD(J,3)"      ";RD(J,7): PRINT
1115  PRINT "****************************************": PRINT
1120  & BUZZ
1125  INPUT "       IF READY, HIT (RETURN)  ";Y$
1130  RETURN
1200  REM  ***********************
1201  REM
1202  REM    SUBROUTINE MAX & MIN
1203  REM
1204  REM  ***********************
1205  REM
1210 M = 8 * (L - 1) + 1
1215  FOR P = 0 TO 3
1220 MAX = LV(M,P)
1225 MIN = LV(M,P)
1230  FOR K = 1 TO 7
1235 I = M + K
```

```
1240  IF MAX < LV(I,P) THEN MAX = LV(I,P)
1245  IF MIN > LV(I,P) THEN MIN = LV(I,P)
1250  NEXT K
1255  PRINT MAX
1260  PRINT MIN
1265  NEXT P
1270  RETURN

9  HOME
100  REM   ********************
110  REM
120  REM       READ TEXT FILE
130  REM
140  REM   ********************
145  DIM RD(200,7): DIM A(200): DIM B(200): DIM C(200)
146  DIM RD$(200,7): DIM A$(200): DIM B$(200): DIM C$(200)
148 EMAX = 105.4:EMIN = 89.3
150 J$ =  CHR$ (4)
160  TEXT : PRINT
170  INPUT " NAME OF TEXT FILE ";A$
180  PRINT : PRINT : PRINT
210  PRINT " I'M READING THE FILE  "
220  PRINT J$;"MON C,I,O"
230  PRINT
240  PRINT J$;"OPEN ";A$
250  PRINT J$;"READ ";A$
260  PRINT
264  INPUT B$
266  INPUT C$
268  INPUT D$
274  INPUT X(1)
276  INPUT X(2)
278  INPUT X(3)
279  INPUT W
295  INPUT CN: INPUT DR
296  INPUT S1: INPUT S2: INPUT S3: INPUT BP
297  INPUT SR
299  INPUT J
300  FOR K = 0 TO J
310  INPUT A(K): INPUT B(K): INPUT C(K)
340  FOR L = 0 TO 7
350  INPUT RD(K,L)
360  NEXT L
370  NEXT K
380  PRINT J$;"CLOSE ";A$
390  PRINT J$;"NOMON C,I,O"
400  REM  END OF READING THE FILE
410 UW = W / X(1) / X(2) / X(3) * 12 ^ 3
500  PR# 2
```

```
505  PRINT  CHR$ (27)"4"
507  PRINT  CHR$ (27)"M"
508  PRINT  CHR$ (9); CHR$ (1)
510  PRINT : PRINT
520  PRINT "          ************************************************
     **********"
530  PRINT
540  PRINT "                              STATIC 3-D TEST ( DATA SHEET - I )
     ": PRINT
550  PRINT "          ************************************************
     **********": PRINT
560  PRINT "            TYPE OF SOIL : ";C$: PRINT
570  PRINT "        DATE OF TESTING : ";D$: PRINT
580  PRINT "              TESTED BY : ";B$;
585  PRINT "                NOTE : ": PRINT : PRINT
590  PRINT "          ====================  INITIAL CONDITION  ========
     ==========": PRINT : PRINT
600  PRINT "    1) SIZES OF SAMPLE ": PRINT
610  PRINT "                X-DIR. (INCH) : ";X(1)
615  PRINT
620  PRINT "                Y-DIR. (INCH) : ";X(2): PRINT
630  PRINT "                Z-DIR. (INCH) : ";X(3): PRINT
640  PRINT "    2) WEIGHTS OF SAMPLE ": PRINT
650  PRINT "                DRY WT.   (LB) : ";W: PRINT
660  PRINT "                UNIT WT. (PCF) : ";UW: PRINT
670  PRINT : PRINT : PRINT
680  PRINT "          ====================    CONSOLIDATION   ==========
     =========="
690  PRINT : PRINT
700  PRINT "    1) CONF. PRESSURE (PSI) : ";S1: PRINT
710  PRINT "    2) VOLUME CHANGE  ": PRINT
720  PRINT "                X-STRAIN (%) : ";RD(3,3): PRINT
730  PRINT "                Y-STRAIN (%) : ";RD(3,4): PRINT
740  PRINT "                Z-STRAIN (%) : ";RD(3,5): PRINT
750 VS = RD(1,1) + RD(3,1) + RD(5,1)
760  PRINT "                V-STRAIN (%) : ";VS: PRINT
770  PRINT  CHR$ (12)
772  FOR K = 0 TO J
774 A$(K) =  STR$ (A(K))
775 B$(K) =  STR$ (B(K))
776 C$(K) =  STR$ (C(K))
777  FOR L = 0 TO 7
778 RD$(K,L) =  STR$ (RD(K,L))
780  NEXT L
782  NEXT K
800  PRINT "          ************************************************
     **********": PRINT
810  PRINT "                              STATIC 3-D TEST ( DATA SHEET - II )
      ": PRINT
```

```
820  PRINT "          ************************************************
     **********": PRINT : PRINT
830  PRINT "           1) STESS-STRAIN RELATION  ": PRINT
850  PRINT  CHR$ (27)"D" CHR$ (1) CHR$ (6) CHR$ (12) CHR$ (180) CHR$ (29
     ) CHR$ (41) CHR$ (55) CHR$ (0)
860 H$ =  CHR$ (9)
870  PRINT "          STEP    D-STRESS    X-STRAIN    Y-STRAIN    Z-STRA
     IN  ": PRINT
880  FOR K = 4 TO J
885 ST = K - 3:ST$ =  STR$ (ST)
900  PRINT H$;ST$;H$;A$(K);H$;B$(K);H$;C$(K);H$;RD$(K,4);H$;RD$(K,5);H$;
     RD$(K,6)
910  PRINT
920  NEXT K
1000  PRINT  CHR$ (12)
1010  PRINT "          ************************************************
     ************": PRINT
1020  PRINT "                          STATIC 3-D TEST ( DATA SHEET - III
      ) ": PRINT
1030  PRINT "          ************************************************
     ************": PRINT : PRINT
1040  PRINT "          2) STRESS-DISPLACEMENT RELATION ": PRINT
1050  PRINT "          STEP    D-STRESS    X-DISPT.    Y-DISPT.  Z-DISPT
     .          ": PRINT : PRINT
1060  FOR K = 4 TO J
1065 ST = K - 3:ST$ =  STR$ (ST)
1070  PRINT H$;ST$;H$;A$(K);H$;B$(K);H$;C$(K);H$;RD$(K,0);H$;RD$(K,1);H$
     ;RD$(K,2)
1080  NEXT K
1100  PRINT  CHR$ (12)
1110  PRINT "          ************************************************
     ************": PRINT
1120  PRINT "                          STATIC 3-D TEST ( DATA SHEET - IV
     ) ": PRINT
1130  PRINT "          ************************************************
     ************": PRINT : PRINT
1140  PRINT "          3) STESS-PORE PRESSURE AND VOLUMETRIC CHANGE ":

1150  PRINT "          STEP    D-STRESS    P-PRESS    V-CHANGE  ": PRINT
     : PRINT
1160  FOR K = 4 TO J
1162 ST = K - 3:ST$ =  STR$ (ST)
1170  PRINT H$;ST$;H$;A$(K);H$;B$(K);H$;C$(K);H$;RD(K,3);H$;RD(K,7)
1180  NEXT K
1190  END
```

APPENDIX B

LIST OF MATRERIALS AND EQUIPMENTS FOR DCSVT1

1. Thin Membrane	Dental Dam One square Yard, 6 inch wide (Thin) The Hygenic Corporation, Akron, Ohio 44310
2. Spaghetti Tube	Teflon Spaghetti Tubing AWG Size 23 Nominal I.D. 0.025" CHEMPLAST Inc., 150 Dey Road, Wayne, NJ.
3-a. Silicone Rubber 3-b. MOLDMAKER	RTV Sicicone Rubber RTV660 General Electric Company Silicone Products Division RTV Products Depertment, Waterford, Yew York 12188
4. Rubber Cement	Victor RUBBER CEMENT, Victor Automative Production Inc., Chicago, Il. 60641
5. Liquid Rubber	Duro Plastic Rubber Loctite Corporation Automotive and Consumer Group Cleveland , Ohio 44129
6. Three way valve	3-Way Ball Valve, Catalog No. 0.43 x S4 Two way valve (Ball Valves), Catalog No. 0.43 x S4 Whitey Co. 318 Bishop Road, Highland Heights Ohio 44143
7. Tube Fitting	Nut, Swagelok Crowford Fitting Co. 295000 Solon Road, Solon Ohio 44139
8-a. Air Regurator 8-b. VPT	Fairchild Model 10 Pneumatic Pressure Regurator The Fairchild T5221 I/P and E/P Transducers

8-c. Air Filter	Fairchild Startos Model 65 Pressure Regurator Fairchild Industrial Products Co., 1501 Fairchild Drive Winston-Salem, NC 27105
9. Pore Pressure Transducer	Pressure Transducer Capacity 0 to 100 psi. Entran Devices Inc.,Fairfield, NJ
10. Differential Transducer	Validyne DP15 Validyne 8626 Wibur Ave, Northridge California, 91324
11-a ISAAC 91A	ISAAC 91A Cyborg Corporation
11-b REFERENCE MANUAL	55 Chapel St., Newton Ma, 02159
11-c HARDWARE MANUAL	
12-A Apple II(Plus)	Apple II (Plus) 48K, Apple Corporaion
12-B Apple Turotial	Cupertino, Cal., 95014
13. VISITERM	Visicorp, San Jose, California 95134

APPENDIX C

TEST RESULTS OF DRAINED CYCLIC LOADING TEST

C.1 INTRODUCTION

Cyclic loading tests were conducted for investigating volumetric changes of uncemented and cemented sand. Totally 10 cyclic loading tests were performed under consolidated-drained condition with volumetric strain measurement on CTX loading of DCSVT1. Basic sample preparation and test condition were succeeded from the previous liquefaction test program.

Both uncemented and cemented samples were prepared by air pluviation technique with Monterey #0/30 sand for their density to be 15.07 (kN/m^3). Cemented samples were cured for 12 days in water at room temperature. Unconfined compressive strength test was conducted for one of seven samples cured for 12 days and its strength is 59 (kN/m^2). Saturation of samples was done with carbon dioxide method and vacuum procedure for uncemented and cemented samples, respectively.

All tests were conducted by the cubical device on CTX loading. The samples were consolidated isotropically under effective confining pressure at 104 (kN/m^2) with back pressure at 208 (kN/m^2) approximately one hour or until no volumetric change was confirmed. For uncemented samples, cyclic loadings were applied in 40 cycles and for cemented samples, 70 cycles.

C.3 TEST RESULTS

Relationship between volumetric change and number of cyclic loadings is shown for uncemented sand in Figure C.1. As seen, the higher the stress level, the larger the volumetric increase;

volumetric increment for each cyclic loading is significantly reduced after half-way to the 40 cycles. In 40 cycles, the final volumetric strains for U-2, U-3, and U-4 are 0.05, 2.1, and 0.33 percent, respectively.

Figure C.2 shows the relationship for cemented sand. The tendency observed for uncemented sand is similar in cemented sand except amount of volumetric strains developed under equivalent stress levels to uncemented sand tests and small increment in volumetric strains at the beginning of the loadings. The volumetric strains in 70 cycles for C-1, C-2, and C-3 are 0.1, 2.7, and 4.1, respectively.

Note that test results of U-1, C-5, and U-6 are similar to those of tests which were done under similar loading conditions, respectively. This indicates that the test results shown are consistent in terms of measurement and loading condition.

Relationships between volumetric strain and octahedral shear strain are shown in Figure C.3 and C.4 for uncemented and cemented sands, respectively. Octahedral shear strain is defined by the following equation:

$$\gamma_{oct} = \frac{2}{3} \times \sqrt{(\varepsilon_1 - \varepsilon_2)^2 + (\varepsilon_2 - \varepsilon_3)^2 + (\varepsilon_3 - \varepsilon_1)^2}$$

Note that in both figures, slight scatters are seen, mainly due to limitation of measuring accuracy of LVDTs and multiplication of small error in three strains by the above equation.

Figure C.3 shows that the higher the stress level the larger the octahedral strains in 40 cycles and the relationships seem to be linear in the range observed. The other remark is that the angles of ascendent linear lines for different stress levels are close one another.

Some of the cemented samples had not been broken in 70 cyclic loadings. C-1 had still unconfined compressive strength at the end of cyclic loadings and it is 23 (kN/m^2). C-2 had the strength to maintain its shape at the end of the test. However, C-3 and C-4 were confirmed as the cemented samples broken when the samples were taken out of the cubical shear box.

The relationship for cemented sand is different from that for uncemented sand (Figure C.4). C-1, C-2, and C-3 remain at small octahedral shear strain level at the beginning of cyclic loadings

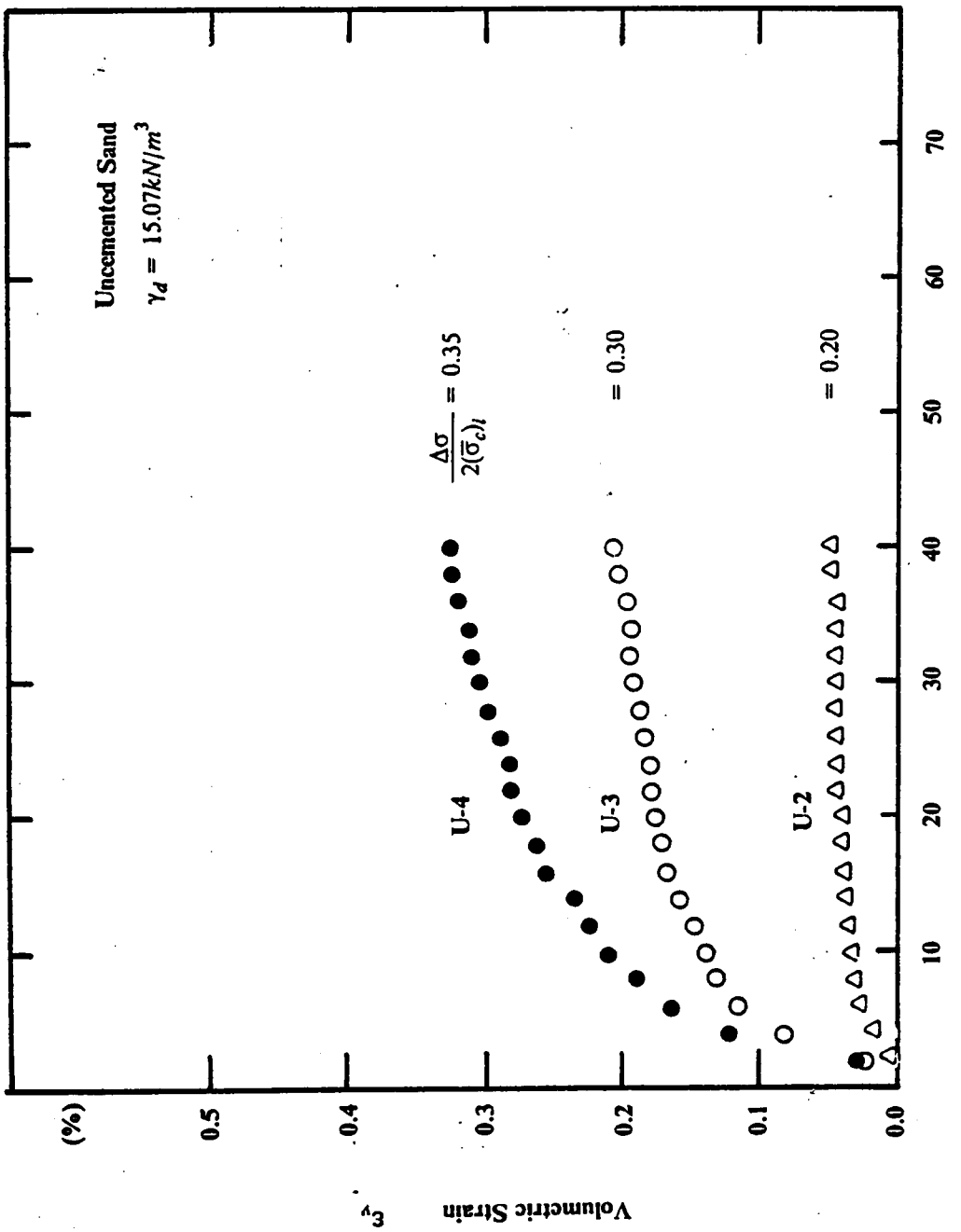

Figure C.1 Volumetric Strain vs. Number of Cyclic Loadings on Uncemented Loose Sand.

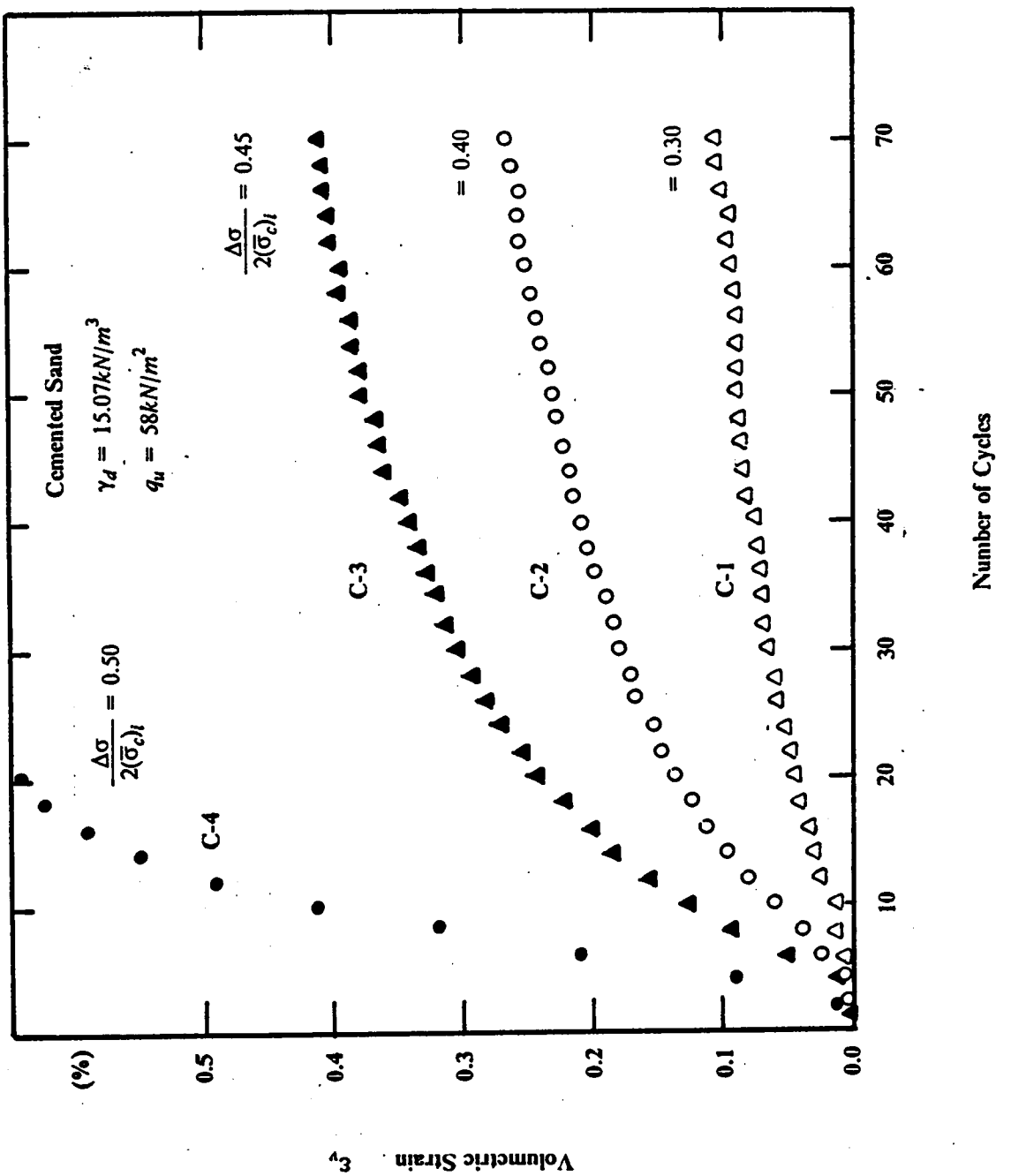

Figure C.2 Volumetric Strain vs. Number of Cyclic Loadings on Cemented Loose Sand.

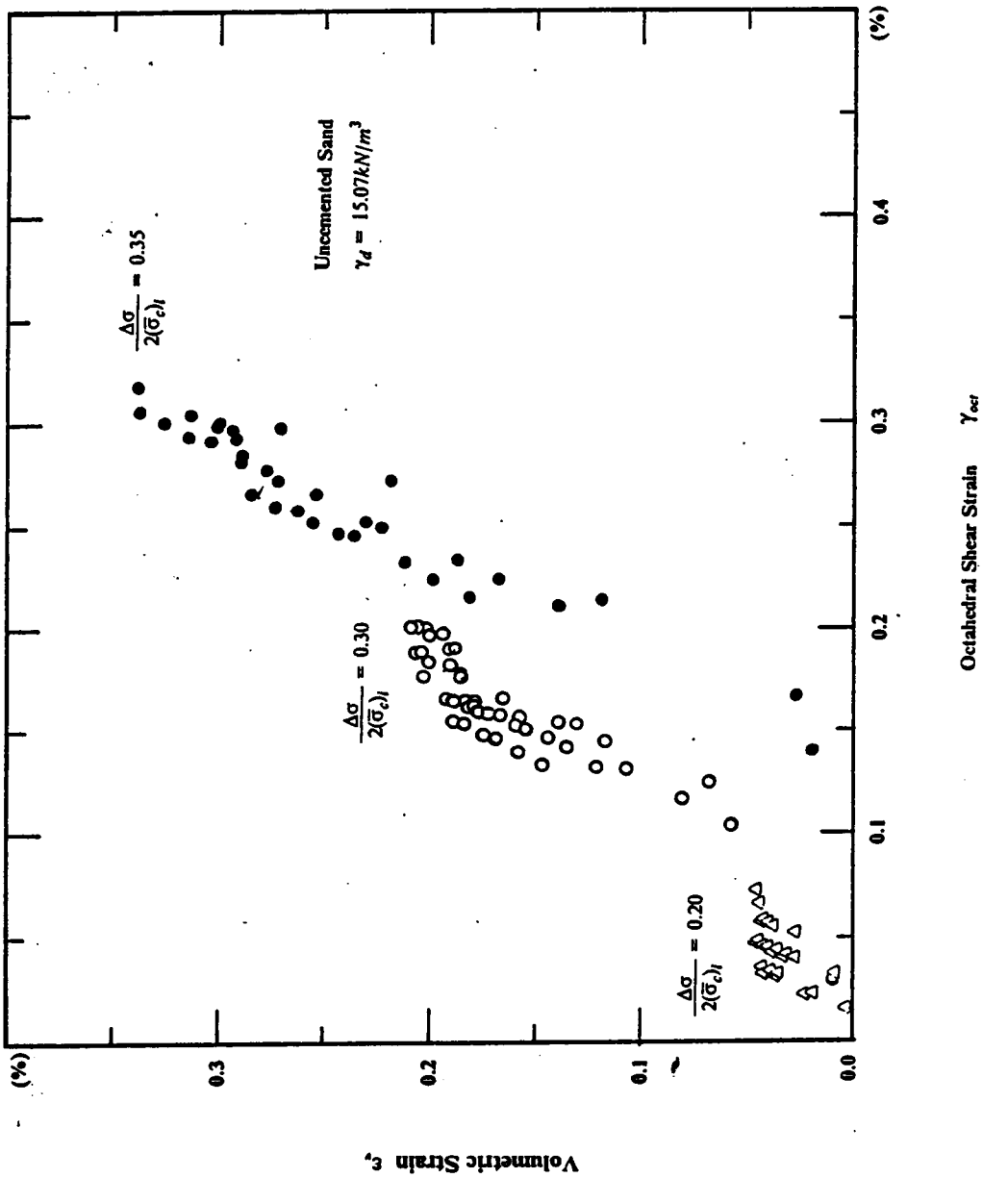

Figure C.3 Volumetric Strain vs. Octahedral Shear Strain on Uncemented Loose Sand.

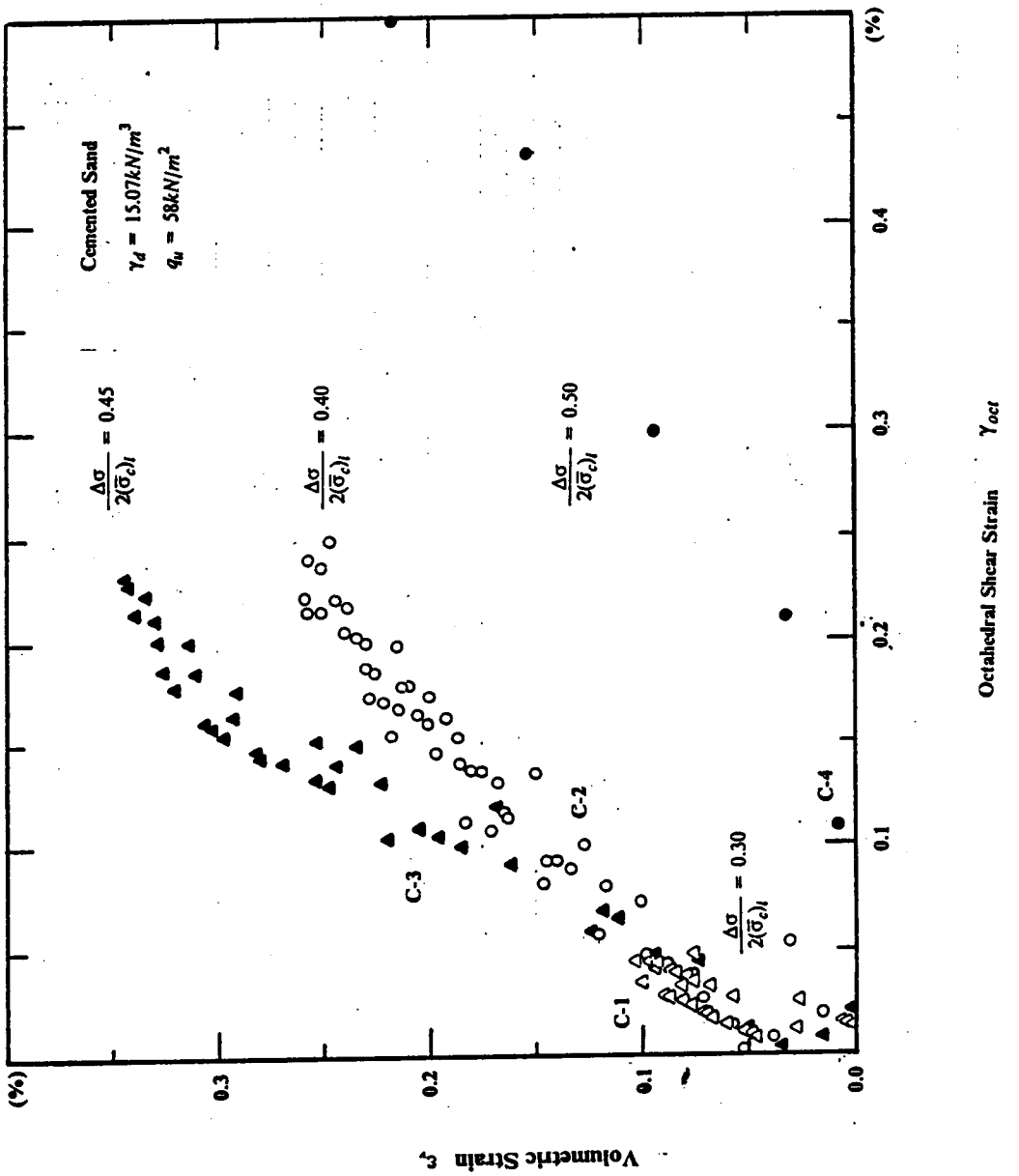

Figure C.4 Volumetric Strain vs. Octahedral Shear Strain on Cemented Loose Sand.

with increment in volumetric strains, and subsequently, curves of these bent and develop volumetric and octahedral shear strains whose relationships seem to linear. The angles of curves after the bent are less than those of uncemented sand, however, the curve of C-3 is somewhat different, showing shape raise after 0.1 percent of octahedral shear strain. The curve of C-4 is totally different to the rest of the curves but similar to that of uncemented samples.

The vita has been removed from the scanned document